To the Graduate Council:

I am submitting herewith a dissertation written by Sangjoon Sohn entitled "A Study of Indentation Creep Using the Finite Element Method." I have examined the final electronic copy of this dissertation for form and content and recommend that it be accepted in partial fulfillment of the requirements for the degree of Doctor of Philosophy, with a major in Materials Science and Engineering.

George M. Pharr, Major Professor

We have read this dissertation
and recommend its acceptance:

Hahn Choo

Warren C. Oliver

Dayakar Penumadu

Accepted for the Council:

Carolyn R. Hodges

Vice Provost and Dean of the
Graduate School

(Original signatures are on file with official student records)

A Study of Indentation Creep Using the Finite Element Method

A Dissertation Presented for the

Degree of Doctor of Philosophy

The University of Tennessee, Knoxville

Sangjoon Sohn

December 2007

Dedication

I dedicate this dissertation to my late grandmother, Soon-Hee Nahm. I am grateful for the inspiration and support she had provided during her lifetime, always believing in me with all her heart.

Acknowledgements

I thank God for being able to complete this journey. I would specially like to thank Dr. George M. Pharr for the endless support he has provided not only as an academic advisor but also as a mentor throughout my graduate studies at the University of Tennessee in Knoxville. I would also like to express my sincere gratitude to Dr. Hahn Choo, Dr. Warren C. Oliver, and Dr. Dayakar Penumadu for accepting to serve as the committee members for my doctoral dissertation and sparing their valuable time to discuss and advise my doctoral research. I would like to acknowledge MTS Nano Instruments for the financial support provided during my doctoral research. I thank my Father, Chang-Moon Sohn, and my Mother, Sook-Hee Kim, for their wonderful support and love. Equally important are my sister and brother and their families in believing in me. My Father-in-Law, Mother-in-Law and their family deserve appreciation for the prayer and support. All the members of Dr. Pharr's research group, past and present, deserve special thanks for the support and friendship they have provided during the long years I have stayed in Knoxville. Above all, I would like to thank my wife, Yujin, for her love and care through both happy and hard times of my doctoral degree program. I would like to say that "I couldn't have done it without her."

Abstract

Indentation is a useful technique for studying the mechanical properties of a material. Measurable mechanical properties from indentation include time-dependent as well as time independent properties. Among these mechanical properties, time-dependent permanent deformation (creep) is of interest in this study. The purpose of this study is to explore the behavior of creep deformation of a solid under indentation. The main scientific research tool will be the finite element method.

Existing works by others provide limited solutions that allow us to correlate uniaxial creep to indentation creep. In this study, the task is taken a step further to enhance and modify previous solutions to more realistic indentation situations. Indentations with spherical and conical indenter geometries are considered. Practical data obtained from indentation creep are usually in the form of displacement (h) – time (t) or load (P) – displacement (h). Results in this study are derived to describe this behavior and obtain fundamental creep parameters from it.

Elasticity may not be ignored in the majority of indentation situations. Therefore, the effect of finite elastic deformation is considered in this study with the intention of characterizing elastic transient phenomena. From the results, certain criteria in terms of an experimentally measurable parameter will be suggested in order to avoid misinterpreting indentation data influenced by the initial elasticity.

The effect of finite strain – finite deformation in indentation is investigated. Creep solutions provided by others usually assume infinitesimal strain – infinitesimal deformation. As a result, only blunt cones approaching the geometry of a flat punch

indenter have been considered for the most part in previous works. In this study, the problem of finite strain – finite deformation is addressed for conical indentation. Various half-included cone angles of the indenter are considered to account for finite strain – finite deformation problems.

The power law relation is the most common general description of creep deformation when strain rate and steady-state stress are involved. However, power law breakdown, due to large strain rates and stresses may occur during the initial parts of indentation, especially for conical indenters. Modeling of power law breakdown in indentation creep is presented and corresponding relations between uniaxial to indentation creep behavior are proposed in this study.

Table of Contents

List of Tables

List of Figures

Nomenclature

A	uniaxial power law creep coefficient
A_1	uniaxial hyperbolic sine law creep coefficient
A_2	uniaxial hyperbolic sine law creep multiplier
$A_{contact}$	projected area of contact under indentation
A_{input}	input uniaxial power law creep coefficient for finite element analysis
A_{output}	output uniaxial power law creep coefficient from finite element analysis
a	contact radius
a_{Hertz}	elastic contact radius for spherical indentation (Hertz)
a_{max}	maximum contact radius
$a_{nominal}$	nominal contact radius computed from the geometry of the indenter
$a_{Sneddon}$	elastic contact radius for conical indentation (Sneddon)
a_{true}	real contact radius accounting for piling up or sinking in of the surface
B	indentation power law creep coefficient
B_1	indentation hyperbolic sine law creep coefficient
B_2	indentation hyperbolic sine law creep multiplier
β	half-included cone angle of a conical indenter
c	pile up – sink in parameter
CLH	constant load and hold
CRL	constant rate of loading
c_{sphere} or $c(m)$	pile up – sink in parameter for spherical indentation
c_{cone} or $c(m,\beta)$	pile up – sink in parameter for conical indentation
D_{eff}	diffusion coefficient

$\frac{dh}{dt}$	displacement velocity of the indenter
$\frac{dP}{dt}$ or $\dot{P}$	loading rate of the indenter
E	elastic modulus
ε	strain
$\varepsilon_{\text{elastic}}$	elastic strain
$\dot{\varepsilon}$	uniaxial strain rate
$\dot{\varepsilon}_I$	indentation strain rate
$(\dot{\varepsilon}_I)_{\text{characteristic}}$	characteristic indentation strain rate
$\dot{\varepsilon}_{\text{ss}}$	steady-state strain rate
$F(m)$	reduced contact pressure for spherical indentation
$F(m,\beta)$	reduced contact pressure for conical indentation
G	shear modulus of a material
h	indentation depth
h_{creep}	creep indentation depth
h_{elastic}	elastic indentation depth
h_{Hertz}	elastic indentation depth for spherical indenter
$h_{\max}$	maximum indentation depth
h_{Sneddon}	elastic indentation depth for conical indenter
$\dot{h}_{\text{Hertz}}$	equivalent elastic indentation strain rate for spherical indenter
$\dot{h}_{\text{Sneddon}}$	equivalent elastic indentation strain rate for conical indenter
$l_{\text{characteristic}}$	characteristic length of indentation
m	uniaxial power law or hyperbolic sine law creep exponent

m_{input}	uniaxial power law or hyperbolic sine law input creep exponent for FEM
m_{output}	uniaxial power law or hyperbolic sine law input creep exponent from FEM
ν	Poisson's ratio
P	load on the indenter
P_{coneCRL}	characteristic load of conical indentation for CRL method
$P_{\text{sphereCRL}}$	characteristic load of spherical indentation for CRL method
p_{mean}	indentation mean pressure (hardness)
$(p_{\text{mean}})_{\text{elastic}}$	elastic mean pressure of indentation
$(p_{\text{mean}})_{\text{Hertz}}$	elastic mean pressure of spherical indentation
$(p_{\text{mean}})_{\text{Sneddon}}$	elastic mean pressure of conical indentation
R or R_{solid}	radius of the specimen solid
S	von Mises stress
σ	stress
σ_{ss}	steady-state stress
σ_{y}	yield stress
t	indentation time
t_{coneCLH}	characteristic time of conical indentation under CLH for power law creep
t_{coneCRL}	characteristic time for conical indentation under CRL
t_{max}	maximum time of indentation
$t_{\text{sinhconeCRL}}$	characteristic time of conical indentation under CRL for hyperbolic sine law creep

$t_{\text{sinhsphereCLH}}$ characteristic time of spherical indentation under CLH for hyperbolic sine law creep

$t_{\text{sphereCLH}}$ characteristic time of spherical indentation under CLH for power law creep

$t_{\text{sphereCRL}}$ characteristic time of spherical indentation under CRL for power law creep

CHAPTER 1 – INTRODUCTION

Uniaxial Creep

Creep may be defined as permanent deformation of a material over a certain period of time [1]. To fully characterize creep phenomenon, it is necessary to develop a constitutive relation among the factors that affect the creep deformation of a material. In the simplest consideration, time, stress, and temperature become the significant influential factors governing the creep deformation. Amongst these factors, time and stress are of interest in this study, and temperature will not be considered explicitly.

For the purpose of measuring creep in uniaxial tension tests, two representative methods are employed in the engineering world. One is to study the rupture induced by creep. The other is characterizing the rate sensitivity of a material using standardized engineering testing methods, which will be the focus of this study.

The generally accepted method to characterize uniaxial creep is to conduct uniaxial creep tests. In a typical uniaxial creep test, a dog-boned shaped test specimen is loaded in tension in a creep testing machine. The load on the specimen is held constant, thereby producing a constant stress condition at small strain levels. Strain is recorded continuously as a function of time. Figure 1 depicts a uniaxial creep test and the resulting strain-time plot. Initially, the specimen undergoes recoverable elastic deformation, which manifests itself as an offset on the vertical axis. Following this initial elastic deformation, the strain-time curve displays three relatively distinct stages of creep deformation.

In the first stage of creep, termed primary creep, a decrease in strain rate (slope of the strain-time curve) is usually observed due to hardening of the material.

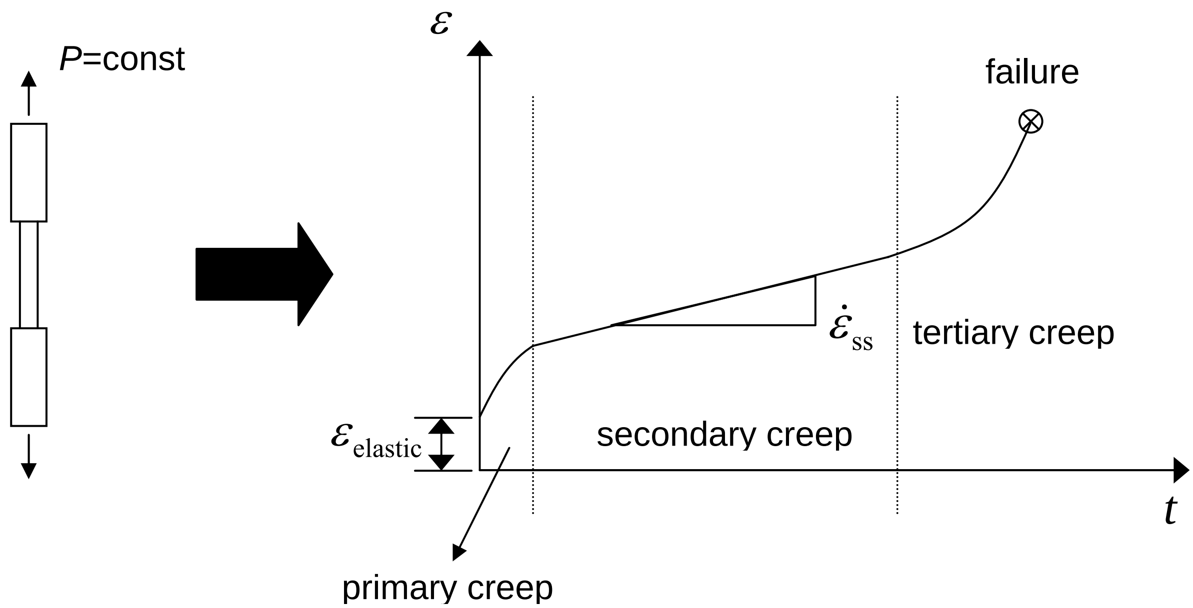

Figure 1. Uniaxial creep test and the resulting creep curve

Then follows a steady-state stage, termed steady-state or secondary creep. Steady-state creep is achieved by a balance of hardening and recovery of the material. Steady-state creep constitutes a major portion of the creep curve and is usually analyzed in characterizing creep behavior. As time elapses, steady state conditions break down and a sharp increase in strain rate is observed. The actual stress in this stage of deformation physically increases, due to voids and damage evolution in the material. This stage is termed "tertiary creep" and generally lasts for a short period of time followed by failure of the material.

Creep Constitutive Relationship

Under a single load, a single creep curve is produced. In order to investigate the rate sensitivity to stress, creep curves analogous to Figure 1 are produced at various levels of stresses. A schematic description of various creep curves for different applied loads is shown in Figure 2. Using the slopes of the steady state regime, a constitutive relation correlating the steady state strain rate and stress is formulated.

Power Law Creep

Figure 3 is a typical example of a steady state strain rate-stress relationship observed for many metals. It is described by a power law constitutive relationship given by

$$\dot{\varepsilon}_{ss} = A\sigma^{m} \tag{1}$$

Here, the steady-state strain rate $\dot{\varepsilon}_{ss}$ is related to stress σ by a power law equation with a creep coefficient A and a creep exponent m.

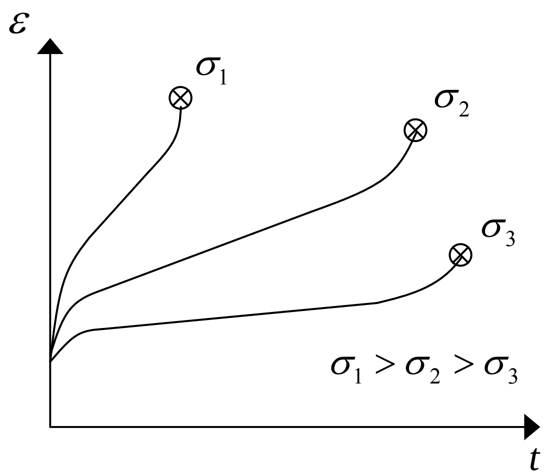

Each test held at constant temperature

Figure 2. Creep curves produced at different stress levels

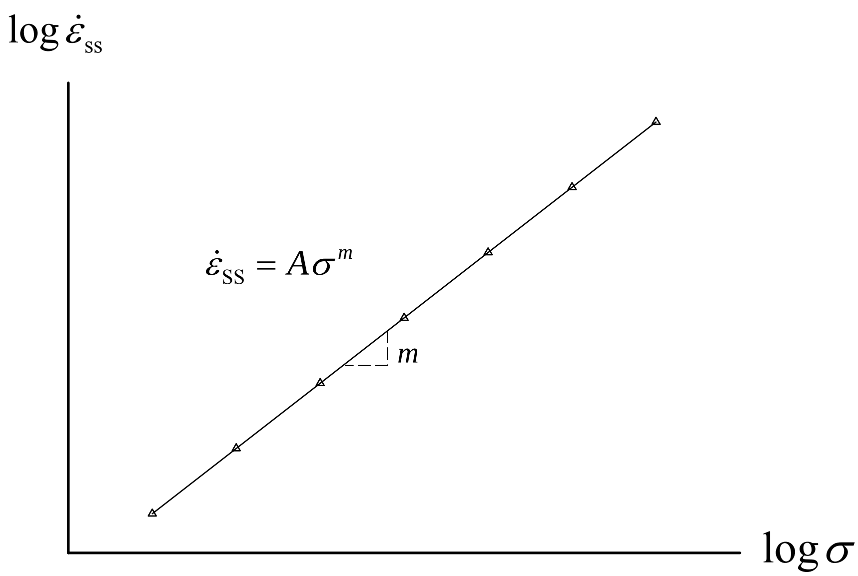

Figure 3. An example of steady state strain rate-stress showing power law relationship

Hyperbolic sine law creep

In some instances, power law breakdown at fast strain rates may be observed. A hyperbolic sine law equation has been used extensively in characterizing creep behavior with power law breakdown. This is described by the relation

$$\dot{\varepsilon}_{ss} = A_1\left[\sinh\left(A_2\sigma\right)\right]^m \tag{2}$$

In hyperbolic sine law creep, creep is characterized by a coefficient A_1, a hyperbolic sine multiplier A_2, and an exponent m. Creep test results on pure aluminum have been described by a modified version of equation (2). Results provided by Luthy *et. al.* [2] are shown in Figure 4. One can observe a breakdown in power law behavior for normalized stresses larger than 4×10^{-4}. A mathematical expression that describes the temperature compensated strain rate to normalized stress is given by

$$\left(\frac{\dot{\varepsilon}_{ss}}{D_{eff}}\right) = K'\left[\sinh\left(\alpha\frac{\sigma}{E}\right)\right]^m \tag{3}$$

Here, D_{eff} is the diffusion coefficient, E is the elastic modulus, and α and K' are material constants. For aluminum, Luthy *et. al.* gives α=2600 and m=4.8.

Indentation Creep

Indentation has been widely used in characterizing mechanical properties. The basic idea is to load or displace a material with an indenter of known geometry and to carefully study the following deformation characteristics. For indenters equipped with load-depth sensing capabilities, loading-unloading curves are produced. Using these curves, elastic and plastic mechanical properties of a material may be estimated.

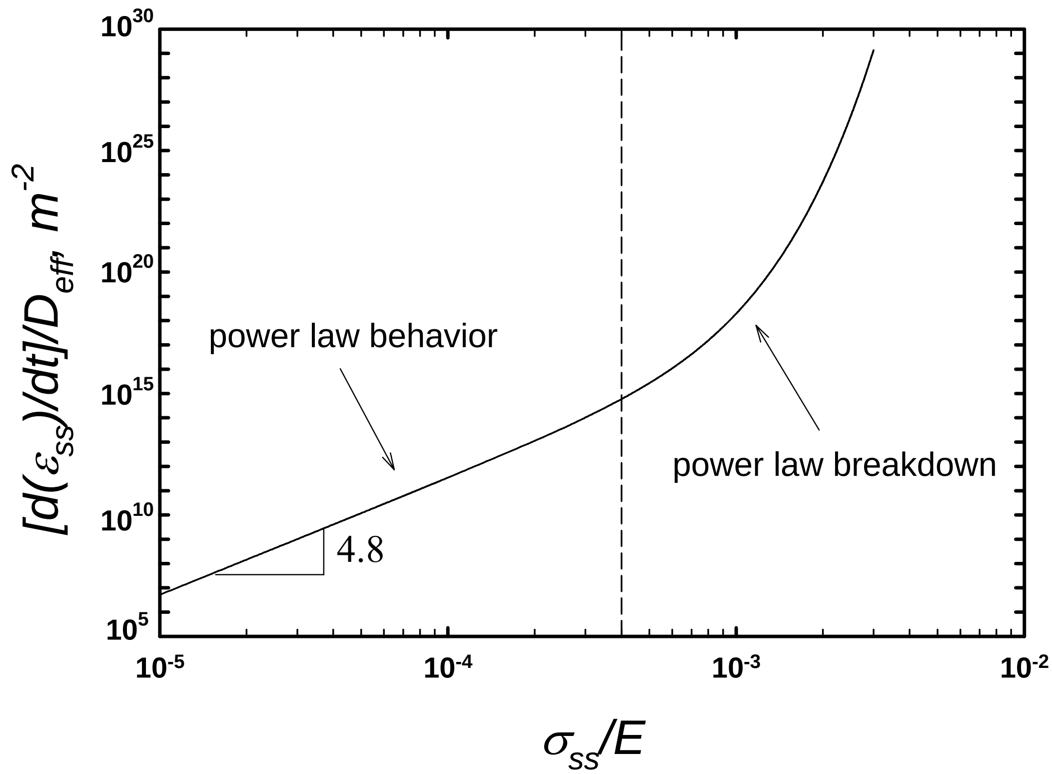

Figure 4. Hyperbolic sine law creep for pure aluminum [2]

These may include instantaneous mechanical properties as well as time dependent mechanical properties.

Indentation creep refers to the creep deformation of a material under indentation. Depending on the creep characteristics, various responses to the loading may be observed. Using these responses, we may be able to deduce a correlation of uniaxial creep to indentation creep. This process is schematically shown in Figure 5. On the left side of the diagram, the material is loaded uniaxially to produce a uniaxial strain rate-stress relationship. When indentation is performed on the same material, we may be able to describe the creep characteristics from the results of indentation. However, to do so, we need to define equivalent stress and equivalent strain rate. In the simplest forms, mean pressure and indentation strain rate represent equivalent stress and equivalent strain rate, respectively [3]. The conventional definition of mean pressure is given by

$$p_{\mathrm{mean}} = \frac{P}{A_{\mathrm{contact}}} \tag{4}$$

Here, P is the load on the indenter and A_{contact} is the projected area of contact. The indentation strain rate may be defined by

$$\dot{\varepsilon}_I = \left(\frac{1}{l_{\mathrm{characteristic}}}\right)\left(\frac{dh}{dt}\right) \tag{5}$$

Here, $l_{\mathrm{characteristic}}$ is the characteristic length in the indentation problem and (dh/dt) is the displacement velocity of the indenter. Generally, either the radius of contact, a, or the depth of indentation, h is used for the characteristic length of indentation. With the use of equations (4) and (5), indentation creep constitutive equation may be formulated. A main goal of this dissertation is to find a suitable correlation between uniaxial creep and indentation creep in terms of constitutive relationships.

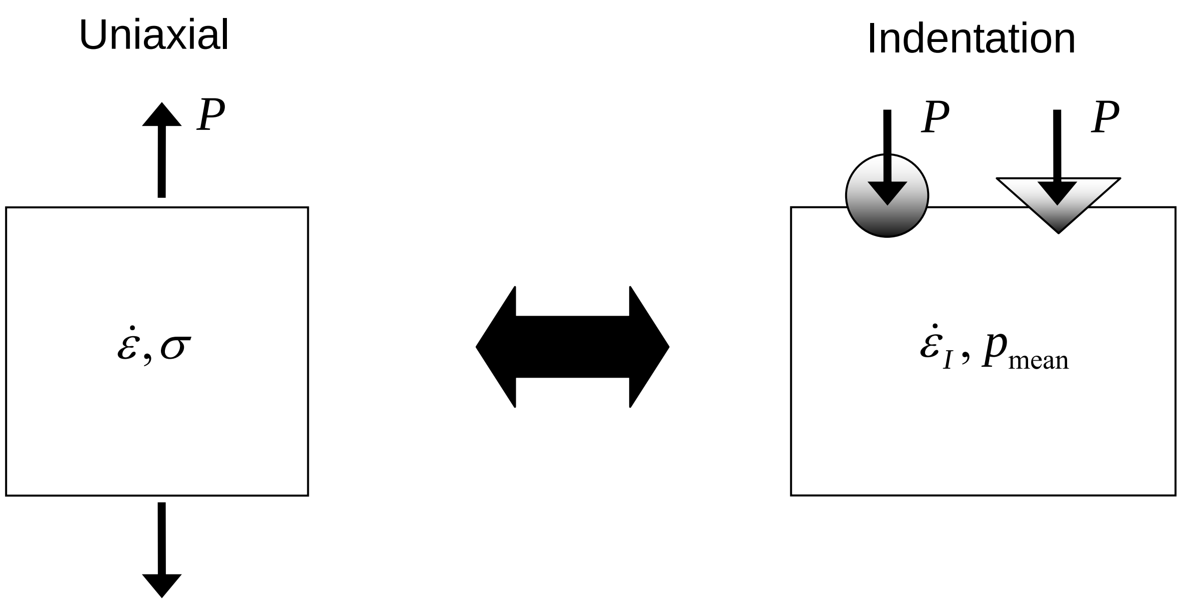

Figure 5. Uniaxial creep versus indentation creep

Literature Review

Previous studies on the issue of correlating uniaxial creep to indentation creep have used several different approaches. Some involve theoretical modeling of the indentation creep boundary value problem [3~8]. Such results provide mathematical formulations and sometimes simple closed form mathematical relationships. With the development and enhancement of instrumented indentation techniques, experimental approaches have been developed to measure uniaxial creep parameters from indentation [9~18]. Subsequent to new experimental approaches, numerical modeling techniques were applied in efforts to better understand the indentation creep process and to find the possible parameters that correlate indentation creep constitutive laws to the uniaxial creep constitutive laws [18~22]. Amongst the different approaches, we first examine significant results and conclusions drawn from indentation experiments on creeping solids.

Critical review of significant indentation creep experiments

For materials exhibiting the power law creep constitutive law given in equation (1), the uniaxial creep exponent m has been estimated empirically from indentation for a few materials [10, 12~17]. One of the earliest attempts in measuring uniaxial creep parameters from small scale indentation used flat punch indentation [10]. For a flat punch indenter, a constant stress condition is maintained when a constant load is applied to the indenter. Therefore, the creep process is relatively analogous to uniaxial creep conditions. Creep exponents estimated using the flat punch indenter showed good agreement with the known literature values obtained from uniaxial creep tests.

For very small scale indentation, the indenter of preference is the three-sided pyramidal indenter. This is termed as the Berkovich indenter, which has an advantage over the four-sided Vickers indenter in that three-sided pyramid culminates in a single point. One other feature of the Berkovich indenter is that the depth to projected contact area ratio is equivalent to a cone with half-included cone angle of 70.3°. Similar to the flat punch indenter, uniaxial creep exponents have been estimated using Berkovich indenters with different loading schemes.

Under constant rate of loading conditions, the load is increased throughout indentation as linear function of time. Mayo and Nix [12] demonstrated the rate sensitivity of a material using a Berkovich indenter under constant rate of loading conditions. They reported that the creep exponents obtained from indentation are similar to the literature values of uniaxial creep exponents.

The simplest method to study creep in indentation is the use of the constant load and hold method. Here, the load on the indenter is held constant and the corresponding changes in depth as a function of time are recorded. Raman and Berriche [13] have investigated indentation creep using constant load and hold method. The results provided by this work also confirm that the indentation creep exponent obtained from a plot of $\dot{\varepsilon}_I$ vs. p_{mean} is very similar to the reported literature values of uniaxial creep exponent.

In both the cases mentioned above, constant mean pressure and accordingly a constant indentation strain rate are not accomplished due to changes in contact area with time. A special type of loading scheme was devised by Lucas and Oliver [17] to resolve this complication. By controlling the load in a way such that the ratio of loading rate to the current load of indentation is held constant, it was reported that mean pressure and indentation strain rate were maintained at constant values. Therefore, one value of constant rate of loading divided by load produced a single mean pressure and corresponding single indentation strain rate. The indentation creep exponent estimated from this loading method was in good agreement with literature reported uniaxial creep exponents.

Summarizing the three significant experimental results, one is able to infer that creep exponent predicted from indentation can be very similar to the unaxial creep exponent. However, none of the above mentioned reports provide any scientific information on the correlation of uniaxial creep coefficient, *A*, to the indentation creep coefficient, *B*. Moreover, the similarity in creep exponents from indentation and uniaxial tests were an observed phenomenon with limited underlying theoretical principles.

Similarity transformation

In the early 1990's, Hill [6] proposed a mathematical approach to simplify the indentation creep problem. By employing a similarity transformation, he was able to convert the generalized power law creep problem into a nonlinear elastic problem, described by:

$$\hat{S}_{ij} = \frac{2}{3}\hat{\varepsilon}_e^{\frac{(1-m)}{m}}\hat{\varepsilon}_{ij} \tag{6}$$

In equation (6), $\hat{S}_{ij}$ is the transformed deviatoric stress; $\hat{\varepsilon}_e = \left(\frac{2}{3}\hat{\varepsilon}_{ij}\hat{\varepsilon}_{ij}\right)^{\frac{1}{2}}$ denotes the stress-strain relationship for a power law elastic body, and *m* is a material constant. When *m*=1, equation (6) describes a linear elastic body. When $m \to \infty$, it describes a rigid – perfectly plastic body. By employing indentation boundary conditions with a flat punch of unit radius, an analytical solution to equation (6) was obtained for certain cases of *m*. For axis-symmetric boundary condition assumptions, Sneddon [23] and Fabrikant [24] have independently provided analytical solutions for linear viscous case (*m*=1). For the rigid – perfectly plastic case, a closed form solution was provided by Prandtl [25] and Hill [26] for a 2-dimensional plane indenter boundary condition. The analytical solutions for notable cases mentioned above are summarized in Table 1. The definitions of *c(m)* and *F(m)* in Table 1 will be explained in detail in later sections of the dissertation.

Significant work of Bower et. al. on indentation creep problem

Bower *et. al.* [19] have examined the indentation of a power law creeping solid more rigorously. For a load history independent material, correlation between uniaxial creep and indentation creep for *m* of 1 ~ 100 has been studied using the similarity transformation concept combined with the finite element method. By using the mean pressure and the indentation strain rate as the variables of analysis, they were able to deduce many significant conclusions. Conclusions drawn from their work form the fundamental basis of this study. The important conclusions are as follows:

1) For a material characterized by the power law creep relation given in equation (1), Bower *et. al.* have analytically proven that the creep exponent deduced from indentation is identical to the uniaxial creep exponent of the material by means of a similarity transformation. According to their results, indentation of a power law creeping solid is described by an analogous power law relation between the mean pressure and the indentation strain rate, $\dot{\varepsilon}_I = B(p_{\mathrm{mean}})^m$.

2) Bower *et. al.* have focused on studying the piling up and sinking in of the material surface. In their work, sinking in or piling up are characterized by a simple parameter, the 'pile up-sink in parameter', *c*. Figure 6 shows the definition of *c*. Figure 6a illustrates an example of piling up for spherical indentation and Figure 6b shows an example of sinking in for conical indentation.

Table 1. Analytical solutions of similarity transformation for limited cases

m	Boundary Conditions	$c(m)$	$F(m)$
1	axis-symmetric, frictionless	$\frac{2}{\pi}$ (cone) $\frac{1}{\sqrt{2}}$ (sphere)	$\frac{8}{3\pi}$
∞	2-D plane, frictionless	1.5 (cone) 1.75 (sphere)	$\frac{(2+\pi)}{\sqrt{3}}$

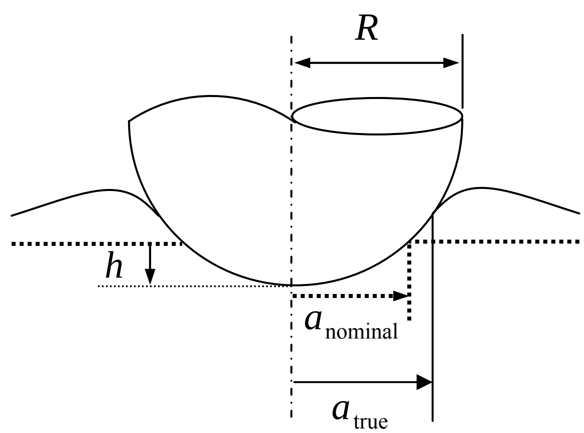

(a) Description of piling up of the surface for spherical indentation

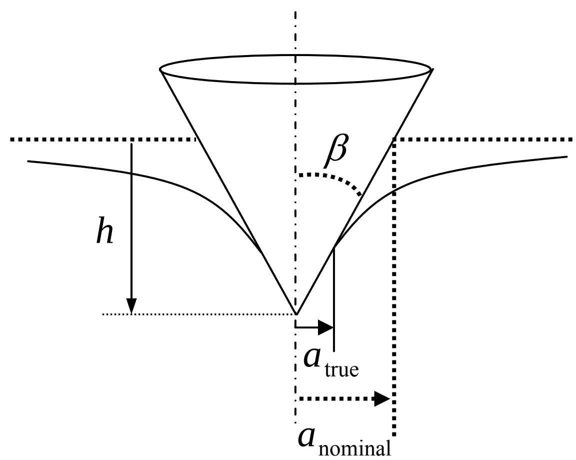

(b) Description of sinking in of the surface for conical indentation

Figure 6. Geometrical representation of piling up or sinking in of the surface

The parameter c is defined as the ratio of the true contact radius (a_{true}) to the nominal contact radius computed from the geometry of the indenter (a_{nominal}). For spherical indentation, c is expressed mathematically by

$$c_{\text{sphere}} = \frac{a_{\text{true}}}{\sqrt{2Rh}} \tag{7}$$

where R is the radius of the indenter and h is the indentation depth. For conical indentation, c is expressed by

$$c_{\text{cone}} = \frac{a_{\text{true}}}{h \tan \beta} \tag{8}$$

where β is the half-included cone angle. From equations (7) and (8), it is clear that when c>1, material piles up around the indenter. Oppositely, c<1 represents sinking in of the surface. When c=1, there is no piling up or sinking in of the surface. Bower *et. al.* showed that c depends only on m for a rigid – power law creeping solid under infinitesimal strain – infinitesimal deformation assumption.

3) Most of the empirical studies on indentation of creeping materials are focused on estimating the uniaxial creep exponent with little or no effort on the correlation of the uniaxial creep coefficient A to indentation creep coefficient B. One of the most significant results presented in the work of Bower *et. al.* is the correlation of uniaxial creep coefficient to indentation creep coefficient by a simple parameter. This parameter, termed as reduced contact pressure *F(m)*, is defined by

$$F(m) = \left(\frac{A}{B}\right)^{\frac{1}{m}} \tag{9}$$

Here, A and B are uniaxial creep coefficient and indentation creep coefficient, respectively and m is the creep exponent. As is observed from equation (9), the correlation between the uniaxial creep coefficient and indentation creep coefficient is a unique function of *m* provided that the infinitesimal strain – infinitesimal deformation assumption is valid. Bower *et. al.* have solved *F(m)* for *m* in the range of 1 ~ 100 using finite element method.

Shortcomings of Bower et. al. results

Although the results of Bower *et. al.* are significant in providing a means to correlate uniaxial creep to indentation creep in an extensive manner, some of the important shortcomings are noted here.

1) Conclusions of their study focus on correlating the mean pressure and indentation strain rate. From an experimental perspective, the mean pressure is not directly available unless a knowledge of piling up or sinking in is provided. Therefore, a practical approach to the problem of correlating uniaxial creep to indentation creep requires data that are readily available from an indentation test. Examples of such data are *h* (indentation depth)-*t* (indentation time) or *P* (indentation load)-*h* (indentation depth) relationships.

2) Although the effects of finite elasticity in indentation of creeping solid were considered to some extent by Bower *et. al.*, a rigorous treatment was not provided. Specifically, transients induced by elasticity were not studied explicitly even though they may have important consequences for the interpretation of indentation creep results.

3) Bower *et. al*. solved the boundary value problem under the assumption of infinitesimal strain – infinitesimal deformation. This has a variety of implications depending on the indenter geometry. For spherical indentation, the contact radius or depth of indentation is the governing variable that determines the effective strain on the solid. Therefore, the depth of indentation must be limited to certain levels that are consistent with infinitesimal deformation. For conical indenters, the half-included cone angle of the indenter is directly

related to effective strain at finite levels. Therefore, conical indentations with various half-included cone angles are expected to produce different results compared to Bower *et. al.* predictions. The effects of finite strain – finite deformation from conical indentation perspective are not addressed in their study.

4) The material is characterized by a simple uniaxial power law constitutive law, given in equation (1). However, material underneath the indenter may experience very large mean pressures and, correspondingly, very fast strain rates. This may lead to power law breakdown that is better described by a hyperbolic sine law constitutive law like that given in equation (2). The hyperbolic sine law creep constitutive law capable of characterizing power law breakdown was not implemented in the previous study.

Objectives of this Dissertation

Based on the shortcomings of previous studies, the objectives of this dissertation are to study the following by means of finite element simulation:

1) The feasibility of correlating uniaxial creep parameters to indentation creep parameters using directly obtainable data from indentation, in particular, *h-t* and *P-h* indentation curves.

2) The influence of elasticity on the creep transient and its effect in uniaxial creep parameter extraction. Spherical and conical indenters will be considered. The loading methods used in this study are generally representative of practical indentation test.

3) Relations for *c(m)* and *F(m)* for conical indentation that account for finite strain – finite deformation. Various half-included cone angles will be considered.

4) Develop a method to extract uniaxial power law creep parameters from indentation

with a special focus on both spherical and conical indenters.

5) Modeling of indentation creep for a hyperbolic sine law creeping solid. In doing so, correlation of the uniaxial hyperbolic sine law creep to the possibility of indentation hyperbolic sine law creep will be investigated with the intention of developing a method to predict the uniaxial hyperbolic sine law creep parameters from indentation.

CHAPTER 2 – FINITE ELEMENT PROCEDURE

Constitutive Laws

Full field finite element simulations for indentation of an elastic – creeping solid were performed using the ABAQUS™ finite element software version 6.3-5 [27]. The finite-strain / finite-deformation features of ABAQUS™ were used in the simulations. Strains calculated in ABAQUS™ also include the effects of material rotations. The stresses calculated for the finite elements are the Cauchy stresses. The elastic-viscoplastic constitutive relation assumes rate-dependent, isotropic, elasto-viscoplasticity using the von Mises yield criteria. The constitutive laws for a power law creeping solid and a hyperbolic sine law creeping solid used in the study were:

$$\dot{\varepsilon} = \left(\frac{\dot{\sigma}}{E}\right) + A\sigma^m \qquad \text{(power law)} \qquad (10)$$

$$\dot{\varepsilon} = \left(\frac{\dot{\sigma}}{E}\right) + A_1\left[\sinh\left(A_2\sigma\right)\right]^m \qquad \text{(hyperbolic sine law)} \qquad (11)$$

Material properties for the constitutive laws are shown in Table 2. Poisson's ratio effects were not considered in this study. Therefore, it is assigned a constant value of 0.3, a typical value for metals. As for power law creep, *m* was carefully chosen to simulate materials with creep exponents ranging from 1 to 10. In hyperbolic sine law creep, *m*=1, 3 and 5 were examined. The indenters in the simulations were modeled as perfectly rigid bodies with infinite modulus of elasticity.

Table 2. Material properties for finite element simulations in this dissertation

Power Law Creep	
E	10~1000 [GPa]
ν	0.3
A	variable
m	1~10

Hyperbolic Sine Law Creep	
E	10~1000 [GPa]
ν	0.3
A_1	variable
A_2	variable
m	1,3, and 5

Boundary Conditions

Indentation of a creeping solid was modeled by the 2-dimensional axis-symmetric boundary conditions shown in Figure 7. The deformable creeping solids were modeled with a free boundary at the outside. A semi infinite half-space condition was achieved by controlling the radius of the creeping solid to exceed the maximum contact radius by at least 100 times. This is more conservative than the previous study of Bower *et. al.* [19], which employed a solid that is 20 times larger than the maximum contact radius. The radius of the spherical indenter was $1\mu m$. In order to compare with Bower's results, strains for spherical indentation were limited to $a/R<0.4$. This condition is satisfied in all spherical indentations in this study. For conical indenters, the half-included cone angle β was chosen as 60°, 70°, and 80°. The 70° cone is of special interest in that the depth-to-contact area ratio is similar to that of Berkovich indenter.

Finite element simulations were performed under load controlled conditions. The two types of loading method employed in this study were constant load and hold (CLH) and constant rate of loading (CRL). Under the CLH condition, a constant load is prescribed on the indenter, and the resulting depth and contact radius are continuously monitored as a function of indentation time. Under the CRL condition, the load is linearly increased as a function of time and the resulting depth and contact radius are recorded. In each of the simulations, the creep deformation process was divided into several hundreds to several thousands of increments.

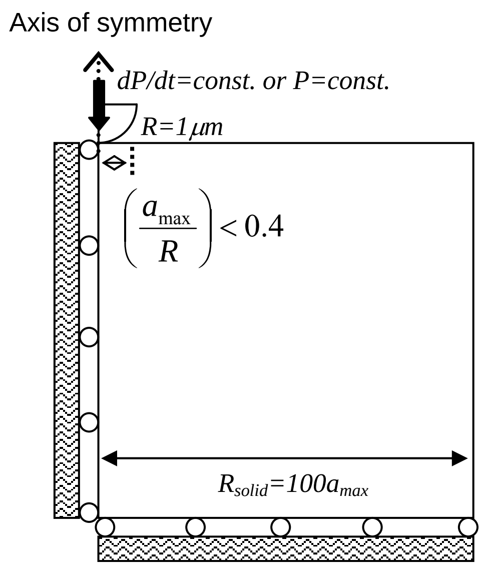

(a) Spherical indentation

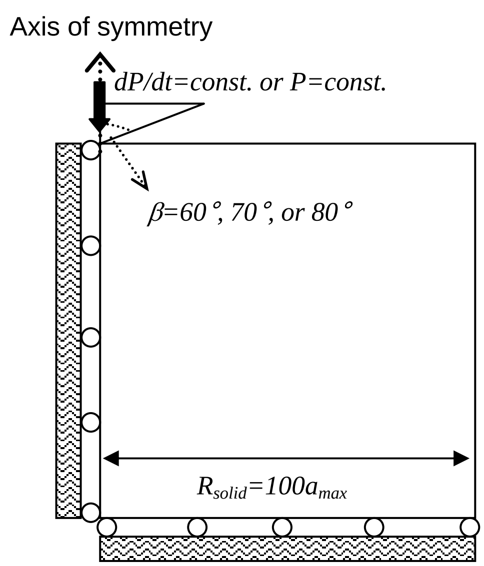

(b) Conical indentation

Figure 7. Boundary and loading conditions used in the finite element modeling

Finite Element Mesh Configuration

The finite element mesh used in this study is shown in Figure 8. A mesh employing 4593 linear, fully-integrated elements was used in modeling the creeping solid. A fine mesh employing smaller elements was used close to the indenter tip region to capture the contact radius accurately. The maximum contact radius was always within the boundary of the fine mesh zone in order to avoid an undesirable transient resulting from mesh zone transitioning.

Dimensional Analysis (π-Theorem)

Dimensional analysis has been found to be a useful tool in reducing the number of experiments or simulations in scientific studies. Adopting Buckingham's π-theorem [28], we are able to obtain several dimensionless variables that describe indentation.

Normalization for CLH Method

In the CLH method, the primary variables of interest are the indentation depth h, indentation time t, and the input indentation load P. By selecting appropriate π-parameters that contain all the dimensions involved in the problem, we are able to normalize the original variables of interest. As for the π-parameters, we select modulus of elasticity E, indenter radius R (for spherical indentation) or maximum depth of indentation $h_{\max}$ (for conical indentation), and maximum time of indentation $t_{\max}$. The result of the normalization is shown in Table 3.

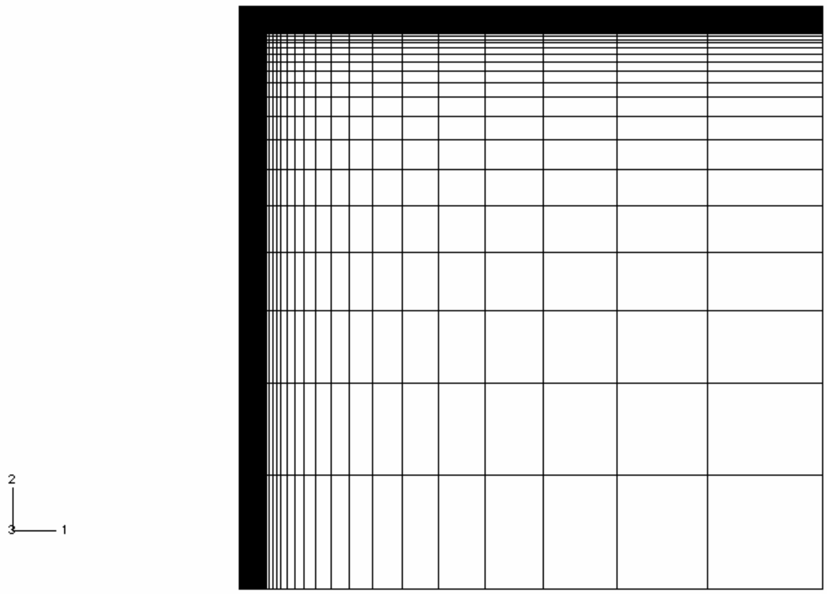

(a) Full mesh description

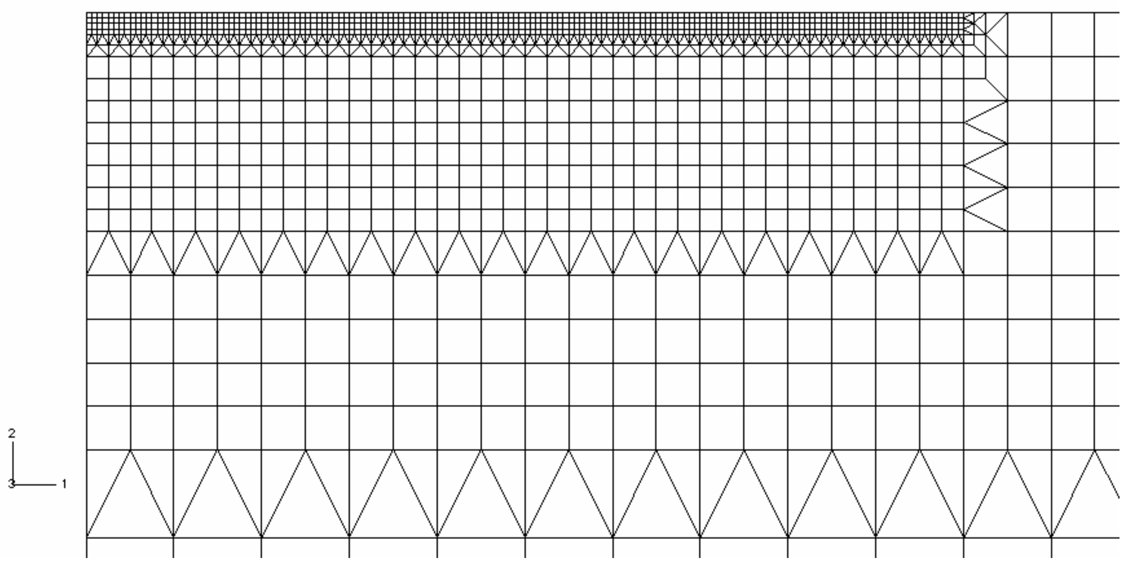

(b) Detail description of the fine mesh zone

Figure 8. Finite element mesh used in the study

Table 3. Results of dimensional analysis for CLH indentation

Original Variable	Normalized Variable (Spherical Indentation)	Normalized Variable (Conical Indentation)
$P \quad [mN]$	$\dfrac{P}{ER^2}$	$\dfrac{P}{E(h_{\max})^2}$
$h \quad [\mu m]$	$\dfrac{h}{R}$	$\dfrac{h}{h_{\max}}$
$t \quad [sec]$	$\dfrac{t}{t_{\max}}$	$\dfrac{t}{t_{\max}}$

Normalization for CRL Method

Applying the π-theorem in a manner analogous to the CLH method, we select elastic modulus E, indenter radius R (for spherical indentation) or maximum indentation depth h_{max} (for conical indentation), and the loading rate dP/dt as the π-parameters. This converts the original boundary value problem into indentation under a unit constant rate of loading. The results of this normalization are given in Table 4.

Data Acquisition

Using the data acquisition capabilities of ABAQUS™, the indentation depth and contact radius were directly obtained at increments when the indenter encountered a new surface node on the creeping solid. An example of data acquisition is shown in Figure 9. Each data point represents a nodal value of indentation depth and contact radius. Average values of load, depth, contact radius, and time at successive nodes were used to calculate the indentation mean pressures and indentation strain rates.

Avoiding Mesh Discretization Problems

Mesh discretization problems may occur when obtaining data at small contact radii due to an insufficiency in the number of nodes and/or elements in contact with the indenter at small contact radius. The effect of this problem is demonstrated in Figure 10, which shows the FEM results for an elastic – power law creeping material using spherical indenter under the CRL method. The creep exponent employed in this figure is m=1.

Table 4. Results of dimensional analysis for CRL indentation

Original Variable	Normalized Variable (Spherical Indentation)	Normalized Variable (Conical Indentation)
P $[mN]$	$\frac{P}{ER^2}$	$\frac{P}{E(h_{\max})^2}$
h $[\mu m]$	$\frac{h}{R}$	$\frac{h}{h_{\max}}$
t $[sec]$	$\frac{t\dot{P}}{ER^2}$	$\frac{t\dot{P}}{E(h_{\max})^2}$
$\dot{P}$ $[mN/sec]$	1	1

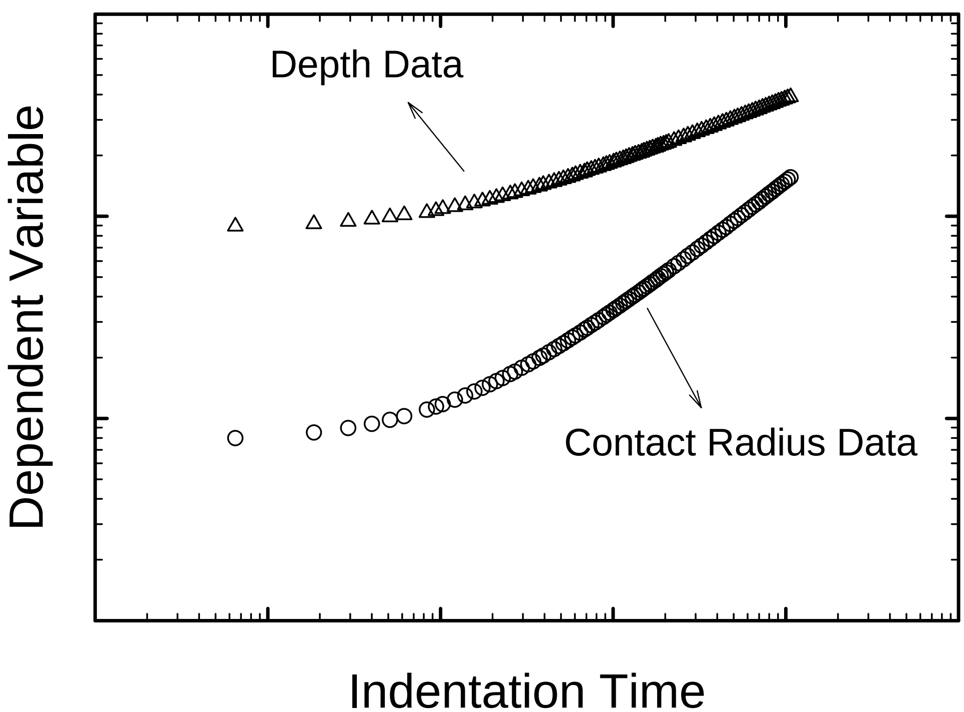

Figure 9. Example of data extraction from ABAQUS™

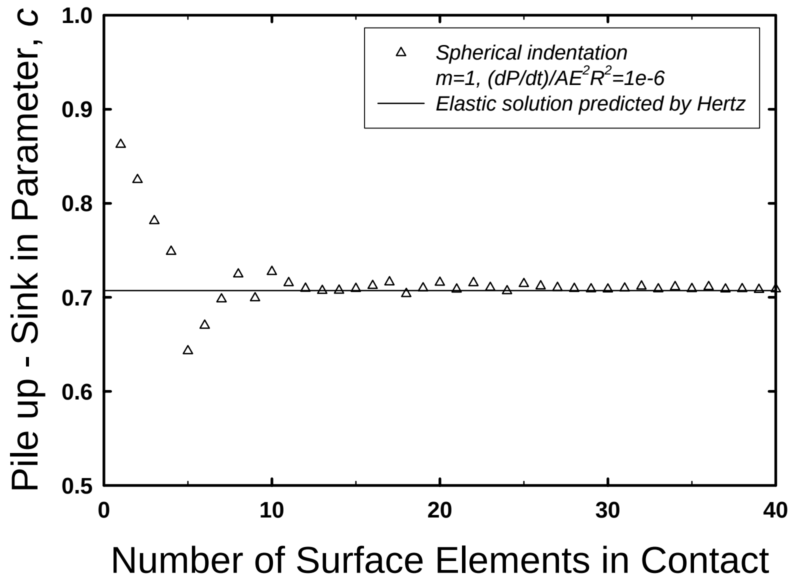

(a) Changes in pile up – sink in prediction due to mesh discretization

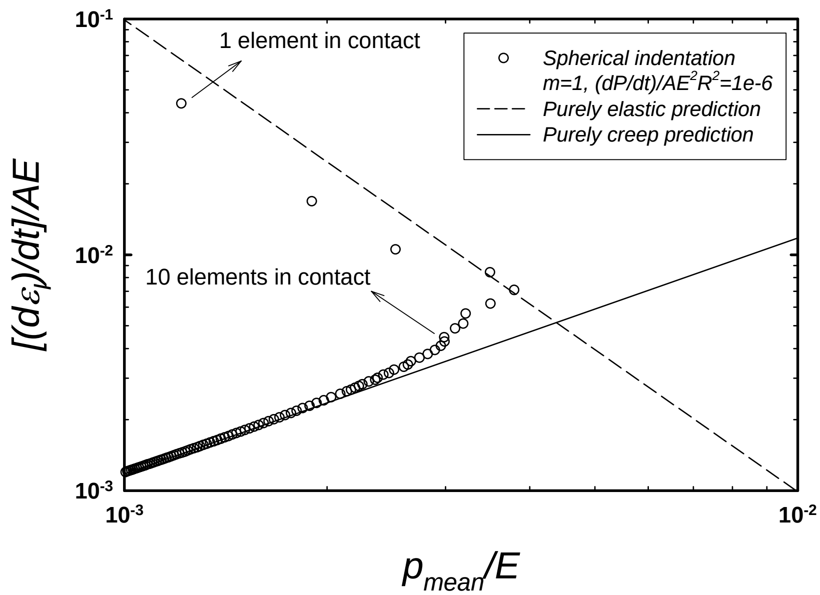

(b) Mesh discretization in terms of indentation strain rate – mean pressure relation

Figure 10. Demonstration of mesh discretization problem

As is explained in detail later in Chapter 4, the Hertzian pressure distribution under spherical indentation for a linear viscous creeping material (m=1) is identical to that of a purely elastic material. This manifests itself as sinking in of the surface in amount equal to that of the elastic prediction for power law creeping materials described by m=1. However, in Figure 10a, we observe significant scatter in the pile up – sink in prediction for m=1 when the indenter is in contact with less than approximately 10 surface elements. This is due to the problems caused by mesh discretization. When the indentation strain rate – mean pressure relation is considered, the indentation strain rate – mean pressure curve is expected to make a gradual transition from the purely elastic prediction to the purely creeping prediction for the constant rate of loading condition in a manner shown by Figure 10b. The nature of this curve will be discussed in detail in Chapter 4. Here again, we observe considerable scatter in the data for results with less than 10 elements in contact. We conclude that with the mesh configuration adopted for this dissertation, results obtained for 10 or less elements in contact are prone to errors caused by discretization, and thus, will be discarded to avoid any further complications in the analysis.

Mesh Verification and Accuracy

The accuracy of the mesh used in this dissertation is verified with respect to known solutions and also to the significant existing results by Bower *et. al.* We first examine the spherical indentation for purely elastic case (Hertzian solution). Figure 11 shows comparison between the results produced from finite element simulation using the mesh for this dissertation and the analytic solution by Hertz. It is seen that the finite element results agree well to the analytic solution in terms of both the description in sinking in of the surface and the *P-h* curve. Although it is impossible to model rigid – power law creeping solid with $m=\infty$ in finite element method, we are able to use elastic – perfectly plastic model to simulate rigid – power law creeping solid with $m=\infty$. The analogy is explained in detail using conical indentation in Chapter 4. In Figure 12, results of spherical indentation with the elastic – perfectly plastic model are obtained using E/σ_y=10000. Therefore, at larger indentation depths, the results are expected to represent rigid – power law creeping situation with $m=\infty$. As expected, this is demonstrated in Figure 12. As for comparing results from mesh employed in this dissertation to existing results from Bower *et. al*, the results and solutions obtained for spherical indentation of elastic – power law creeping solid at larger depth are constantly compared to Bower *et. al.* predictions in Chapter 4. Therefore, the mesh verification in this section provides partial evidence to the accuracy of the mesh employed in this dissertation.

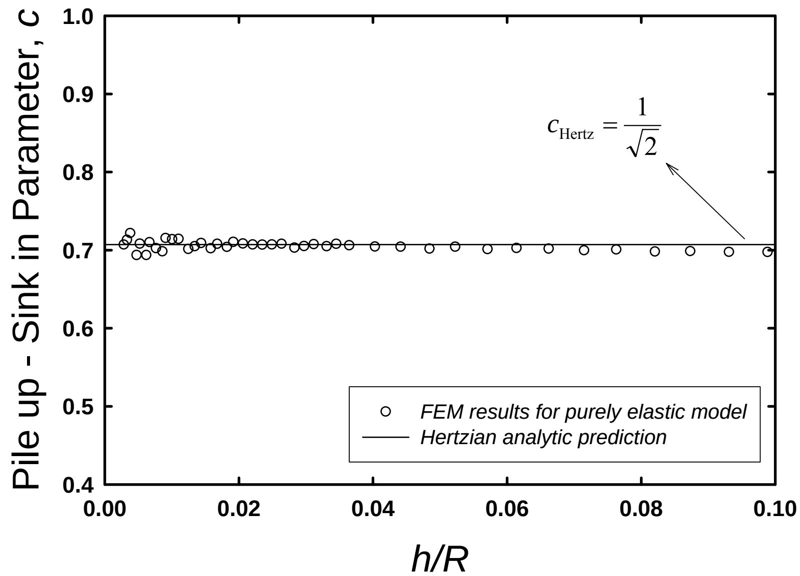

(a) comparison in pile up – sink in parameter, *c*

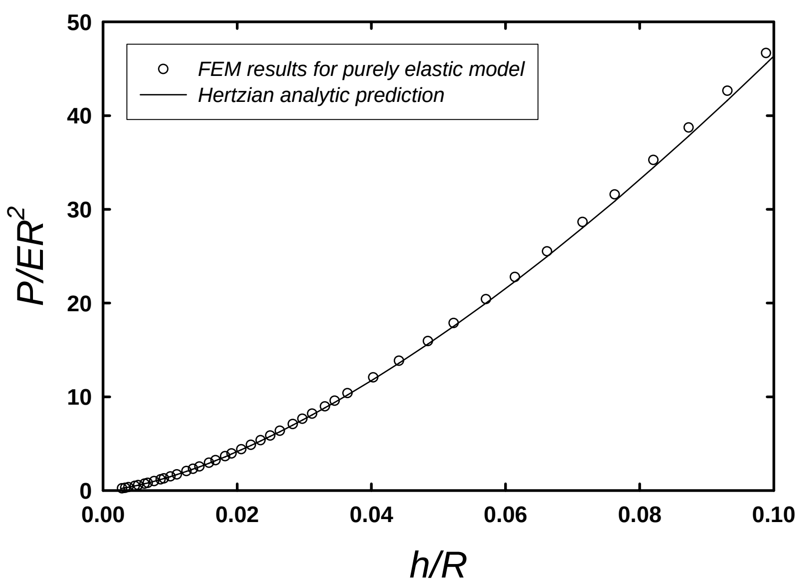

(b) comparison in *P-h* curves

Figure 11. Mesh verification using elastic solution

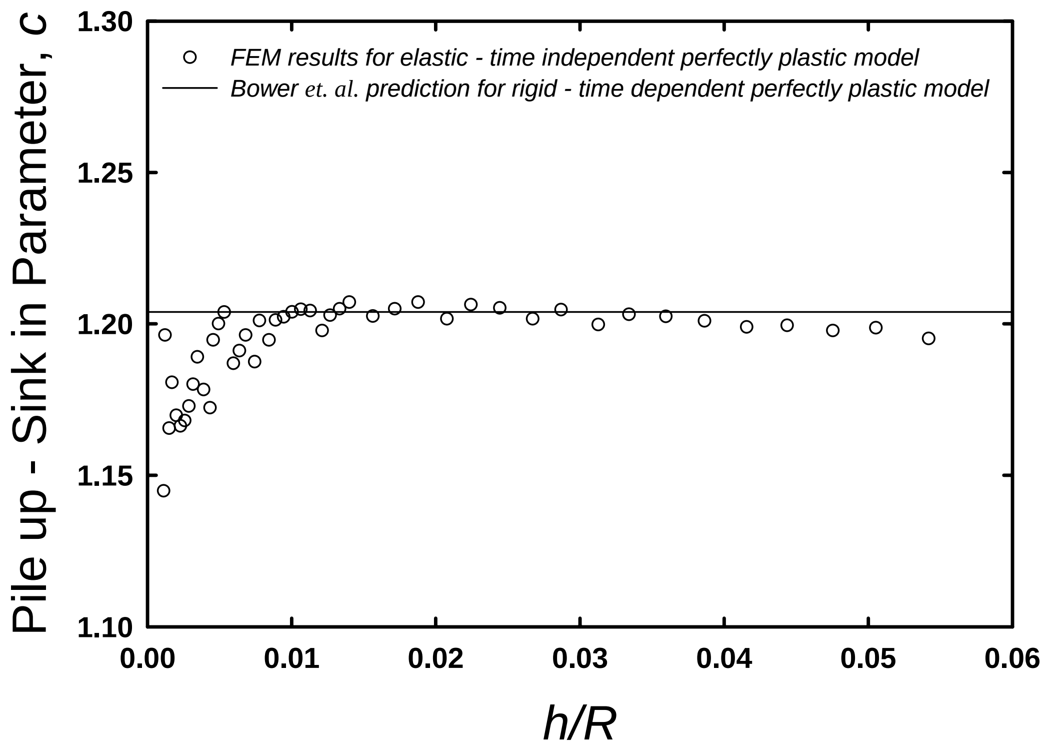

Figure 12. Mesh verification using perfectly plastic solution

CHAPTER 3 – *h-t* OR *P-h* RELATIONSHIP FOR RIGID – POWER LAW CREEPING SOLID

In this chapter, we present the theoretical derivation of the indentation depth – indentation time (h-t) or indentation load – indentation depth (P-h) relations for a power law creeping solid based on the results of Bower *et. al.* [19]. These mathematical formulations are developed under the assumption of rigid – power law creep constitutive law.

Spherical Indentation under the CLH Method

Based on a similarity analysis, Bower *et. al.* showed that the indentation of a power law creeping solid is characterized by an analogous power law relation. Therefore, indentation of a solid characterized by

$$\dot{\varepsilon} = A\sigma^m \tag{12}$$

is characterized by

$$\dot{\varepsilon}_I = B\left(p_{\text{mean}}\right)^m \tag{13}$$

Equation (13) may be rewritten in terms of indentation variables as

$$\left(\frac{1}{a}\right)\left(\frac{dh_{\text{creep}}}{dt}\right) = B\left(\frac{P}{\pi a^2}\right)^m \tag{14}$$

Here, the indentation creep constitutive law is expressed in terms of contact radius a, depth h, time t, and load P on the indenter. Employing the definition of pile up – sink in parameter c to substitute for the contact radius, equation (14) becomes

$$\left(\frac{1}{c\sqrt{2Rh_{\text{creep}}}}\right)\left(\frac{dh_{\text{creep}}}{dt}\right) = B\left(\frac{P}{2\pi Rc^2 h_{\text{creep}}}\right)^m \tag{15}$$

Solving this first-order differential equation with respect to h_{creep} yields

$$h_{\text{creep}} = \left[\left(\frac{2m+1}{2}\right)B\left(\frac{P}{\pi}\right)^m \left(c^{1-2m}\right)\left(2R\right)^{\frac{1-2m}{2}}\right]^{\frac{2}{2m+1}} t^{\frac{2}{2m+1}} \tag{16}$$

which is the theoretical *h*-*t* relationship for indentation of a power law creeping solid using spherical indenter under the constant load and hold method. Here, *B* is the indentation creep coefficient and *R* is the radius of the indenter.

Spherical Indentation under the CRL Method

For the CRL method, the load on the indenter may be expressed in terms of the loading rate $\dot{P}$ and indentation time *t* as

$$P = \dot{P}t \tag{17}$$

Analogous to the procedure for deriving equation (16), we write the indentation strain rate to indentation mean pressure relation in terms of primary indentation variables and the pile up – sink in parameter *c*. This yields

$$\left(\frac{1}{c\sqrt{2Rh_{\text{creep}}}}\right)\left(\frac{dh_{\text{creep}}}{dt}\right) = B\left(\frac{\dot{P}t}{2\pi Rc^2 h_{\text{creep}}}\right)^m \tag{18}$$

Solution of equation (18) yields

$$h_{\text{creep}} = \left[\left(\frac{2m+1}{2m+2}\right)B\left(\frac{\dot{P}}{\pi}\right)^m \left(c^{1-2m}\right)\left(2R\right)^{\frac{1-2m}{2}}\right]^{\frac{2}{2m+1}} t^{\frac{2m+2}{2m+1}} \tag{19}$$

This is the *h*-*t* relationship for indentation of power law creeping solid using spherical indenter under the CRL method.

For the CRL method, the load changes continuously as a function of time or depth of indentation. Therefore, the *P*-*h* relation may also be deduced from the indentation constitutive law. Substituting *t* with $P/\dot{P}$ in equation (19), we obtain the *P*-*h* relation for spherical indentation under the CRL method:

$$P = \left[\left(\frac{2m+2}{2m+1}\right)\left(\frac{1}{B}\right)\dot{P}\pi^{m}\left(c^{2m-1}\right)\left(2R\right)^{\frac{2m-1}{2}}\right]^{\frac{1}{m+1}} h_{\text{creep}}^{\frac{2m+1}{2m+2}} \tag{20}$$

Conical Indenter under the CLH Method

For conical indentation, we may rewrite equation (13) with primary variables of indentation and the pile up – sink in parameter *c* as

$$\left(\frac{1}{ch_{\text{creep}}\tan\beta}\right)\left(\frac{dh_{\text{creep}}}{dt}\right) = B\left[\frac{P}{\pi c^{2}\left(h_{\text{creep}}\right)^{2}\left(\tan\beta\right)^{2}}\right]^{m} \tag{21}$$

Here, β is the half-included cone angle of the conical indenter as defined in Figure 6b. Similar to spherical indentation, closed form solution of equation (21) yields the *h*-*t* relation for indentation of power law creeping solid using conical indenter under the CLH method. This is given by:

$$h_{\text{creep}} = \left[2mB\left(\frac{P}{\pi}\right)^{m}\left(c\tan\beta\right)^{1-2m}\right]^{\frac{1}{2m}} t^{\frac{1}{2m}} \tag{22}$$

Conical Indenter under the CRL Method

Substituting *P* with $\dot{P}t$ in equation (21), we obtain

$$\left(\frac{1}{ch_{\text{creep}}\tan\beta}\right)\left(\frac{dh_{\text{creep}}}{dt}\right)=B\left[\frac{\dot{P}t}{\pi c^2\left(h_{\text{creep}}\right)^2\left(\tan\beta\right)^2}\right]^m \tag{23}$$

which describes indentation of a power creeping solid using a conical indenter under the CRL method. Equation (23) may be solved for h_{creep} yielding the h-t or P-h relations for indentation of a power law creeping solid using a conical indenter under the CRL method. These are given by:

$$h_{\text{creep}}=\left[\left(\frac{2m}{m+1}\right)B\left(\frac{\dot{P}}{\pi}\right)^m\left(c\tan\beta\right)^{1-2m}\right]^{\frac{1}{2m}}t^{\frac{m+1}{2m1}} \qquad (h\text{-}t \text{ relation}) \tag{24}$$

$$P=\left[\left(\frac{m+1}{2m}\right)\frac{\dot{P}\pi^m\left(c\tan\beta\right)^{2m-1}}{B}\right]^{\frac{1}{m+1}}h_{\text{creep}}^{\frac{2m}{m+1}} \qquad (P\text{-}h \text{ relation}) \tag{25}$$

Prediction of Uniaxial Power Law Creep Parameters from *h-t* or *P-h* Curves

The h-t or P-h relations for indentation of a rigid – power law creeping solid are summarized in Table 5. These relationships enable us to predict the uniaxial power law creep parameters. The uniaxial creep exponent m is obtained directly from the slope of log$h$-log$t$ or log$P$-log$h$ relationship. Prediction of the uniaxial creep coefficient A is more complicated and requires the knowledge of other relations that will be developed later in this study.

Table 5. *h-t* and *P-h* relations for indentation of rigid – power law creeping solid

Indenter Geometry	Loading Method	*h-t* or *P-h* Relationship
Sphere	CLH	$h_{\text{creep}} = \left[\left(\frac{2m+1}{2} \right) B \left(\frac{P}{\pi} \right)^m \left(c^{1-2m} \right) (2R)^{\frac{1-2m}{2}} \right]^{\frac{2}{2m+1}} t^{\frac{2}{2m+1}}$
	CRL	$h_{\text{creep}} = \left[\left(\frac{2m+1}{2m+2} \right) B \left(\frac{\dot{P}}{\pi} \right)^m \left(c^{1-2m} \right) (2R)^{\frac{1-2m}{2}} \right]^{\frac{2}{2m+1}} t^{\frac{2m+2}{2m+1}}$
		$P = \left[\left(\frac{2m+2}{2m+1} \right) \left(\frac{1}{B} \right) \dot{P} \pi^m \left(c^{2m-1} \right) (2R)^{\frac{2m-1}{2}} \right]^{\frac{1}{m+1}} h_{\text{creep}}^{\frac{2m+1}{2m+2}}$
Cone	CLH	$h_{\text{creep}} = \left[2mB \left(\frac{P}{\pi} \right)^m (c \tan \beta)^{1-2m} \right]^{\frac{1}{2m}} t^{\frac{1}{2m}}$
	CRL	$h_{\text{creep}} = \left[\left(\frac{2m}{m+1} \right) B \left(\frac{\dot{P}}{\pi} \right)^m (c \tan \beta)^{1-2m} \right]^{\frac{1}{2m}} t^{\frac{m+1}{2m}}$
		$P = \left[\left(\frac{m+1}{2m} \right) \frac{\dot{P} \pi^m (c \tan \beta)^{2m-1}}{B} \right]^{\frac{1}{m+1}} h_{\text{creep}}^{\frac{2m}{m+1}}$

CHAPTER 4 – INDENTATION OF AN ELASTIC – POWER LAW CREEPING SOLID

Previous studies of the indentation of a power law creeping solid provided solutions that are subject to certain limitations such as the assumption of indentation satisfying infinitesimal strain – infinitesimal deformation condition, the creeping solid behaving as elastically rigid, and the application of a power law constitutive relationship between stress and strain rate [19]. In this chapter, indentation of power law creeping solid is further studied with the intention of providing enhanced and/or modified solutions

Taking advantage of existing solution for spherical indentation [19] satisfying the infinitesimal strain – infinitesimal deformation condition, the elastic-creep transient will be studied in detail. This transient is carefully documented, and qualitative/quantitative conclusions are provided with recommendations and procedures that will be useful to the indentation experimentalist.

For conical indentation, the finite deformation problem is explored in terms of the half-included cone angle of the indenter [30]. Modified creep solutions incorporating the effects of the half-included cone angle are necessary before the transient can be understood. Based on the creep solution for conical indentation, transients occurring from elasticity will be explained in detail.

Overall, recommendations to the indentation experimentalist will be provided for extracting uniaxial creep parameters from load and depth sensing indentation results.

Elastic-Creep Transients for Spherical Indentation under the CLH Method

Indentation process under the CLH method

As shown in Figure 13a, the indenter is initially at rest on the surface of the creeping solid. Upon loading, the surface is subjected to instantaneous elastic deformation. According to the elastic solution for spherical indentation, the material surface sinks in, as shown in Figure 13b. After creep commences, the deformation undergoes a transient resulting in changes in the surface deformation and pressure distribution (Figure 13c). This behavior is influenced by the creep exponent, *m*.

Existing creep solution for spherical indentation

The study of indentation creep under spherical indentation may be summarized by two significant parameters, *c(m)* and *F(m)*, as introduced in Chapter 1. *c(m)* characterizes the extent of piling up or sinking in of the surface. It is seen from the solution by Bower *et. al.* [19] that when *m*=1, the amount of sinking in is equivalent to that of the elastic deformation. The dependence of *c(m)* on *m* determined by Bower *et. al*. is given in Figure 14. A simple empirical correlation between *c(m)* and *m* is given by

$$c(m) = 1.204 - \left(\frac{0.766}{m}\right) + \left(\frac{0.497}{m^2}\right) - \left(\frac{0.231}{m^3}\right) \tag{26}$$

F(m) provides a correlation between the uniaxial creep coefficient *A*, and the indentation creep coefficient, *B*. This is shown in Figure 15 and can be well described by the empirical correlation

$$F(m) = \left(\frac{A}{B}\right)^{\frac{1}{m}} = 3.048 + \left(\frac{1.440}{m}\right) - \left(\frac{11.360}{m^2}\right) + \left(\frac{12.191}{m^3}\right) - \left(\frac{4.475}{m^4}\right) \tag{27}$$

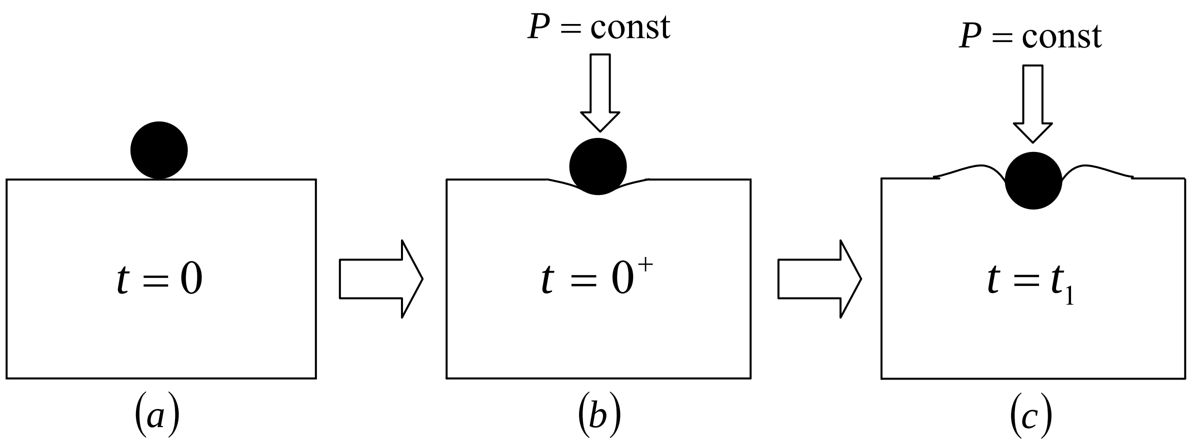

Figure 13. Indentation process under CLH method

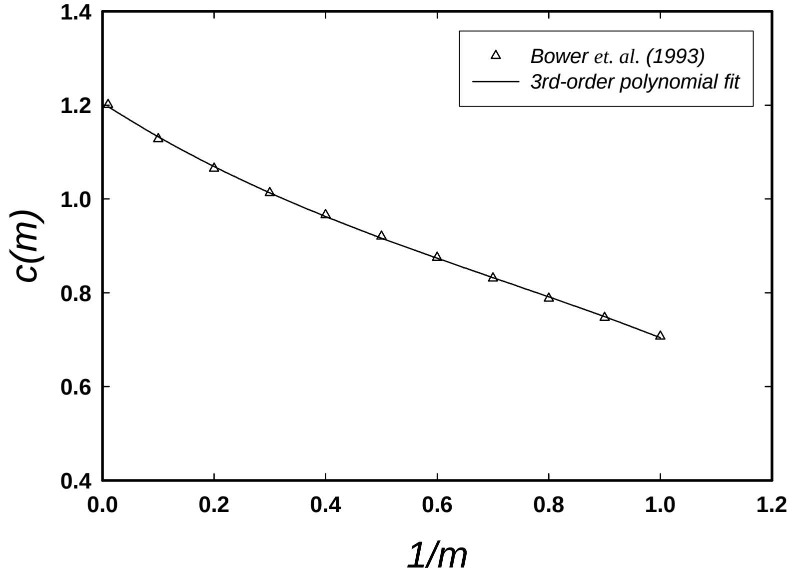

Figure 14. Pile up – sink in parameter, *c*, dependence on *m* for spherical indentation

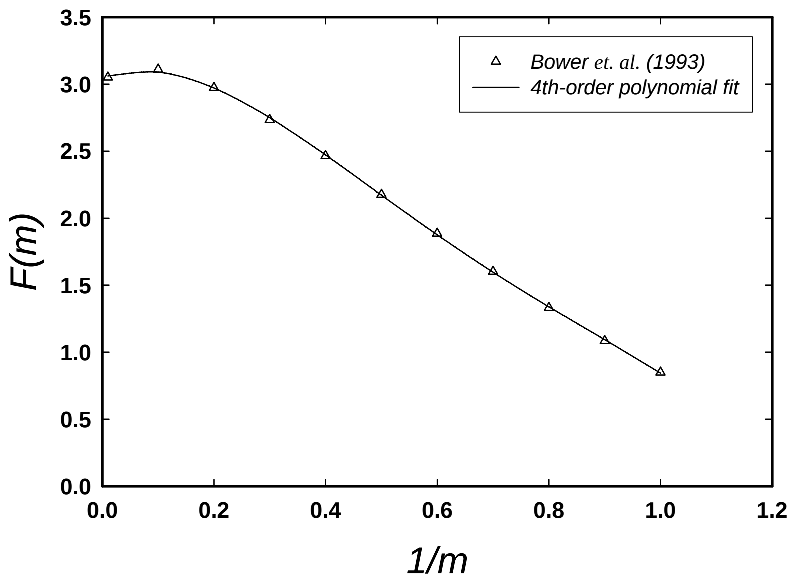

Figure 15. Creep coefficient correlation dependence on *m* for infinitesimal strain – infinitesimal deformation condition

c(m) and *F(m)* derived from equations (26) and (27) will be used extensively throughout the analysis of indentation creep for spherical indentation.

Indentation h-t curves for various creep exponents

Using the dimensionless parameters outlined in Chapter 2, we use the finite element method to produce indentation *h-t* curves for various values of *m*. Figure 16 shows normalized *h-t* curves for *m*=1. By prescribing an identical normalized load, $\frac{P}{ER^2} = 0.001$, perfect overlapping of two of the *h-t* curves occurs. This is evidence of successful dimensional analysis. Figure 17 and Figure 18 show normalized *h-t* curves for *m*=3 and 5, respectively. Analogously, results of successful dimensional analysis are shown in the figures.

In all the *h-t* plots, the *h-t* relation tends to approach a log-linear regime at longer times or larger depths of indentation. This log-linear regime is representative of the theoretical *h-t* relationship for creep given in equation (16). The deviation at shorter times or shallower depths is due to a transient occurring from elasticity. Due to elasticity, a finite depth of indentation is observed at time t/t_{max}=0. As creep deformation starts, the *h-t* relationship approaches the rigid – power law creeping solid behavior, thereby producing the elastic transient from the initially predicted elastic indentation depth. This manifests itself as a breakdown of the linear relationship in the log*h*-log*t* curve.

A new concept of normalization – the elastic normalization

We now take advantage of known elastic solutions to further normalize the indentation *h-t* curves. The purpose of this normalization is to explore the feasibility of producing *h-t* curves that depend only on the creep exponent regardless of elasticity.

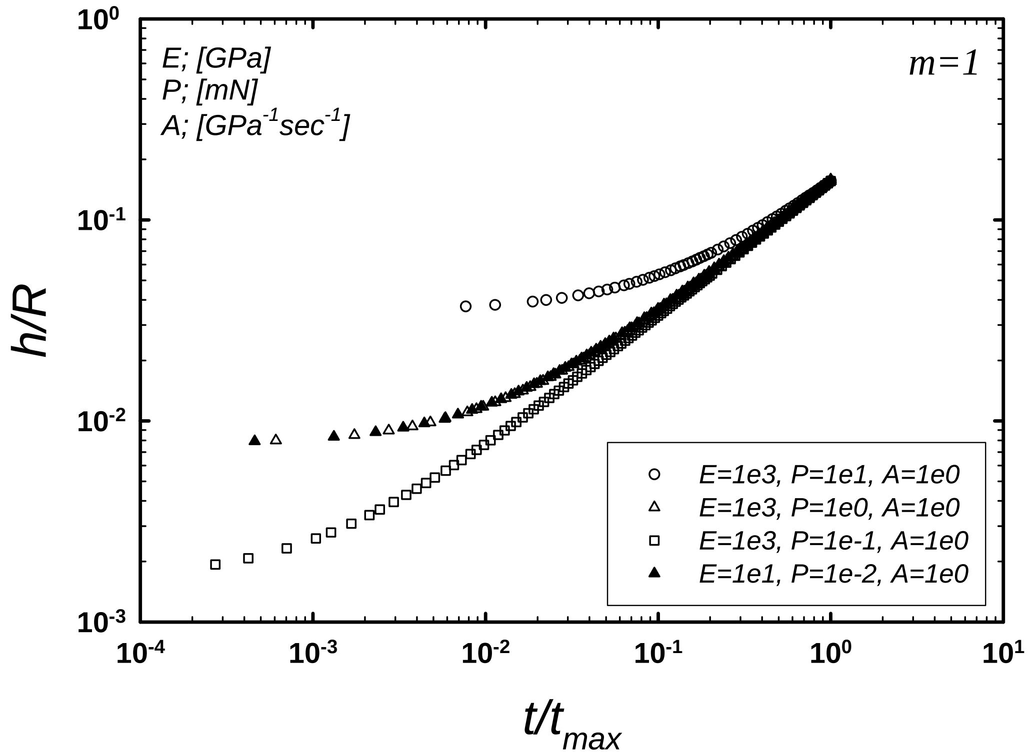

Figure 16. *h-t* curves for *m*=1 (sphere, CLH)

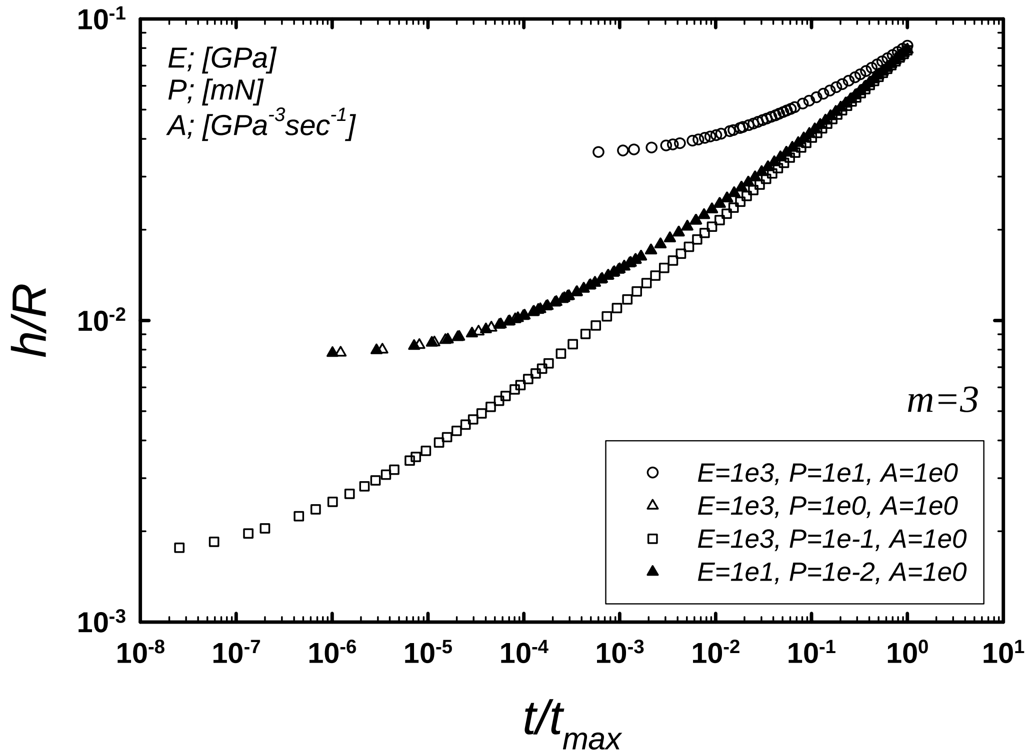

Figure 17. *h*-*t* curves for *m*=3 (sphere, CLH)

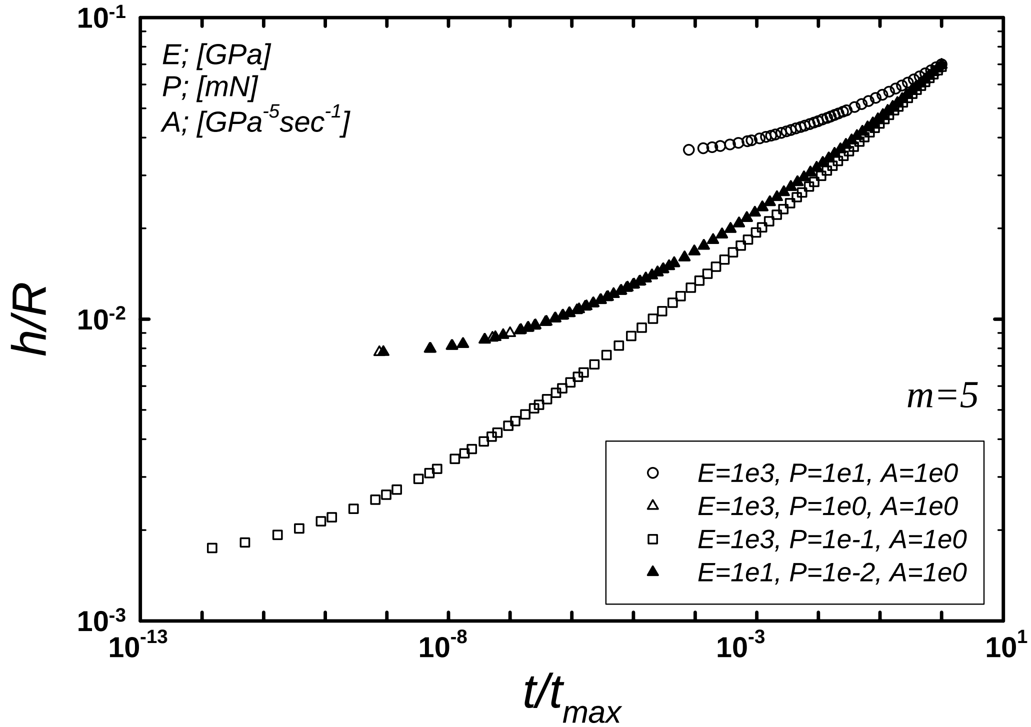

Figure 18. *h-t* curves for *m*=5 (sphere, CLH)

Therefore, we introduce a new concept of normalization incorporating elastic material properties and the geometric features of the indenter. For indentation depth, normalization is performed with respect to the elastic depth for spherical Hertzian contact h_{Hertz} [29], which is given by

$$h_{\mathrm{Hertz}} = \left[\frac{9\left(1-\nu^2\right)^2 P^2}{16RE^2}\right]^{\frac{1}{3}} \tag{28}$$

Normalization of the indentation time requires a characteristic time derived from known variables. By combining the rigid – power law creep relation for spherical indentation under the CLH method (equation (16)), and the elastic depth h_{Hertz}, we obtain a characteristic time incorporating both finite elasticity and power law creep. Substituting h_{creep} into equation (16) with h_{Hertz} and solving for time t, we obtain a characteristic time. This is termed as the characteristic time for spherical indentation under the CLH method, $t_{\mathrm{sphereCLH}}$, and is given by:

$$t_{\mathrm{sphereCLH}} = \frac{\left[\dfrac{3\left(1-\nu^2\right)}{E}\right]^{\frac{2m+1}{3}} \left(\pi^m\right)\left(P^{\frac{1-m}{3}}\right)}{B\left(\dfrac{2m+1}{2}\right)\left(c^{1-2m}\right)\left(2^{\frac{2m+7}{6}}\right)\left[R^{\frac{2}{3}(1-m)}\right]} \tag{29}$$

Physically, $t_{\mathrm{sphereCLH}}$ represents the indentation time required to achieve twice the elastic depth. In equation (29), all the variables except c and B are assumed to be known from elasticity or from the boundary conditions of the problem. At larger depths or longer times, c is independent of depth and is a unique function of m. B can be obtained from the intercept of the log$h$-log$t$ curve in the log-linear regime.

Despite the difficulty in obtaining the indentation strain rate – mean pressure relation from indentation experiments, FEM provides us with the tools to examine indentation strain rate – mean pressure data, and they are discussed here to illustrate several important points. In accordance with the normalization techniques used in this section, the indentation strain rate and the mean pressure are normalized with respect to elastic properties and geometric parameters of the indenter. The elastic mean pressure, $(p_{\text{mean}})_{\text{Hertz}}$ [29], given by:

$$(p_{\text{mean}})_{\text{Hertz}} = \left[\frac{16PE^2}{9\pi^3(1-\nu^2)^2 R^2}\right]^{\frac{1}{3}} \tag{30}$$

is used in normalizing the mean pressure. A characteristic indentation strain rate, $(\dot{\varepsilon}_I)_{\text{characteristic}}$, is derived by substituting $(p_{\text{mean}})_{\text{Hertz}}$ into equation (13), which gives:

$$(\dot{\varepsilon}_I)_{\text{characteristic}} = B\left[(p_{\text{mean}})_{\text{elastic}}\right]^m \tag{31}$$

Since the mean pressure decreases with time in a CLH experiment, equation (31) represents the maximum indentation strain rate for the elastic – power law creeping material.

Using the normalization method outlined above, Figures 16-18 have been normalized and replotted as Figures 19-21. For the master *h*-*t* curves shown in Figure 19a, 20a and 21a, the solution of Bower *et. al.* is derived by normalizing equation (16) with h_{Hertz} and $t_{\text{sphereCLH}}$, which gives:

$$\left(\frac{h}{h_{\text{Hertz}}}\right) = \left(\frac{t}{t_{\text{sphereCLH}}}\right)^{\frac{2}{2m+1}} \tag{32}$$

Regardless of the load, elastic modulus, or sphere radius, elastic normalization produces master *h*-*t* curves that are solely dependent on *m*. In each of the master *h*-*t* curves, the deviation from the Bower *et. al.* prediction accounts for the transient induced by finite elasticity.

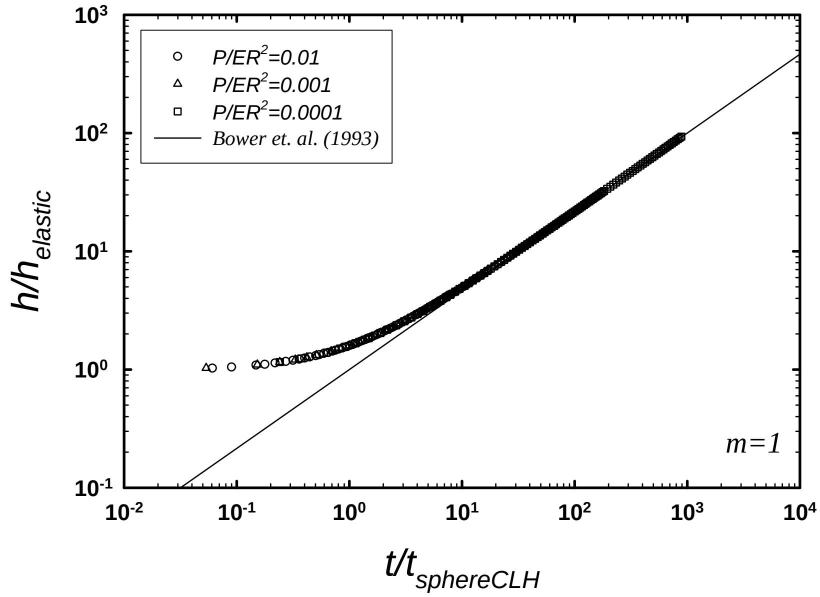

(a) Master *h*-*t* curve

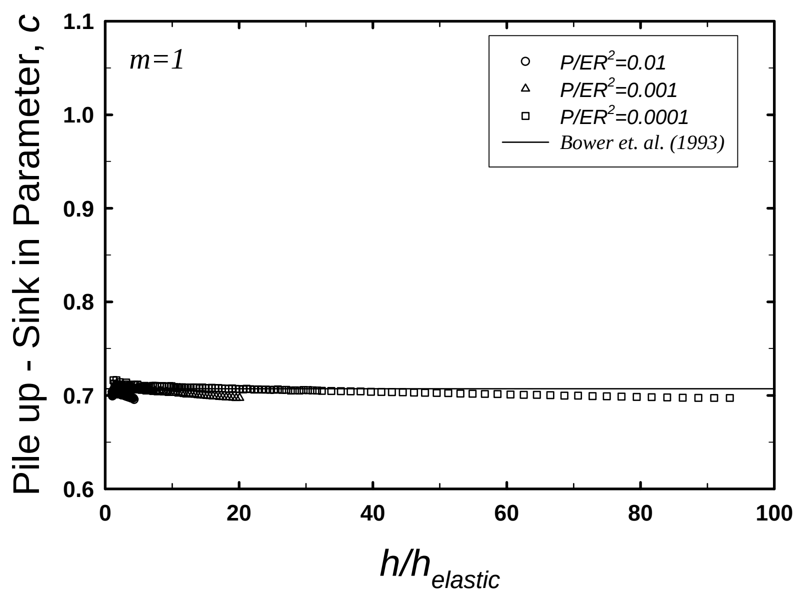

(b) Pile up-sink in variation

Figure 19. Elastic normalized results for *m*=1 (sphere, CLH)

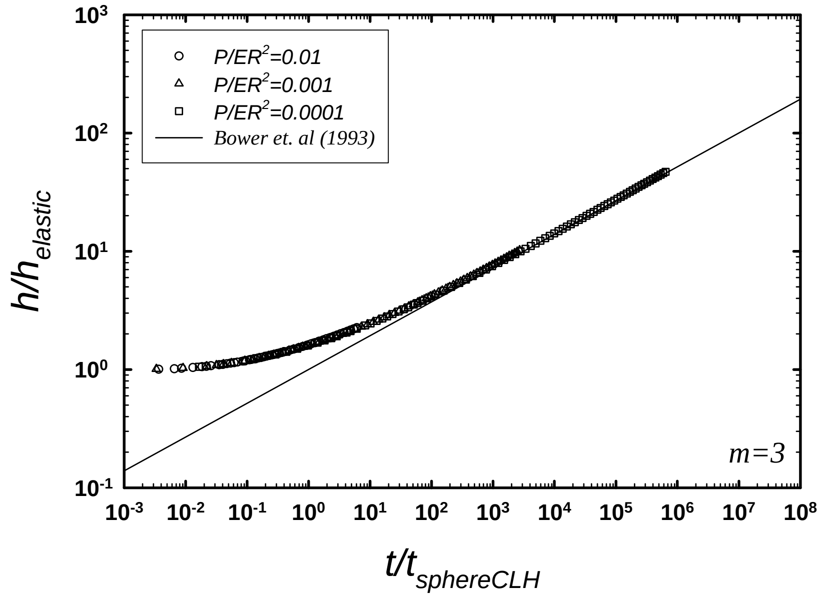

(a) Master *h*-*t* curve

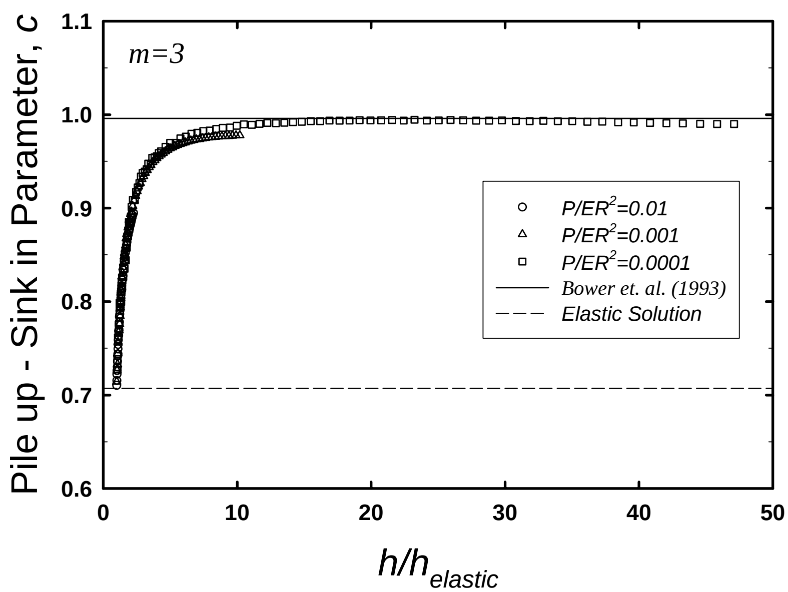

(b) Pile up-sink in variation

Figure 20. Elastic normalized results for *m*=3 (sphere, CLH)

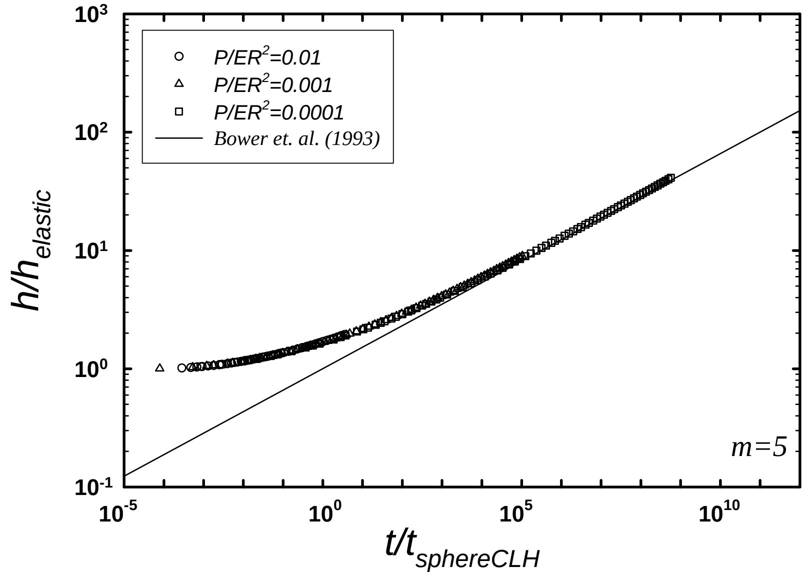

(a) Master *h*-*t* curve

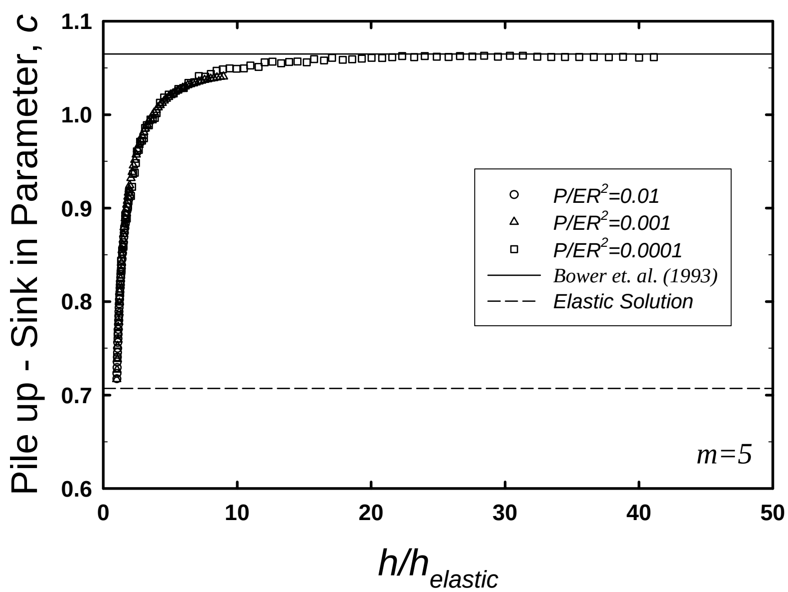

(b) Pile up-sink in variation

Figure 21. Elastic normalized results for *m*=5 (sphere, CLH)

Transient phenomena are now explained in detail using the pile up-sink in variations. Initially, the surface of the creeping solid sinks in due to instantaneous elasticity, with the amount of sinking in equal to the elastic prediction. With the progression of creep deformation, the initially sunk in surface undergoes a change in shape which depends on *m*.

According to the Hertzian contact analysis for spherical indentation [29], the pile up – sink in parameter, *c* is equal to $\frac{1}{\sqrt{2}}$ for elastic contact. In Figure 19b, pile up – sink in parameter shows a constant value equal to $\frac{1}{\sqrt{2}}$, which is that for the elastic solution. Therefore, materials with *m*=1 do not exhibit transient induced by finite elasticity because the amount of sink in for a creeping material is exactly that produced by elastic deformation. When *m*=3, the initially sunk in surface gradually recovers from the sinking in. This process is shown in Figure 20b, where *c* approaches approximately 1. Therefore, *m*=3 represents surface deformation with no apparent piling up or sinking in. Similarly, the initially sunk in surface transitions to piling up for *m*=5, as shown in Figure 21b, and the resulting surface deformation is characterized by appreciable pile up after creep has occurred.

The transient occurring from elasticity may also be observed in terms of the stress distribution on the deforming solid underneath the indenter. Figures 22-24 illustrate the constant von Mises contour plots for indentation of an elastic – power law creeping solid for spherical indentation under the CLH method with an applied normalized load of $\frac{P}{ER^2} = 0.0001$. The von Mises stress, S, in these plots has been normalized with respect to the elastic modulus, *E*.

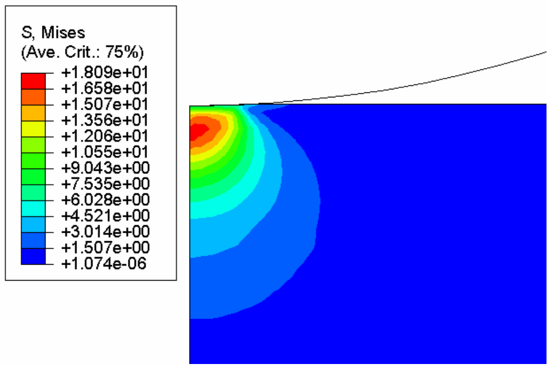

(a) h/h_{elastic}=1

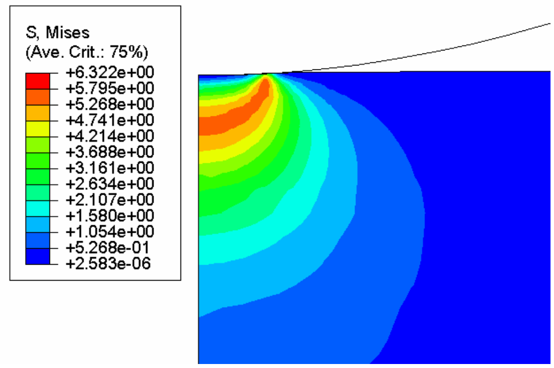

(b) h/h_{elastic}=2

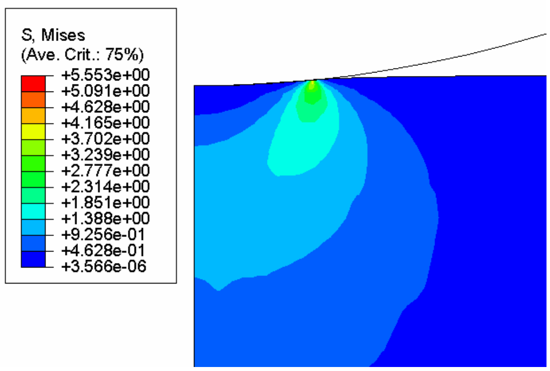

(c) h/h_{elastic}=6

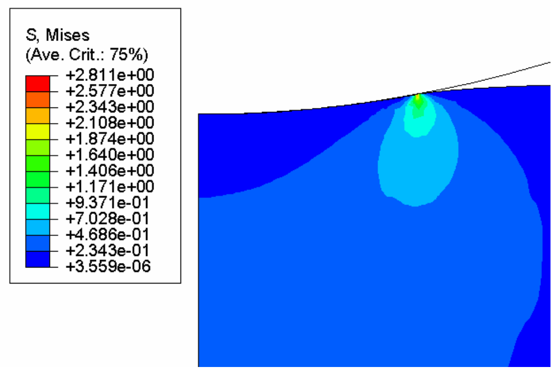

(d) h/h_{elastic}=20

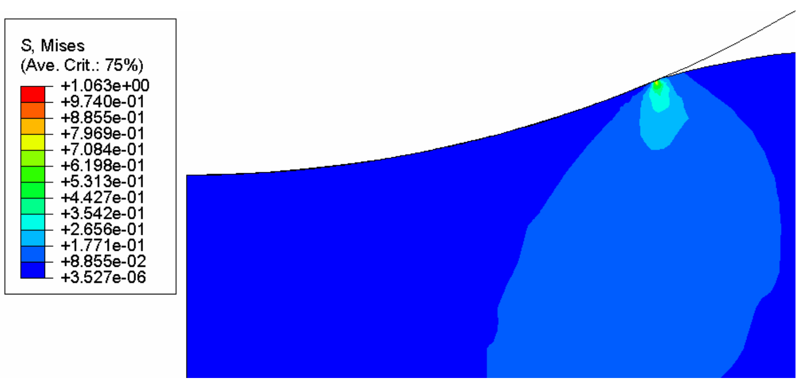

(e) h/h_{elastic}=93 (maximum depth)

Figure 22. von Mises stress distribution for m=1 (sphere, CLH)

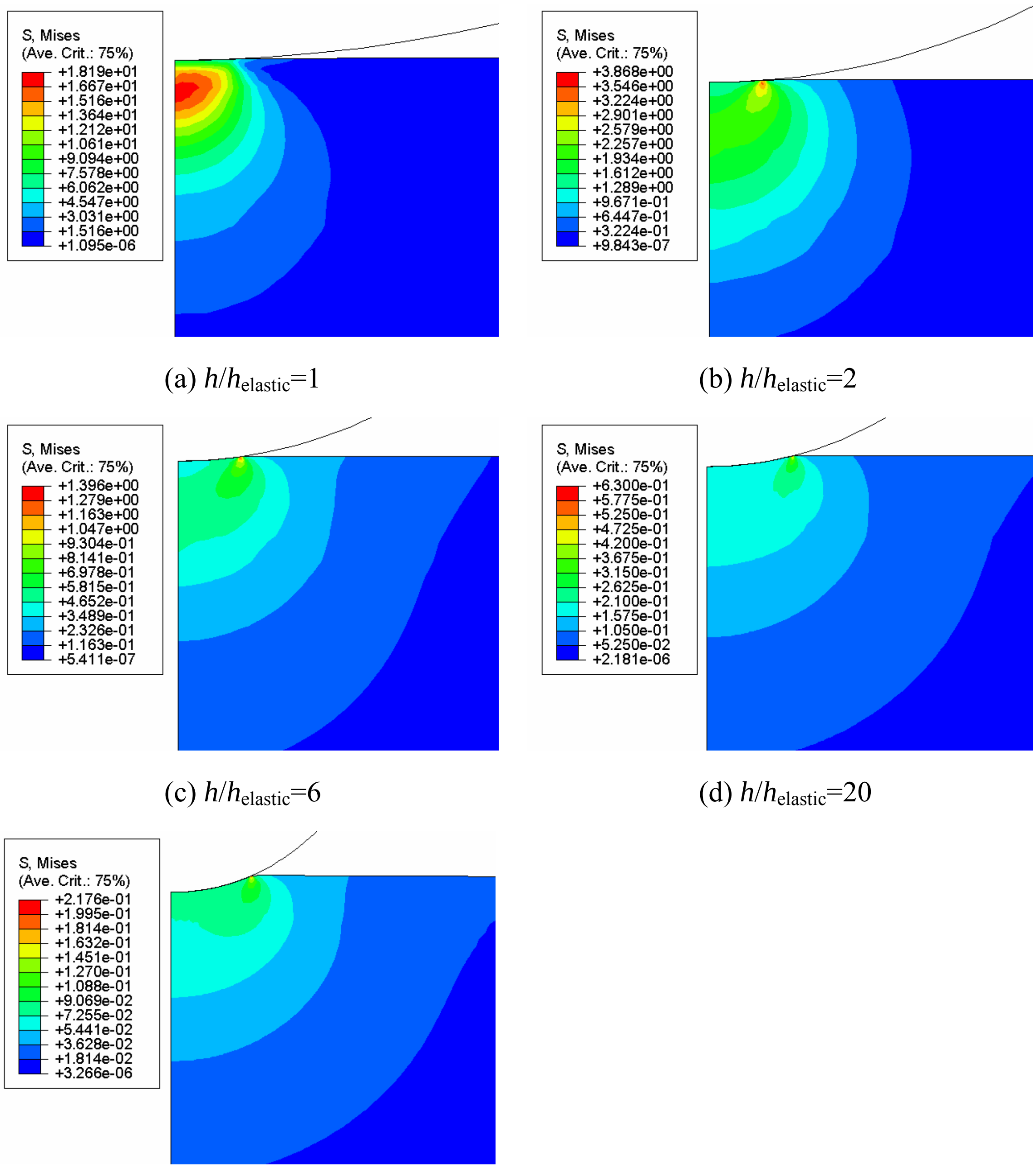

(a) h/h_{elastic}=1

(b) h/h_{elastic}=2

(c) h/h_{elastic}=6

(d) h/h_{elastic}=20

(e) h/h_{elastic}=47 (maximum depth)

Figure 23. von Mises stress distribution for *m*=3 (sphere, CLH)

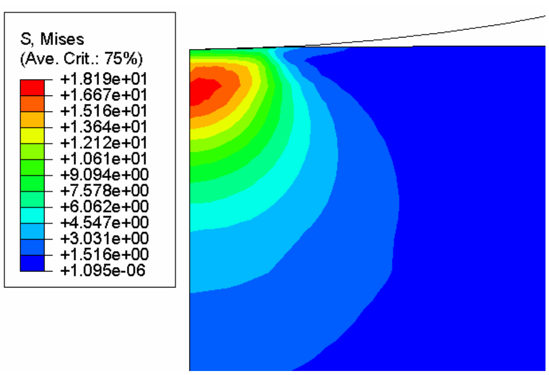

(a) h/h_{elastic}=1

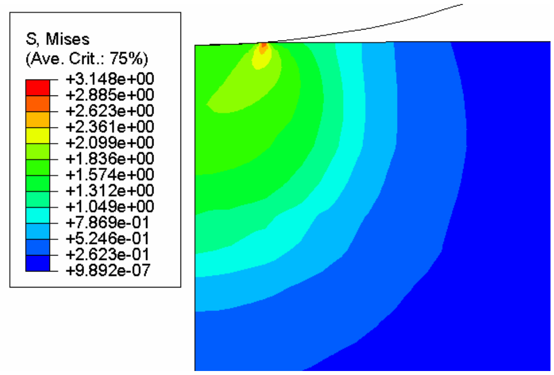

(b) h/h_{elastic}=2

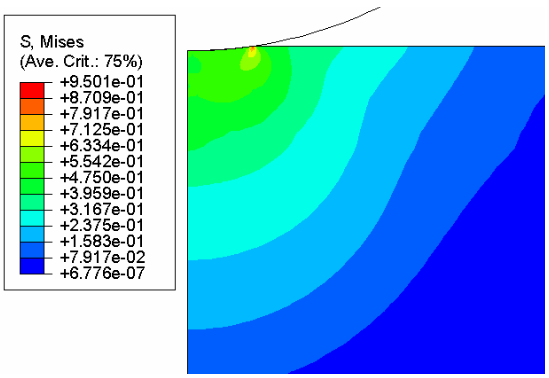

(c) h/h_{elastic}=6

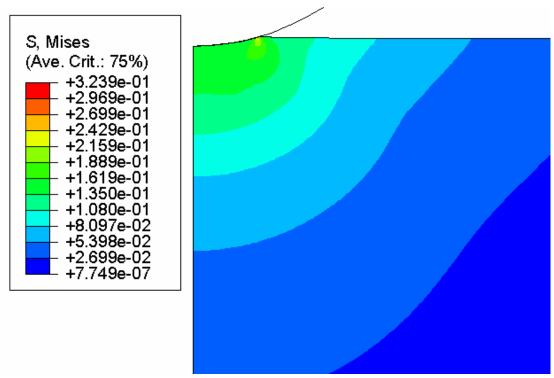

(d) h/h_{elastic}=20

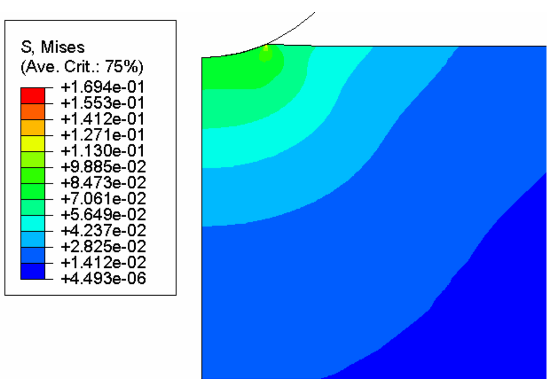

(e) h/h_{elastic}=41 (maximum depth)

Figure 24. von Mises stress distribution for m=5 (sphere, CLH)

In each of the figures, the changes in stress distribution are displayed with respective to the progression of indentation. According to elastic analysis for spherical indentations, the maximum von Mises stress develops below the surface of the solid [32]. This corresponds to $h/h_{elastic}=1$ in terms of elastic normalized depth. As is observed from the figures, this is indeed the case, regardless of creep exponents. As indentation progresses, the stress distribution changes according to the creeping nature of the material. These changes in stress distribution are a consequence of the transient occurring from elasticity. For m=1, 3, and 5, we observe that the stress distribution at a depth of $h/h_{elastic}=20$ is similar to that of the maximum depth.

The normalized indentation strain rate – mean pressure relation is shown in Figure 25. For the CLH method, creep commences upon completion of elastic indentation. Therefore, the maximum values of mean pressure and indentation strain rate correspond to a single point at the upper right of the indentation strain rate – mean pressure curve. Irrespective of m, using the Hertzian elastic solution and the Bower *et. al.* prediction for power law creep, these values may be predicted analytically. The elastic mean pressure is the maximum mean pressure, and the corresponding maximum indentation strain rate can be evaluated from equation (31). The Bower *et. al.* solution for the indentation strain rate – mean pressure curve assumes a power law creep constitutive relation only, that is, no elasticity. Therefore, deviation from the Bower *et. al.* solution in the indentation strain rate – mean pressure curve is indicative of a transient induced by elastic deformation. When $m>1$, the maximum indentation strain rate for the elastic – power law creeping situation exceeds the predicted rigid – power law creep values.

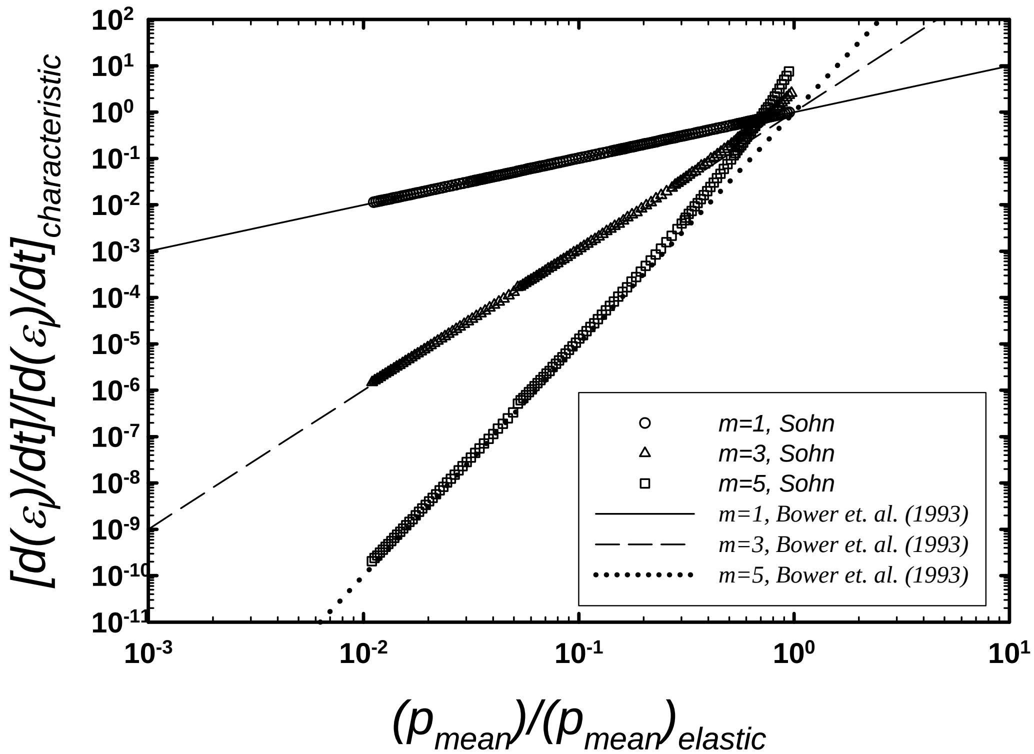

Figure 25. Indentation strain rate – mean pressure curves (sphere, CLH)

This is due to the sinking in of the surface induced by elasticity in the transient regime resulting in smaller contact area and accordingly faster indentation strain rates. Also, the pressure distribution initially equal to the Hertzian elastic prediction changes as creep commences. The slopes of the linear regime of each of the curves represent the uniaxial creep exponent.

Effects of elastic transient in the prediction of creep parameters

Prediction of uniaxial creep parameters from indentation *h*-*t* curves is based on determining the slope of the linear regime and the corresponding intercept on log scales. The elastic transient may alter the slope of *h*-*t* curves. This results in a poor prediction of the uniaxial creep exponent and the corresponding uniaxial creep coefficient in the elastic transient. Figure 26 shows this influence. Here, the uniaxial creep exponents are estimated using a power law fit to local data of log*h*-log*t* curve to determine values for *m* and *B*. Approximately 10 local *h*-*t* data points are collected for determining the slope and intercept. The representative depth chosen is the average depth of the 10 local values. Uniaxial creep coefficients are estimated from the computed local *m* and Bower *et. al.* solutions corresponding to the computed local *m*. It is seen from Figure 26a that the error associated with the creep exponent estimation decreases as the indentation progresses to greater depths. The estimated error is less than 10% at a depth of $h/h_{elastic}$=15. An analogous analysis on the uniaxial creep coefficient *A* shows that $h/h_{elastic}$ must be about 20 for the error to reduce to 10%. Overall, this implies that the indentation should proceed to a depth of $h/h_{elastic}$=20 for the elastic transient to diminish and the effects of elasticity in predicting the uniaxial creep exponent to be ignorable within a 10% of error margin.

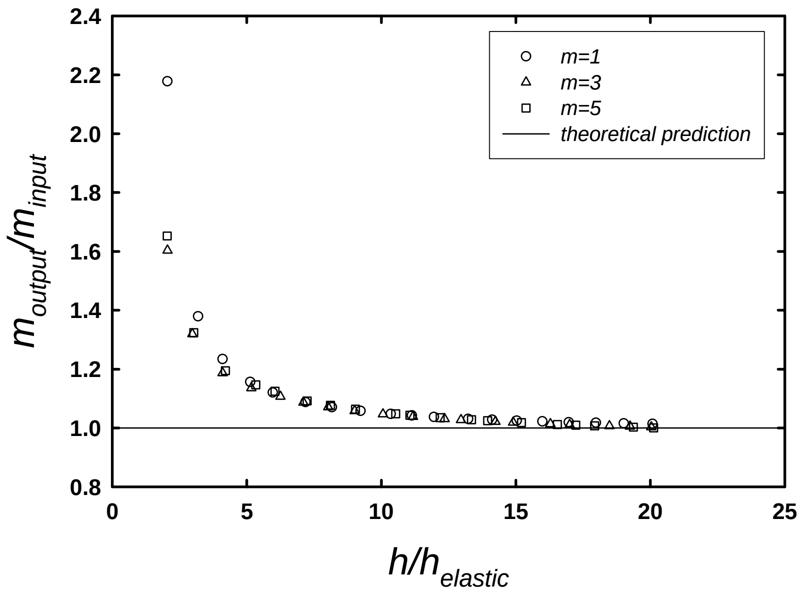

(a) Changes in output creep exponent

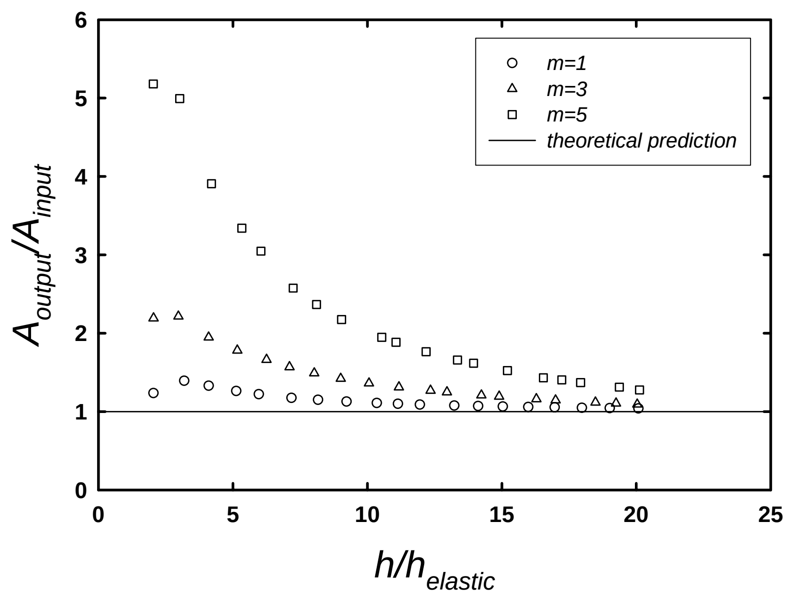

(b) Changes in output creep coefficient

Figure 26. Changes in output uniaxial creep parameters (sphere, CLH)

Elastic-Creep Transients for Spherical Indentation under the CRL Method

Indentation process under the CRL method

Under the CRL method, the load is continuously increased as a linear function of time. The distinction between elastic and creep indentation is not clear due to the inability to define a discrete elastic indentation depth, which is calculated for a constant load. As a consequence, it is difficult to explain the indentation process in a manner similar to the case under the CLH method that displayed discrete stages of deformation (Figure 13). The process of indentation is explained with a different approach, as shown in Figure 27. Initially, the indenter is at rest at time t=0. Upon loading, the deforming solid exhibits deformation characterized both by creep and elasticity (t=t_1). The applied loading rate governs the manner in which the surface deforms. For extremely fast loading rates, surface deformation is dominated by purely elastic deformation due to insufficient time for the creep to take place. This is depicted in Figure 27a. Figure 27a shows the constant loading rate process at very fast rates for which the surface sinks in according to the predicted elastic solution. On the other hand, for very slow loading rates, a sufficient amount of time occurs for the creep deformation to dominate the whole indentation process. This is depicted in Figure 27b. Figure 27b shows a very slow loading rate that produces piling up of the surface, with the amount of pile up dependent upon the creep exponent.

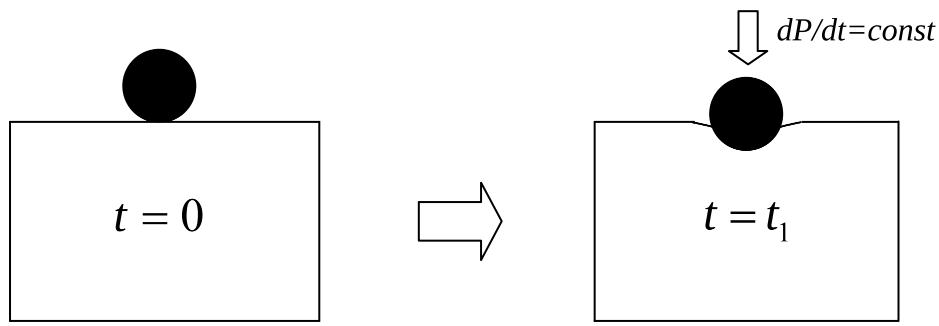

(a) Sinking in of the surface under very fast loading rates

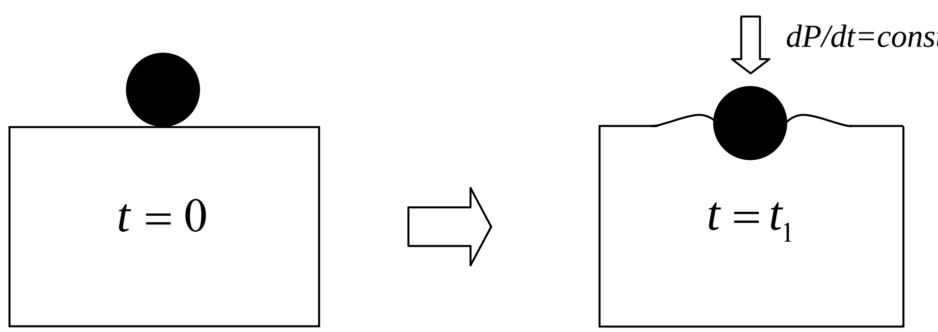

(b) Piling up of the surface under very slow loading rates

Figure 27. Extreme surface behaviors governed by loading rates for the CRL method

Indentation h-t and P-h curves for various creep exponents

CRL can be analyzed in terms of both *h-t* and *P-h* curves. The *h-t* curve for m=1 is shown in Figure 28. In addition to the *h-t* curve, the corresponding *P-h* curve is also presented. Both the *h-t* and the *P-h* curves are presented in dimensionless forms using the techniques outlined in Chapter 2 Overlapping of two of the curves occurs for the same values of dimensionless loads $\frac{\dot{P}}{AE^{m+1}R^2}$. According to the Bower *et. al.* results in equations (19) and (20), the rigid – power law creep *h-t* or *P-h* curves should show a log-linear relationship. Therefore, the breakdown of log linearity in the *h-t* or *P-h* curves at faster loading rates indicates the elastic transient effect. At faster loading rates, indentation is governed by more elastic effects than creep effects due to lack of time for creep deformation to accumulate. Figures 29 and 30 are plots of the *h-t* and *P-h* curves for m=3 and 5, respectively. Once again, successful dimensional analysis produces overlapped *h-t* or *P-h* curves under identical values of dimensionless loading rate, $\frac{\dot{P}}{AE^{m+1}R^2}$.

Elastic normalization for the CRL method

Under the CRL method, the load on the indenter changes continuously. As a consequence, the elastic depth is not defined as a unique value but varies according to equation (28). However, since the applied load is a known at any time, we are still able to normalize indentation depth with elastic depth. For deriving the characteristic time, we adopt a procedure similar to the CLH method. Substituting h_{creep} with h_{Hertz} in equation (19) and solving for t, we obtain a characteristic time for spherical indentation under the CRL method, $t_{\text{sphereCRL}}$, given by:

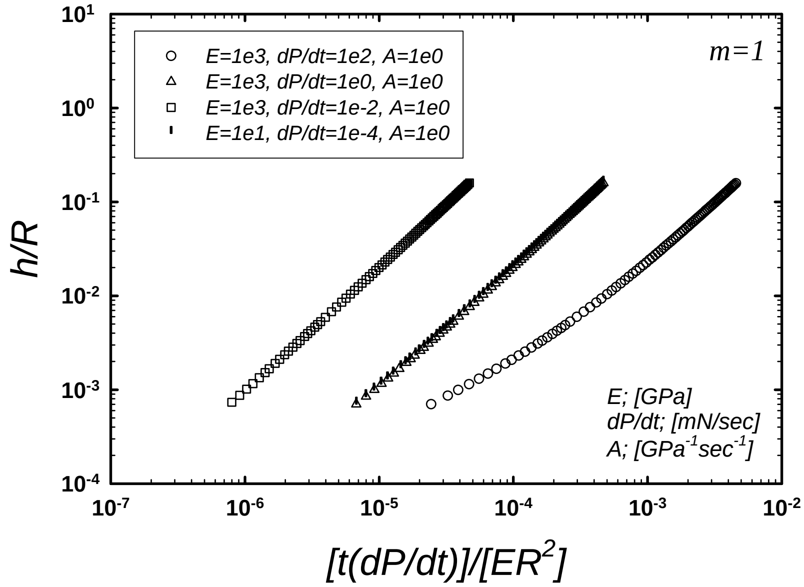

(a) *h*-*t* curves

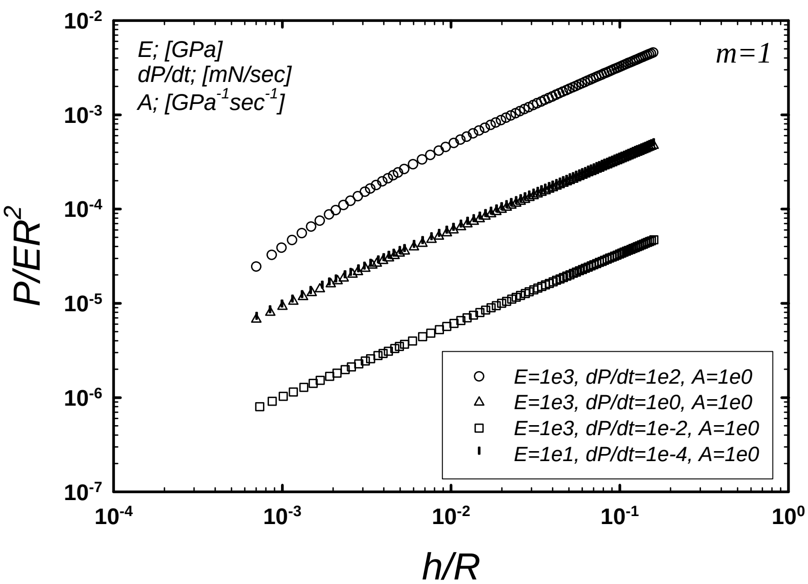

(b) *P*-*h* curves

Figure 28. *h*-*t* and *P*-*h* curves *m*=1 (sphere, CRL)

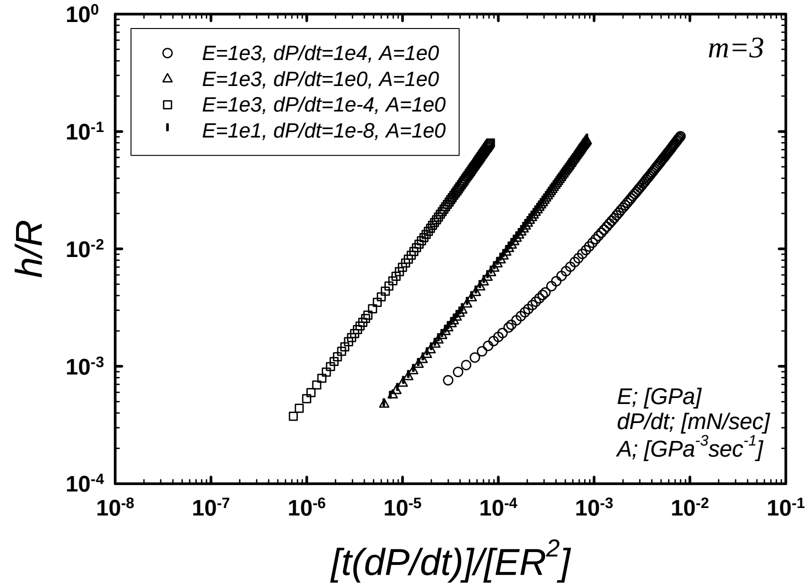

(a) *h-t* curves

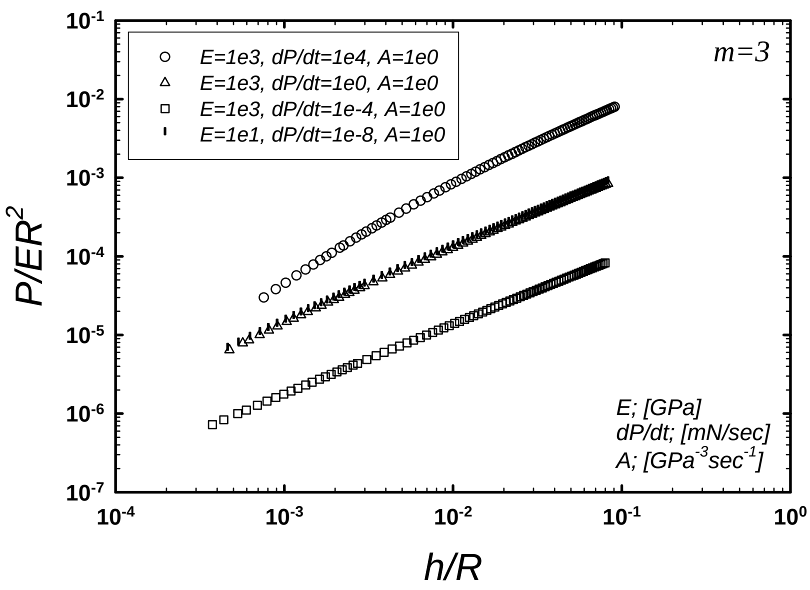

(b) *P-h* curves

Figure 29. *h-t* and *P-h* curves *m*=3 (sphere, CRL)

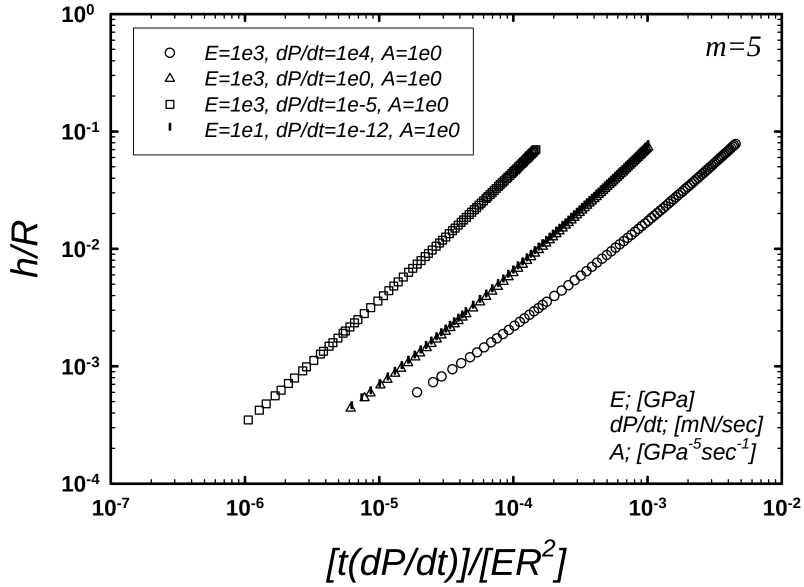

(a) *h*-*t* curves

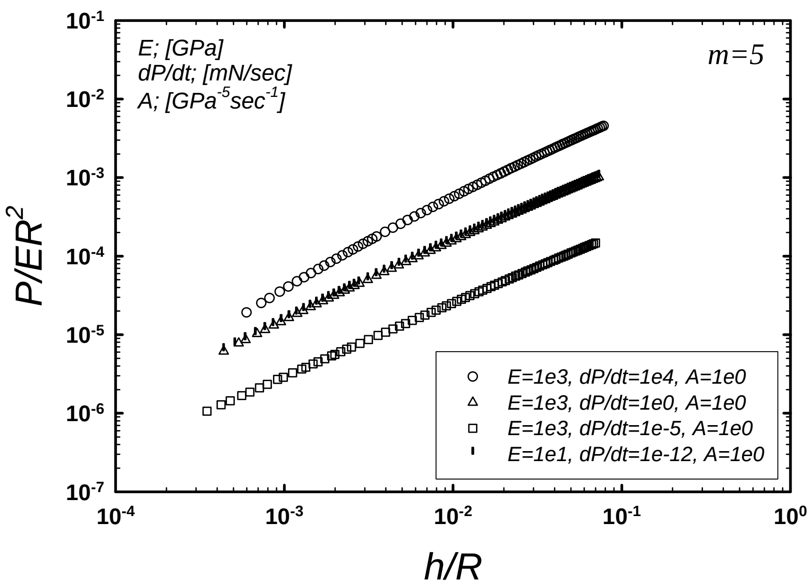

(b) *P*-*h* curves

Figure 30. *h*-*t* and *P*-*h* curves *m*=5 (sphere, CRL)

$$t_{\text{sphereCRL}} = \left\{ \left(\frac{2m+2}{2m+1} \right)^2 \left[\frac{3(1-\nu^2)P}{E} \right]^{\frac{4m+2}{3}} \left(\frac{c^{2m-1}}{B} \right)^2 \left(\frac{\pi}{\dot{P}} \right)^{2m} \left(2^{-\frac{2m+7}{3}} \right) \left[R^{\frac{4}{3}(m-1)} \right] \right\}^{\frac{1}{2m+2}} \tag{33}$$

In addition to the characteristic time, a characteristic load is required to normalize the indentation load. The characteristic load for spherical indentation under the CRL method is derived by replacing h_{creep} with h_{Hertz} in the power law creep *P*-*h* relationship (equation (20)). The result is given by

$$P_{\text{sphereCRL}} = \left\{ \left(\frac{2m+2}{2m+1} \right) \left[\frac{3(1-\nu^2)P}{E} \right]^{\frac{2m+1}{3}} \left(\frac{\pi^m \dot{P}}{B} \right) \left(c^{2m-1} \right) \left(2^{-\frac{2m+7}{6}} \right) \left[R^{\frac{2}{3}(m-1)} \right] \right\}^{\frac{1}{m+1}} \tag{34}$$

Physically, $P_{\text{sphereCLH}}$ represents the indentation load required to achieve twice the elastic depth.

For elastic normalization of the mean pressure and indentation strain rate, equations (30) and (31) are used, respectively. Figures 28-30 are normalized and replotted as master curves in Figures 31-33. The Bower *et. al.* prediction for the *h*-*t* curve is derived by normalizing equation (19) with h_{Hertz} and $t_{\text{sphereCRL}}$ giving

$$\left(\frac{h}{h_{\text{Hertz}}} \right) = \left(\frac{t}{t_{\text{sphereCRL}}} \right)^{\frac{2m+2}{2m+1}} \tag{35}$$

The Bower *et. al.* prediction for *P*-*h* curve is derived by normalizing equation (20) with $P_{\text{sphereCRL}}$ and h_{Hertz} to give

$$\left(\frac{P}{P_{\text{sphereCRL}}} \right) = \left(\frac{h}{h_{\text{Hertz}}} \right)^{\frac{2m+1}{2m+2}} \tag{36}$$

Deviation from the Bower *et. al.* prediction indicates a transient induced by elasticity.

The elastic transient may also be examined from changes in surface deformation.

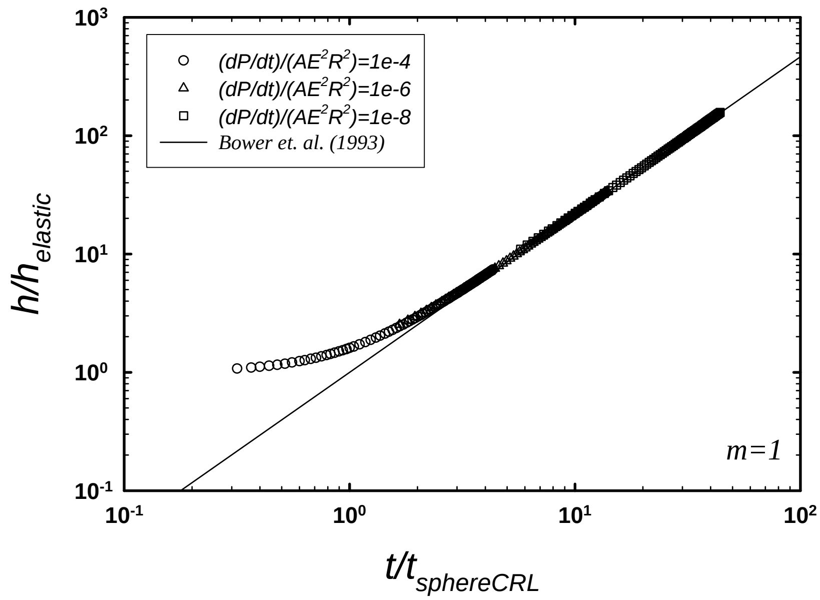

(a) Master *h*-*t* curve

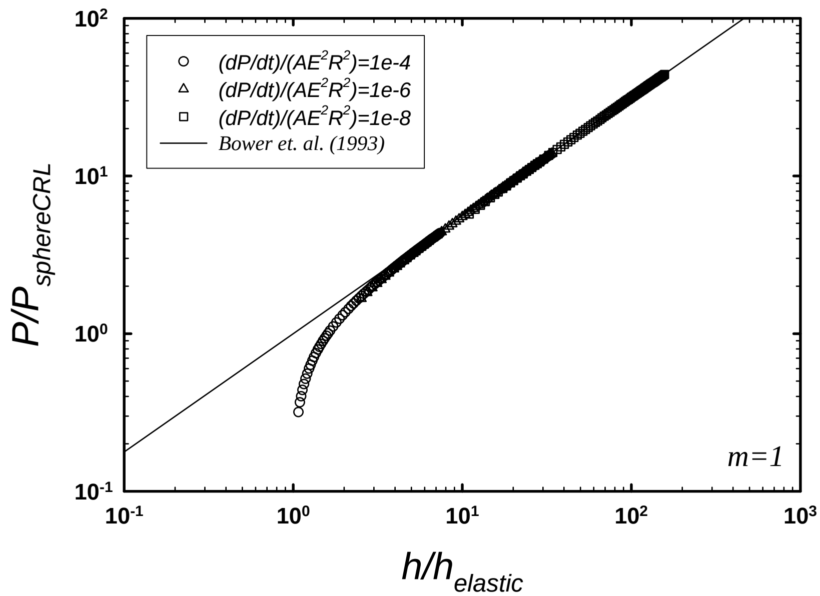

(b) Master *P*-*h* curve

Figure 31. Elastic normalization results for *m*=1 (sphere, CRL)

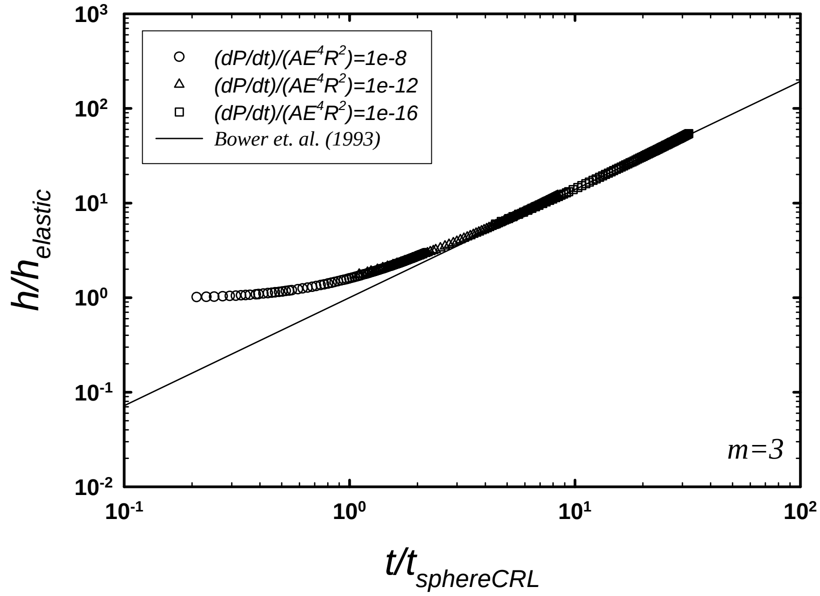

(a) Master *h*-*t* curve

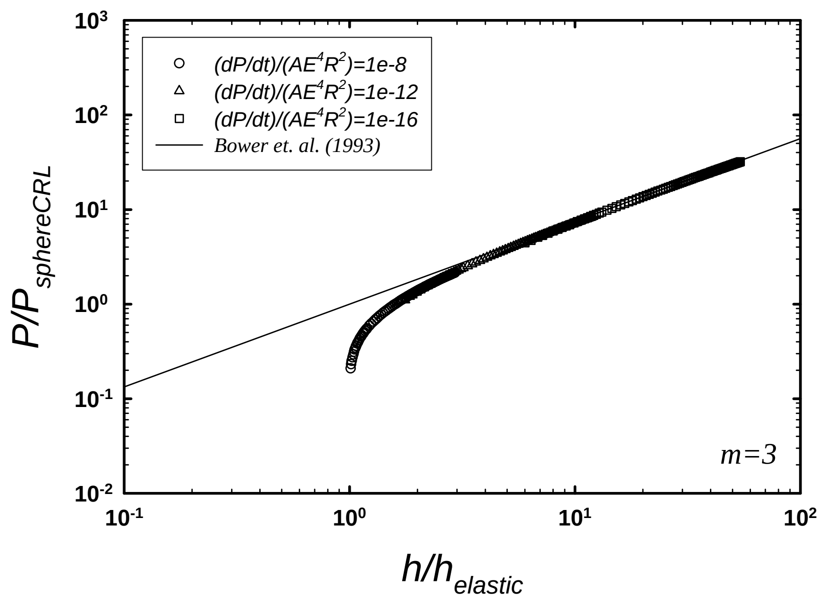

(b) Master *P*-*h* curve

Figure 32. Elastic normalization results for *m*=3 (sphere, CRL)

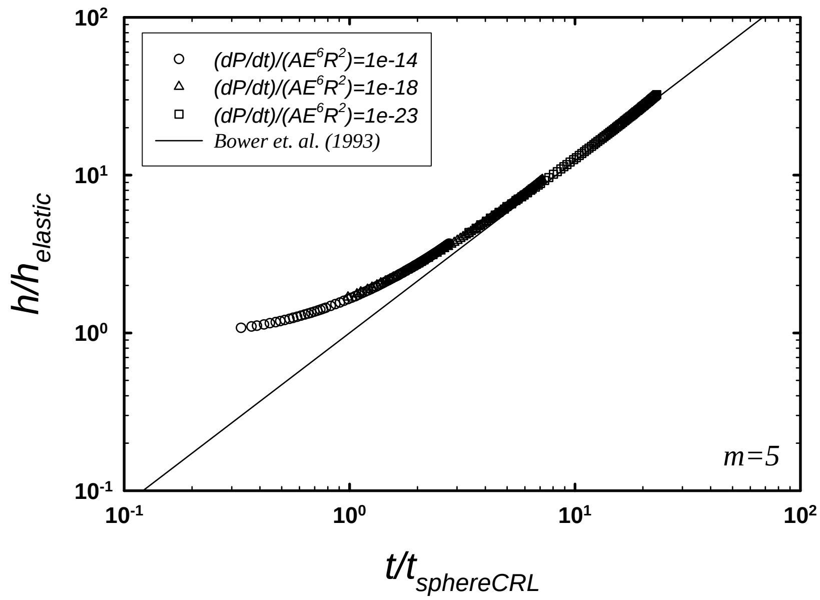

(a) Master *h*-*t* curve

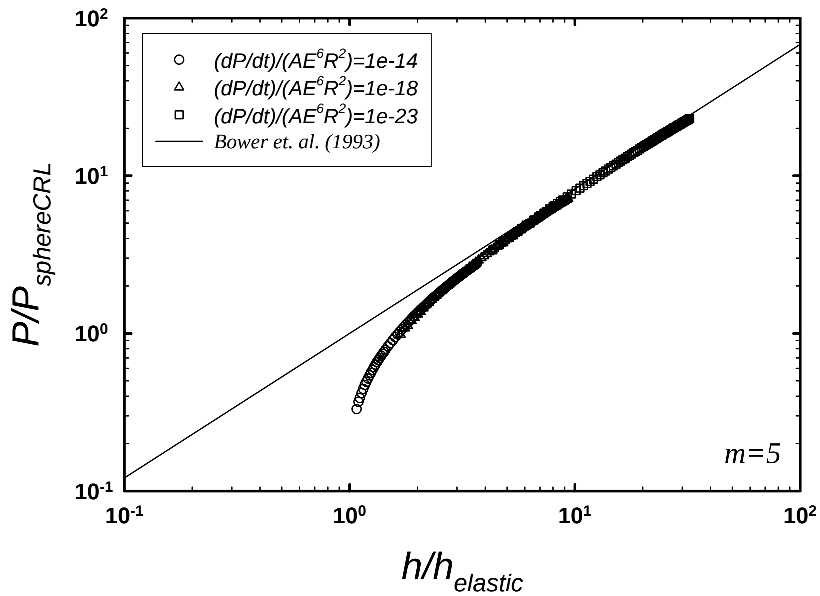

(b) Master *P*-*h* curve

Figure 33. Elastic normalization results for *m*=5 (sphere, CRL)

Results of the progressive piling up or sinking in are shown in Figures 34-36. For m=1, a transient is not observed, which is in agreement with the theoretical prediction. This is due to the similarity in pressure distribution for Hertzian elastic contact and linear viscous creep. For m>1, c is initially equivalent to the elastic value, which is $\frac{1}{\sqrt{2}}$, but as indentation progresses, it approaches the Bower *et. al.* predictions. The transient depends on the creep exponent: for larger creep exponents, larger depths are required for the elastic transient to diminish and the indentation to be dominated by pure creep deformation.

We now examine the stress distribution for spherical indentation under the CRL method. Note that due to discretization problems, we are only able to acquire stress distribution results after 10 surface elements are in contact with the indenter. Since the loading rate has a direct influence on the indentation process, stress distribution for different loading rates are investigated.

Figure 37 depicts the changes in stress distribution with respect to the indentation depth for m=1. Figure 37a represents a relatively faster loading rate ($\frac{\dot{P}}{AE^2R^2}=10^{-4}$) and Figure 37b represents a relatively slower loading rate ($\frac{\dot{P}}{AE^2R^2}=10^{-8}$). Load varies as a function of the indentation depth for the CRL method. The geometries of the deformed surfaces at different values of loading rates are not directly comparable to each other due to the elastic normalization process employed. However, we observe that the changes in stress distribution with respect to the normalized depth show results analogous to the stress distribution changes for the CLH method; that is, at very shallow depths ($h/h_{elastic}$=1.1), the stress distribution is similar to that of the elastic prediction.

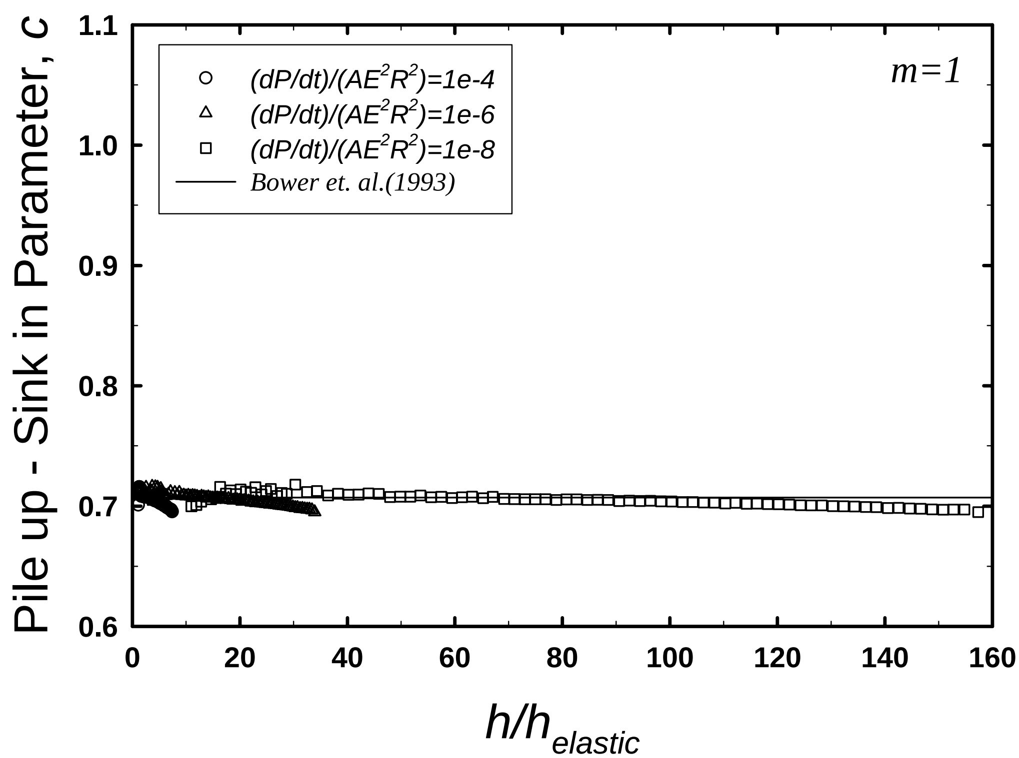

Figure 34. Changes in surface deformation for *m*=1 (sphere, CRL)

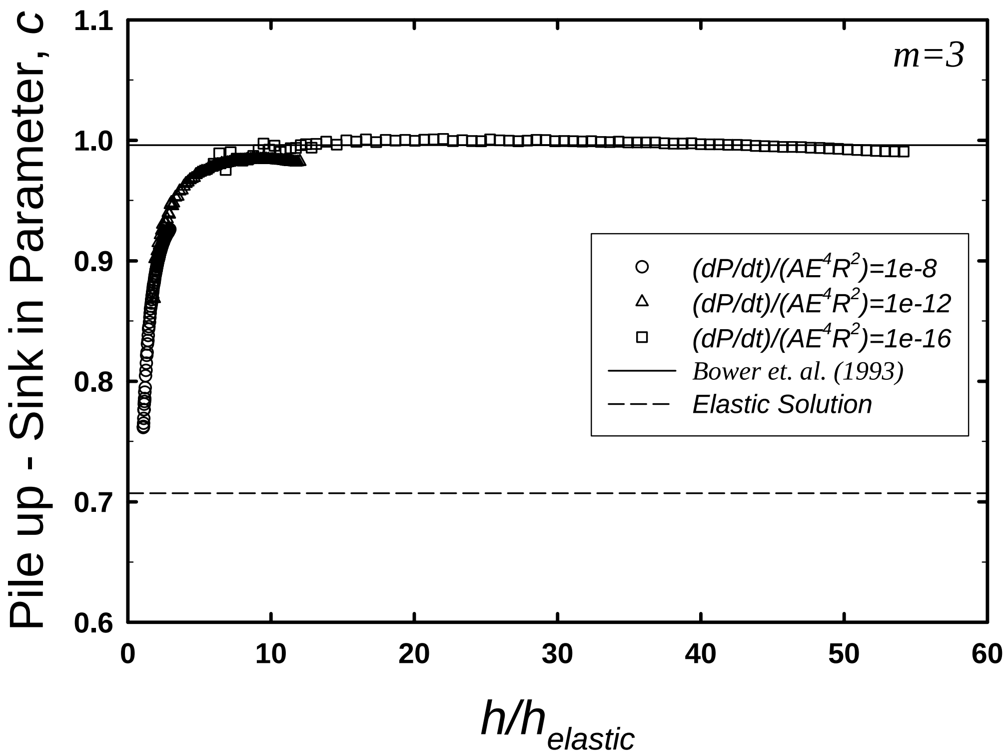

Figure 35. Changes in surface deformation for *m*=3 (sphere, CRL)

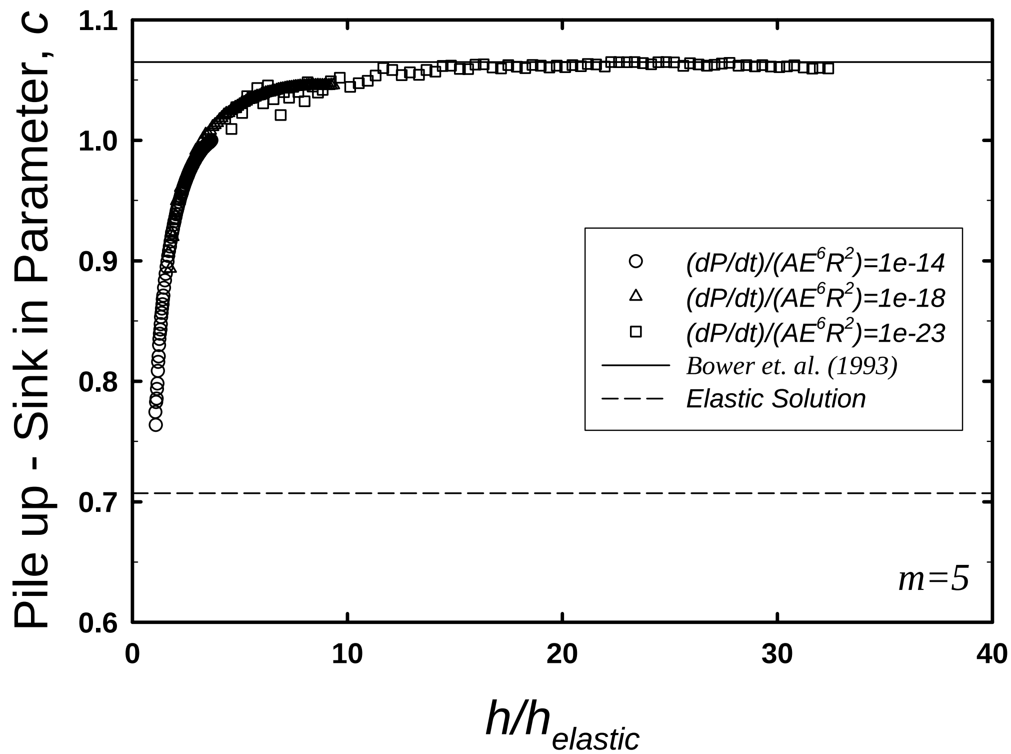

Figure 36. Changes in surface deformation for *m*=5 (sphere, CRL)

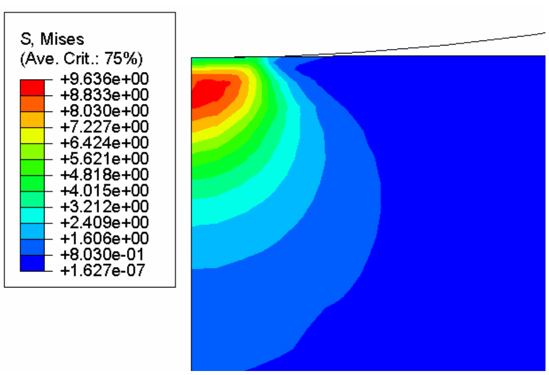

h/h_{elastic}=1.1

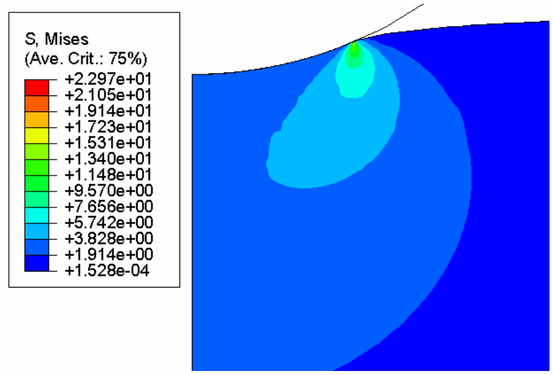

h/h_{elastic}=7.4 (maximum depth)

(a) stress distribution for m=1 at $\dfrac{\dot{P}}{AE^2R^2} = 10^{-4}$

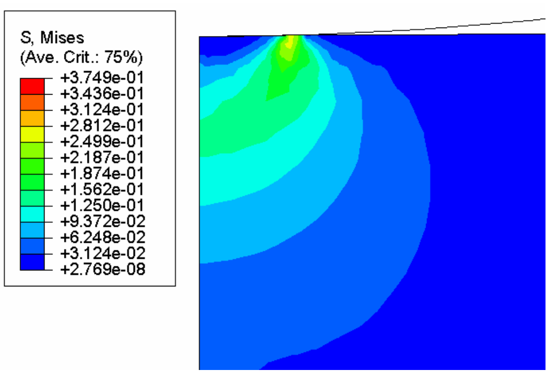

h/h_{elastic}=11

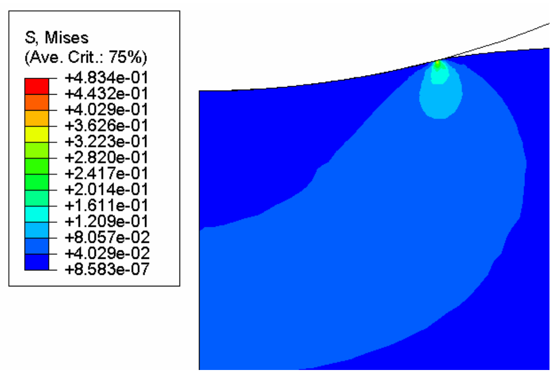

h/h_{elastic}=100 (maximum depth)

(b) stress distribution for m=1 at $\dfrac{\dot{P}}{AE^2R^2} = 10^{-8}$

Figure 37. von Mises stress distributions for m=1 (sphere, CRL)

As the indentation progresses, the von Mises stress distribution gradually changes to a fully developed creep prediction. Similar changes in stress distribution starting from the elastic prediction to the creep prediction are shown for *m*=3 and 5 in Figures 38 and 39, respectively.

The indentation strain rate – mean pressure curves are shown in Figure 40. Decoupling elasticity from creep is extremely complicated for the CRL method. Therefore, examining the behavior of changes in elastic mean pressure under varying load and the corresponding equivalent indentation strain rate is critical in order to understand the indentation strain rate – mean pressure relation. First, we need to examine the limits imposed by elasticity. To do so, we begin with Hertzian elastic solution given by equation (28). Differentiating equation (28) with respect to time, we obtain

$$\dot{h}_{\text{Hertz}} = \left[\frac{9\left(1-\nu^2\right)}{16RE^2}\right]\left(\frac{2P^{-\frac{1}{3}}}{3}\right)\left(\dot{P}\right) \tag{37}$$

where the elastic contact radius [29] is given by equation (38):

$$a_{\text{Hertz}} = \left[\frac{3\left(1-\nu^2\right)PR}{4E}\right]^{\frac{1}{3}} \tag{38}$$

Dividing equation (37) by equation (38), we obtain a variable analogous to an indentation strain rate:

$$\left(\frac{\dot{h}_{\text{Hertz}}}{a_{Hertz}}\right) = \left[\frac{2\left(1-\nu^2\right)}{9ER^2P^2}\right]^{\frac{1}{3}}\left(\dot{P}\right) \tag{39}$$

We may rewrite equation (39) in terms of elastic mean pressure, giving

$$\left(\frac{\dot{h}_{\text{Hertz}}}{a_{\text{Hertz}}}\right) = \frac{8\dot{P}E}{9\left(1-\nu^2\right)\pi^2R^2\left[\left(p_{\text{mean}}\right)_{\text{Hertz}}\right]^2} \tag{40}$$

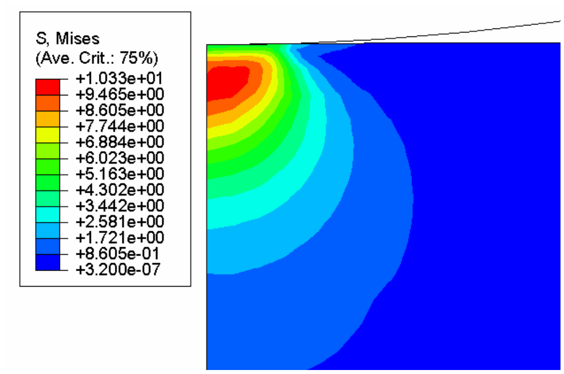

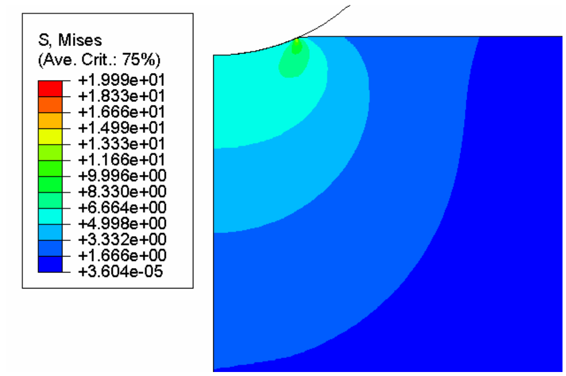

h/h_{elastic}=1.01 h/h_{elastic}=3 (maximum depth)

(a) stress distribution for m=3 at $\dfrac{\dot{P}}{AE^4R^2} = 10^{-8}$

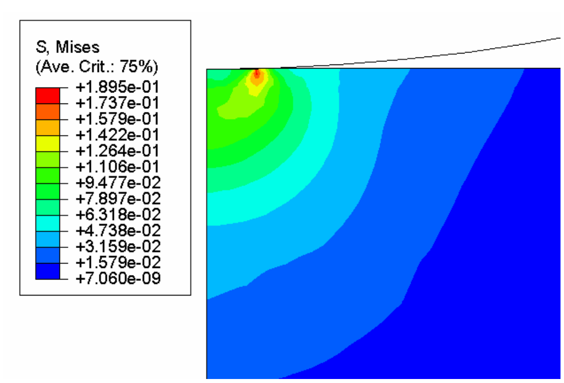

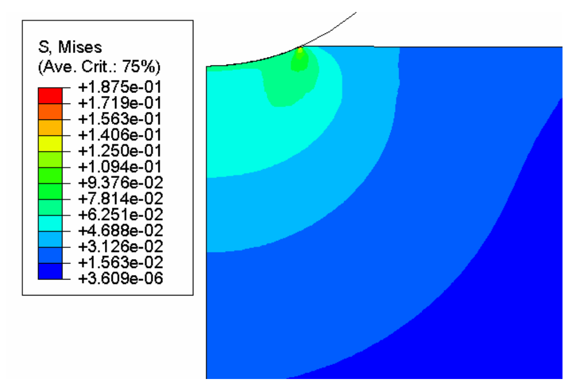

h/h_{elastic}=6 h/h_{elastic}=54 (maximum depth)

(b) stress distribution for m=3 at $\dfrac{\dot{P}}{AE^4R^2} = 10^{-16}$

Figure 38. von Mises stress distributions for *m*=3 (sphere, CRL)

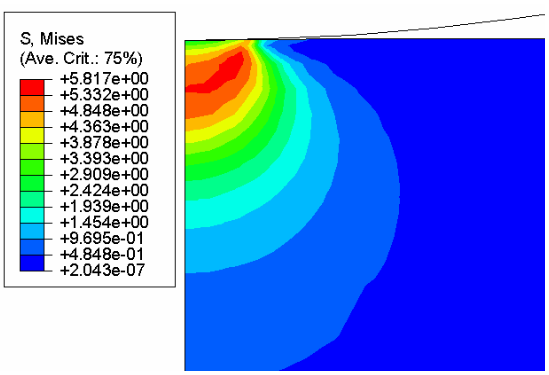

h/h_{elastic}=1.1

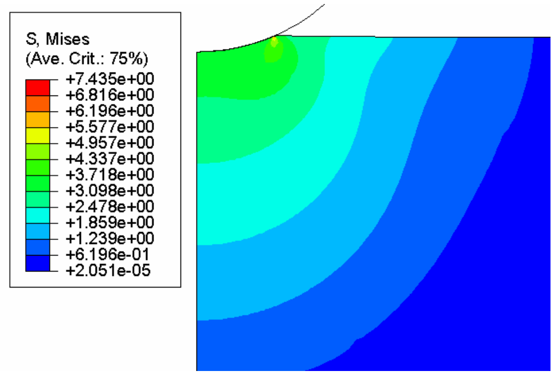

h/h_{elastic}=3.7 (maximum depth)

(a) stress distribution for m=5 at $\dfrac{\dot{P}}{AE^6R^2} = 10^{-14}$

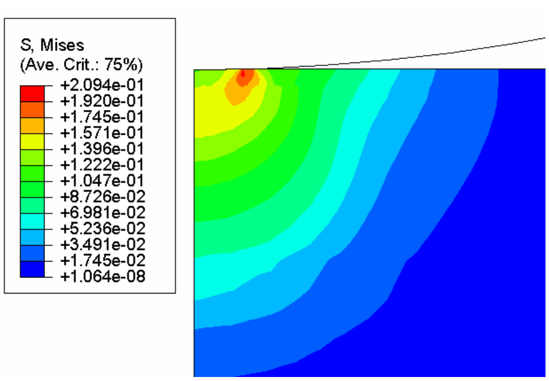

h/h_{elastic}=4.3

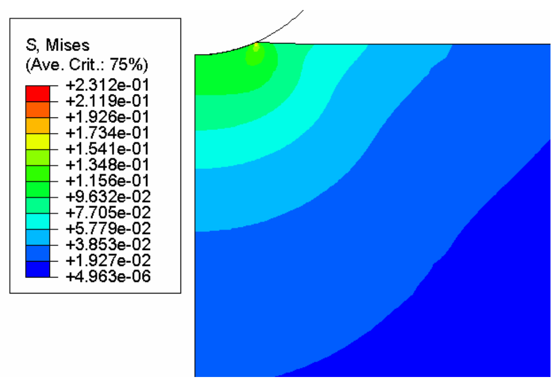

h/h_{elastic}=32 (maximum depth)

(a) stress distribution for m=5 at $\dfrac{\dot{P}}{AE^6R^2} = 10^{-23}$

Figure 39. von Mises stress distributions for *m*=5 (sphere, CRL)

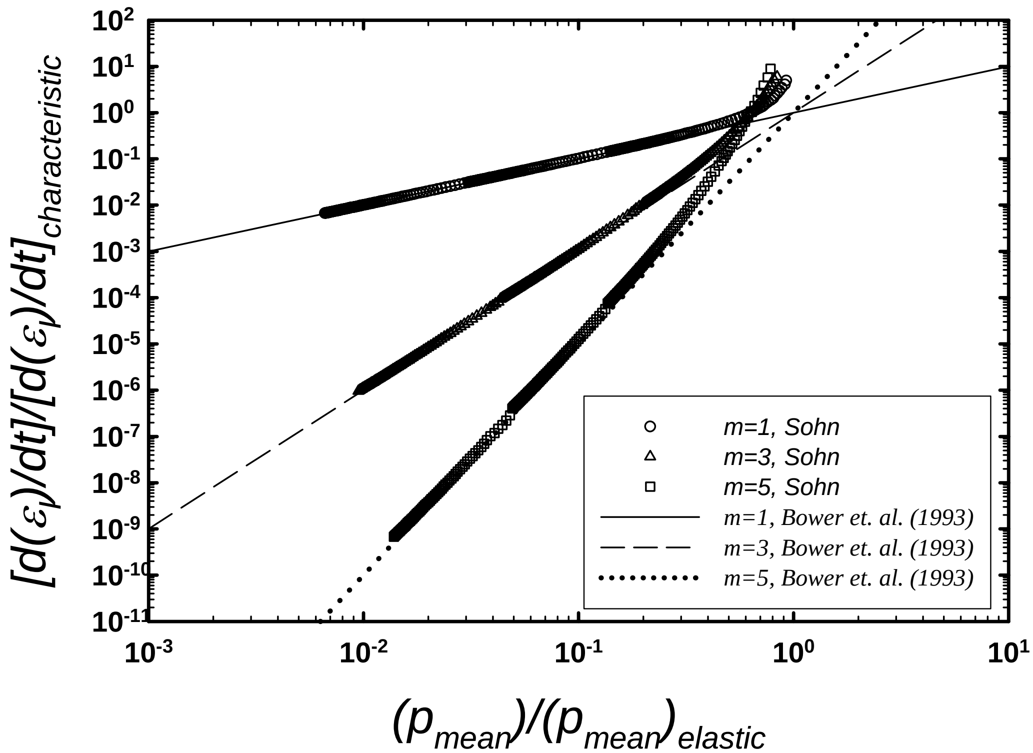

Figure 40. Indentation strain rate – mean pressure curves (sphere, CRL)

Physical interpretation of equation (40) is ambiguous due to the rate-dependent terms displayed in elastic solutions. However, equation (40) should yield the maximum permissible equivalent indentation strain rate under varying elastic mean pressure. For clarification, we rewrite equation (40) as:

$$\left(\dot{\varepsilon}_I\right)_{\text{Maximum}} = \frac{8\dot{P}E}{9\left(1-\nu^2\right)\pi^2 R^2\left[\left(p_{\text{mean}}\right)_{\text{Hertz}}\right]^2} \tag{41}$$

Figure 41 schematically shows the maximum permissible indentation strain rate combined with the Bower *et. al.* prediction of the creep indentation strain rate as a function of mean pressure. During the initial stages of indentation, the indentation strain rate – mean pressure relation follows the upper portion of the curve represented by a slope of negative 2. If the deformation was governed entirely by elasticity, the indentation strain rate – mean pressure relation would proceed along this curve described with slope of negative 2. As power law creep starts to have influence on the deformation, indentation strain rate – mean pressure relation makes a gradual transition to the power law creep curve shown as the dotted line in Figure 41. This results in a knee-shaped curve in the transient regime. Therefore, we conclude from Figure 41 that regardless of the creep exponent, the indentation strain rate – mean pressure relation for an elastic – power law creeping solid under the CRL method exhibits transient phenomena. Evidence of this is shown Figure 40 as the deviations from the Bower *et. al.* solution, even for m=1.

Sensitivity of output data analysis influenced by elasticity

The sensitivity of creep parameter prediction to the elastic transient in the CRL method is illustrated in Figure 42, which shows results for both the *h-t* and *P-h* behaviors. Both of these data sets produce the same results.

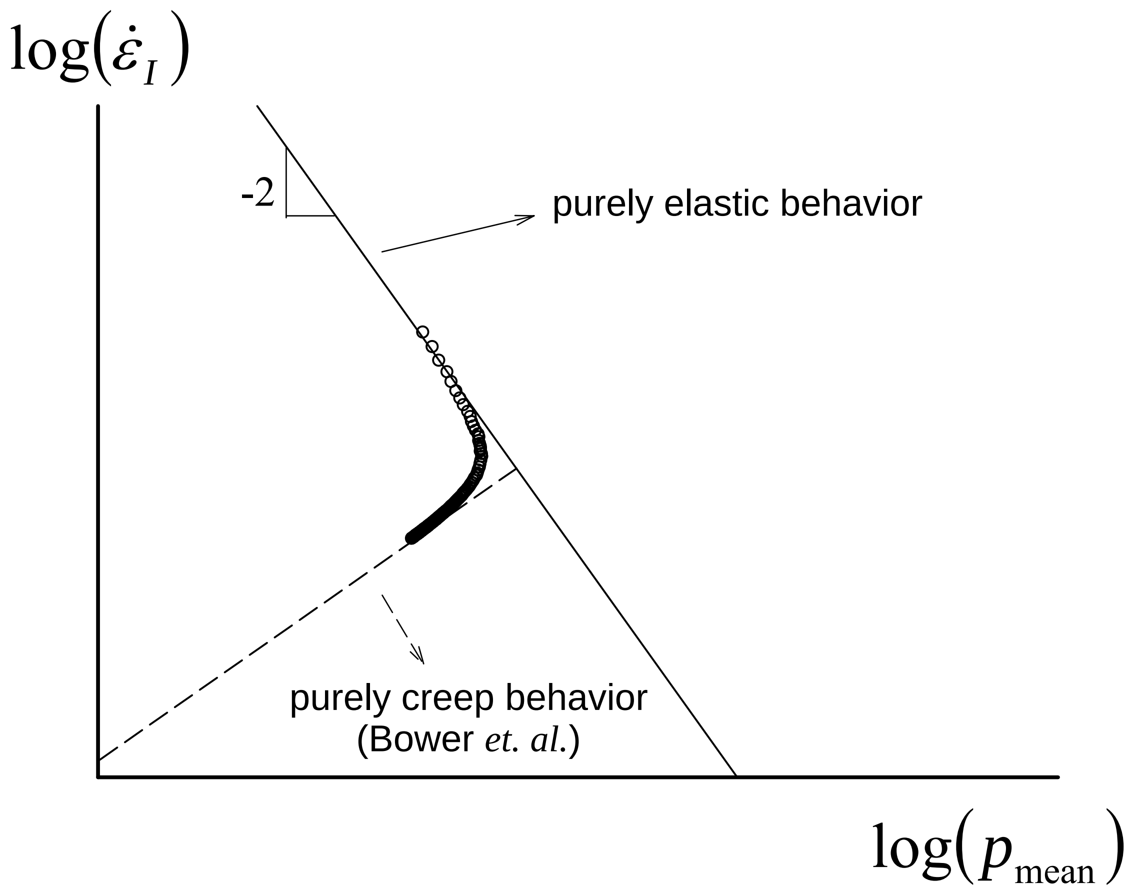

Figure 41. Limiting curves of indentation strain – mean pressure (sphere, CRL)

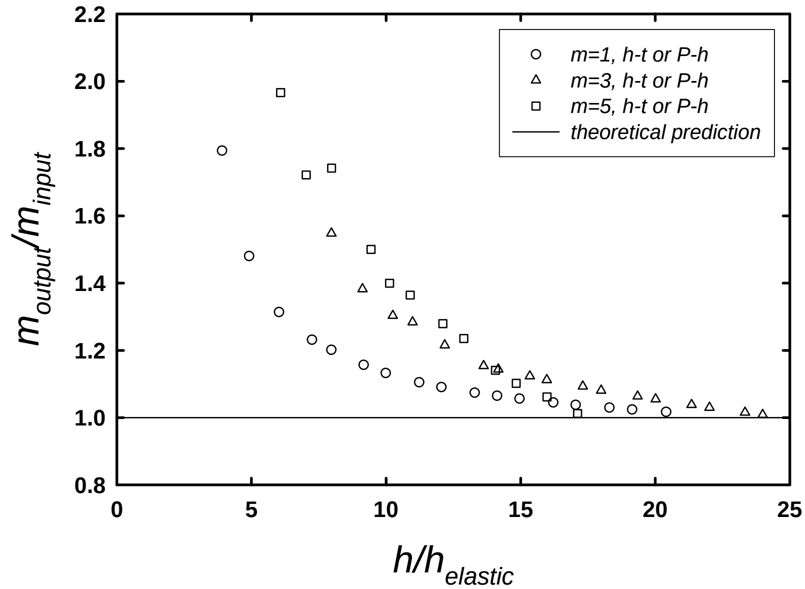

(a) Changes in output creep exponent

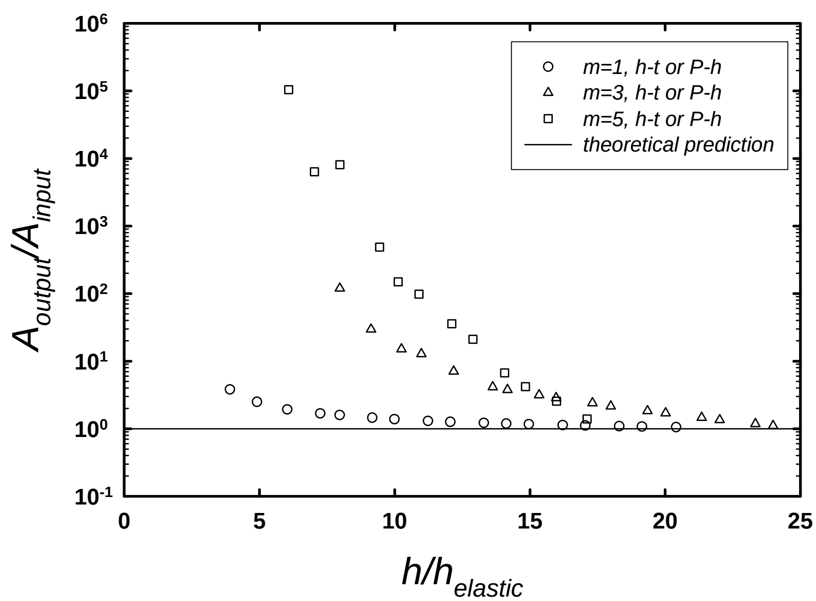

(b) Changes output uniaxial creep coefficient

Figure 42. Changes in output uniaxial creep parameters (sphere, CRL)

The error in the creep exponent reduces to less than 10% only at a depth of h/h_{elastic}=20. The uniaxial creep coefficient A is very sensitive to elasticity, as seen in Figure 40b. The error covers several orders of magnitude. Thus, caution must be exercised when estimating the uniaxial creep coefficient from spherical indentation under the CRL method.

c(m) and *F(m)* for Rigid – Power Law Creeping Solid Using Conical Indenters

Uniaxial creep parameter prediction from indentation based on the similarity transformation [6] assumes infinitesimal deformation – infinitesimal strain. For spherical indentation, the effective strain [30] is described by

$$\varepsilon_{\text{sphere}} = \left(\frac{a}{R}\right) \tag{42}$$

The radius of contact or correspondingly the depth of indentation thus clearly has a direct influence on the effective strain. Bower *et. al.* suggest that $\left(\frac{a}{R}\right) < 0.4$ to avoid difficulties [19]. For conical indentation, the effective strain [29] is often described by

$$\varepsilon_{\text{cone}} = 0.2\cot\beta \tag{43}$$

Thus, for indenters with smaller half-included cone angles β, the influences of finite strain may be important.

Here, the influences of finite deformation – finite strain for conical indentation are addressed. The main purpose is to provide *c(m)* and *F(m)* for conical indentation in a manner that accounts for the finite strains. Half-included cone angles of 60°, 70°, and 80° will be considered with emphasis on the 70° half-included cone angle, which is the conical equivalent of the Berkovich indenter. The CRL method is employed to conduct this study, with the *P-h* curve being the preferred data for analysis. In the CRL method, the applied load starts at zero and increases with time. From a simulation perspective, this enables better convergence when larger creep exponents are considered. Therefore, simulation results for larger creep exponents are more easily obtained using the CRL method.

Determining the uniaxial creep exponent from h-t or P-h curves

m can be predicted from either the *h-t* or *P-h* curve as outlined in Chapter 3, provided that the solid behaves in a rigid – power law creeping manner. Unfortunately, finite element modeling does not provide the capabilities of rigid – power law creeping constitutive relation [27]. As a consequence, elasticity must be built in to the constitutive law, and accordingly, a transient due to this elasticity is unavoidable. Accuracy is examined by comparing the FEM *h-t* or *P-h* curve for a given creep exponent to the theoretical rigid – power law creep *h-t* or *P-h* curves. This is demonstrated in Figure 43. Figure 43a shows the *h-t* curves obtained from indentation for several different creep exponents at very long times after the elastic transient has subsided. A conical indenter with half-included cone angle of 70° was used to generate the data. The *h-t* data have been produced at different loading rates for different creep exponents, all of which are representative of relatively slow loading rates. Each *h-t* curve shown is a power law regression to the FEM data. The creep exponent has been calculated from the slope of log*h*-log*t* curves by means of equation (24). For, the input values are noted. For a truly rigid elastic – power law creeping solid, output slope should be identical to the input slope. The output slopes are all within 1% of deviation from the input, implying that elasticity does not have a significant influence on these results.

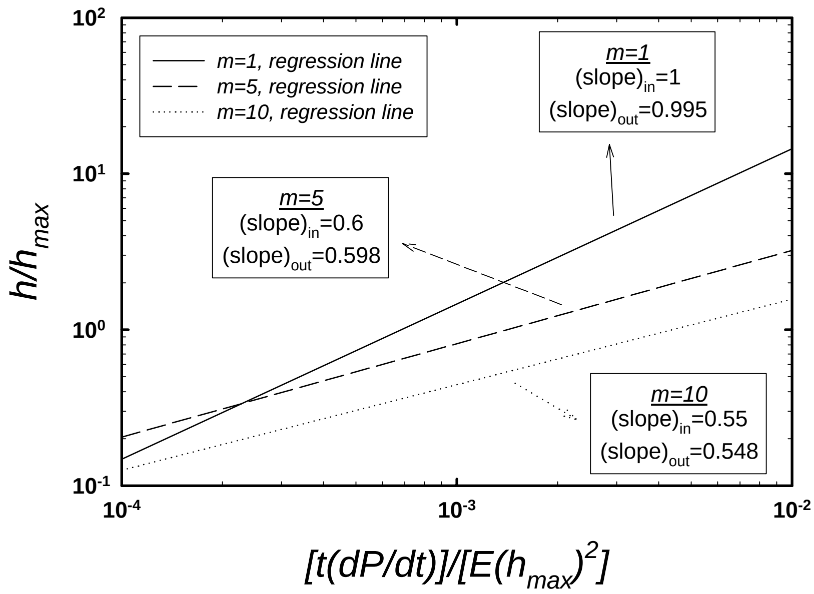

(a) *h*-*t* curves for various *m*

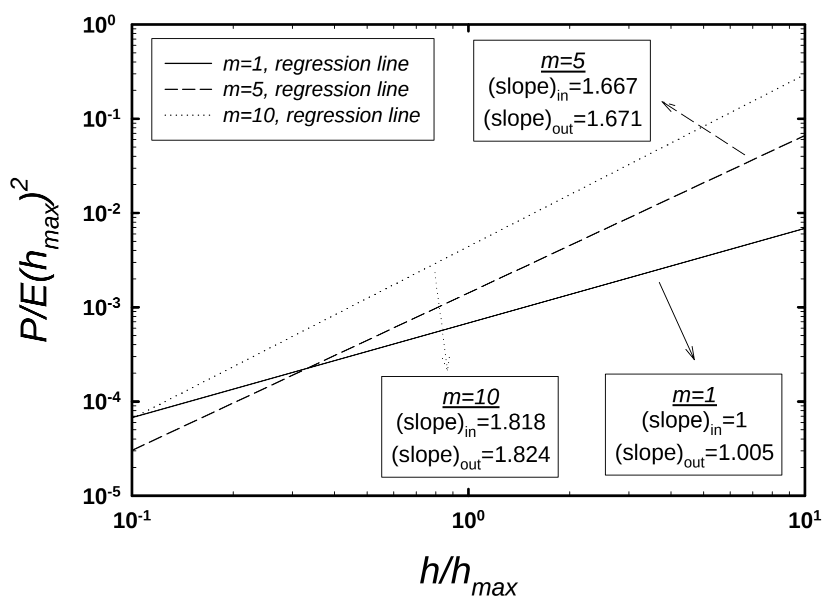

(b) *P*-*h* curves for various *m*

Figure 43. Comparison of output to input *h-t* or *P-h* slopes (70° cone, CRL)

Similar results are shown for of P-h curves in Figure 41b, where the output slopes have been extracted using equation (25). Therefore, we are capable of simulating rigid – power law creeping behavior by controlling the loading rates to small values, and the output creep exponents obtained from relatively slow loading rates should be representative of a rigid – power law creeping solid. Figure 44 depicts the accuracy of output creep exponent produced by finite element simulation. Results are shown for the three different half-included cone angles used in this study. Intuitively, the simulations performed with larger creep exponents are expected to yield results with larger errors induced by the nonlinearity in the constitutive law. The maximum deviation of output creep exponent from the input value is less than 3%. Based on the output creep exponent analysis, we conclude that the creep results derived in this section are free from errors caused by the elastic transient. Supplementary proof of the unimportance of the elastic transient is given in Figure 45. For a rigid – power law creeping solid, piling up or sinking in of the surface should be independent of indentation depth and only a function of the creep exponent for infinitesimal strain – infinitesimal deformation assumption [19]. Figure 45 demonstrates this fact for indentation with a conical indenter of 70° half-included cone angle. In Figure 45, it is seen that by selecting data for depths that are larger than 40% of the maximum depth, the pile up – sink in parameter c is constant. Therefore transients are unimportant when small depth data are discarded. This procedure has been exercised throughout the analysis in this section.

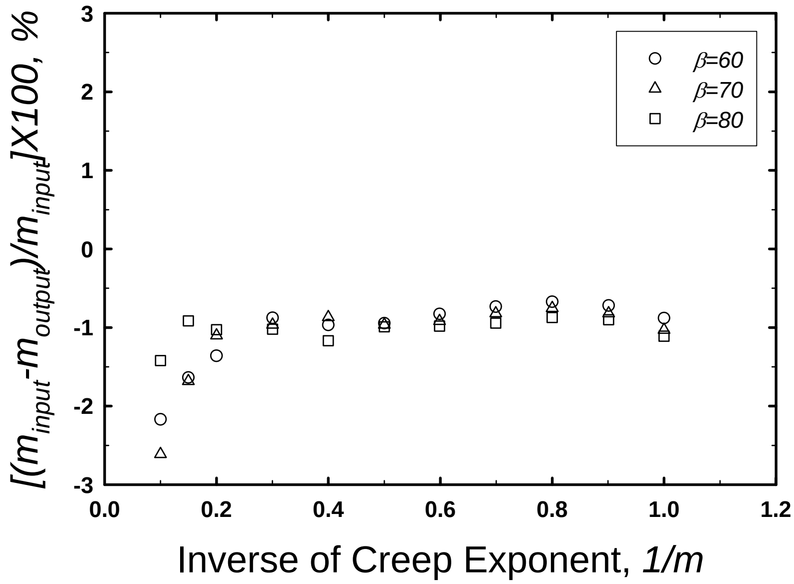

Figure 44. Accuracy of modeling rigid – power law creeping behavior

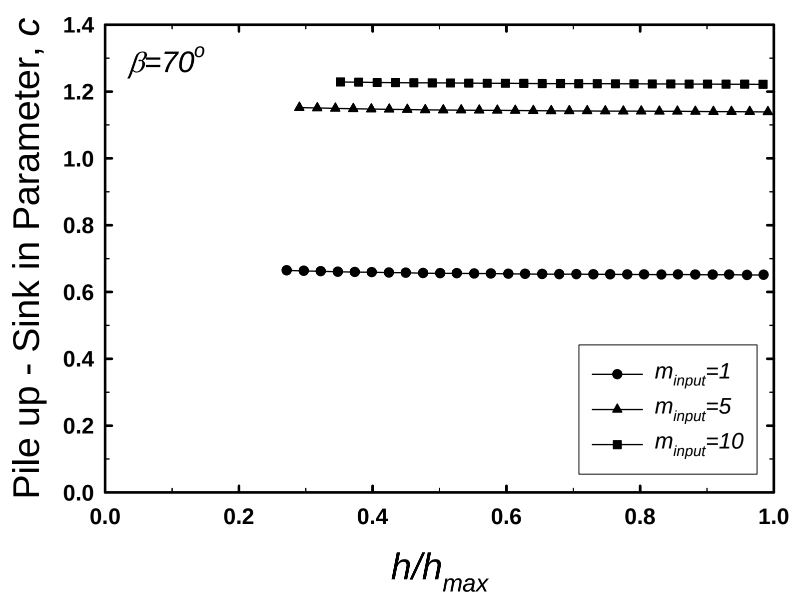

Figure 45. *c* independent of depth

Indentation creep solutions for conical indenters

According to equation (25), m is directly derivable from the *P*-*h* creep relationship. However, the uniaxial creep coefficient A is not readily available, but may be obtained from the intercept of a log*P*-log*h* plot, which gives the indentation creep coefficient B. Therefore, a knowledge of the relationship between the two creep coefficients is required in order to fully predict uniaxial creep parameters from indentation. Most of the variables in the lumped coefficient representing the intercept in equation (25) are known values from the loading conditions, the geometry of the indenter, or the slope of the log*P*-log*h* in the log linear regime. The only exception is c. The dependence of c on the creep exponent for different half-included cone angles is shown in Figure 46. The Bower *et. al.* solution also shown in the figure is derived under the assumption of infinitesimal strain – infinitesimal deformation. For the conical indenter, the half-included cone angle has to approach 90° for this assumption to be strictly valid. Therefore, blunt cones approaching the geometry of a flat punch indenter have to be used in order to produce such results. The results in Figure 46 show that the blunt indenter behavior is approached, but the non-90° cone angles produce deviations from the Bower *et. al*. prediction that could be significant. Solutions for the relations of pile up – sink in parameter c and the inverse of creep exponent $1/m$ derived in this study for different half-included cone angles fit well to a 3rd order polynomial regression.

$$c(m,\beta) = c_0 + c_1\left(\frac{1}{m}\right) + c_2\left(\frac{1}{m}\right)^2 + c_3\left(\frac{1}{m}\right)^3 \tag{44}$$

The parameters of the regression are given in Table 6.

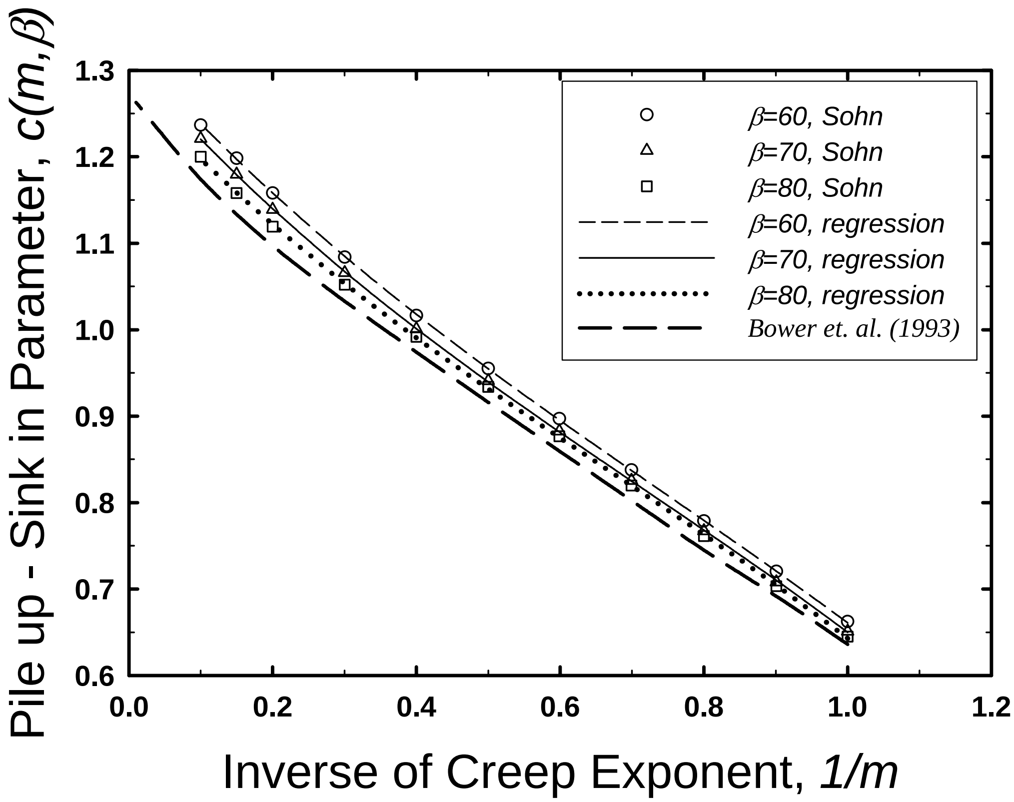

Figure 46. Pile up – sink in solution for conical indenters

Table 6. Fit parameters for *c(m,β)* equations

β	c_0	c_1	c_2	c_3
60°	1.326	-0.925	0.470	-0.210
70°	1.310	-0.948	0.540	-0.252
80°	1.281	-0.884	0.493	-0.247

We note that piling up or sinking in of the surface as a function of creep exponent has a weak but possibly important dependence on the half-included cone angle of the conical indenter.

With the information regarding *c*, we are now able to determine the indentation creep coefficient, *B*. The prediction of unaxial creep coefficient from indentation involves a functional relationship between *B* and *A*. This is achieved by the reduced contact pressure, $F(m)=(A/B)^{1/m}$. The definition of *F(m)* is given in equation (9). The dependence of $F(m,\beta)$ on β and *m* is shown in Figure 47. The relations between *F(m)* and *1/m* derived here fit well to a 4th order polynomial regression:

$$F(m,\beta) = F_0 + F_1\left(\frac{1}{m}\right) + F_2\left(\frac{1}{m}\right)^2 + F_3\left(\frac{1}{m}\right)^3 + F_4\left(\frac{1}{m}\right)^4 \tag{45}$$

The parameters of the regression are given in Table 7. The functional relationship in Figure 47 shows weak dependence on the half-included cone angle for small creep exponent values. For larger creep exponents, the half-included cone angle is more important. The $c(m,\beta)$ and $F(m,\beta)$ functions presented here should serve as references in predicting uniaxial power law creep parameters from indentation when conical indentations are considered.

$c(m,\beta)$ and $F(m,\beta)$ in the limiting cases

$c(m,\beta)$ and $F(m,\beta)$ are bounded by two natural limiting values when plotted as the inverse of the creep exponent, $1/m$. $1/m=1$ implies a linear viscous solid, which behaves analogous to a linear elastic solid. When $1/m=0$, *m* approaches infinity. This represents a rigid – perfectly plastic solid. For this special case, we are able to redefine $F(m,\beta)$ in terms of purely plastic deformation.

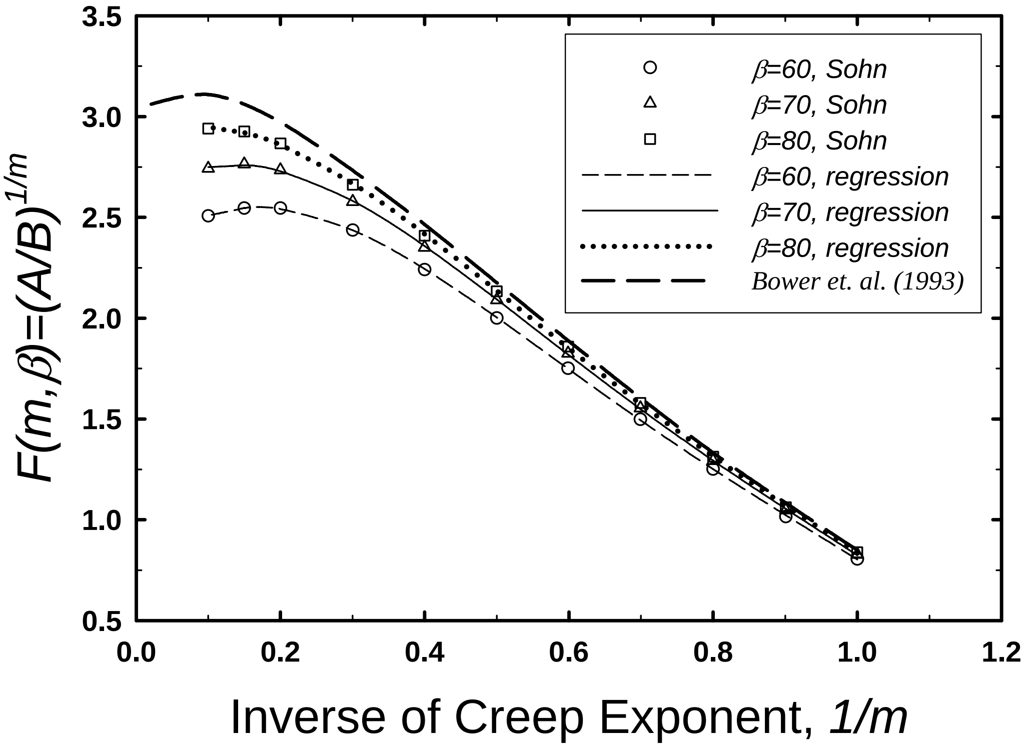

Figure 47. Creep coefficients correlation for conical indenters

Table 7. Fit parameters for *F(m,β)* equations

β	F_0	F_1	F_2	F_3	F_4
60°	2.280	3.496	-13.253	12.349	-4.069
70°	2.588	2.745	-12.428	11.915	-3.996
80°	2.889	1.522	-10.242	10.074	-3.407

Rewriting $F(m,\beta)$ with equations (12) and (13), $F(m,\beta)$ is given by

$$F(m,\beta)=\left(\frac{A}{B}\right)^{\frac{1}{m}}=\left[\frac{\dfrac{\dot{\varepsilon}}{\sigma^{m}}}{\dfrac{\dot{\varepsilon}_{I}}{\left(p_{\text{mean}}\right)^{m}}}\right]^{\frac{1}{m}} \tag{46}$$

Rearranging equation (46) yields

$$F(m,\beta)=\left(\frac{\dot{\varepsilon}}{\dot{\varepsilon}_{I}}\right)^{\frac{1}{m}}\left(\frac{p_{\text{mean}}}{\sigma}\right) \tag{47}$$

For a rigid – plastic solid with $m=\infty$, σ becomes σ_y. Thus, equation (47) may be rewritten as:

$$F(\infty,\beta)=\left(\frac{p_{\text{mean}}}{\sigma_{y}}\right) \tag{48}$$

provided that the ratio of uniaxial strain rate to indentation strain rate is finite. Equation (48) is the definition of constraint factor [31] for a rigid – perfectly plastic solid. Therefore, we are able to obtain creep solutions for m approaching infinity by simulating elastic – time independent perfectly plastic behavior. Figure 48 shows FEM results for $c(\beta)$ and $F_c(\beta)$ for time independent plasticity. $c(\beta)$ is the pile up – sink in parameter and $F_c(\beta)$ is the constraint factor, both of which show a dependence on the half-included cone angle. $c(\beta)$ is apparently affected by elasticity for smaller values of E/σ_y. As E/σ_y increases, $c(\beta)$ approaches constant values which represent rigid – perfectly plastic solutions. The same trend is observed for $F_c(\beta)$. Figures 46 and 47 are replotted to include the limiting case of m approaching infinity in Figures 49 and 50, respectively. In Figure 48, a decrease in $F(m,\beta)$ for small $1/m$ after experiencing a peak is observed for results with conical indenters. Bower *et. al.* also observed this peak.

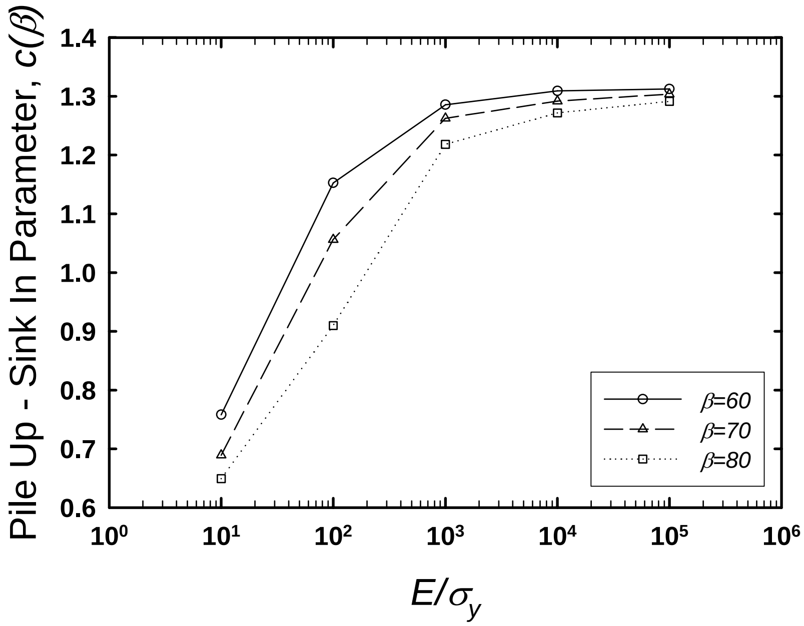

(a) c for various half-included cone angles

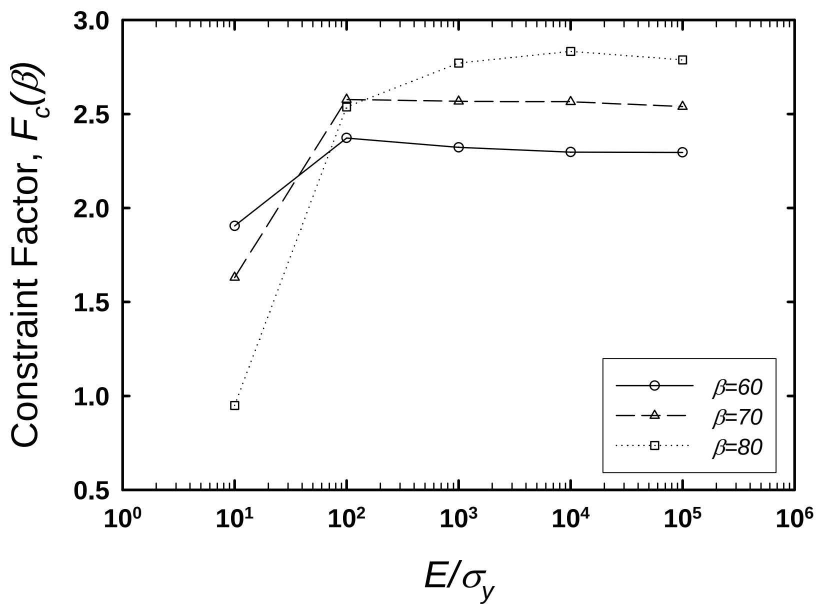

(b) F_c for various half-included cone angles

Figure 48. *c* and F_c for time independent plasticity

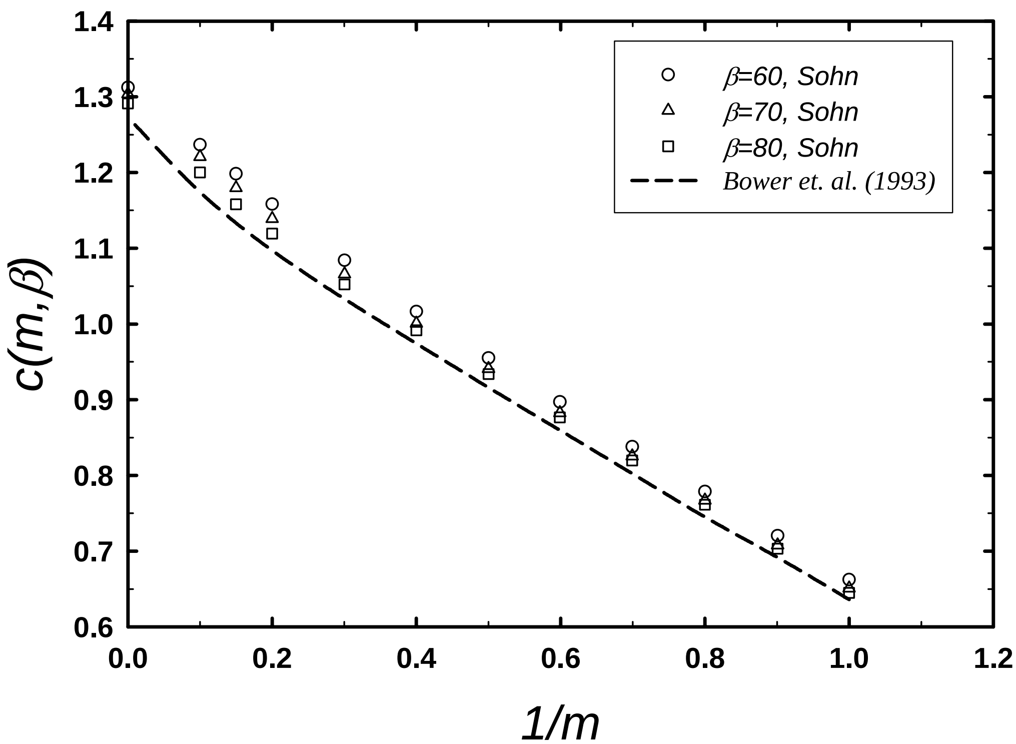

Figure 49. Extended *c(m,β)* curve

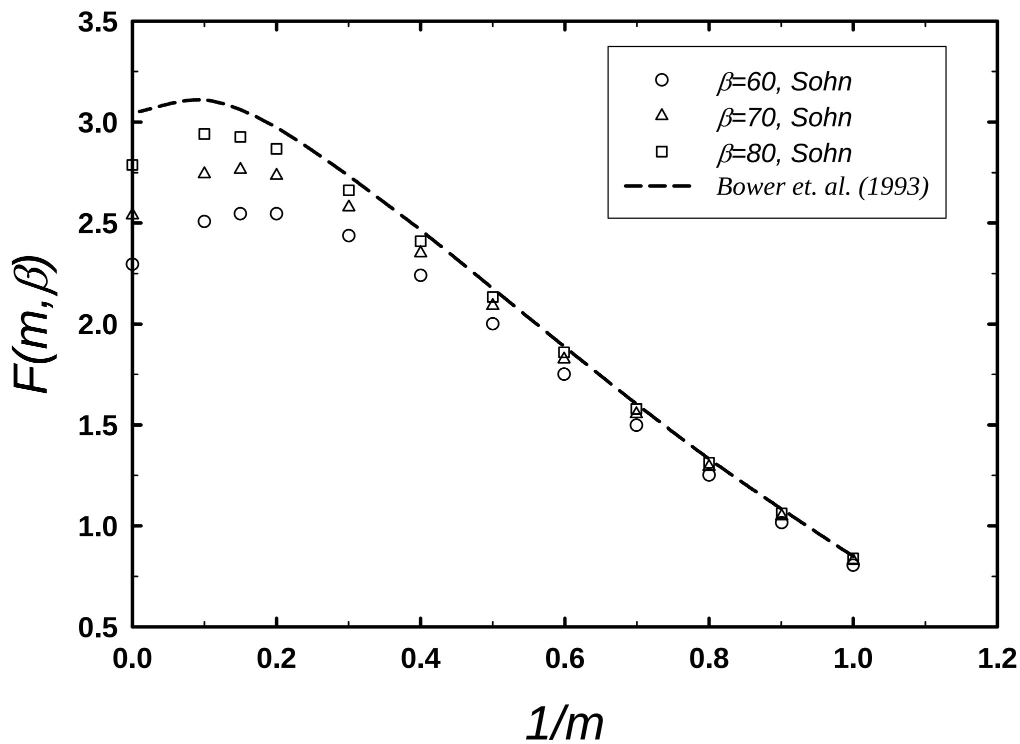

Figure 50. Extended *F(m,β)* curve

Elastic-Creep Transients for Conical Indentation under the CLH Method

The functions $c(m,\beta)$ and $F(m,\beta)$ obtained for conical indentation in the previous section allow us to investigate the elastic creep transient phenomenon for conical indenters. The manner in which the study is carried out is similar to the study of the elastic transient for spherical indentation, as given earlier in this chapter. We will initially explore the transient under the CLH method for various half-included cone angles.

Indentation process under the CLH method with conical indenters

The deformation process for the CLH indentation under conical indenters is described by a procedure analogous to spherical indentation under the CLH method, with the exception that the indenter is treated as conical shape. Upon loading, instantaneous elastic impression is followed by creep deformation. Similar to indentation with the spherical indenter, data is collected as creep progresses, thereby representing time dependent deformation with a transient appearing in the early stages of the *h-t* curves. Conical indenters with half-included cone angles of 70° and 80° are considered.

Simulation attempts with a 60° cone were unsuccessful due to convergence problems. In finite element simulation, the process of indentation is partitioned into small increments. Force equilibrium and moment equilibrium must be satisfied in order to progress to the next increment. When convergence is not satisfied at any given increment, the finite element code automatically recalculates the given time increment, with a smaller increase in input values, until equilibrium is satisfied. Convergence becomes a problem when the minimum value in the increment reaches a limit set by the code. In viscoplastic analysis, this limit is set by time. The time limit for the minimum range of creep integration is 10^{-40} [27]. For indentation with a 60° cone, this limit was reached in the first few attempts due to relatively large amount of effective strain imposed on the deformable solid. Therefore, convergence was not achieved and the calculation aborted. However, for 70° and 80° cones, the effective strain was small enough to achieve equilibrium at a finite number of calculation attempts.

Indentation h-t curves for conical indentation

Figure 51 shows the indentation *h-t* curves from conical indentation with the CLH method for m=1. All indentations were performed to the same maximum depth. Overlapping of *h-t* curves is achieved when normalized load, $\frac{P}{E(h_{\max})^2}$ is identical. Figures 52 and 53 are similar *h-t* curves for m=3 and 5, respectively. Analogous results demonstrating successful dimensional analysis are observed in these figures. Transients are shown as deviations from log linearity at shallower depths or shorter times of indentation.

Elastic normalization for conical indentation under the CLH method

Similar to spherical indentations, elasticity provides a way to further normalize the results for conical indentations. In the elastic normalization process for conical indentation, we use Sneddon's [31] elastic solutions for indentation by a rigid cone. The elastic depth for conical indentation is employed in normalizing the indentation depth. The equation for the elastic depth is

$$h_{\text{Sneddon}} = \left[\frac{\pi P\left(1-\nu^2\right)}{2E\tan\beta}\right]^{\frac{1}{2}} \tag{49}$$

For derivation of a characteristic time, we adopt the same procedure used for spherical indentation under the CLH method.

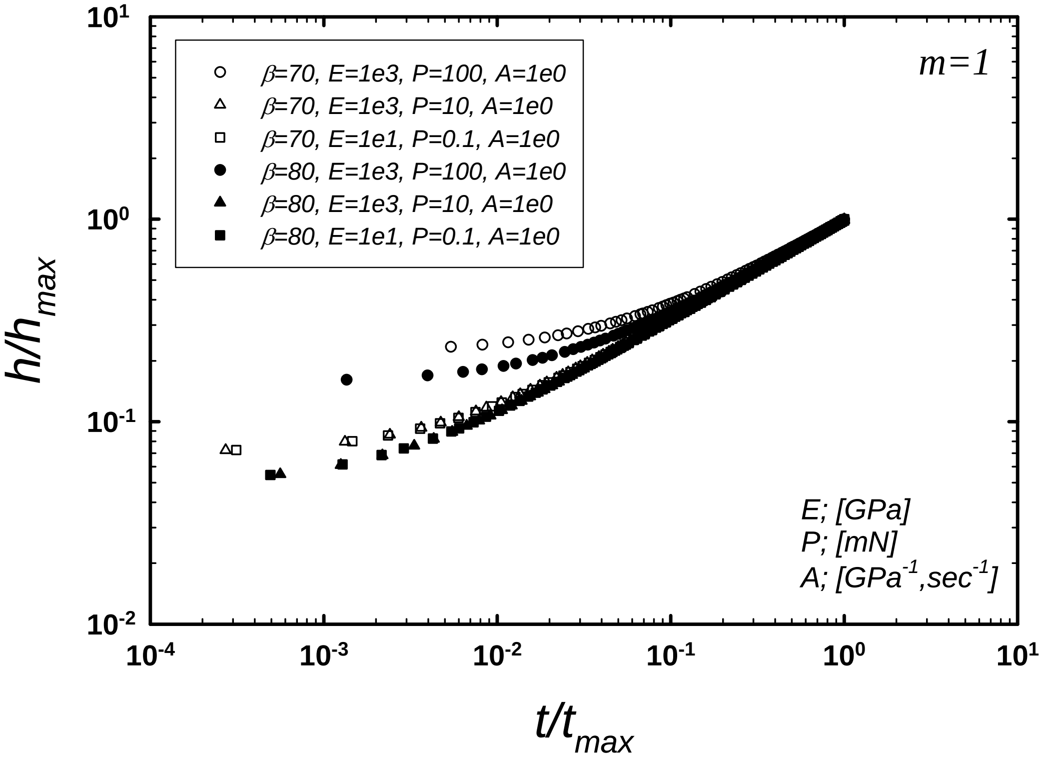

Figure 51. ***h-t*** **curves for** ***m*****=1 (cone, CLH)**

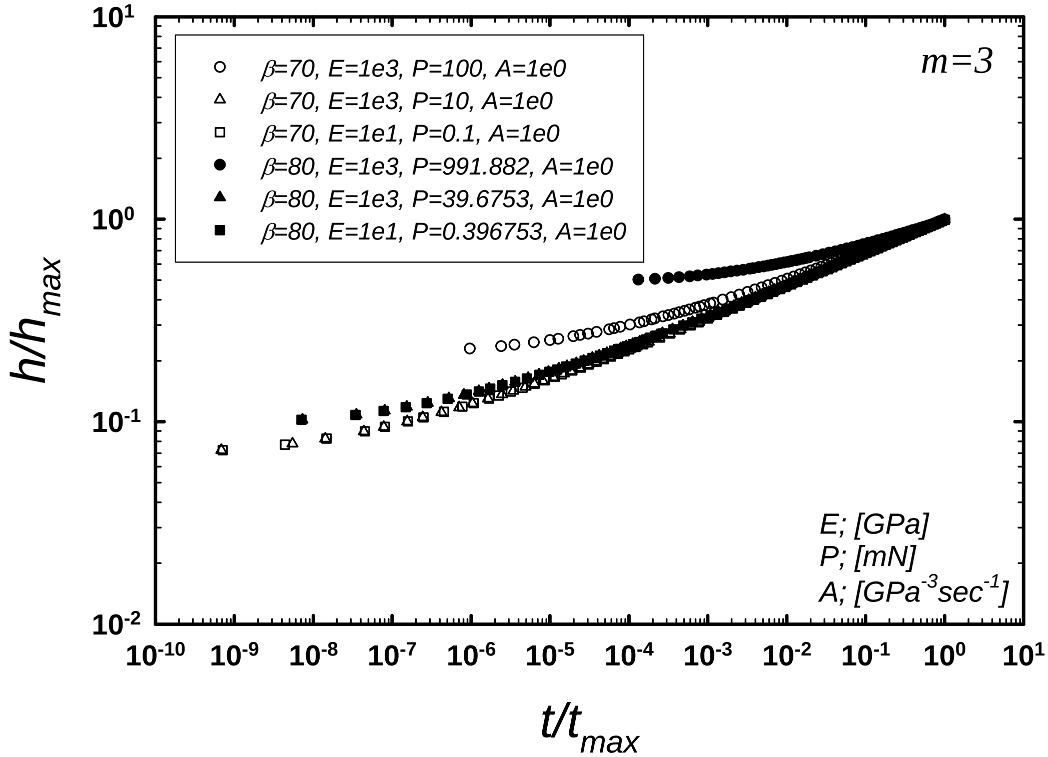

Figure 52. ***h-t*** **curves for** ***m*****=3 (cone, CLH)**

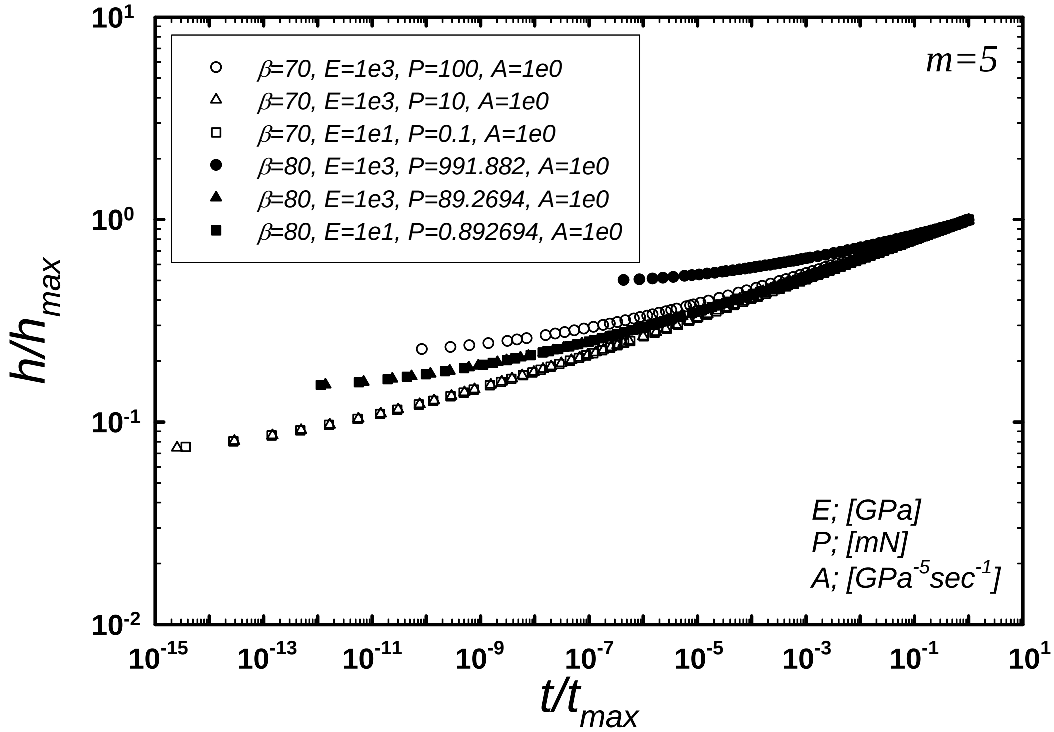

Figure 53. *h*-*t* curves for *m*=5 (cone, CLH)

From the rigid – power law creep *h-t* relationship for conical indentation under the CLH method (equation (22)), we replace h_{creep} with h_{Sneddon} in equation (22) and solve for *t*. We define this variable as the characteristic time for conical indentation under the CLH method, t_{coneCLH}. The mathematical expression for t_{coneCLH} is

$$t_{\text{coneCLH}} = \left[\frac{\pi^{2m}\left(1-\nu^2\right)^m}{E^m Bm\left(2^{m+1}\right)\left(c^{1-2m}\right)\left(\tan\beta\right)^{1-m}} \right] \tag{50}$$

Physically, t_{coneCLH} is indentation time required to achieve twice the elastic depth. Note that this variable has no dependence on the applied load. In equation (50), all the other variables, except for *m*, *B* and *c*, are known from elastic properties or geometric features of the indenter. *m* is acquired from the slope of log*h*-log*t* relationship in the log linear regime. *B* is obtained from the intercept of this log-linear curve. Once *m* is known, *c* may be estimated according to equation (44).

When considering the mean pressure to indentation strain rate relationship, the elastic mean pressure [31] and indentation strain rate at the elastic mean pressure are used to normalize respective variables, which are given by

$$\left(p_{\text{mean}}\right)_{\text{Sneddon}} = \frac{E}{2\left(1-\nu^2\right)\tan\beta} \tag{51}$$

$$\left(\dot{\varepsilon}_I\right)_{\text{characteristic}} = B\left[\left(p_{\text{mean}}\right)_{\text{Sneddon}}\right]^m \tag{52}$$

Using equations (49) and (50), master *h-t* curves can be produced, that depend only on *m*. First, we examine the linear viscous case, *m*=1. The master *h-t* curve for *m*=1 is shown in Figure 54a. Modified Bower results are predictions of indentation of a rigid – power law creeping solid modified to account for the effects of finite deformation. The term 'modified Bower' is used since *c(m)* and *F(m)* for conical indentation must include the effects of half-included cone angle.

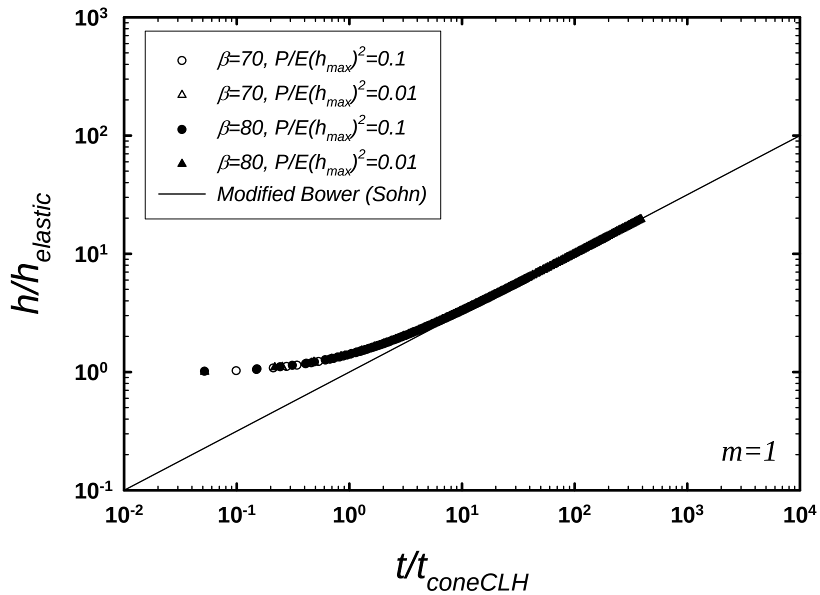

(a) Master *h*-*t* curve

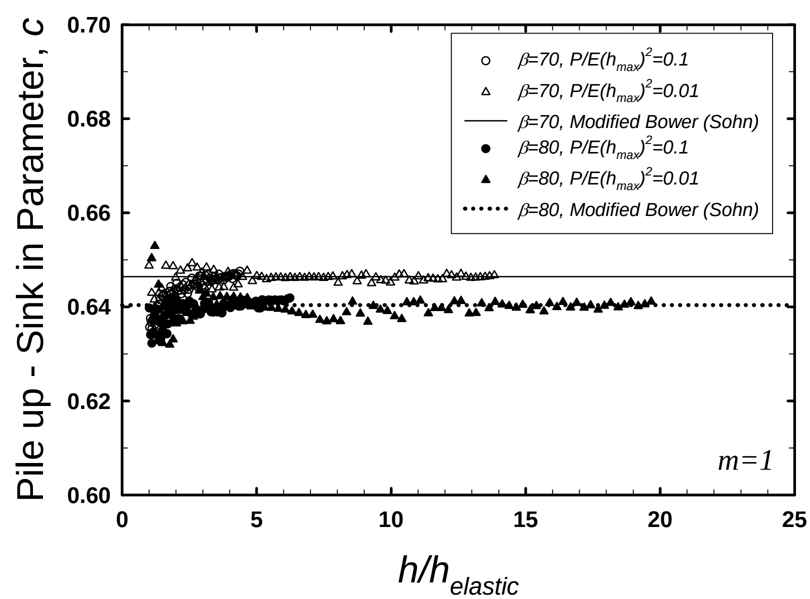

(b) Surface deformation changes during indentation

Figure 54. Elastic normalization results for *m*=1 (cone, CLH)

The modified Bower line in Figure 54a is described by

$$\left(\frac{h}{h_{\mathrm{elastic}}}\right)=\left(\frac{t}{t_{\mathrm{coneCLH}}}\right)^{\frac{1}{2m}} \tag{53}$$

The transient in the master *h*-*t* curve is due to the elasticity and manifests itself as a deviation from the modified Bower relation. The corresponding surface deformation is depicted in Figure 54b. As expected, a transient behavior is not observed for m=1.

Figures 55 and 56 illustrate the master *h*-*t* curves for m=3 and 5, respectively. In both of the cases, a transient is observed not only in the *h*-*t* relationship but also in the surface deformation. Figure 55b and 56b show the sinking in of the surface. This sinking in of the surface is due to the elastic nature of the initial deformation. As indentation progresses, the surface deformation starts to exhibit the effects of creep, and, at sufficiently larger depths or longer indentation times, the amount of sinking in or piling up is equivalent to the predicted value for rigid – power law creep.

In a manner similar to the analysis of spherical indentation under the CLH method, constant von Mises stress contours for 70° conical indentation are shown in Figures 57-59. Here, the von Mises stress is normalized with respect to E. In Figure 57-59, the initial stress distribution at depth of h/h_{elastic}=1 is typical of an elastic stress distribution. As indentation progresses, the stress distribution changes to reflect the permanent deformation of the material governed by power law creep. The stress distribution at maximum depth of each of the creep exponents, as shown in Figures 57f, 58f, and 59f, represents the typical stress distribution of indentation for fully developed creep at the given creep exponent.

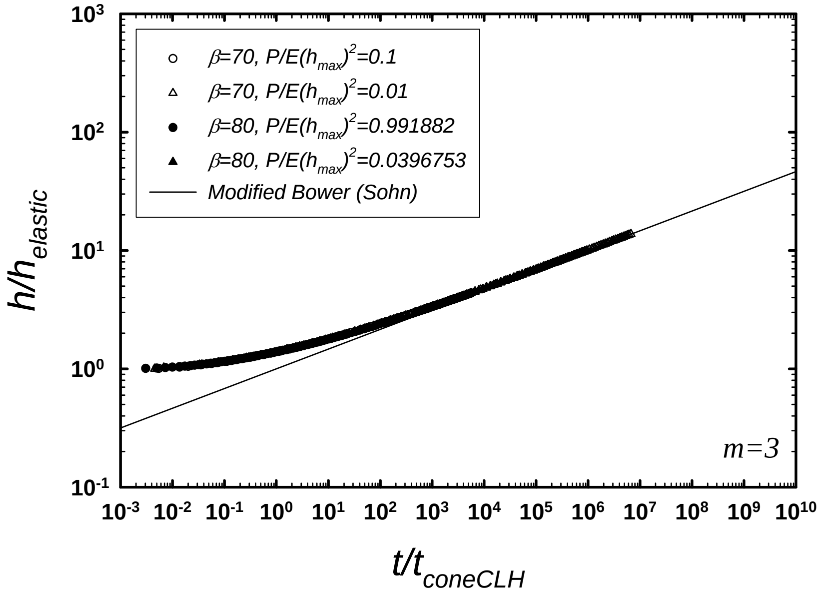

(a) Master *h*-*t* curve

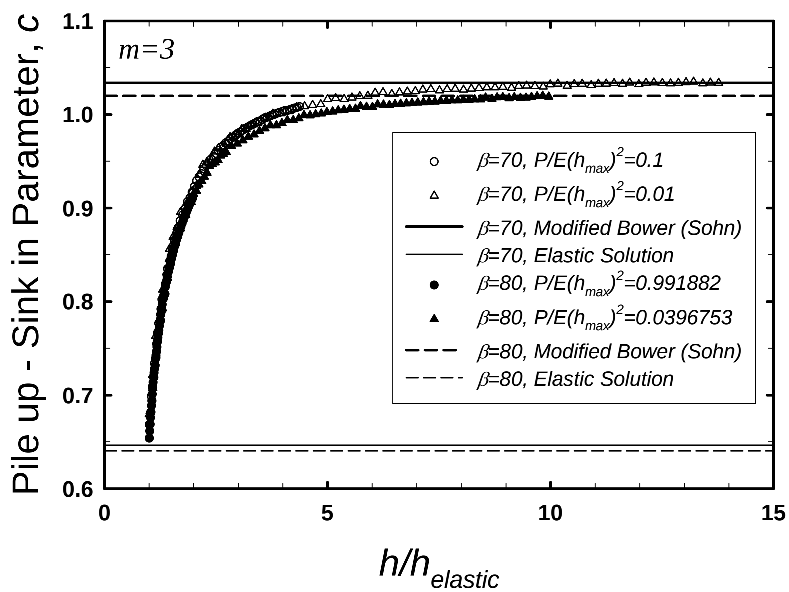

(b) Surface deformation changes during indentation

Figure 55. Elastic normalization results for *m*=3 (cone, CLH)

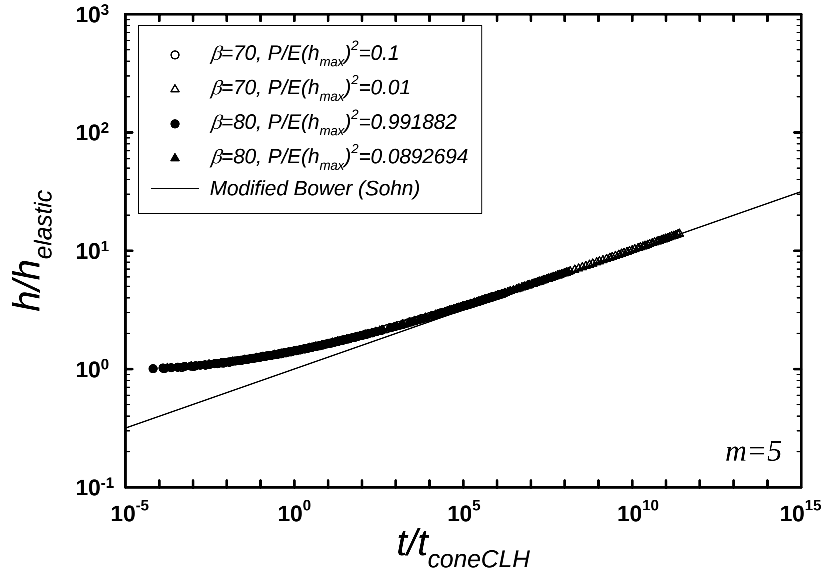

(a) Master *h*-*t* curve

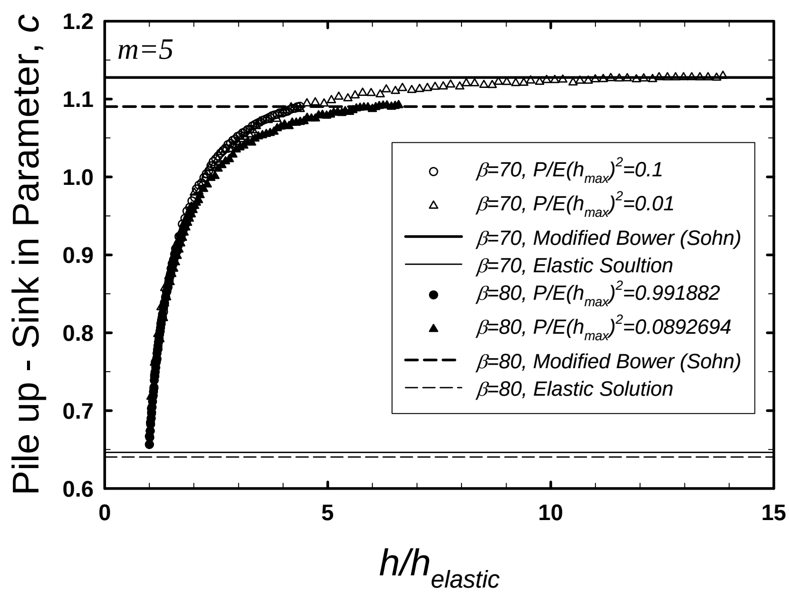

(b) Surface deformation changes during indentation

Figure 56. Elastic normalization results for *m*=5 (cone, CLH)

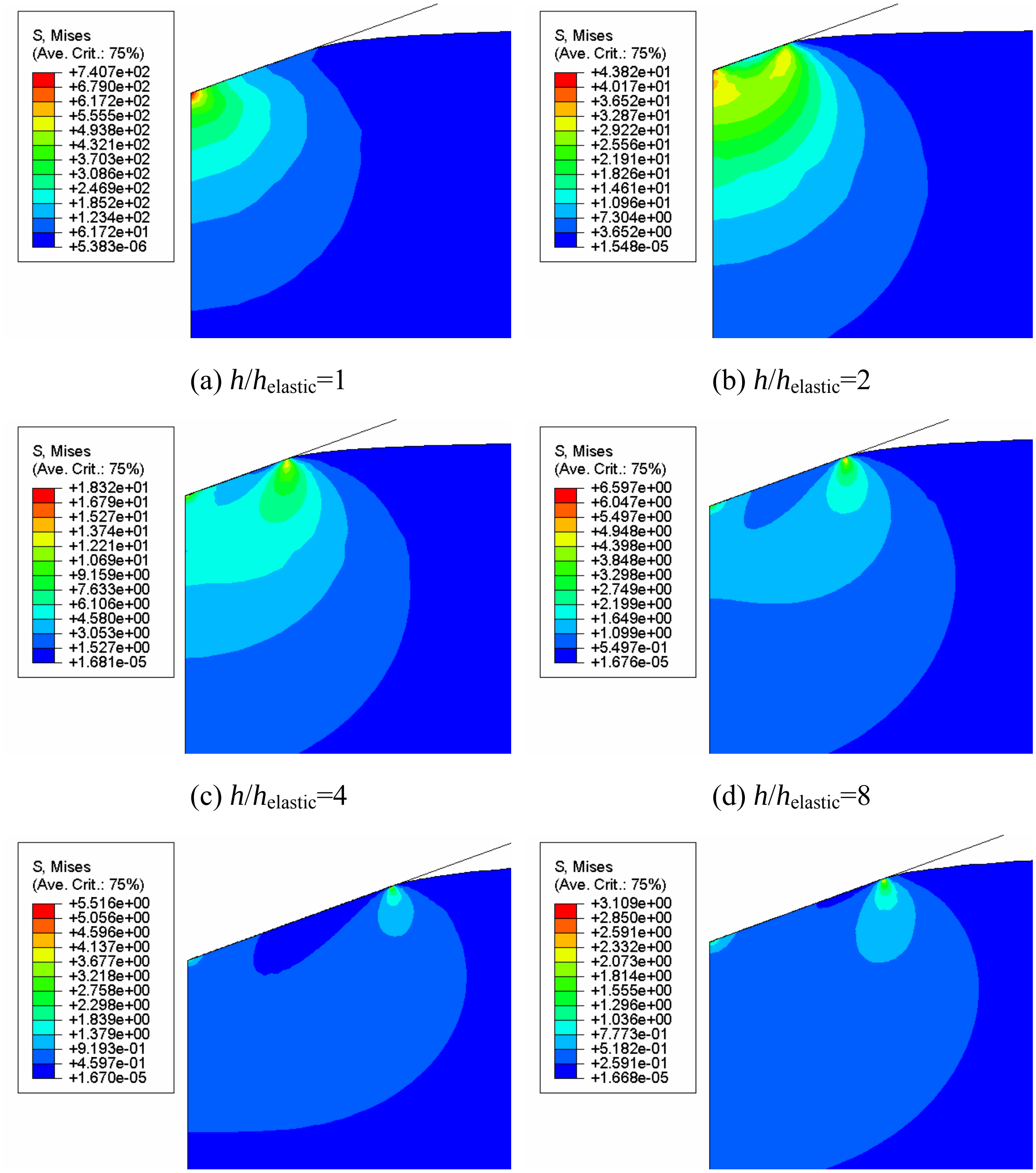

(a) h/h_{elastic}=1

(b) h/h_{elastic}=2

(c) h/h_{elastic}=4

(d) h/h_{elastic}=8

(e) h/h_{elastic}= 12

(f) h/h_{elastic}= 13.8

(maximum depth)

Figure 57. von Mises stress distribution for *m*=1 (70° cone, CLH)

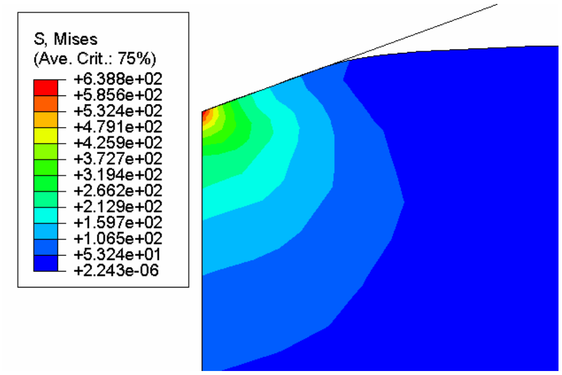

(a) h/h_{elastic}=1

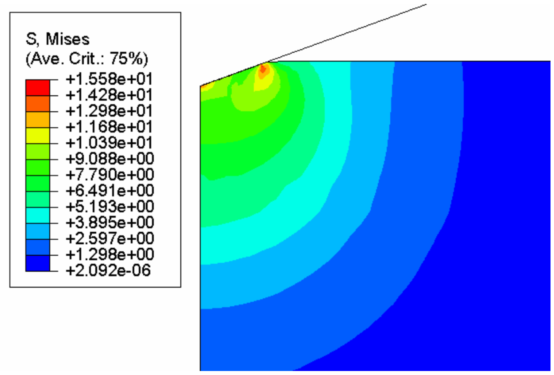

(b) h/h_{elastic}=2

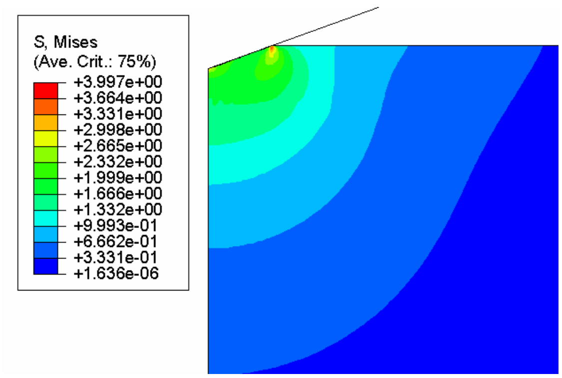

(c) h/h_{elastic}=4

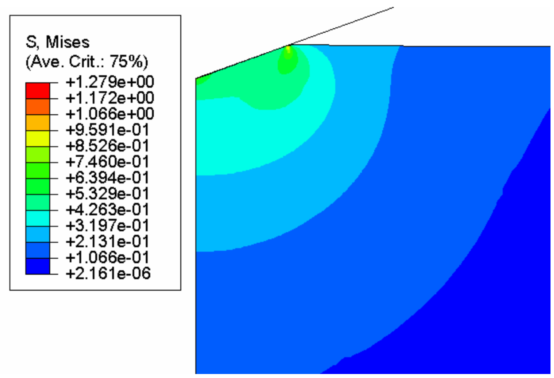

(d) h/h_{elastic}=8

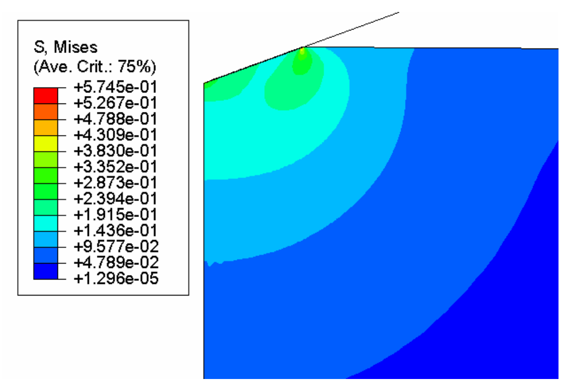

(e) h/h_{elastic}=12

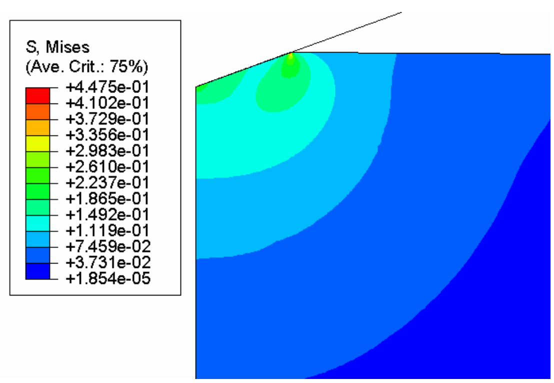

(f) h/h_{elastic}=13.8

(maximum depth)

Figure 58. von Mises stress distribution for *m*=3 (70° cone, CLH)

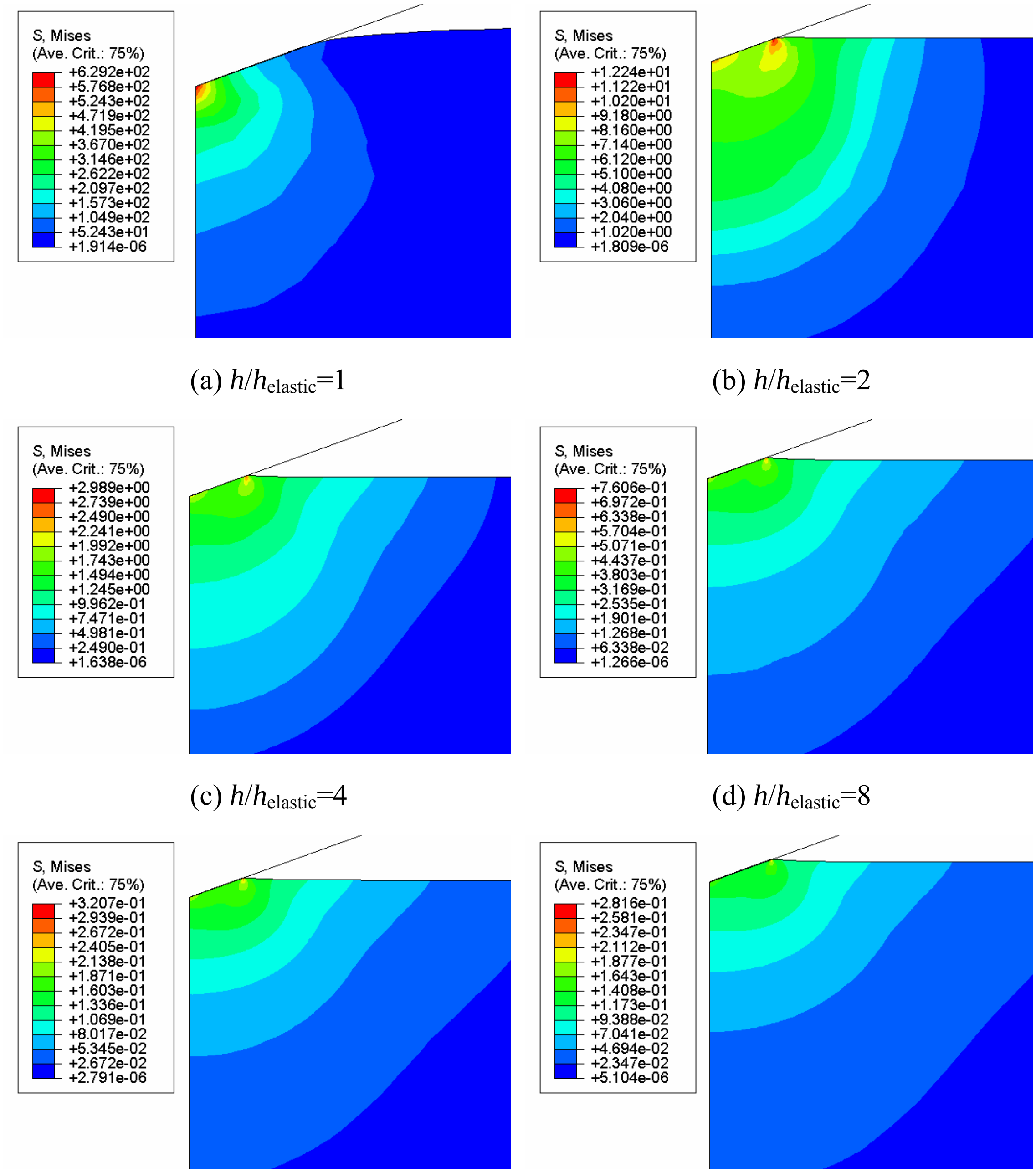

(a) h/h_{elastic}=1

(b) h/h_{elastic}=2

(c) h/h_{elastic}=4

(d) h/h_{elastic}=8

(e) h/h_{elastic}=12

(f) h/h_{elastic}=13.9

(maximum depth)

Figure 59. von Mises stress distribution for *m*=5 (70° cone, CLH)

Therefore, the transient induced by elasticity manifests itself as different stress distributions with respect to the progression of indentation for different creep exponents.

Results for the relations between indentation strain rate and mean pressure are shown in Figure 60. A transient induced by elasticity is not observed when m=1, in agreement with the theoretical prediction. However, when m>1, a transient manifests itself as a deviation from the proposed modified Bower solution in each of the curves. The slopes of indentation strain rate – mean pressure curve at longer indentation times are equal to the creep exponents of the material.

Error in uniaxial creep parameter prediction due to elastic transient

We now predict uniaxial creep parameters from the h-t curves of an elastic – power law creeping solid. The uniaxial creep parameters are computed from local finite element h-t results with approximately 10 data points fitted to power law regression. The representative depth of each result is the average depth of the selected data range. The uniaxial creep exponent is estimated from the slope of log$h$-log$t$ data, and the uniaxial creep coefficient B is determined using the local exponent and relevant values for other variables by the expression in equation (22). Figure 61 shows the results. When estimating the uniaxial creep exponent, a depth of h/h_{elastic}=5 yields output results within 10% of the input values. However, the uniaxial creep coefficient is more affected, producing relatively larger errors. For m=5, h/h_{elastic}=10 yields an output uniaxial coefficient 30% larger than the input value. Despite this error in estimating the uniaxial creep coefficient, the worst overestimation of uniaxial creep coefficient is still within 40% of the input value.

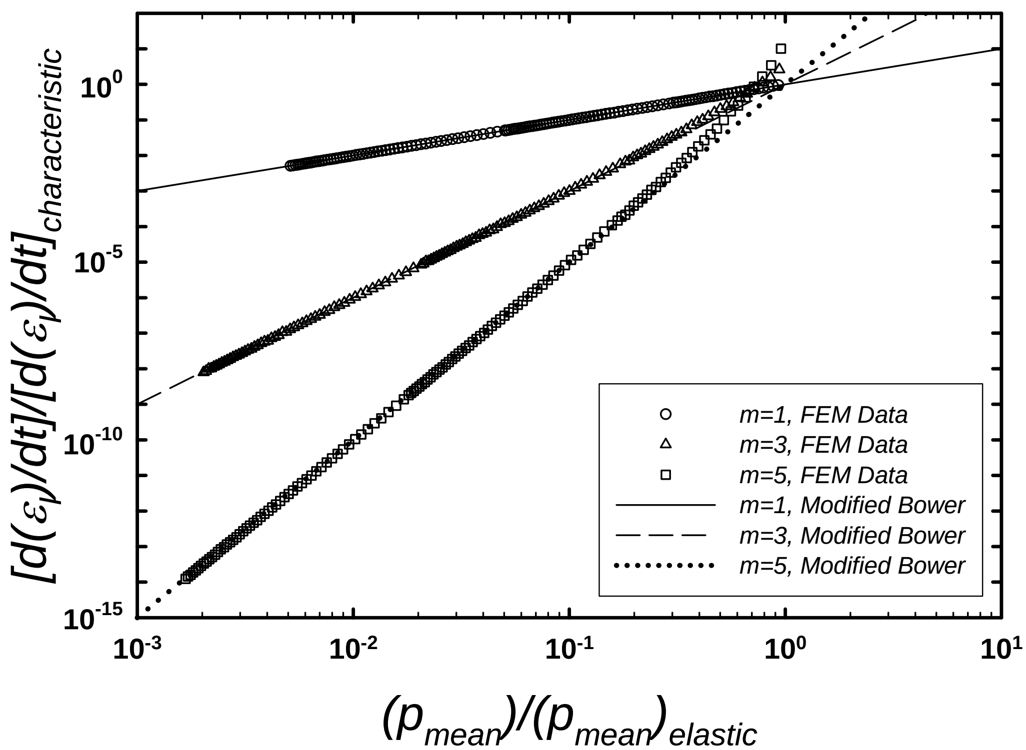

Figure 60. Indentation strain rate – mean pressure curves (70 ° cone, CLH)

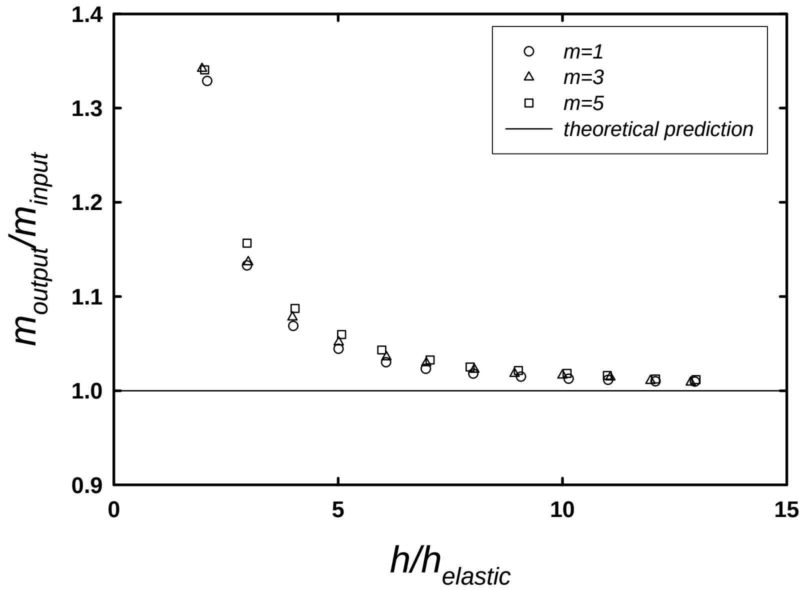

(a) Output uniaxial creep exponent calculation

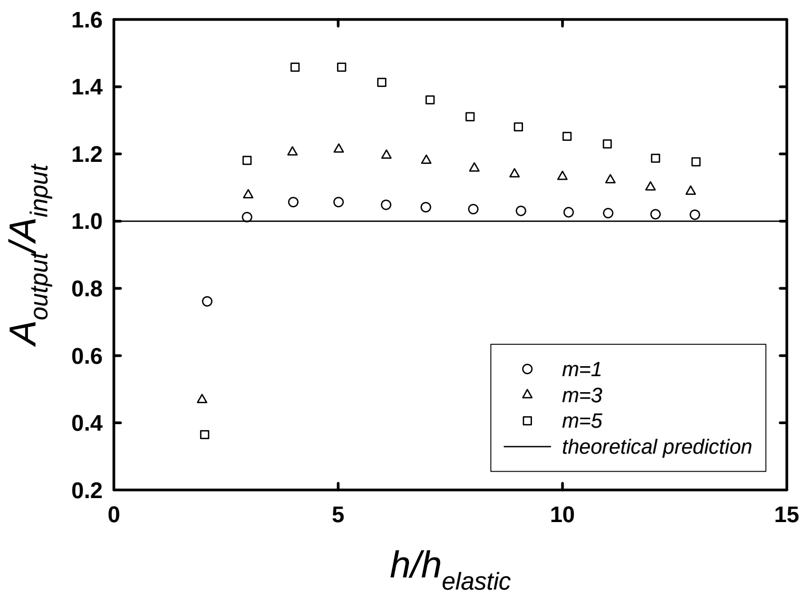

(b) Output uniaxial creep coefficient calculation

Figure 61. Effects of the elasticity on uniaxial creep parameters (70° cone, CLH)

Compared to the errors in estimating the uniaxial creep coefficient from spherical indentation using the CLH method (400%), errors from conical indentation under the CLH method are relatively small. One possible explanation for the smaller errors for conical indentation is the nature of the geometry of the indenter. The conical indenter has a singularity at its tip that promotes plasticity. Therefore, the effects of elasticity disperse more quickly and easily than for a spherical indenter.

Elastic-Creep Transients for Conical Indentation under the CRL Method

Indentation process for conical indentation under the CRL method

The process of indentation under the CRL method using a conical indenter is explained in a manner analogous to spherical indentation under the CRL method. Note once again that the distinction between discrete elastic deformation and plasticity caused by creep is complicated. This process is shown in Figure 62. For extremely fast loading rates, surface deformation is dominated by purely elastic deformation. On the other hand, for very slow loading rates, creep deformation may dominate the whole indentation process.

Indentation h-t and P-h curves for various creep exponents

Using dimensional analysis, *h-t* and *P-h* curves from conical indentation under the CRL method are presented in Figures 63-65, for m=1, 3, and 5, respectively. For each of creep exponent, three different half-included cone angles are considered with different loading rates. The breakdown in log-linearity at faster loading rates is associated with elastic transients.

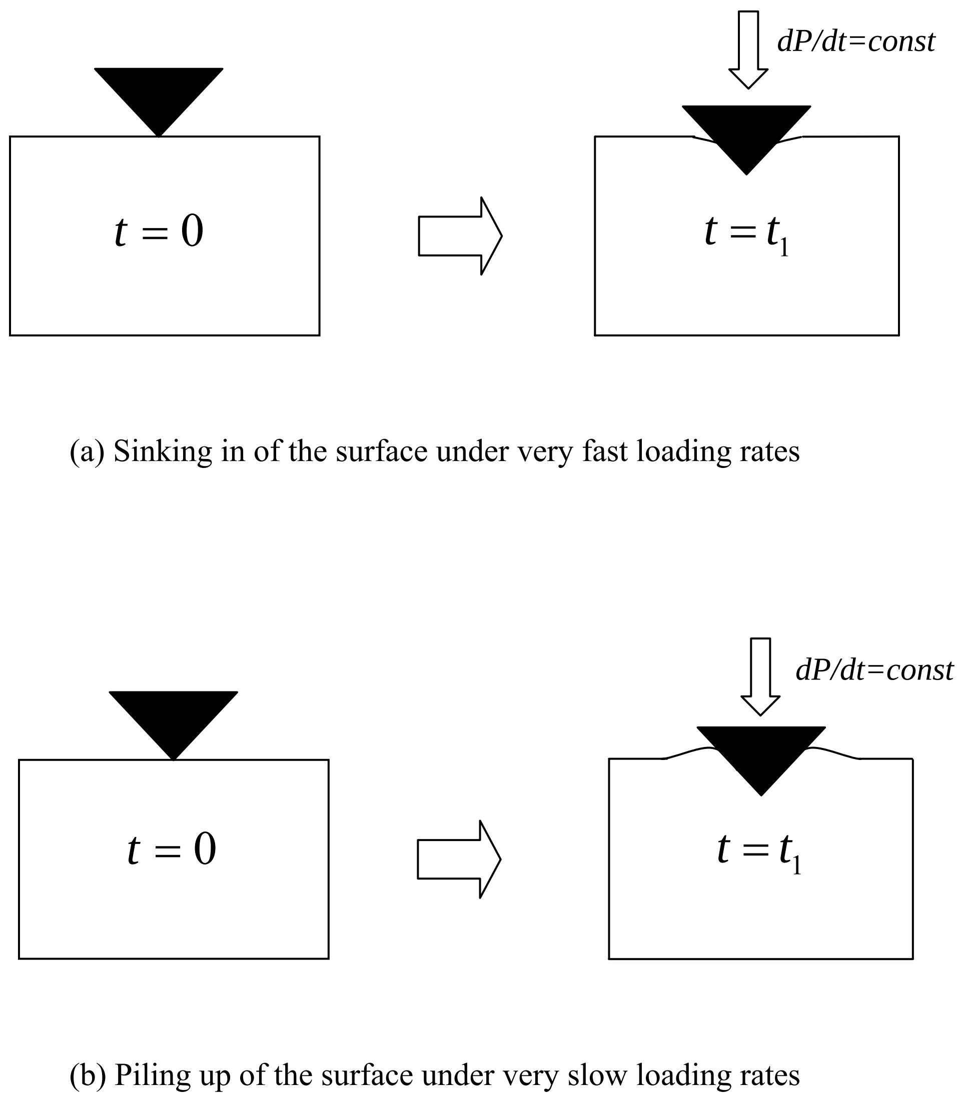

Figure 62. Extreme surface behaviors governed by loading rates

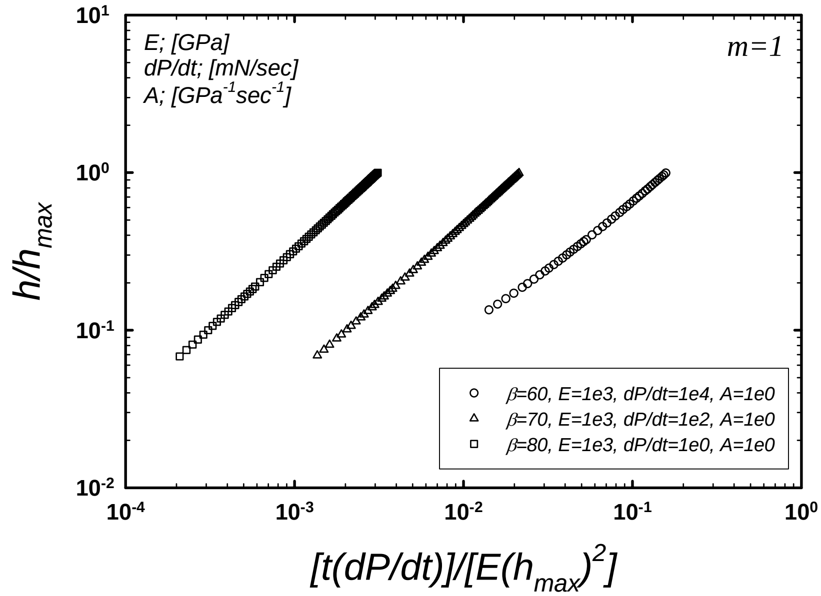

(a) *h*-*t* curves

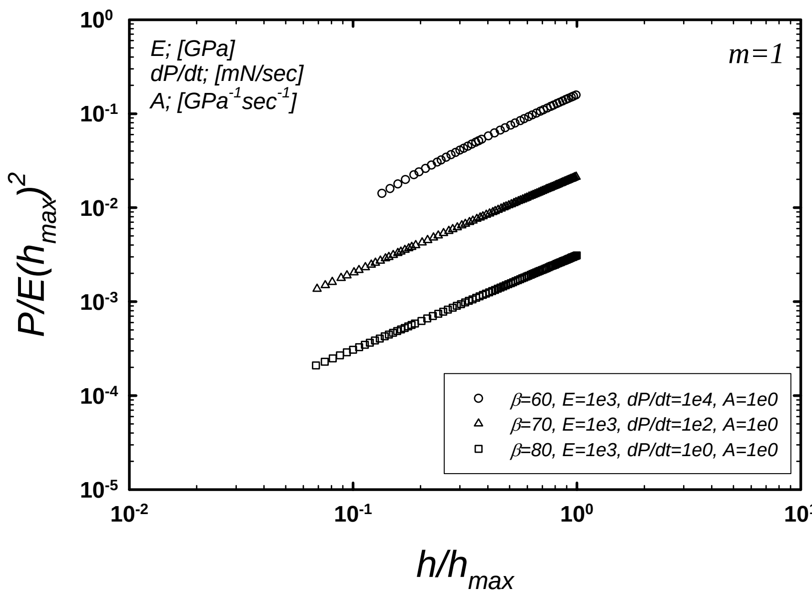

(b) *P*-*h* curves

Figure 63. *h*-*t* and *P*-*h* curves for *m*=1 (cone, CRL)

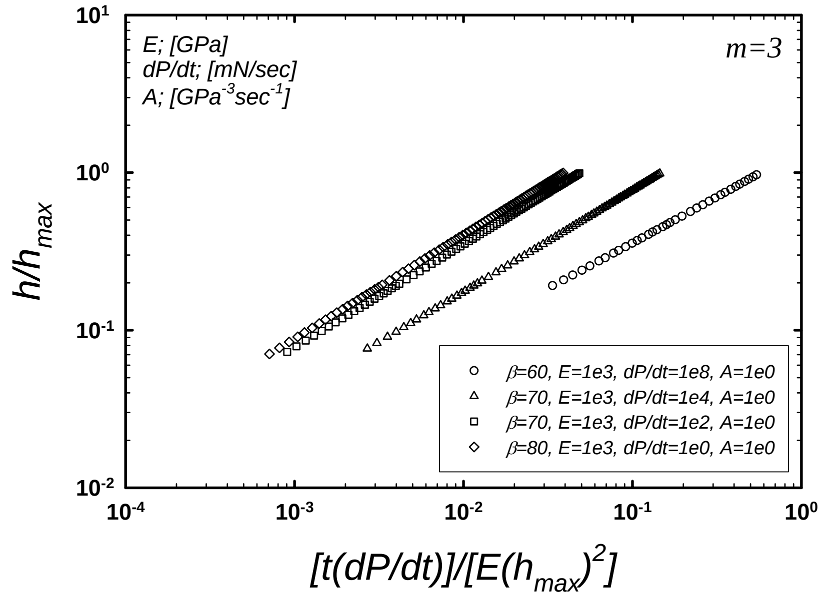

(a) *h*-*t* curves

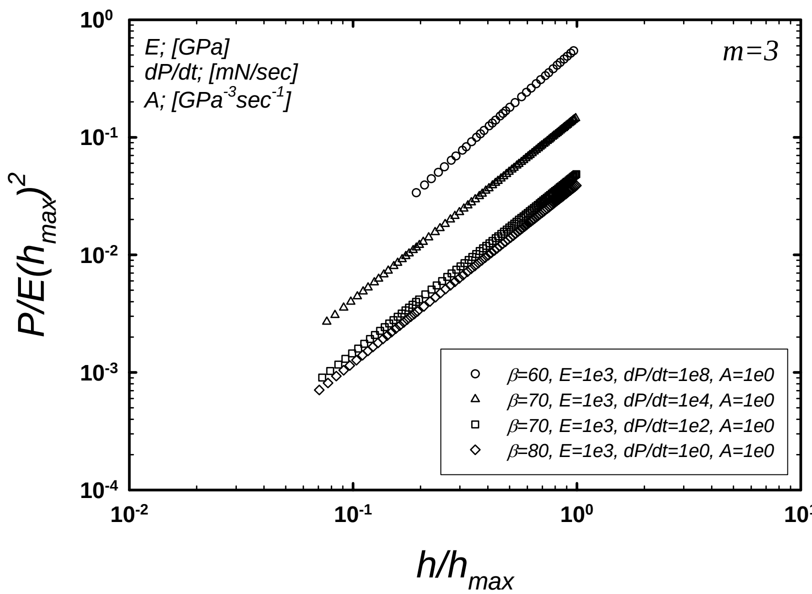

(b) *P*-*h* curves

Figure 64. *h*-*t* and *P*-*h* curves for *m*=3 (cone, CRL)

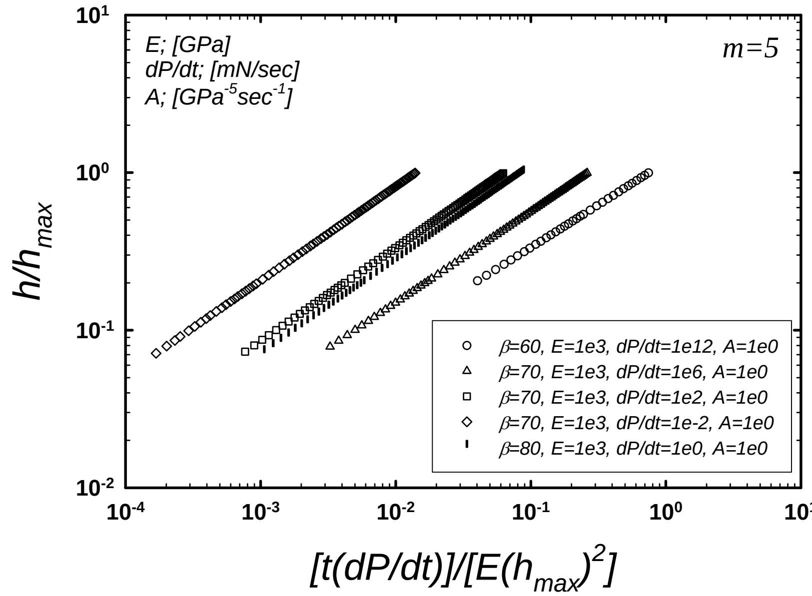

(a) *h*-*t* curves

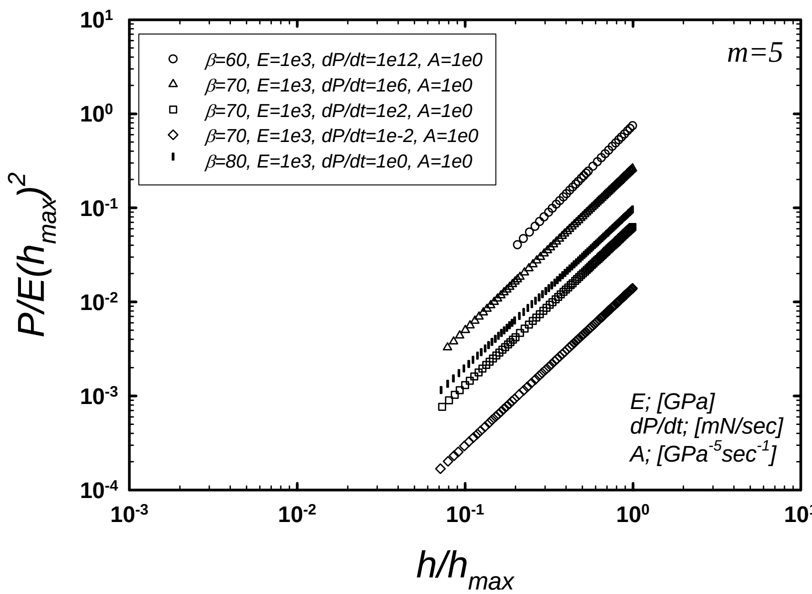

(b) *P*-*h* curves

Figure 65. *h*-*t* and *P*-*h* curves for *m*=5 (cone, CRL)

Application of elastic normalization

Elastic properties and known geometric parameters of the indenter may be used to normalize the *h-t* and *P-h* curves to produce master *h-t* or *P-h* curves. The procedures to determine the appropriate normalizing variables are similar to those for spherical indentation under the CRL method. The indentation depth is normalized using the elastic depth for conical indentation (equation (49)). In order to normalize indentation time and indentation load, characteristic time and characteristic load are required. This is achieved in a manner similar to spherical indentation under the CRL method. We first examine the rigid – power law creep *h-t* relationship for conical indentation under the CRL method. By substituting equation (49) into equation (24) and solving for *t*, we obtain a characteristic time, t_{coneCRL}. This is given by:

$$t_{\mathrm{coneCRL}} = \left\{ \left(\frac{m+1}{2m} \right) \left[\frac{P\left(1-\nu^2\right)}{2\dot{P}E} \right]^m \left(\frac{\pi^{2m}}{B} \right) \left(c^{2m-1}\right) (\tan\beta)^{m-1} \right\}^{\frac{1}{m+1}} \tag{54}$$

Likewise, the characteristic load is derived from the rigid – power law creep *P-h* relationship. By replacing h_{creep} in equation (25) with the elastic depth of equation (49), we obtain a characteristic load for conical indentation under CRL method, $P_{\mathrm{coneCRL},}$ given by:

$$P_{\mathrm{coneCRL}} = \left\{ \left(\frac{m+1}{2m} \right) \left[\frac{P\left(1-\nu^2\right)}{2E} \right]^m \left(\frac{\pi^{2m}\dot{P}}{B} \right) \left(c^{2m-1}\right) (\tan\beta)^{m-1} \right\}^{\frac{1}{m+1}} \tag{55}$$

Characteristic loading rates are obtained by dividing equation (55) with equation (54). The result is a unit loading rate, in agreement with the result of dimensional analysis for conical indentation under the CRL method (Table 4).

The mean pressure and indentation strain rate can be normalized with equations

(51) and (52), respectively. The result of this elastic normalization yields master h-t and P-h curves as demonstrated in Figures 66-68. The modified Bower results in Figures 66a, 67a and 68a have been described by:

$$\left(\frac{h}{h_{\text{elastic}}}\right)=\left(\frac{t}{t_{\text{coneCRL}}}\right)^{\frac{m+1}{2m}} \tag{56}$$

Similarly, modified Bower results in Figures 66b, 67b and 68b are described by equation (57).

$$\left(\frac{P}{P_{\text{coneCRL}}}\right)=\left(\frac{h}{h_{\text{elastic}}}\right)^{\frac{2m}{m+1}} \tag{57}$$

The master h-t and P-h curves show deviations from the modified Bower results, which are effects induced by elasticity. Regardless of the creep exponent, the h-t or P-h curves approach the predicted rigid – power law creeping prediction at longer indentation times or larger indentation depths. The purpose of these master curves is to demonstrate the feasibility of elastic normalization and to study the effects of the elastic transient on the h-t and P-h curves. For m=3 and 5, the half-included cone angles of the conical indenter and the loading rates were selected to represent important portions of these master curves. Therefore, breaks in the master h-t and P-h curves for m=3 and 5 are observed in the resulting plots.

Implications of the elastic transient may be explained in detail in terms of the surface deformation. When m=1, c should be a constant equal to the elastic prediction. For a 70° cone, this is shown to be the case in Figure 69. For m>1, a transient regime appears in the pile up – sink in parameter plot. Figures 70 and 71 depict the changes in surface deformation for m=3 and 5, respectively.

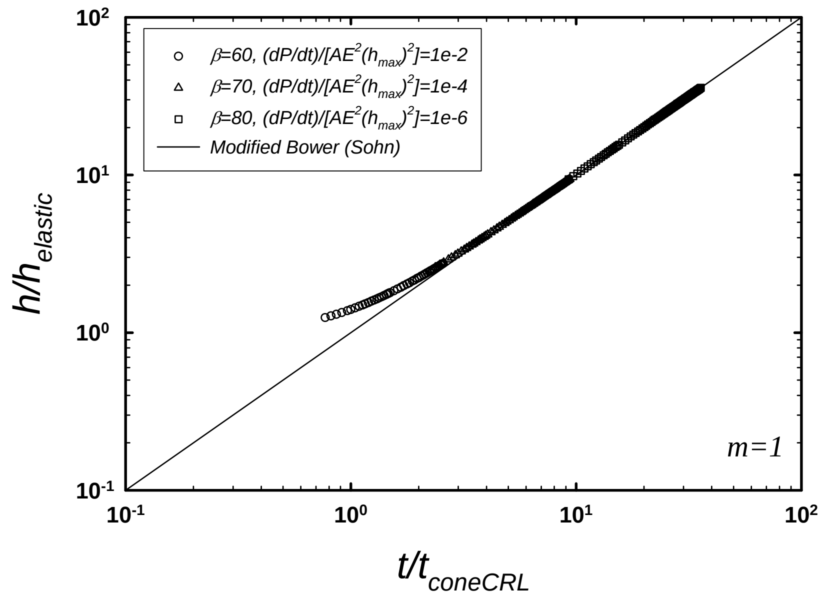

(a) Master *h*-*t* curve

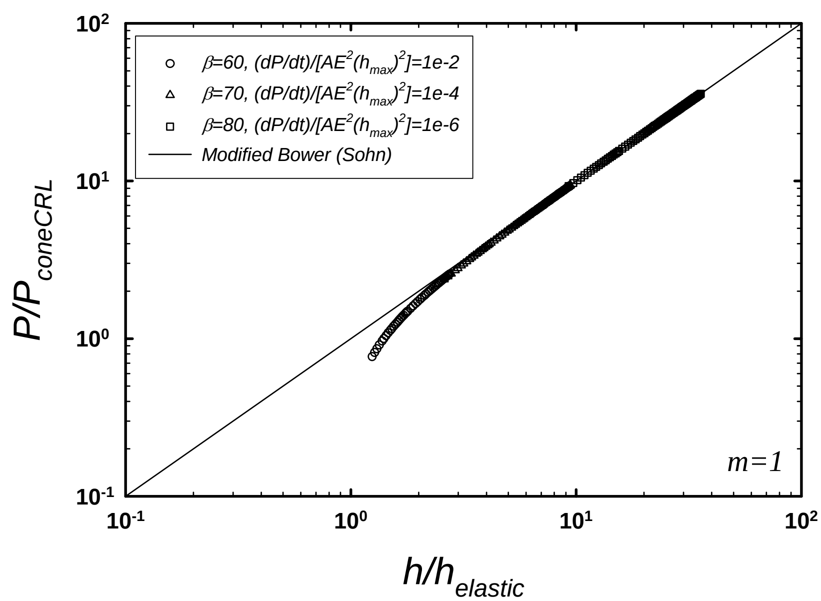

(b) Master *P*-*h* curve

Figure 66. Elastic normalization results for *m*=1 (cone, CRL)

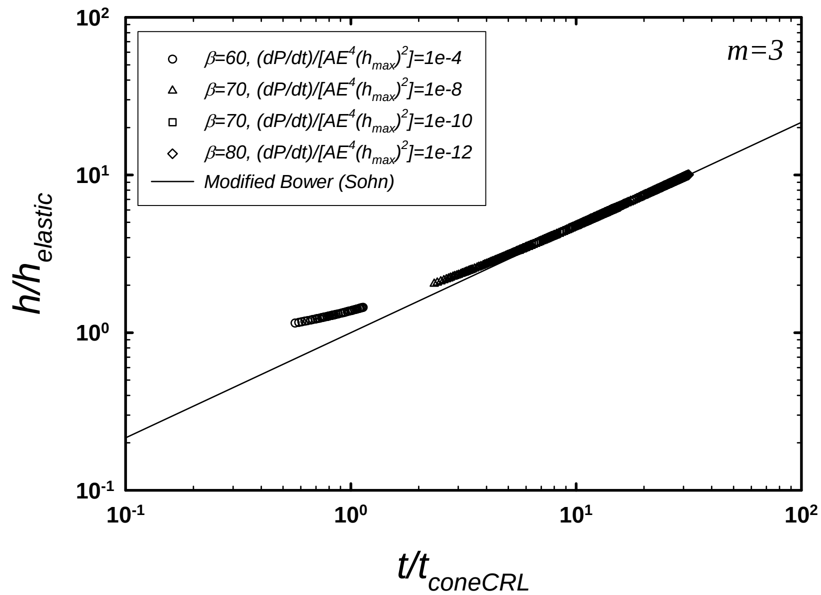

(a) Master *h*-*t* curve

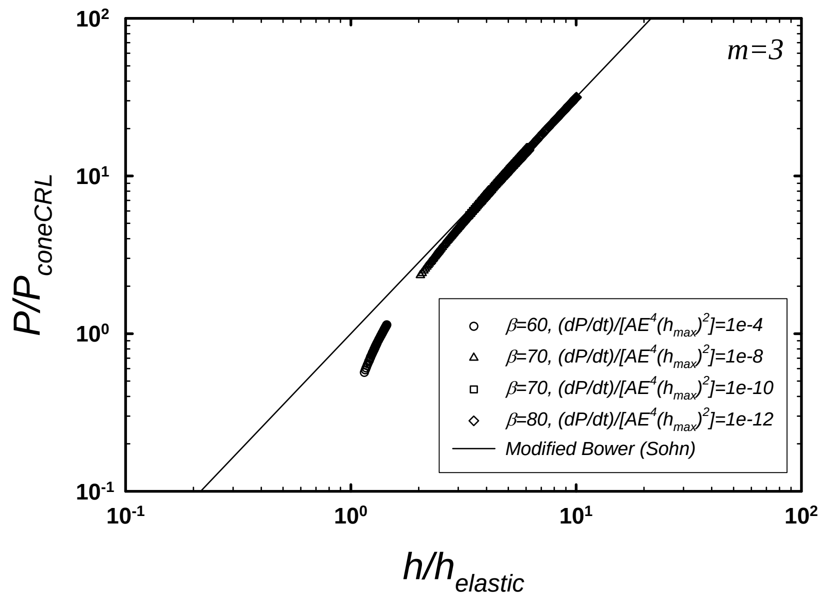

(b) Master *P*-*h* curve

Figure 67. Elastic normalization results for *m*=3 (cone, CRL)

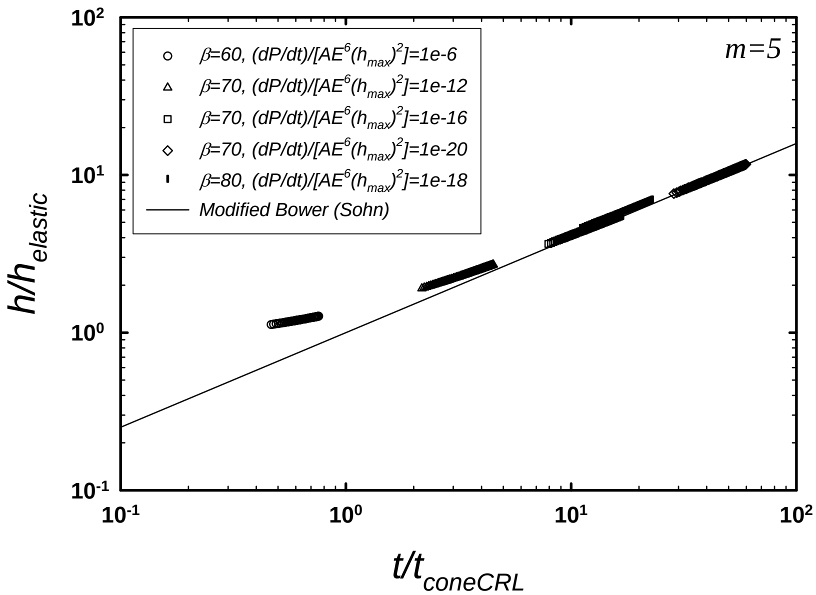

(a) Master *h*-*t* curve

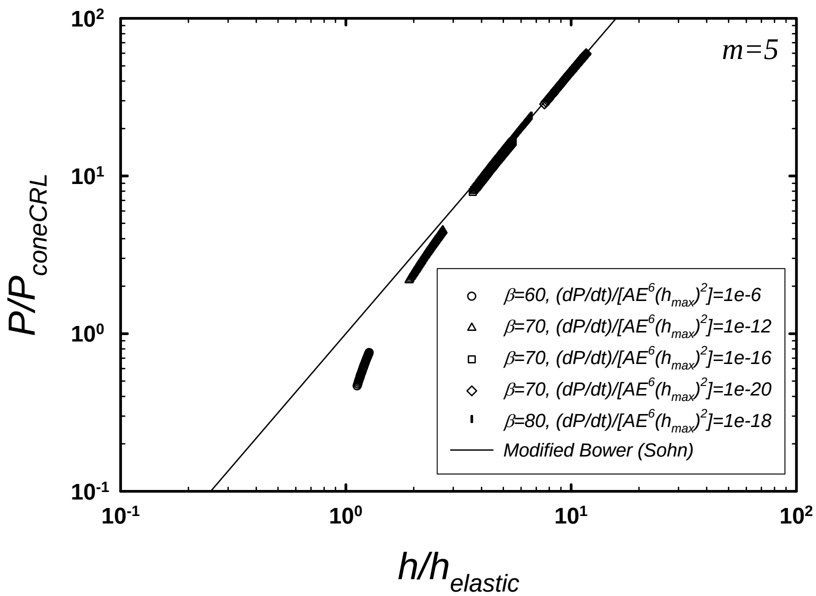

(b) Master *P*-*h* curve

Figure 68. Elastic normalization results for *m*=5 (cone, CRL)

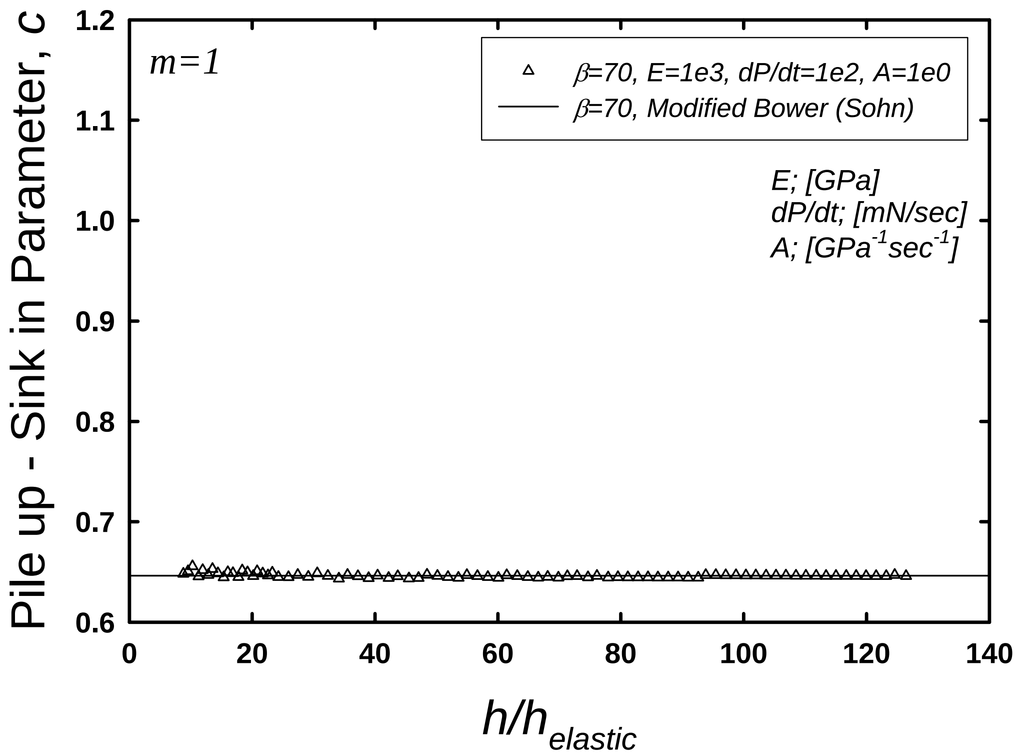

Figure 69. Changes in surface deformation for *m*=1 (70° cone, CRL)

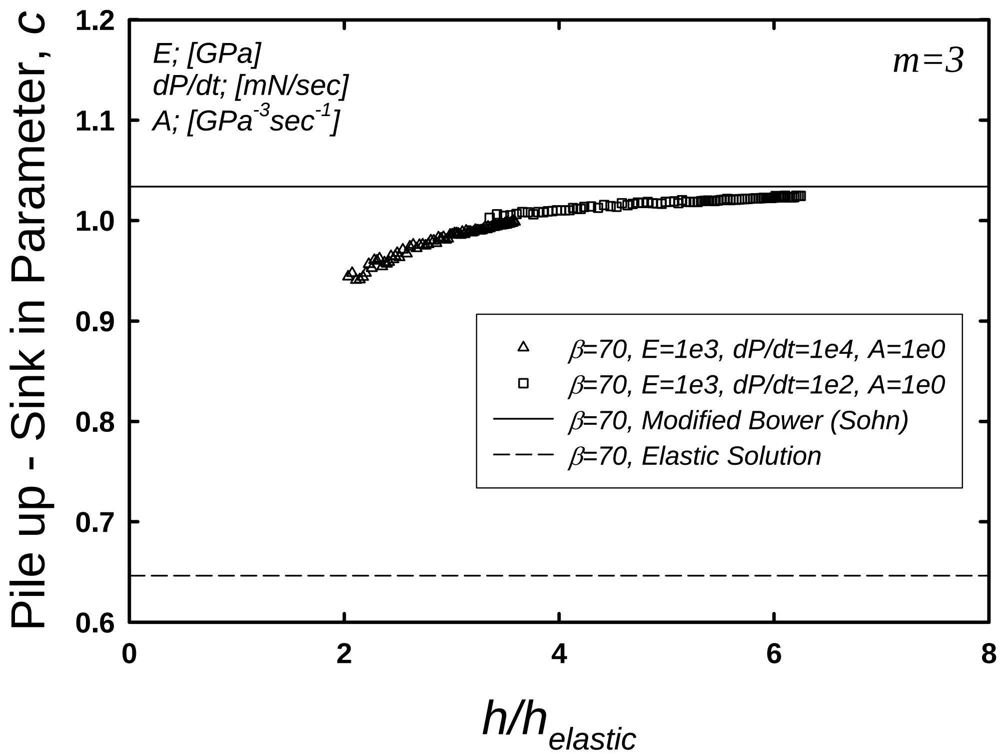

Figure 70. Changes in surface deformation for *m*=3 (70° cone, CRL)

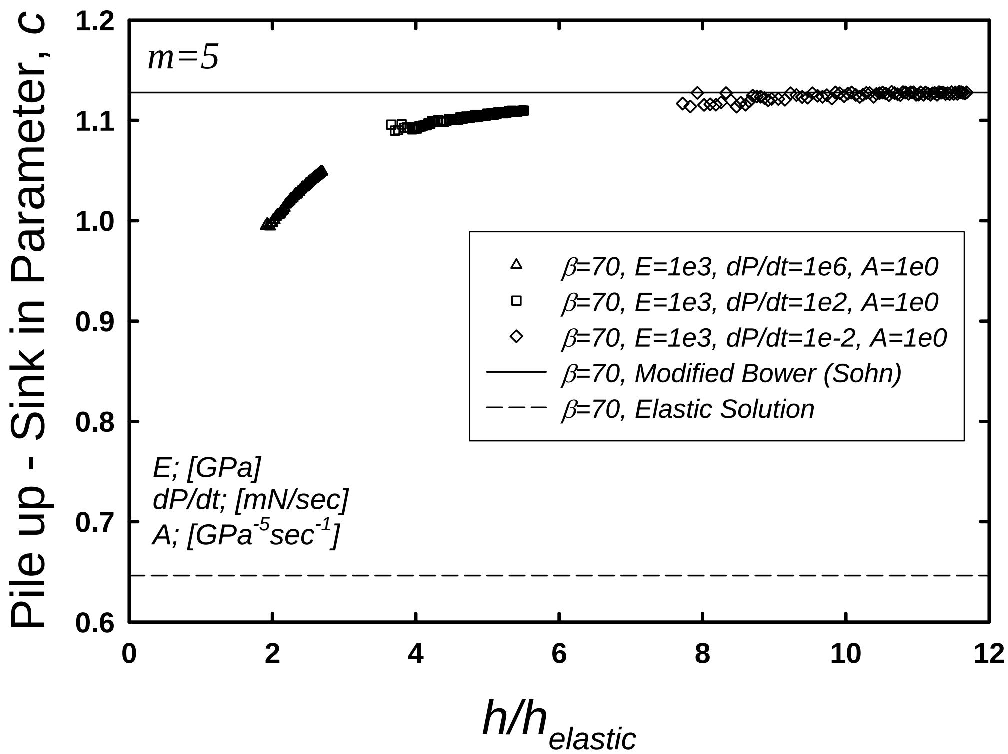

Figure 71. Changes in surface deformation for *m*=5 (70° cone, CRL)

The initial value of c is consistent with Sneddon's [31] elastic predictions. In Figures 70 and 71, c exhibits a transient as it approaches the rigid – power law creep prediction as indentation progresses.

Figures 72-74 show stress distributions at different normalized indentation depths for m=1, 3, and 5, respectively. These contour diagrams indicate the changes in stress distribution with respect to the indentation depth. Figure 72 depicts results for m=1. For m=1, stress distribution is shown at normalized loading rate of $\frac{\dot{P}}{AE^2(h_{\max})^2}=10^{-4}$, since at this normalized loading rate, indentation covers normalized depths representative of elastic dominated to fully creep dominated regime. Figures 73 and 74 show the changes in stress distribution for m=3 and 5, respectively. Here, results are shown for relatively faster loading rates and relatively slower loading rates in order to demonstrate the changes in stress distribution for both small and large indentation depths.

Figure 75 shows the indentation strain rate – mean pressure curves for different values of m. The indentation strain rate – mean pressure data is in a good agreement with rigid – power law creep predictions at small mean pressures and indentation strain rates. The deviation from the rigid – power law creep prediction at high mean pressure (i.e, at the beginning of an indentation experiment) is an indication of the elastic transient. Note that a transient is observed even for m=1 in Figure 75. This transient may be explained in a manner similar to the transients for m=1 from spherical indentation under the CRL method. As the load changes during indentation, the corresponding elastic depth changes as a function of load and other variables.

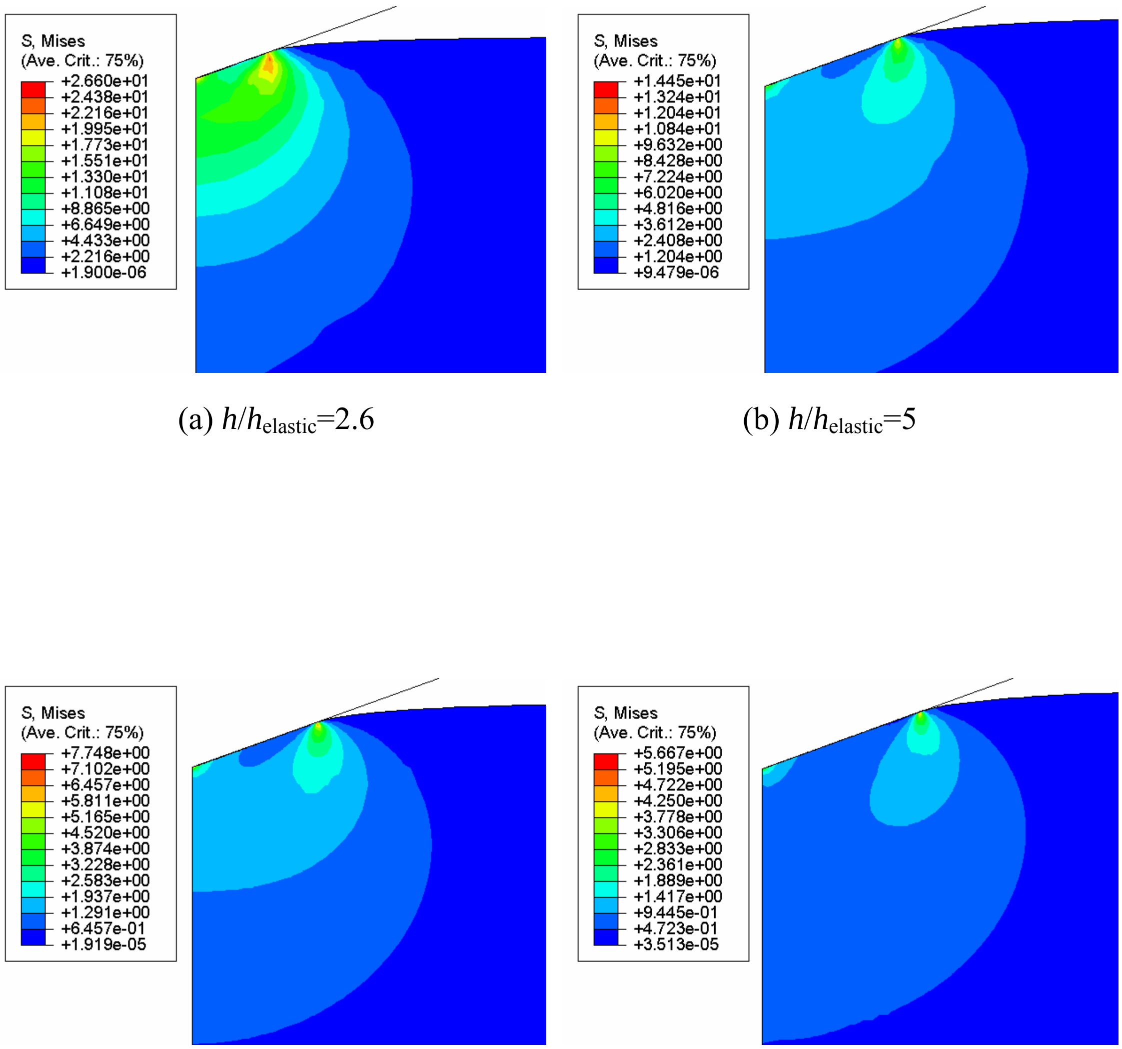

(a) h/h_{elastic}=2.6 (b) h/h_{elastic}=5

(c) h/h_{elastic}=7 (d) h/h_{elastic}=9.4

(maximum depth)

Figure 72. von Mises stress distribution for *m*=1 (70° cone, CRL) at

$$\frac{\dot{P}}{AE^2(h_{\max})^2} = 10^{-4}$$

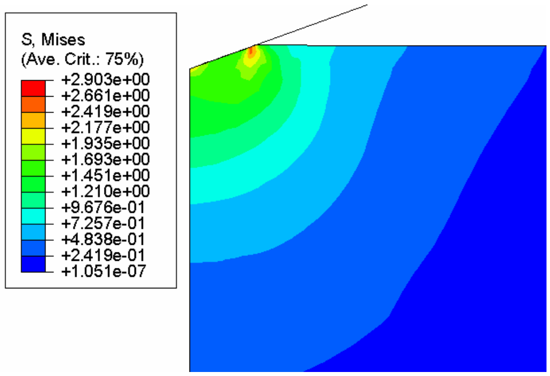

h/h_{elastic}=2

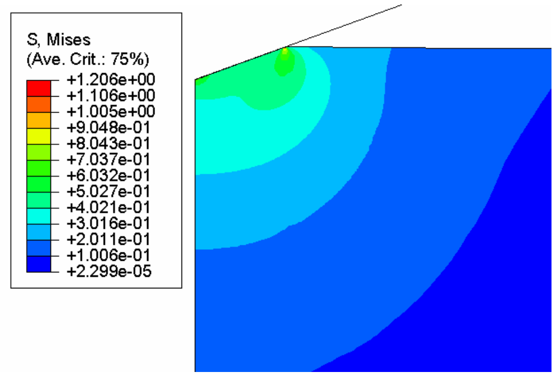

h/h_{elastic}=3.6

(a) stress distribution for m=3 at $\dfrac{\dot{P}}{AE^4(h_{\max})^2}=10^{-8}$

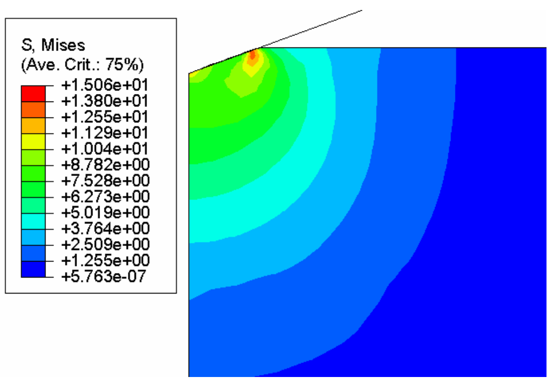

h/h_{elastic}=4.4

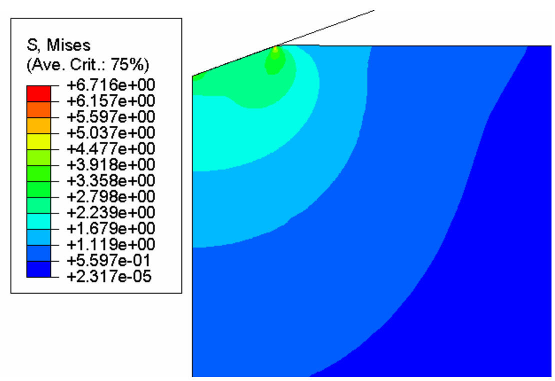

h/h_{elastic}=8.3

(b) stress distribution for m=3 at $\dfrac{\dot{P}}{AE^4(h_{\max})^2}=10^{-11}$

Figure 73. von Mises stress distribution for *m*=3 (70° cone, CRL)

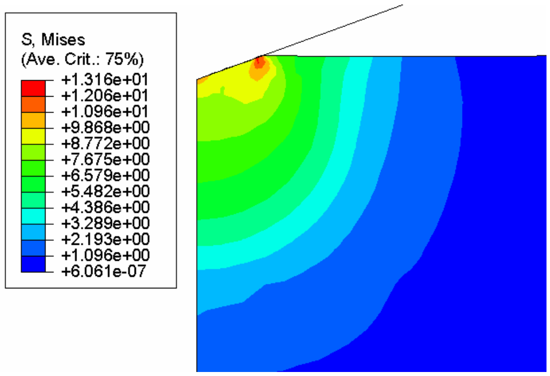

h/h_{elastic}=1.9

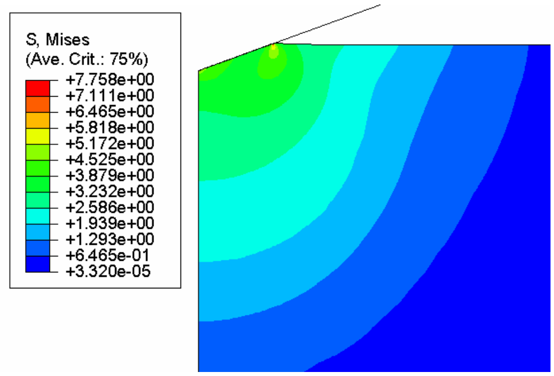

h/h_{elastic}=2.7

(a) stress distribution for m=5 at $\dfrac{\dot{P}}{AE^6\left(h_{\max}\right)^2}=10^{-12}$

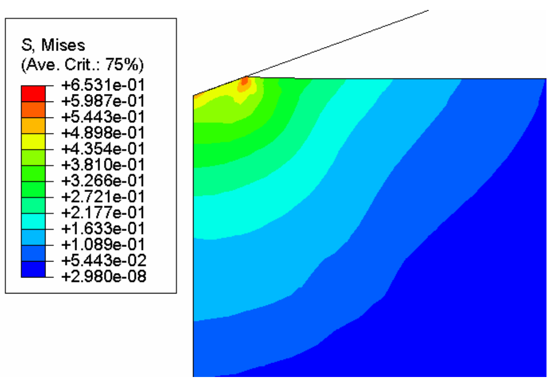

h/h_{elastic}=7.6

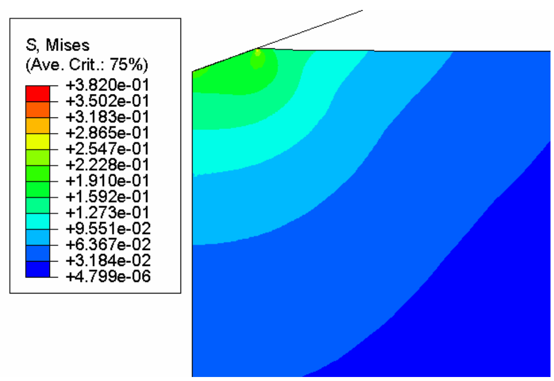

h/h_{elastic}=11.7

(a) stress distribution for m=5 at $\dfrac{\dot{P}}{AE^6\left(h_{\max}\right)^2}=10^{-20}$

Figure 74. von Mises stress distribution for *m*=5 (70° cone, CRL)

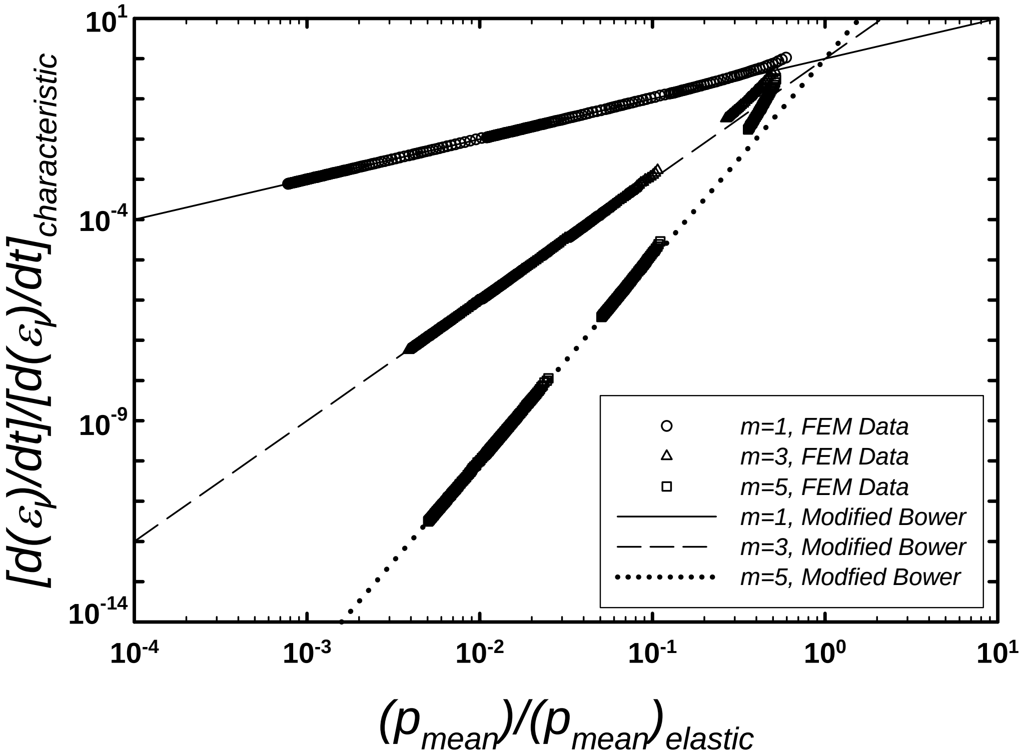

Figure 75. Indentation strain rate – mean pressure curves (70° cone, CRL)

Therefore, differentiating equation (49) with respect to time, we obtain

$$\dot{h}_{\text{Sneddon}} = \left[\frac{\pi\left(1-\nu^2\right)}{2PE\tan\beta}\right]^{\frac{1}{2}}\left(\frac{\dot{P}}{2}\right) \tag{58}$$

Dividing equation (58) by the elastic contact radius [31] for conical indentation, we arrive at an expression for the elastic strain rate:

$$\left(\frac{\dot{h}_{\text{Sneddon}}}{a_{\text{Sneddon}}}\right) = \frac{\pi\dot{P}}{4P\tan\beta} \tag{59}$$

Rewriting equation (59) in terms of the elastic mean pressure, we obtain

$$\left(\frac{\dot{h}_{\text{Sneddon}}}{a_{\text{Sneddon}}}\right) = \left[\frac{\pi\left(1-\nu^2\right)\dot{P}}{2E}\right]\left[\frac{\left(p_{\text{mean}}\right)_{\text{Sneddon}}}{P}\right] \tag{60}$$

The left-hand side of equation (60) is a strain rate equivalent variable that defines the maximum indentation strain rate at the elastic mean pressures. For conical indentation, the elastic mean pressure is not dependent on load. Therefore, according to equation (60), load variation during indentation results in elastic indentation strain rates that do not change, thus giving a vertical line in a plot of $\log\dot{\varepsilon}_I$ versus $\log\left(p_{\text{mean}}\right)$. This is depicted in Figure 76 as the solid vertical line. The pressure at which this occurs is the elastic mean pressure. As creep commences, the initially elastically dominated indentation strain rate – mean pressure curve makes a gradual transition toward the rigid – power law creep regime. This curve is shown as the dotted line in Figure 76. Therefore, the indentation strain rate – mean pressure curves exhibit a transient regardless of the creep exponent involved.

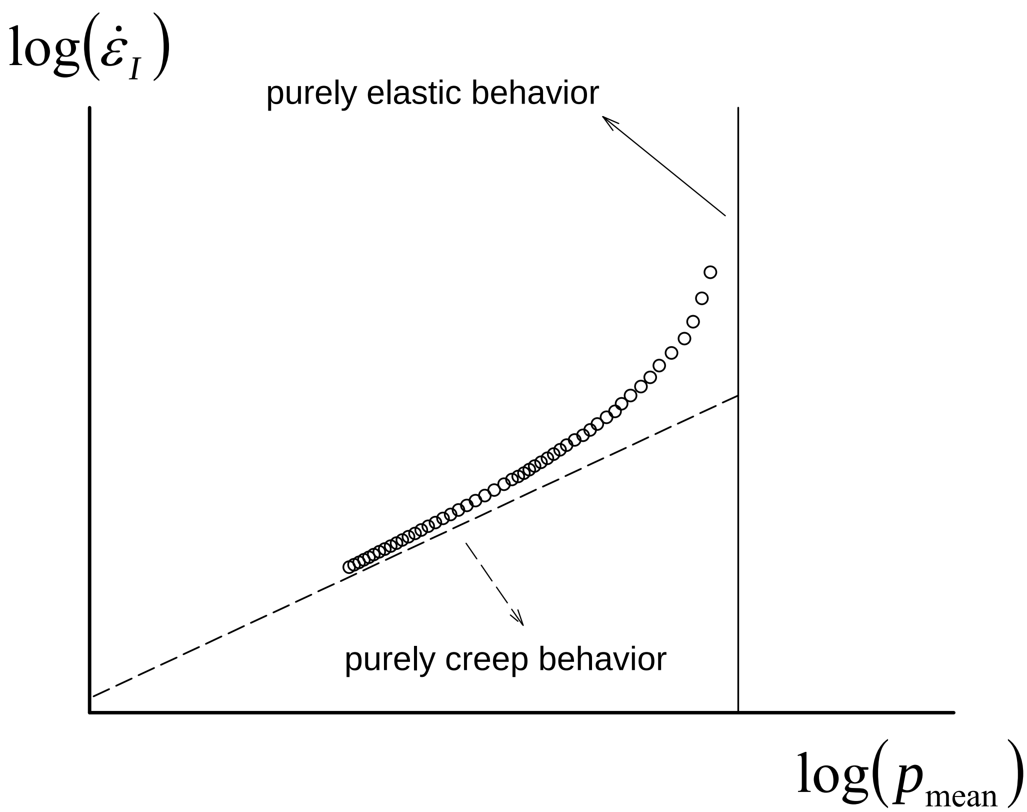

Figure 76. Limiting curves of indentation strain rate – mean pressure (cone, CRL)

Precision of uniaxial creep parameters

The effect of elasticity in precisely determining unaxial creep parameters of a material with a 70° conical indenter under the CRL method is demonstrated in Figure 77. Uniaxial creep exponents and uniaxial creep coefficients were computed from 10 local data points on the *h-t* or *P-h* curve. For the uniaxial creep exponent, the maximum estimated error at the shallow depth of $h/h_{elastic}$=2 is within 40%, and at a depth of $h/h_{elastic}$=5, the prediction yields results with errors less than 10%. The uniaxial creep coefficient is slightly more sensitive with a maximum overestimation of 70%. Note that the magnitudes of the errors in predicting the uniaxial creep coefficient using conical indentation under the CRL method are much smaller than those of spherical indentation under the CRL method. This shows again that the conical indenter diminishes elastic effects.

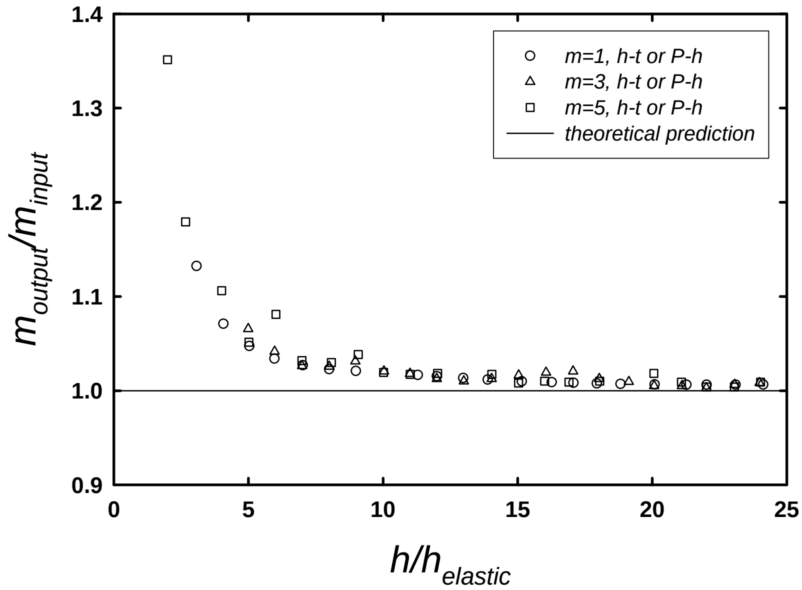

(a) Output uniaxial creep exponent calculation

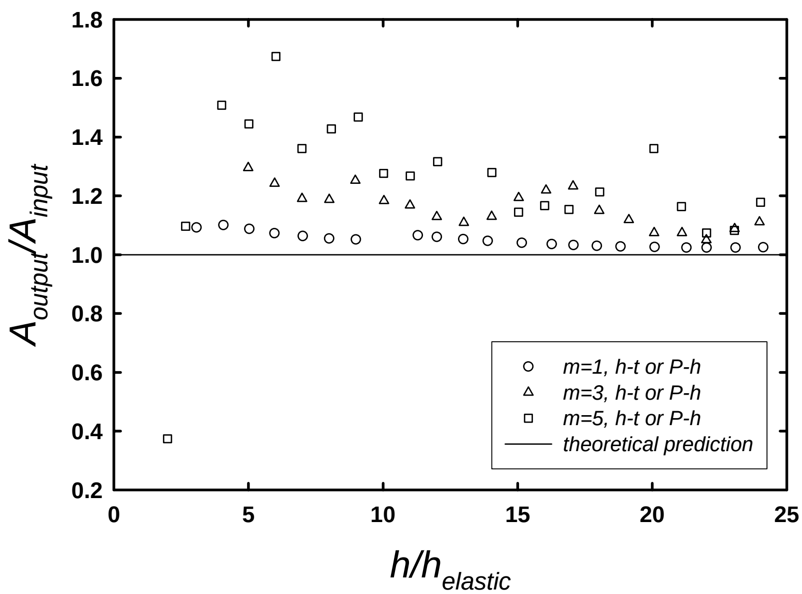

(b) Output uniaxial creep coefficient calculation

Figure 77. Effects of the elasticity on uniaxial creep parameters (70° cone, CRL)

CHAPTER 5 – CONCLUSIONS FOR INDENTATION OF AN ELASTIC – POWER LAW CREEPING SOLID

The primary conclusions drawn from the study of indentation of an elastic – power law creeping solid are presented in this chapter. The conclusions provide recommendations to experimentalists on how to best conduct indentation creep experiments to make meaningful measurements of fundamental creep parameters, especially m and A.

Conclusions

1) The use of h-t or P-h curves produced from spherical or conical indentation enables us to predict the uniaxial power law creep parameters from indentation. For an elastic – power law creeping solid, the uniaxial creep exponent can be obtained from the slope of $\log h$-$\log t$ or $\log P$-$\log h$ curve at long times or large depths. With auxiliary functional relationships, the uniaxial creep coefficient can be computed from the intercept of $\log h$-$\log t$ or $\log P$-$\log h$ curve. A flowchart showing this process is shown in Figure 78.

2) For spherical indentation, $c(m)$ and $F(m)$ by Bower *et. al.* may be used as the auxiliary functional relationships. For conical indentation, $c(m,\beta)$ and $F(m,\beta)$ must be redefined as introduced in this dissertation. Table 8 lists the auxiliary functional relationships for spherical and conical indentations.

3) With elastic normalization, master h-t or P-h curves are available from FEM for different indenter geometries and different loading methods. The normalizations are summarized in Table 9 and Table 10.

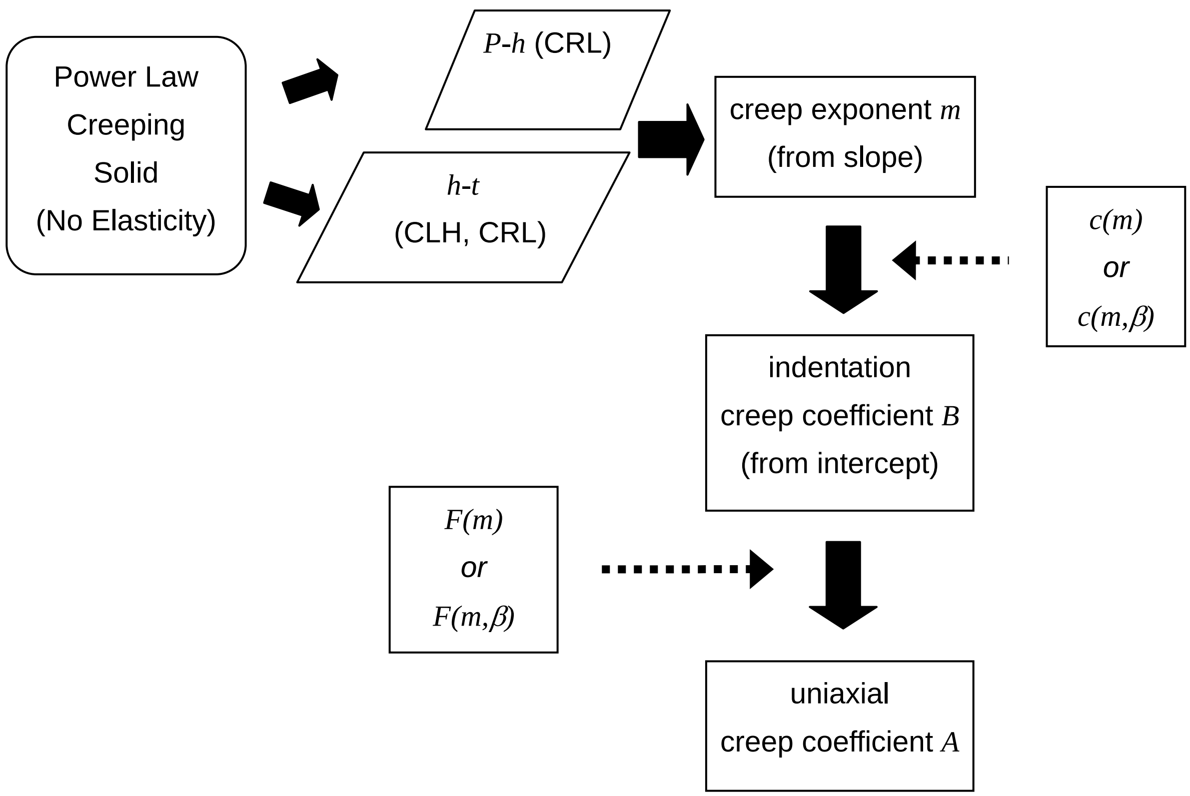

Figure 78. Flowchart of uniaxial power law creep parameter extraction process from indentation

Table 8. Auxiliary functional relationship for spherical and conical indentations

	$c(m)$ or $c(m,\beta)$
Sphere	$c(m)=1.204-\left(\frac{0.766}{m}\right)+\left(\frac{0.497}{m^2}\right)-\left(\frac{0.231}{m^3}\right)$
Cone (β=60°)	$c(m,60^{\circ})=1.326-\left(\frac{0.925}{m}\right)+\left(\frac{0.470}{m^2}\right)-\left(\frac{0.210}{m^3}\right)$
Cone (β=70°)	$c(m,70^{\circ})=1.310-\left(\frac{0.948}{m}\right)+\left(\frac{0.540}{m^2}\right)-\left(\frac{0.252}{m^3}\right)$
Cone (β=80°)	$c(m,80^{\circ})=1.281-\left(\frac{0.884}{m}\right)+\left(\frac{0.493}{m^2}\right)-\left(\frac{0.247}{m^3}\right)$

	$F(m)$ or $F(m,\beta)$
Sphere	$F(m)=3.048+\left(\frac{1.440}{m}\right)-\left(\frac{11.360}{m^2}\right)+\left(\frac{12.191}{m^3}\right)-\left(\frac{4.475}{m^4}\right)$
Cone (β=60°)	$F(m,60^{\circ})=2.280+\left(\frac{3.496}{m}\right)-\left(\frac{13.253}{m^2}\right)+\left(\frac{12.349}{m^3}\right)-\left(\frac{4.069}{m^4}\right)$
Cone (β=70°)	$F(m,70^{\circ})=2.588+\left(\frac{2.745}{m}\right)-\left(\frac{12.428}{m^2}\right)+\left(\frac{11.915}{m^3}\right)-\left(\frac{3.996}{m^4}\right)$
Cone (β=80°)	$F(m,80^{\circ})=2.889+\left(\frac{1.522}{m}\right)-\left(\frac{10.242}{m^2}\right)+\left(\frac{10.074}{m^3}\right)-\left(\frac{3.407}{m^4}\right)$

Table 9. Summary of elastic normalizations for spherical indentation

	Sphere, CLH	Sphere, CRL
Normalized Depth	$\dfrac{h}{h_{\mathrm{Hertz}}}$	$\dfrac{h}{h_{\mathrm{Hertz}}}$
Normalized Time	$\dfrac{t}{t_{\mathrm{sphereCLH}}}$	$\dfrac{t}{t_{\mathrm{sphereCRL}}}$
Normalized Load	Not Applicable	$\dfrac{P}{P_{\mathrm{sphereCRL}}}$
h_{Hertz}	$\left[\dfrac{9\left(1-\nu^2\right)^2 P^2}{16RE^2}\right]^{\frac{1}{3}}$	
$t_{\mathrm{sphereCLH}}$	$\dfrac{\left[\dfrac{3\left(1-\nu^2\right)}{E}\right]^{\frac{2m+1}{3}}\left(\pi^m\right)\left(P^{\frac{1-m}{3}}\right)}{B\left(\dfrac{2m+1}{2}\right)\left(c^{1-2m}\right)\left(2^{\frac{2m+7}{6}}\right)\left[R^{\frac{2}{3}(1-m)}\right]}$	
$t_{\mathrm{sphereCRL}}$	$\left\{\left(\dfrac{2m+2}{2m+1}\right)^2\left[\dfrac{3\left(1-\nu^2\right)P}{E}\right]^{\frac{4m+2}{3}}\left(\dfrac{c^{2m-1}}{B}\right)^2\left(\dfrac{\pi}{\dot{P}}\right)^{2m}\left(2^{-\frac{2m+7}{3}}\right)\left[R^{\frac{4}{3}(m-1)}\right]\right\}^{\frac{1}{2m+2}}$	
$P_{\mathrm{sphereCRL}}$	$\left\{\left(\dfrac{2m+2}{2m+1}\right)\left[\dfrac{3\left(1-\nu^2\right)P}{E}\right]^{\frac{2m+1}{3}}\left(\dfrac{\pi^m\dot{P}}{B}\right)\left(c^{2m-1}\right)\left(2^{-\frac{2m+7}{6}}\right)\left[R^{\frac{2}{3}(m-1)}\right]\right\}^{\frac{1}{m+1}}$	

Table 10. Summary of elastic normalizations for conical indentation

	Cone, CLH	Cone, CRL
Normalized Depth	$\dfrac{h}{h_{\text{Sneddon}}}$	$\dfrac{h}{h_{\text{Sneddon}}}$
Normalized Time	$\dfrac{t}{t_{\text{coneCLH}}}$	$\dfrac{t}{t_{\text{coneCRL}}}$
Normalized Load	Not Applicable	$\dfrac{P}{P_{\text{coneCRL}}}$
h_{Sneddon}	$\left[\dfrac{\pi P\left(1-\nu^{2}\right)}{2E\tan\beta}\right]^{\frac{1}{2}}$	
t_{coneCLH}	$\left[\dfrac{\pi^{2m}\left(1-\nu^{2}\right)^{m}}{E^{m}Bm\left(2^{m+1}\right)\left(c^{1-2m}\right)\left(\tan\beta\right)^{1-m}}\right]$	
t_{coneCRL}	$\left\{\left(\dfrac{m+1}{2m}\right)\left[\dfrac{P\left(1-\nu^{2}\right)}{2\dot{P}E}\right]^{m}\left(\dfrac{\pi^{2m}}{B}\right)\left(c^{2m-1}\right)\left(\tan\beta\right)^{m-1}\right\}^{\frac{1}{m+1}}$	
P_{coneCRL}	$\left\{\left(\dfrac{m+1}{2m}\right)\left[\dfrac{P\left(1-\nu^{2}\right)}{2E}\right]^{m}\left(\dfrac{\pi^{2m}\dot{P}}{B}\right)\left(c^{2m-1}\right)\left(\tan\beta\right)^{m-1}\right\}^{\frac{1}{m+1}}$	

The master curves produced from elastic normalizations are unique functions of the creep exponent. The master *h*-*t* curves for the CLH method are shown in Figures 79-81. In each of these plots, the FEM produced master *h*-*t* curves fit well to a 7-parameter fit equation given by

$$y = 1 + x_0 x + x_1 x^{0.5} + x_2 x^{0.4} + x_3 x^{0.3} + x_4 x^{0.2} + x_5 x^{0.1} + x_6 x^{0.01} \quad (61)$$

Fit parameters for master *h*-*t* curves of the CLH method are listed in Table 11. In a similar manner, master *P*-*h* curves for the CRL method are shown in Figures 82-84. Again, the master *P*-*h* curves fit well to equation (61). Table 12 lists the fit parameters for master *P*-*h* curves for Figures 82-84.

4) Rigid – power law creep conditions are achieved when the indentation depth exceeds a certain criteria. The parameter $h/h_{elastic}$ can be used to determine the depth. The depth criteria to avoid elastic transient for both spherical and conical indentations are shown in Table 13.

Recommendations to the Indentation Experimentalists

The first uniaxial power law creep parameter available from the indentation *h*-*t* or *P*-*h* curve is the uniaxial creep exponent. Since we know the rigid – power law creep *h*-*t* or *P*-*h* relationship, creep exponents determined from the slopes of log*h*-log*t* or log*P*-log*h* may be examined for limiting cases of *m*. As *m* varies from 0 to ∞, the corresponding variations in the slopes of *h*-*t* or *P*-*h* curves are shown in Table 14. In the majority of the cases, only a slight change in the slope results in creep exponents varying from 0 to ∞.

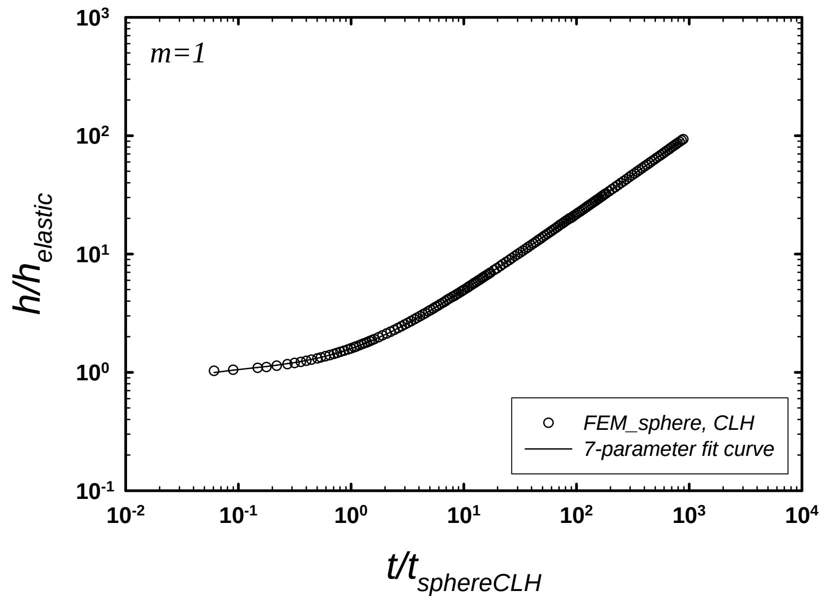

(a) spherical indentation

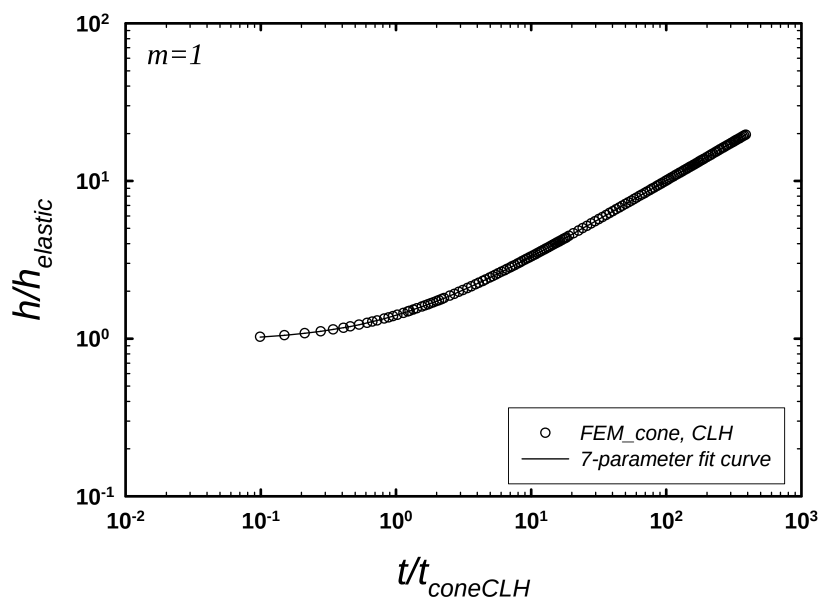

(b) conical indentation

Figure 79. Master *h*-*t* and fit curves for *m*=1 (CLH method)

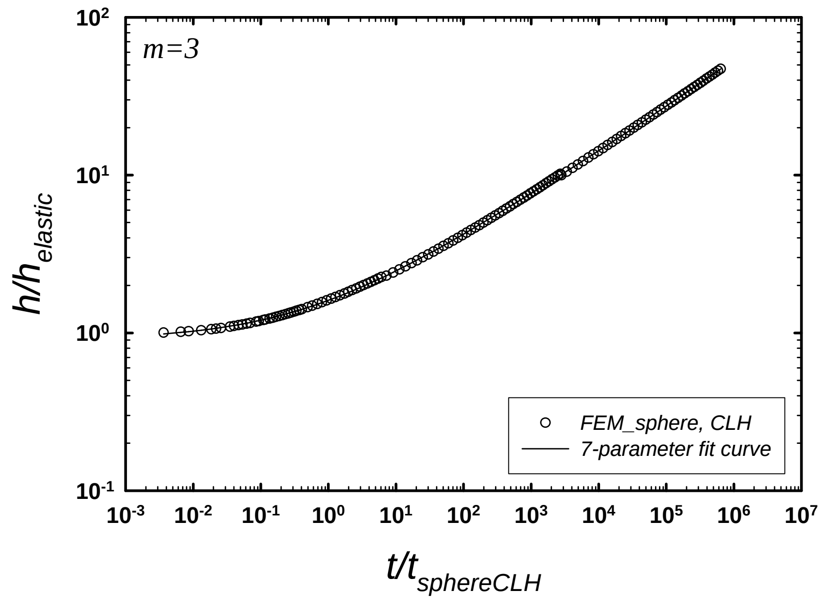

(a) spherical indentation

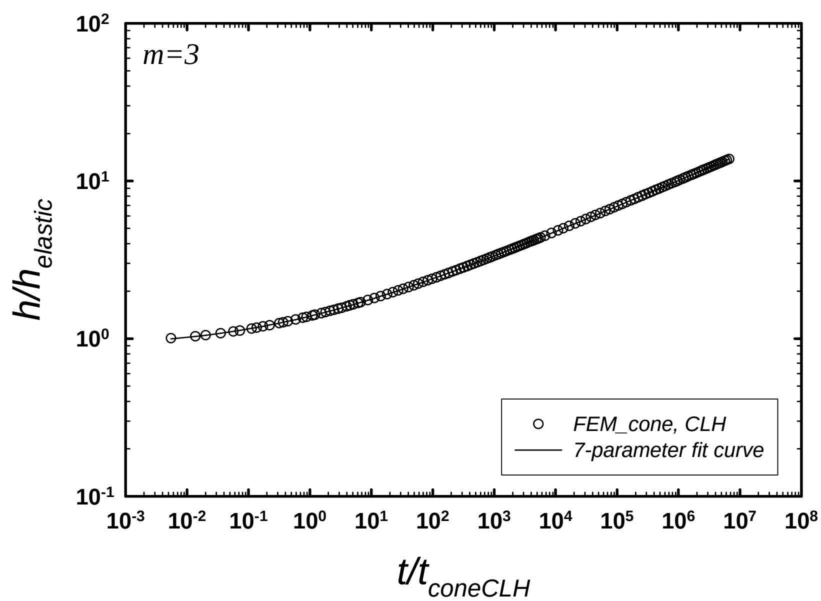

(b) conical indentation

Figure 80. Master *h-t* and fit curves for *m*=3 (CLH method)

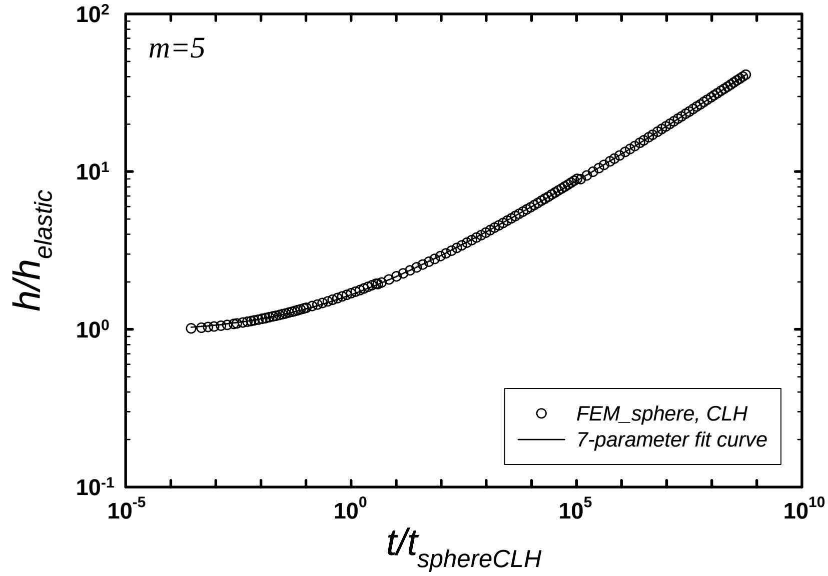

(a) spherical indentation

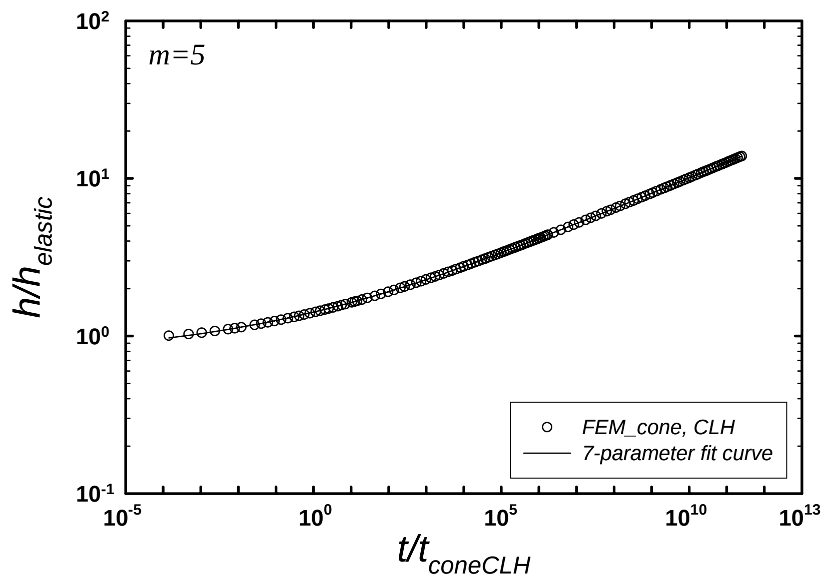

(b) conical indentation

Figure 81. Master *h-t* and fit curves for *m*=5 (CLH method)

Table 11. Fit parameters for the master *h-t* curves (CLH method)

Indenter Geometry	m	x_0	x_1	x_2	x_3	x_4	x_5	x_6
sphere	1	4.06e-3	2.85e1	-1.34e2	2.88e2	-3.26e2	1.92e2	-4.81e1
	3	-7.14e-6	1.13e-1	-8.64e-1	3.16e0	-2.51e0	9.89e-1	-2.79e-1
	5	3.49e-9	-2.73e-3	4.91e-2	-3.34e-1	1.68e0	-8.44e-1	1.11e-1
cone	1	-2.36e-3	6.74e0	-3.57e1	8.88e1	-1.09e2	6.60e1	-1.64e1
	3	6.28e-8	-5.51e-3	7.18e-2	-4.02e-2	1.62e0	-9.87e-1	9.00e-2
	5	3.39e-12	-4.05e-5	1.28e-3	-1.59e-2	9.67e-2	6.95e-1	-3.60e-1

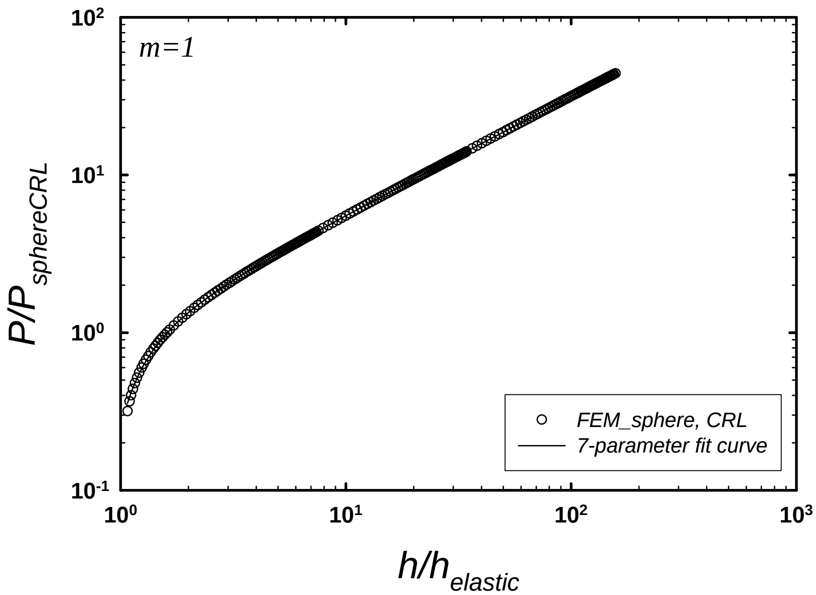

(a) spherical indentation

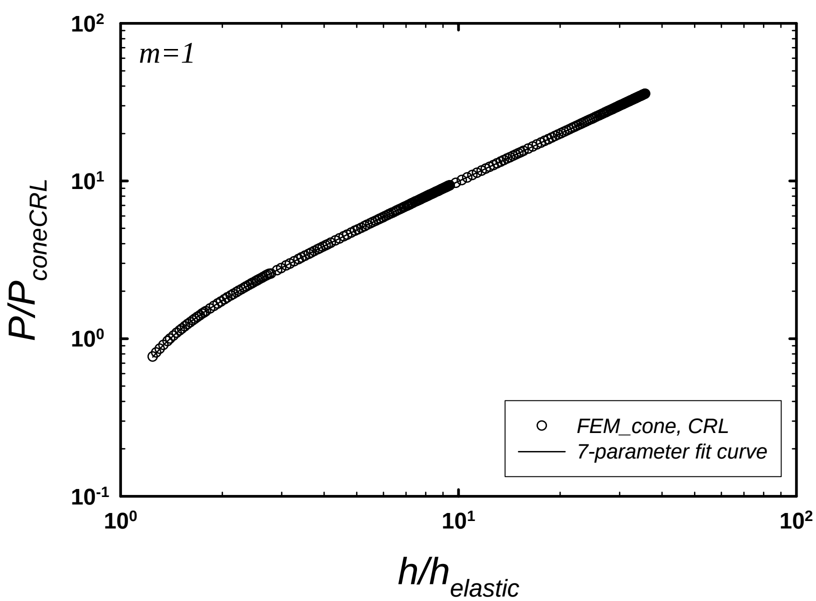

(b) conical indentation

Figure 82. Master *P-h* and fit curves for *m*=1 (CRL method)

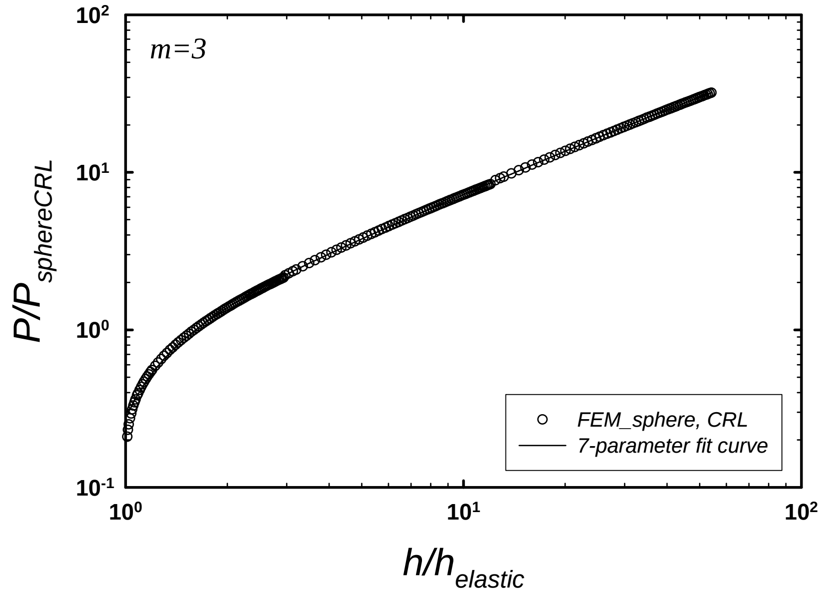

(a) spherical indentation

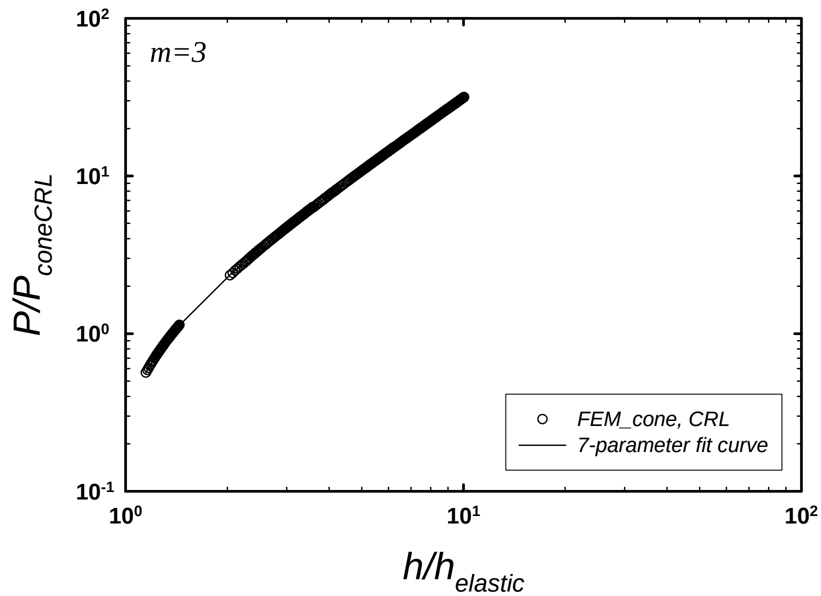

(b) conical indentation

Figure 83. Master *P-h* and fit curves for *m*=3 (CRL method)

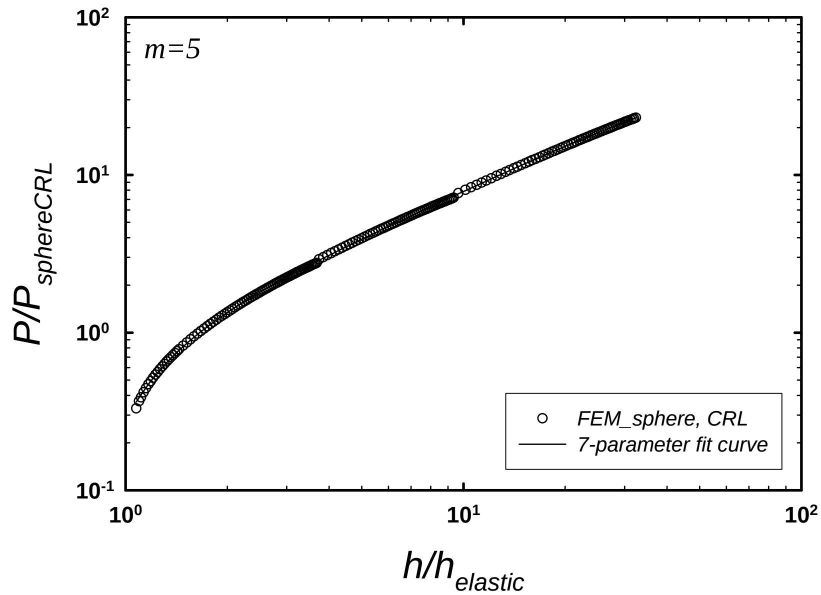

(a) spherical indentation

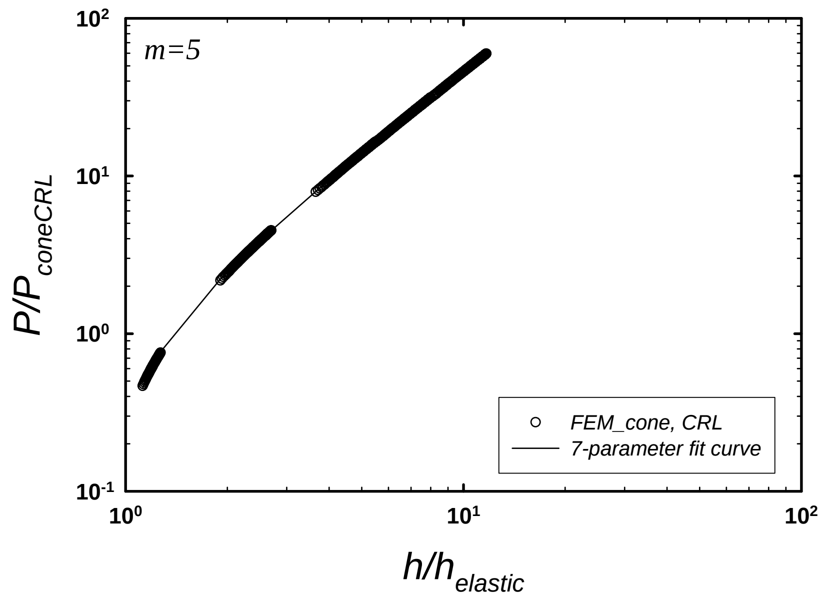

(b) conical indentation

Figure 84. Master *P-h* and fit curves for *m*=5 (CRL method)

Table 12. Fit parameters for the master *P-h* curves (CRL method)

Indenter Geometry	m	x_0	x_1	x_2	x_3	x_4	x_5	x_6
sphere	1	-7.67e-1	9.03e2	-4.96e3	1.13e4	-1.32e4	8.16e3	-2.16e3
	3	-8.35e-1	2.06e2	-5.33e2	2.08e2	5.77e2	-6.77e2	2.19e2
	5	-3.24e0	6.20e2	-1.62e3	5.65e2	2.07e3	-2.48e3	8.55e2
cone	1	-8.33e0	7.15e3	-3.70e4	7.90e4	-8.65e4	4.99e4	-1.24e4
	3	4.29e1	-4.35e3	1.10e4	-4.31e3	-1.17e4	1.42e4	-4.84e3
	5	9.27e1	-1.00e4	2.60e4	-1.23e4	-2.37e4	3.04e4	-1.06e4

Table 13. Criteria for avoiding elastic transient

	spherical indentation	70° conical indentation
CLH method	$\frac{h}{h_{\mathrm{Hertz}}} \geq 20$	$\frac{h}{h_{\mathrm{Sneddon}}} \geq 10$
CRL method	$\frac{h}{h_{\mathrm{Hertz}}} \geq 20$	$\frac{h}{h_{\mathrm{Sneddon}}} \geq 10$

Table 14. Sensitivity of the slope of *h-t* or *P-h* curves to *m*

Indenter Geometry	Sphere (m=1~∞)			Cone (m=1~∞)		
Loading Method & Data Analysis	CLH *h-t*	CRL *h-t*	CRL *P-h*	CLH *h-t*	CRL *h-t*	CRL *P-h*
slope of the curve (log-log scale)	$\frac{2}{3} \sim 0$	$\frac{4}{3} \sim 1$	$\frac{3}{4} \sim 1$	$\frac{1}{2} \sim 0$	$1 \sim \frac{1}{2}$	$1 \sim 2$

Therefore, estimated creep exponents are highly sensitive to the slope of indentation $\log h$-$\log t$ or $\log P$-$\log h$ curves.

Based on the analysis and results provided from this dissertation, conical indentation compared to spherical indentation is more capable of avoiding elasticity at relatively shallower normalized depth, $h/h_{elastic}$. Therefore, employing conical indenter in indentation experiments may be a preferable choice. However, recommendation on which loading method (CLH versus CRL) to adopt is not clear and may require more sophisticated analysis.

CHAPTER 6 – APPLICATION OF INDENTATION CREEP TO PURE ALUMINUM UNIAXIAL CREEP DATA

In this chapter, we compare the results and conclusions drawn from the previous chapters in this dissertation to a practical material with known power law creep parameters for the purpose of examining the feasibility of extracting realistic uniaxial power law creep parameters from indentation. Pure aluminum is selected as the material of interest. Luthy *et. al.* have provided extensive uniaxial creep parameters for pure aluminum at various temperatures [2].

Temperature Dependent Uniaxial Power Law Creep Parameters for Pure Aluminum

Luthy *et. al.*'s uniaxial creep test results describe power law as well as power law breakdown behavior of creep for pure aluminum [2]. The correlation between normalized stress and temperature compensated strain rate is given by

$$\left(\frac{\dot{\varepsilon}_{\mathrm{ss}}}{D_{\mathrm{eff}}}\right) = K'\left[\sinh\left(\alpha\frac{\sigma}{E}\right)\right]^{m} \tag{3}$$

with m=4.8 and α=2600. According to their analysis, the data exhibit power law breakdown behavior for $\sigma/E>4\times10^{-4}$. For stresses less than $\sigma/E<4\times10^{-4}$, a power law constitutive relation well describes the creep deformation process. Therefore, equation (3) reduces to

$$\left(\frac{\dot{\varepsilon}_{ss}}{D_{eff}}\right) = K'\left(\alpha\frac{\sigma_{ss}}{E}\right)^m \tag{62}$$

for small normalized stresses. Rewriting equation (62) yields

$$\dot{\varepsilon}_{ss} = \left[K'D_{eff}\left(\frac{\alpha}{E}\right)^m\right](\sigma_{ss})^m \tag{63}$$

The relationship is now expressed in terms of steady-state strain rate and steady-state stress with a coefficient and exponent in the mathematical form we adopt for this dissertation. By comparing equations (63) and (1), we are able to determine the creep coefficient. The relationship between *A* and the temperature compensated term is expressed by

$$A = K'D_{eff}\left(\frac{\alpha}{E}\right)^m \tag{64}$$

Here, α, *m*, and *E* are known values. By reanalyzing Luthy *et. al.*'s results, we are able to estimate K'=2.03×10^{14} [m^{-2}]. The only other term requiring numerical evaluation is the D_{eff}, which is the diffusion coefficient. Luthy *et. al.* use existing literature to suggest the following correlation for D_{eff}.

$$\begin{aligned} D_{eff} &= \left[\left(1.7\times10^{-4}\right)\exp\left(-\frac{142}{RT}\right)\right] + \left[\left(6\times10^{-7}\right)\exp\left(-\frac{115}{RT}\right)\right] \\ &+ \left[\left(2.8\times10^{-6}\right)\exp\left(-\frac{82}{RT}\right)\right]\left[80\left(\frac{\sigma}{E}\right)^2\right], \quad \left[\frac{m^2}{s}\right] \end{aligned} \tag{65}$$

Here, *R* is the universal gas constant and *T* is the absolute test temperature. The first two terms in the right side of equation (65) represents diffusion coefficient for self-lattice diffusion. These two additive terms in the self-lattice diffusion is due to two existing self-lattice diffusion coefficient for pure aluminum, as explained in detail by Luthy *et. al.* [2].

The last term in the right side of equation (65) with the dependence on normalized stress (σ/E) accounts for the dislocation pipe diffusion [2]. Combining equations (64), (65), and the known values for K', α, E, and m, A in terms of temperature compensated parameters for pure aluminum is given by

$$\begin{aligned} A = & \left[\left(1.183\times10^{14}\right)\exp\left(-\frac{142}{RT}\right)\right] + \left[\left(4.175\times10^{11}\right)\exp\left(-\frac{115}{RT}\right)\right] \\ & + \left[\left(1.948\times10^{12}\right)\exp\left(-\frac{82}{RT}\right)\right]\left[80\left(\frac{\sigma}{E}\right)^2\right], \quad \left[\frac{1}{GPa^{4.8}s}\right] \end{aligned} \tag{66}$$

The typical range [33] over which majority of creep data are typically acquired is

$$10^{-4} < \frac{\sigma}{G} < 10^{-3} \tag{67}$$

In equation (67), σ is the applied stress and G is the shear modulus of the material. Rewriting equation (67) with the elastic modulus (E=70GPa) and Poisson's ratio of pure aluminum (ν≈0.3) yields

$$3.85\times10^{-5} < \frac{\sigma}{E} < 3.85\times10^{-4} \tag{68}$$

For simplicity, accepting the average value of typical σ/E in uniaxial creep test (σ/E=2.12×10^{-4}), the correlation of the uniaxial creep coefficient A to the test temperature considered in Luthy *et. al.* is shown in Figure 85.

Application of Indentation Creep to Pure Aluminum

According to Luthy *et. al.*, the uniaxial creep exponent of pure aluminum is 4.8 and the uniaxial creep coefficient is given by Figure 85 for a typical σ/E value. Approximating the uniaxial creep exponent of the pure aluminum to be 5 (thus, the

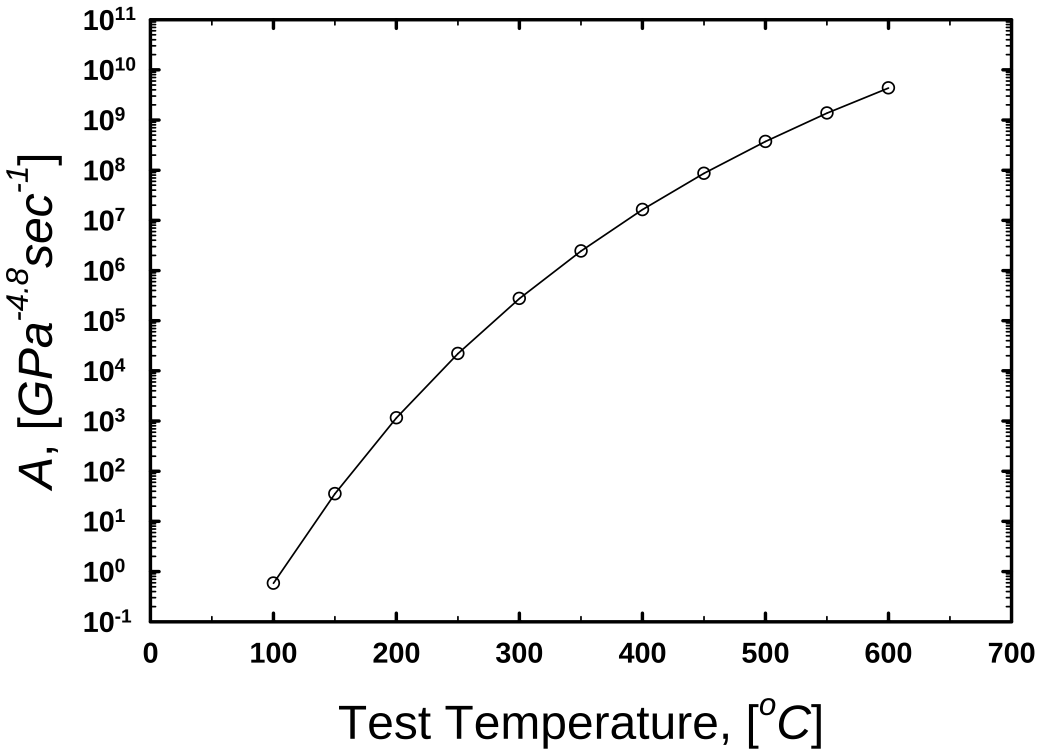

Figure 85. Correlation of *A* to test temperature for pure aluminum [2]

indentation creep exponent is 5), we are able to apply the results and conclusions drawn from previous chapters of this dissertation to determine the necessary experimental conditions needed to extract the uniaxial creep coefficient of pure aluminum. Note that since a temperature dependence was not built into the creep model used in this dissertation, we simply assume that the activation energy for creep calculated from indentation is identical to the activation energy for creep from the uniaxial creep test. Therefore, the temperature dependence in indentation creep is assumed to be same as the temperature dependence of uniaxial creep. With this assumption, we proceed to propose required indentation experimental conditions for spherical and 70° conical indenters. In order to avoid estimation errors caused by elasticity from indentation, the criteria of interest in estimating the uniaxial creep parameters is the depth of indentation with respect to the elastic depth.

Application of pure aluminum data to spherical indentation under the CLH method

In Chapter 4, it was suggested that a depth of at least h/h_{elastic}=20 should be achieved to avoid elastic transients in predicting the uniaxial creep parameters for spherical indentation under the CLH method. Therefore, the depth of indentation should satisfy

$$\left(\frac{h}{h_{\mathrm{Hertz}}}\right)_{\mathrm{sphere,\ CLH}} \geq 20 \tag{69}$$

When condition set by equation (69) is applied to equation (32), which is the master curve *h*-*t* relation, we are able to rewrite equation (69) as

$$\left(\frac{t}{t_{\mathrm{sphereCLH}}}\right)^{\frac{2}{11}} \geq 20 \tag{70}$$

for m=5. Substituting $t_{\text{sphereCLH}}$ with equation (29) for m=5 and rearranging equation (70) yields

$$t \geq \frac{\left(20^{\frac{11}{2}}\right)\left[\frac{3\left(1-\nu^{2}\right)}{E}\right]^{\frac{11}{3}}\left(\pi^{5}\right)\left(P^{-\frac{4}{3}}\right)}{B\left(\frac{11}{2}\right)\left(c^{-9}\right)\left(2^{\frac{17}{6}}\right)\left(R^{-\frac{8}{3}}\right)} \tag{71}$$

Substituting the known variables and parameters into equation (71), the required time for indentation to produce valid data may be expressed as a function of the uniaxial creep coefficient, applied load, and the radius of the indenter as

$$t \geq \frac{312002R^{\frac{8}{3}}}{AP^{\frac{4}{3}}} \tag{72}$$

To visualize this problem explicitly, we choose an indenter of R=50μm with an applied load of P=10mN. Note that, due to restrictions on infinitesimal strain – infinitesimal deformation issue (a/R<0.4), the maximum depth of indentation in this case should be limited to 3.5μm. We now define the critical time of indentation according to the relation provided by equation (72), t_{critical}, to be the minimum time for the indenter to be driven in to yield an h-t curve free from elastic transient. Then t_{critical} can be calculated for the given indentation conditions and the result is shown in Figure 86. Note that at this given indentation experiment condition, the initial elastic depth is h_{elastic}≈58nm. It is seen from Figure 86 that, it takes an unrealistic amount of time (impossible in a real indentation experiment) for the effects of elasticity to diminish in the h-t curve at 100℃. The temperature dependence of t_{critical} is very strong, and at approximately 300℃, the critical time decreases to a value that may be achieved in a

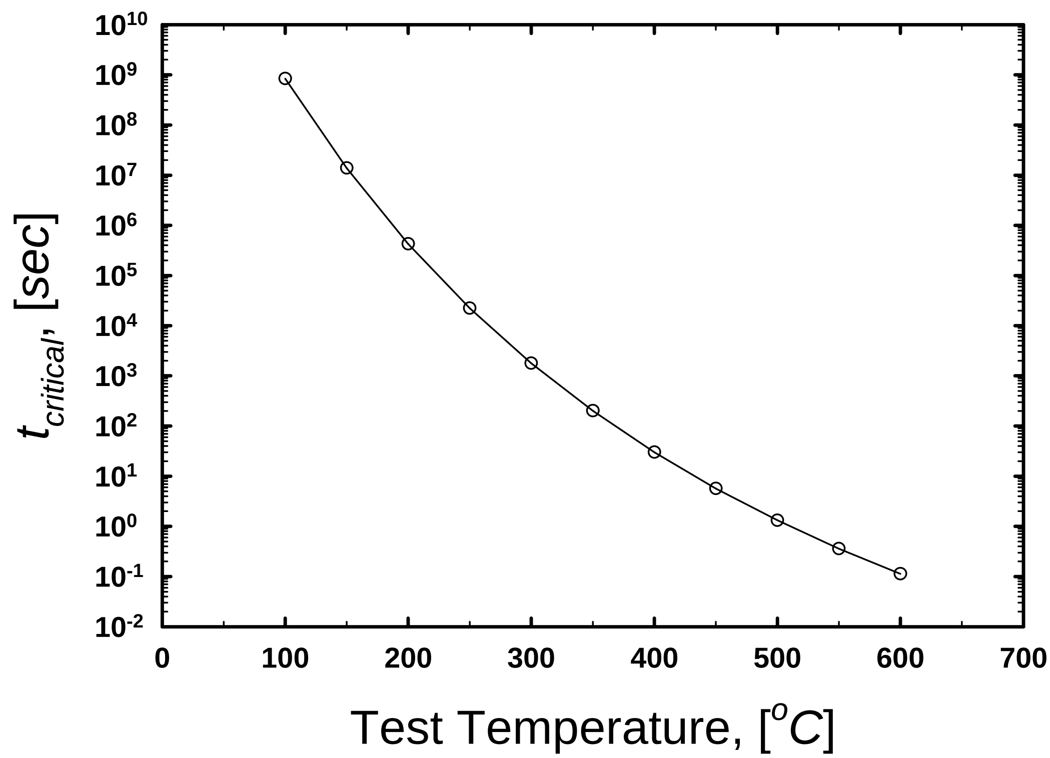

Figure 86. An example of critical time as a function of test temperature (sphere, CLH)

real indentation experiment (t_{critical}=1781*sec* or 30*min*). Thus, assuming that indentation test can be conducted at this temperature, the uniaxial creep exponent *m* may be estimated within 5% of error and the uniaxial creep coefficient *A* may be estimated within 20% of error according to the results from this dissertation.

Application of pure aluminum data to spherical indentation under the CRL method

Similar to the situation for spherical indentation under the CLH method, depth of indentation should satisfy

$$\left(\frac{h}{h_{\text{Hertz}}}\right)_{\text{sphere, CRL}} \geq 20 \tag{73}$$

in order to avoid the elastic transient. In terms of the master curve *P-h* relation (equation (36)), equation (73) may be rewritten as

$$\left(\frac{P}{P_{\text{sphereCRL}}}\right)^{\frac{12}{11}} \geq 20 \tag{74}$$

for *m*=5. Substituting $P_{\text{sphereCRL}}$ with equation (34) for *m*=5 and rearranging equation (74) yields

$$P \geq \left\{ \frac{\left(20^{\frac{11}{2}}\right)\left[\frac{3\left(1-\nu^{2}\right)}{E}\right]^{\frac{11}{3}}\left(\pi^{5}\right)\left(\dot{P}\right)\left(c^{9}\right)\left(2^{\frac{17}{6}}\right)\left(R^{\frac{8}{3}}\right)}{B} \right\}^{\frac{3}{7}} \tag{75}$$

Substituting the known variables and parameters into equation (75), the required load for indentation to produce valid data may be expressed as a function of the uniaxial creep coefficient, applied loading rate, and the radius of the indenter as

$$P \geq \left[\frac{487\dot{P}\left(R^{\frac{8}{3}}\right)}{A} \right]^{\frac{3}{7}} \tag{76}$$

For practical application, we choose an indenter of R=50μm with an applied loading rate of $dP/dt=1\mu N/sec$. Once again, infinitesimal strain – infinitesimal deformation issue (a/R<0.4) imposes a restriction on the depth of indentation. Thus, the maximum depth of indentation in this case is limited to 3.5μm. We now define the critical load of indentation according to the relation provided by equation (76), P_{critical}, to be the minimum load for the indenter to be driven in to yield *h-t* or *P-h* curve free from elastic transient. Then P_{critical} can be calculated for the given indentation conditions and the result is shown in Figure 87. It is demonstrated in Figure 87 that, an unrealistic load of 2786 *mN* should be achieved before valid data is acquired at a test temperature of 100 ℃. Again, the temperature dependence of P_{critical} is very strong, and at approximately 350 ℃, this critical load drops to 4*mN*. In terms of time, this corresponds to 4038 seconds (or 1.1 hours), which is achievable in experimental conditions, provided that the test temperature is stabilized at 350 ℃.

Application of pure aluminum data to 70° conical indentation under the CLH method

The depth criteria to avoid the elastic transient for conical indentation under the CLH method is

$$\left(\frac{h}{h_{\text{Sneddon}}}\right)_{\text{cone, CLH}} \geq 10 \tag{77}$$

When condition set by equation (77) is applied to the master curve *h-t* relation (equation (53)), we are able to rewrite equation (77) as

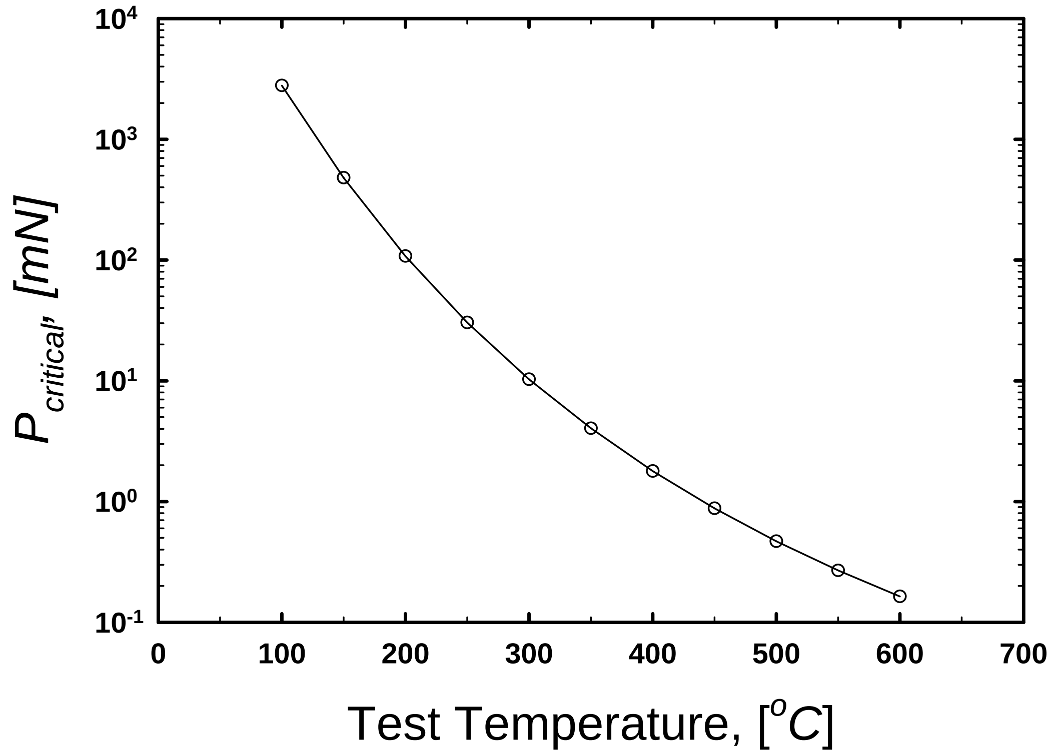

Figure 87. An example of critical load as a function of test temperature (sphere, CRL)

$$\left(\frac{t}{t_{\mathrm{coneCLH}}}\right)^{\frac{1}{10}} \geq 10 \tag{78}$$

for m=5. Substituting t_{coneCLH} with equation (50) for m=5 and rearranging equation (78) yields

$$t \geq \frac{\left(10^{10}\right)\left(\pi^{10}\right)\left(1-\nu^{2}\right)^{5}\left(c^{9}\right)\left(\tan\beta\right)^{4}}{(5)\left(2^{6}\right)\left(E^{5}\right)(B)} \tag{79}$$

Substituting the known variables and parameters into equation (79), the required time for indentation to produce valid data may be expressed as a function of the uniaxial creep coefficient as

$$t \geq \frac{30570476}{A} \tag{80}$$

We define the critical time of indentation in a manner analogous to the analysis for spherical indentation under the CLH method. Therefore, t_{critical} is the minimum time for the indenter to be driven in to yield an *h*-*t* curve free from elastic transient. Then t_{critical} can be calculated for the given indentation conditions and the result is shown in Figure 88. From Figure 88, we observe that an unrealistic amount of time (impossible in a real indentation experiment) is required for the effects of elasticity to diminish in the *h*-*t* curve at 100 ℃. However, at 250 ℃, the critical time decreases to a value that may be achieved in a real indentation experiment (t_{critical}=1386*sec* or 23*min*).

Application of pure aluminum data to 70° conical indentation under the CRL method

Analogous to conical indentation under the CLH method, the depth of indentation should satisfy

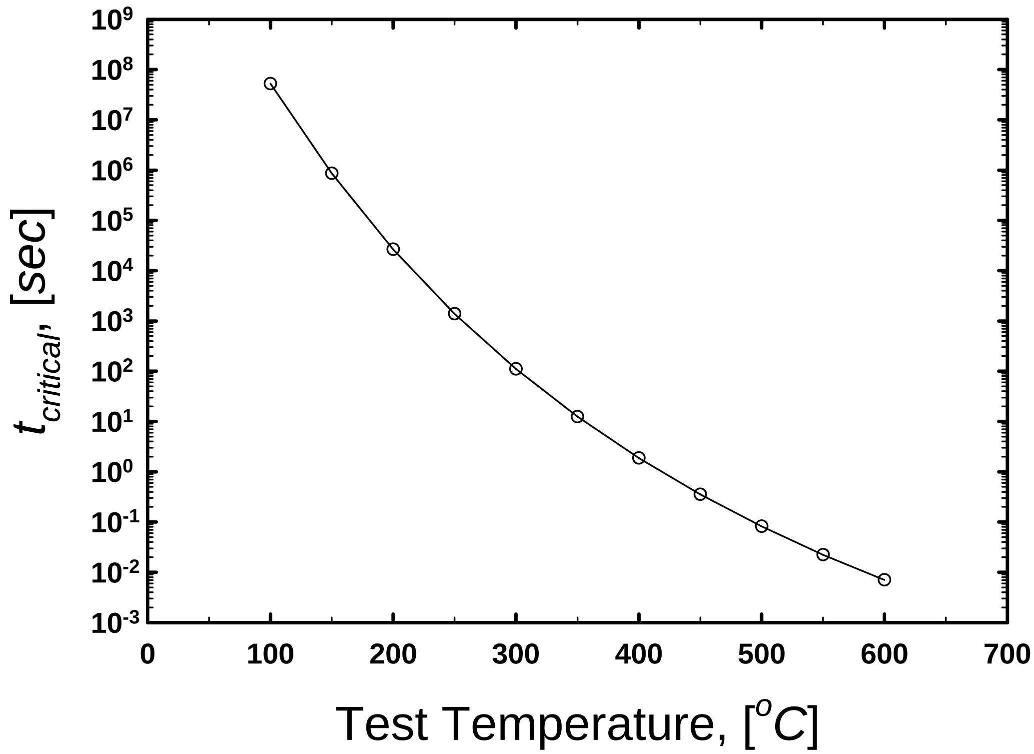

Figure 88. An example of critical time as a function of test temperature (70° cone, CLH)

$$\left(\frac{h}{h_{\text{Sneddon}}}\right)_{\text{cone, CRL}} \geq 10 \tag{81}$$

in order to avoid the elastic transient. Examining the master *P-h* curve for *m*=5 for conical indentation under the CRL method, the corresponding condition in terms of the load should be

$$\left(\frac{P}{P_{\text{coneCRL}}}\right)^{\frac{6}{10}} \geq 10 \tag{82}$$

Rewriting equation (82) with P_{coneCRL} given by equation (55) yields

$$P \geq \left(10^{\frac{10}{6}}\right)\left\{\left(\frac{6}{10}\right)\left(\frac{\pi^{10}\dot{P}}{B}\right)\left[\frac{P\left(1-\nu^{2}\right)}{2E}\right]^{5}\left(c^{9}\right)\left(\tan\beta\right)^{4}\right\}^{\frac{1}{6}} \tag{83}$$

Substituting the known variables and parameters into equation (83), the required load for indentation to produce valid data may be expressed as a function of uniaxial creep coefficient and applied loading rate as

$$P \geq \frac{183422859\dot{P}}{A} \tag{84}$$

For a practical application, a loading rate of $dP/dt=1\mu N/sec$ is considered. P_{critical} is the minimum load for the indentation to achieve in order to avoid the effects of elasticity for the CRL method. Figure 89 shows the correlation of P_{critical} to test temperature. An unrealistic load of 3.15×10^{5} *mN* should be achieved before valid data is acquired at a test temperature of 100 ℃. The critical load drops to 0.66*mN* at 300 ℃. In terms of time, this corresponds to 11 minutes, which is achievable in experimental conditions, provided that the test temperature is stabilized at 300 ℃.

Examples of predicted *h-t* and *P-h* curves for pure aluminum with the CRL

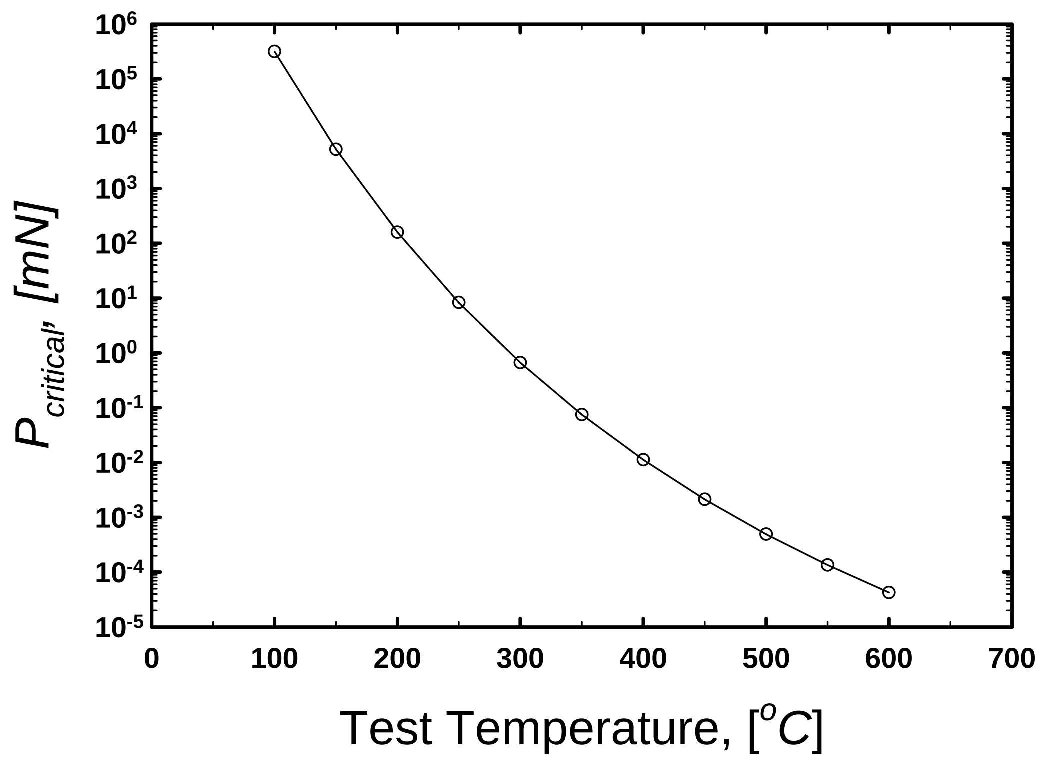

Figure 89. An example of critical load as a function of test temperature (70° cone, CRL)

indentation experiment condition outlined in the above sections are presented in Figures 90 and 91. Based on the analyses and results in this dissertation, these curves are realistic h-t and P-h curves at the intended test temperatures.

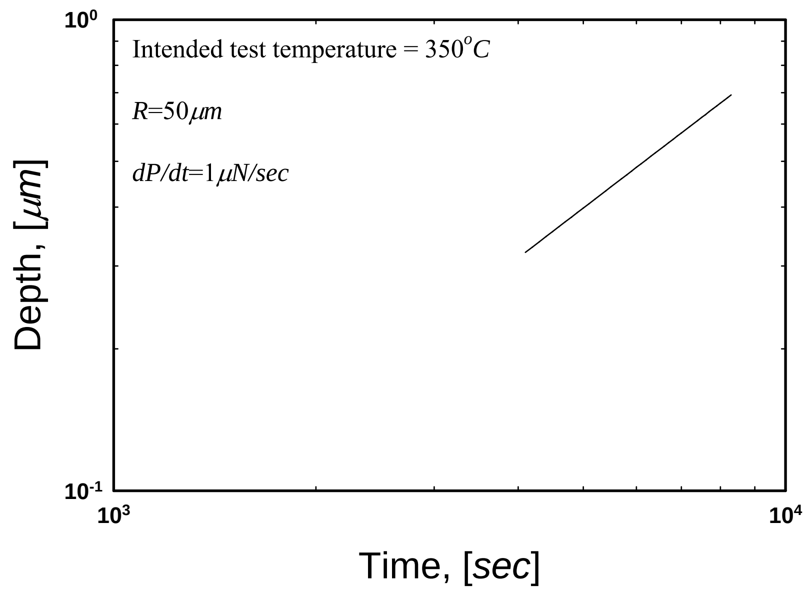

(a) *h-t* curve

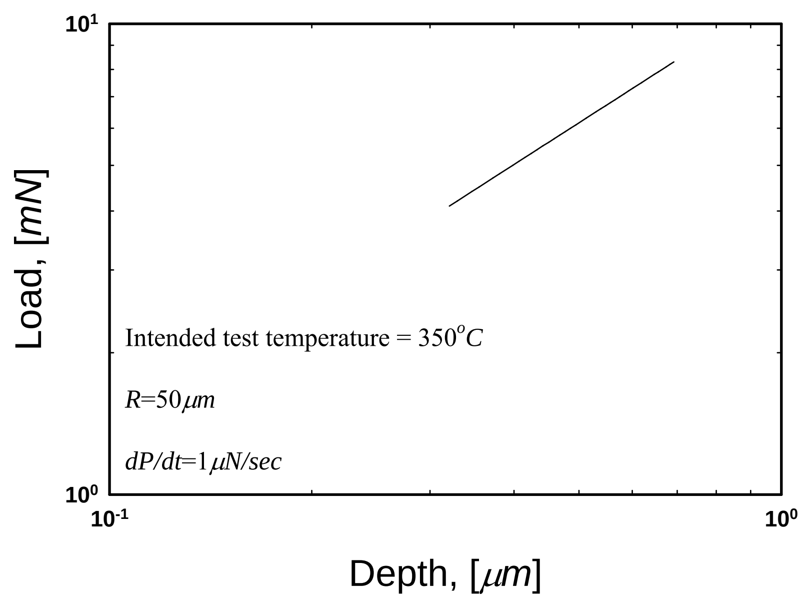

(b) *P-h* curve

Figure 90. Predicted *h-t* and *P-h* curve for pure aluminum (sphere, CRL)

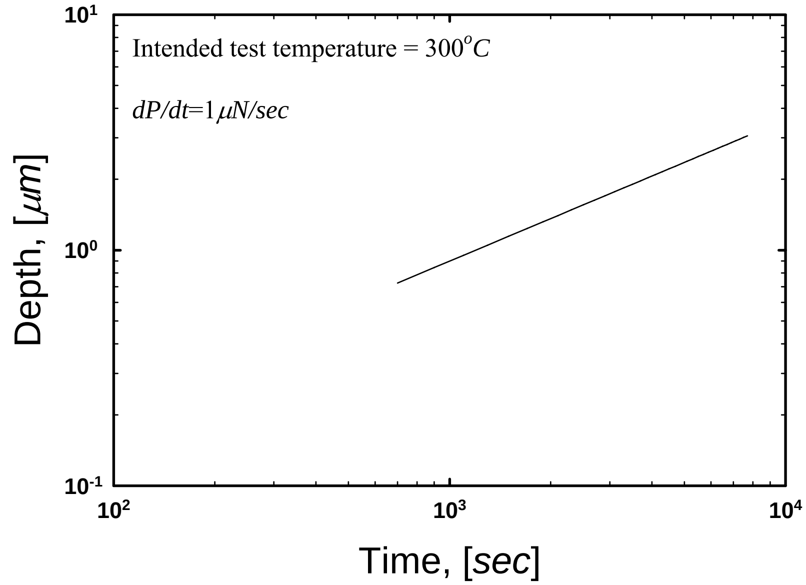

(a) *h*-*t* curve

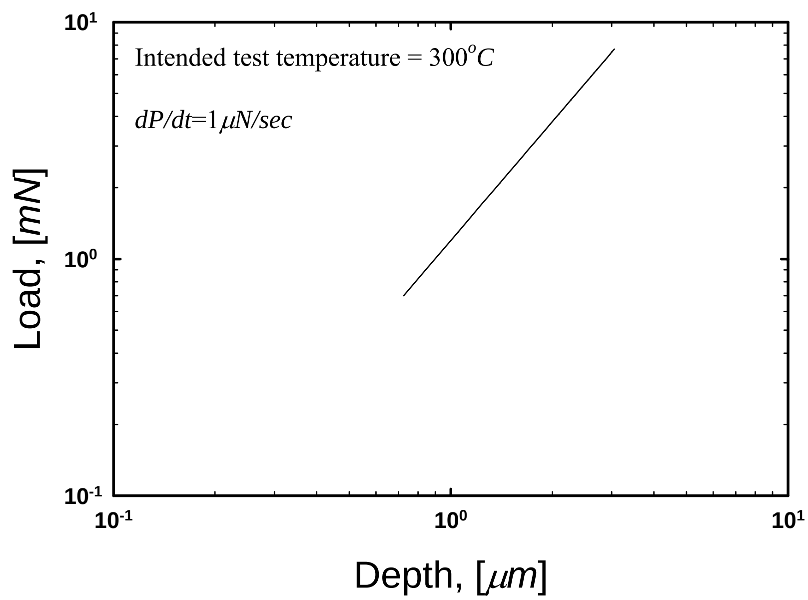

(b) *P*-*h* curve

Figure 91. Predicted *h-t* and *P-h* curve for pure aluminum (70° cone, CRL)

CHAPTER 7 – INDENTATION OF AN ELASTIC – HYPERBOLIC SINE LAW CREEPING SOLID

Extension of similarity transformation methods to rigid – hyperbolic sine law creep is not straightforward, and a simple analytical correlation between uniaxial creep and indentation creep may is not available. A previous study using the finite element method to simulate an elastic – hyperbolic sine law creeping solid assumed similarity in the constitutive relationships [22]. In studying indentation of a hyperbolic sine law creeping solid, we assume without proof that a simple correlation similar to the case of a power law creeping solid exists between uniaxial and indentation creep. Specifically, indentation of a hyperbolic sine law creeping solid is also characterized by a hyperbolic sine law equation of the form

$$\dot{\varepsilon}_I \approx B_1 \left[\sinh\left(B_2\, p_{\text{mean}}\right)\right]^m \tag{85}$$

where B_1 and B_2 are material constants. The validity of this assumption based on finite element simulation is demonstrated in Figure 92. In this figure, a hyperbolic sine law equation is fit to the results from FEM, and these are compared to the input constitutive relationship. To avoid the effects of elasticity, the mean pressure and indentation strain rate data are taken at relatively long indentation times and large indentation depths. Therefore, the resulting input constitutive relation may be characterized by hyperbolic sine law without the addition of elasticity. When this condition is satisfied, it is seen from Figure 92 that the output constitutive law is well described by a 3-parameter hyperbolic sine law fit with a coefficient, a hyperbolic multiplier, and an exponent.

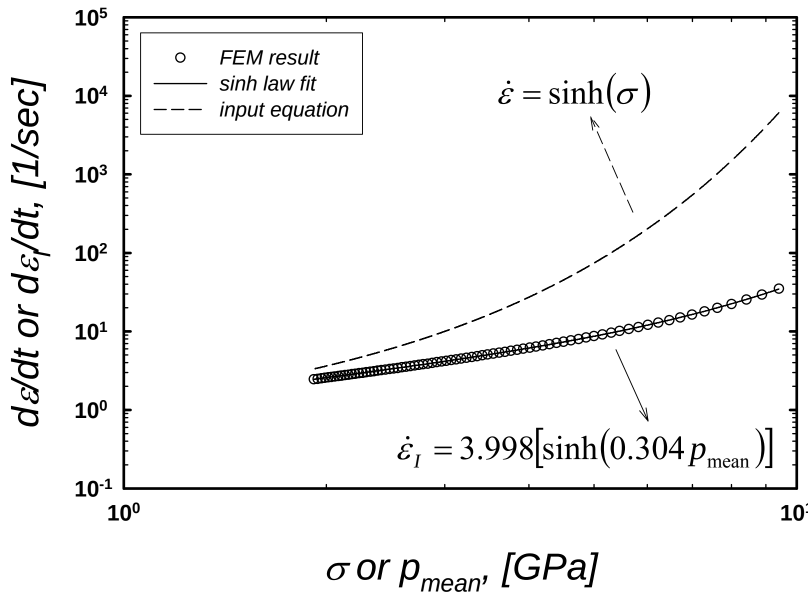

(a) conical indentation (70° cone, CRL)

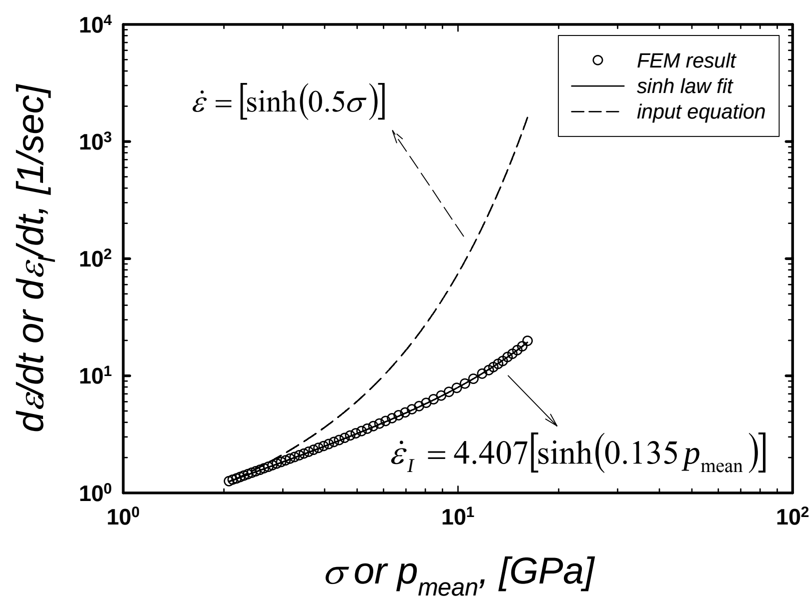

(a) spherical indentation (CLH)

Figure 92. Similarity in constitutive relation between uniaxial and indentation creep for hyperbolic sine law equation

The input constitutive relationship is characterized an analogous 3-parameter hyperbolic sine law implying that there is an analogy between the uniaxial and indentation creep constitutive relationships. When the argument within the hyperbolic sine function in equation (2) is small, equation (2) reduces to the power law relationship

$$\dot{\varepsilon} \approx A_1 \left(A_2 \sigma\right)^m \tag{86}$$

In a similar manner, equation (85) reduces to

$$\dot{\varepsilon}_I \approx B_1 \left(B_2 p_{\text{mean}}\right)^m \tag{87}$$

for small arguments. Comparing equations (86) and (87), we hypothesize that a hyperbolic sine law creeping solid should be similar to indentation of a power law creeping solid at relatively small mean pressures and small indentation strain rates. Applying the power law solutions for spherical and conical indentation, we obtain the following important relationships for indentation of hyperbolic sine law creeping solid:

$$c = c(m) \tag{88}$$

$$F(m) = \left[\frac{A_1 \left(A_2\right)^m}{B_1 \left(B_2\right)^m}\right]^{\frac{1}{m}} \tag{89}$$

In this chapter, we present methods for determining uniaxial creep parameters from indentation of an elastic – hyperbolic sine law creeping solid. Due to finite element difficulties, only indentation with a conical indenter under the CRL method and indentation with spherical indenter under the CLH method will be examined in detail. Detailed explanations for the cause of technical restrictions for other cases will be given later.

Application of Solutions Obtained for Indentation of a Power Law Creeping Solid

Accepting the hypothesis that the indentation creep constitutive relation for hyperbolic sine law creep at longer indentation times and larger indentation depths is characterized by equation (87), we apply the same analytical reasoning developed in Chapter 3. By replacing the indentation strain rate and mean pressure in equation (87) with primary variables of indentation, we obtain

$$h_{\text{creep}} \approx \left[\left(\frac{2m}{m+1}\right)B_1\left(B_2\right)^m\left(\frac{\dot{P}}{\pi}\right)^m\left(c\tan\beta\right)^{1-2m}\right]^{\frac{1}{2m}} t^{\frac{m+1}{2m}} \tag{90}$$

$$h_{\text{creep}} \approx \left[\left(m+\frac{1}{2}\right)B_1\left(B_2\right)^m\left(\frac{P}{\pi}\right)^m\left(c^{1-2m}\right)\left(2R\right)^{\frac{1}{2}-m}\right]^{\frac{2}{2m+1}} t^{\frac{2}{2m+1}} \tag{91}$$

Equation (90) is the rigid – power law creep *h*-*t* relation for conical indentation under the CRL method. Equation (91) is the rigid – power law creep *h*-*t* relation for spherical indentation under the CLH method. In a manner similar to Chapter 3, the hyperbolic sine law creep exponent, m, is determined from the slope of log*h*-log*t* curves in equations (90) and (91) at long times. The distinction between *h*-*t* curves from power law creep and hyperbolic sine law creep is observed in terms of the intercept of the log*h*-log*t* curves. Instead of obtaining a single coefficient B, we obtain a lumped coefficient $B_1(B_2)^m$ from equations (90) and (91), provided that c is known. Figure 93 shows that the pile up – sink in parameter c for hyperbolic sine law creep approaches the power law creep prediction. This power law prediction is used as the known c value. Applying equation (89), $A_1(A_2)^m$ is determined from $B_1(B_2)^m$.

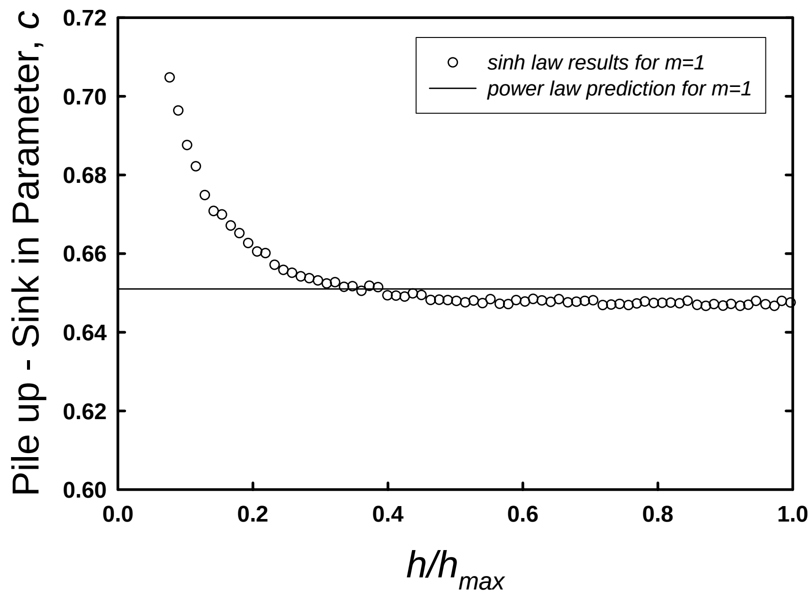

(a) conical indentation (70° cone, CRL)

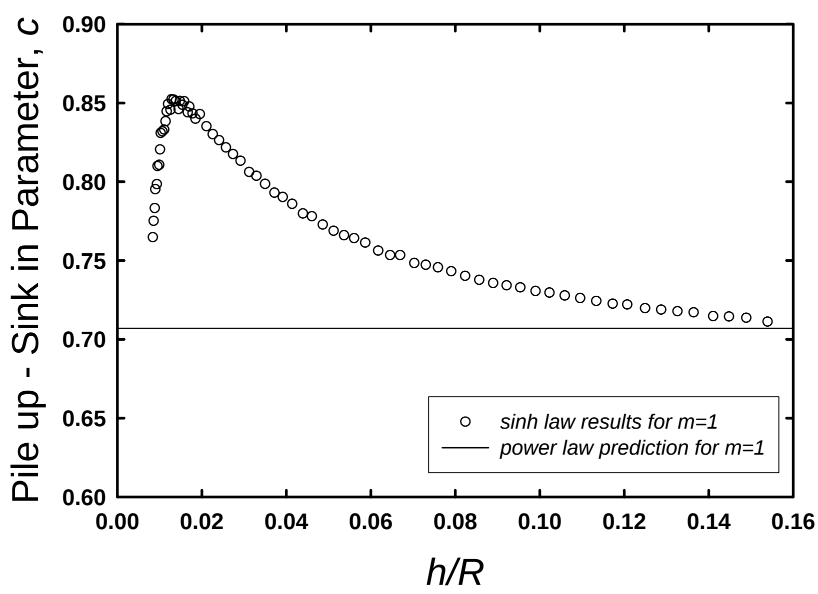

(b) spherical indentation (CLH)

Figure 93. *c* approaching the power law prediction (sphere, CLH)

In summary, application of power law creep indentation results provides methods in determining the uniaxial hyperbolic sine law creep exponent. In addition, the lumped coefficient $A_1(A_2)^m$ can be determined. This is demonstrated in Figure 94. In Figure 94, h-t curves produced from an elastic – hyperbolic sine law creep solid are shown with power law regression results. The power law regression lines are taken from data at long times. For the conical indentation using the CRL method shown in Figure 94a, the output exponent from the slope of the h-t curve (m_{output}=3.106) is within 5% error with respect to the input value (m_{input}=3). Using the power law predictions of c (equations (44)) at the computed output exponent values, the indentation lumped coefficient $B_1(B_2)^m$ is calculated from the intercept of h-t curve. Using equation (89), the output uniaxial lumped coefficient is estimated to be 0.154, which is approximately 23% larger than the input unaxial lumped coefficient (0.125). Analogous analysis for the results of spherical indentation using the CLH method (Figure 94b) yield output creep exponent (m_{output}=2.89) within 5% of the input value (m_{input}=3). Corresponding output uniaxial lumped coefficient computed in a manner similar to Figure 94a is 0.734, which is approximately 27% smaller than the input value (1.000).

Nature of Power Law Breakdown in Hyperbolic Sine Function

The analyses and results discussed above do not provide a complete solution for obtaining all the uniaxial hyperbolic sine law creep parameters. In order to accomplish this, knowledge of either A_1 or A_2 is independently required. For this purpose, we examine the nature of hyperbolic sine law equation. Figure 95 is a numerically generated plot of the hyperbolic sine equation.

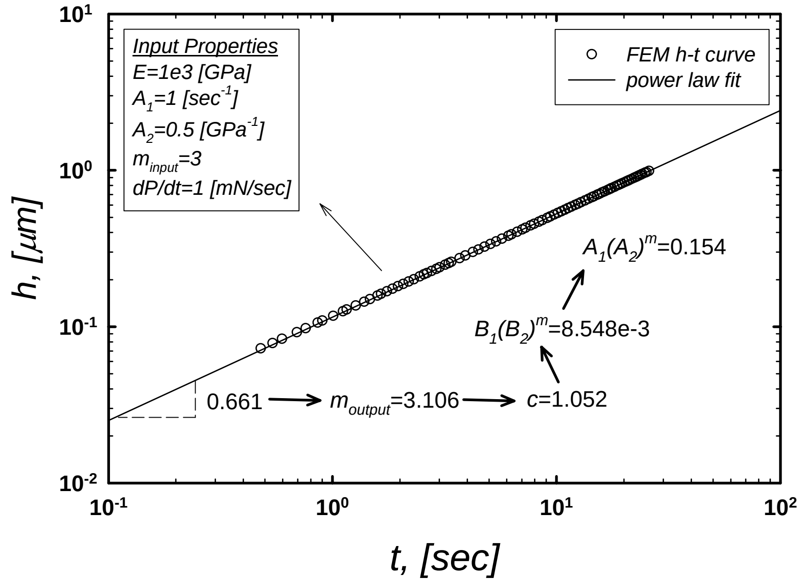

(a) conical indentation (70° cone, CRL)

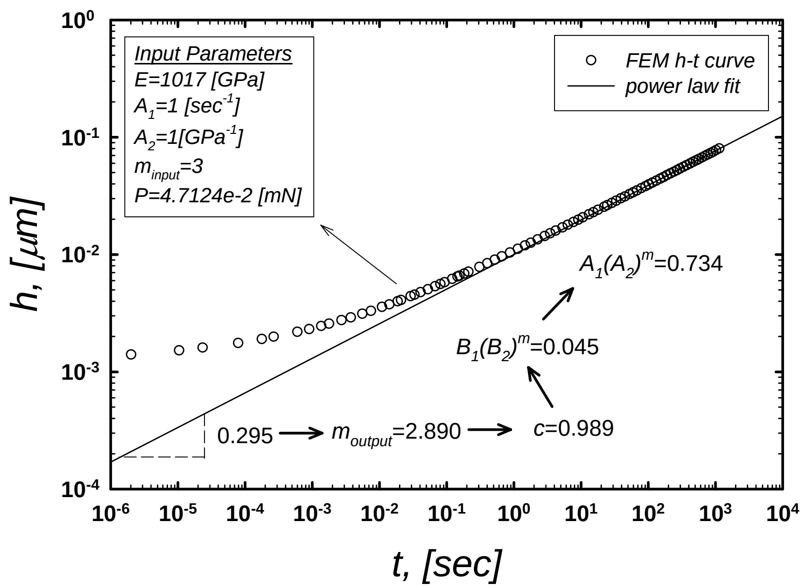

(b) spherical indentation (CLH)

Figure 94. Example of creep parameters extraction from *h-t* curves of sinh law creep

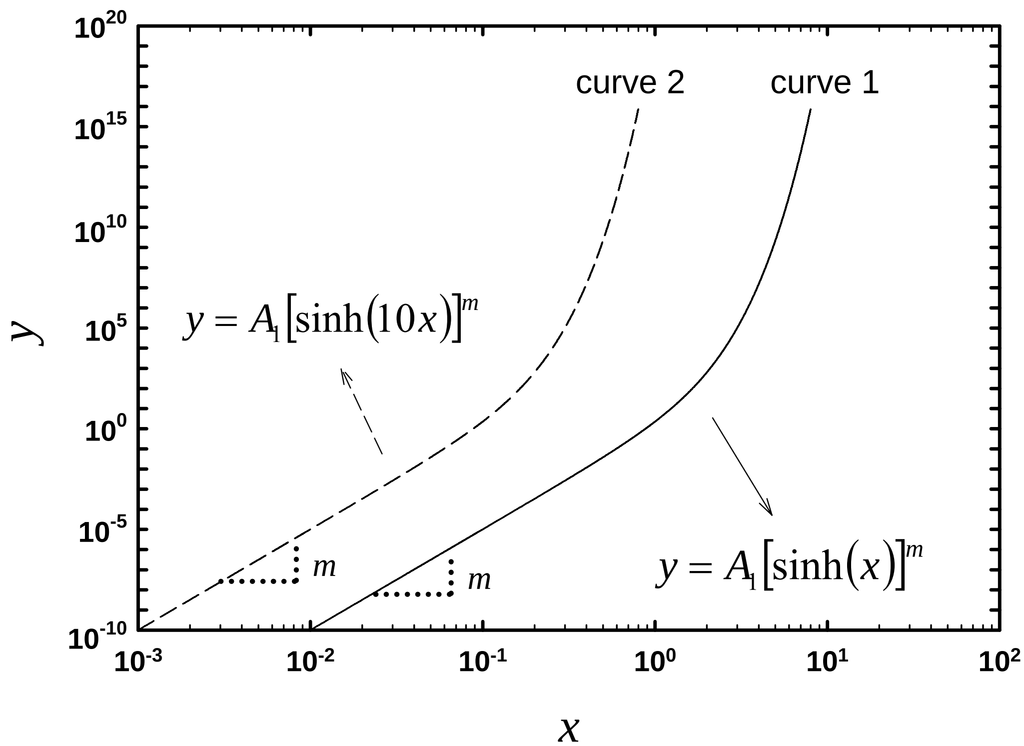

Figure 95. Shift in power law breakdown for hyperbolic sine law equation

Both curve 1 and curve 2 are characterized by a hyperbolic sine equation with three parameters; A_1, A_2, and m. The slopes in the log-linear regime for both of the curves are represented by the exponent, m. Careful observation yields information regarding the initiation of power law breakdown. The only distinction between the two curves is the difference of A_2 within the argument of the hyperbolic sine function. As a consequence, there is a shift in the location of the initiation of power law breakdown. Therefore, A_2 is the critical parameter governing where on the x-axis the breakdown in power law behavior commences. This argument will be used as the additional piece of information in determining the uniaxial hyperbolic creep parameters from indentation.

Prediction of Uniaxial Hyperbolic Sine Law Creep Parameters from Indentation

With the arguments outlined in the previous sections, methods for determining uniaxial hyperbolic sine law creep parameters from indentation are now presented. We consider conical indentation under the CRL method and spherical indentation under the CLH method.

Indentation h-t curves

Transients induced by power law breakdown originating from hyperbolic sine function manifest themselves as deviations from a log linear relationship in h-t curves. Figure 94 illustrates the examples of deviations for a linear (m=1) and a non-linear (m=3) creep constitutive relation. In Figure 96, the input constitutive law for hyperbolic sine law creep is equation (2). The input constitutive relation for power law creep in Figure 96 is equation (86).

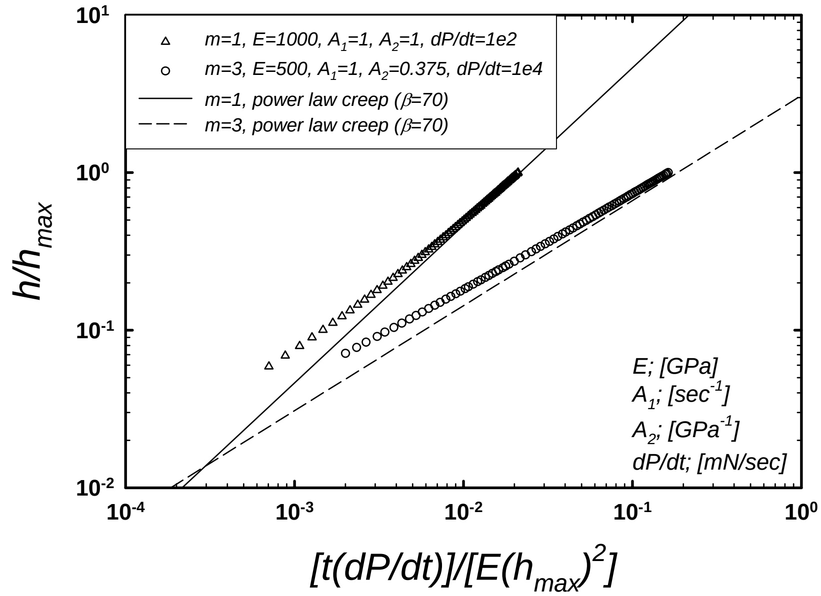

(a) conical indentation (70° cone, CRL)

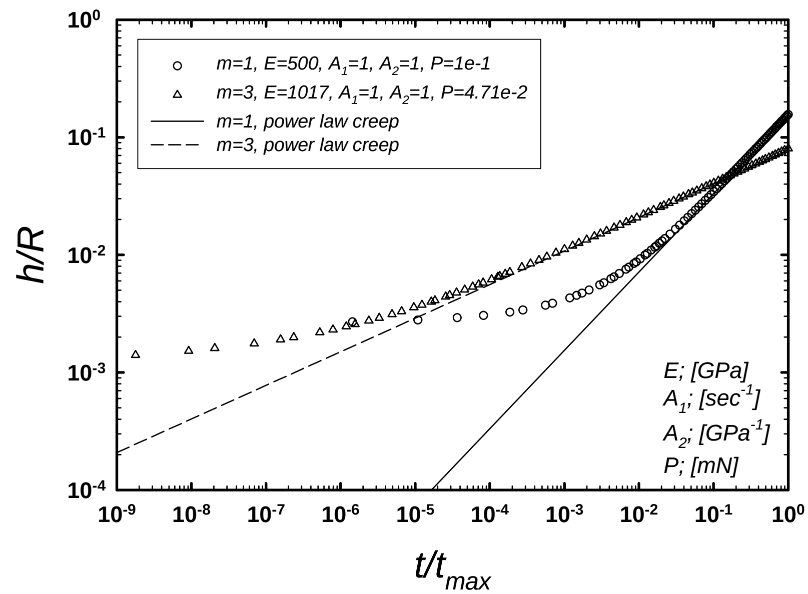

(b) spherical indentation (CLH)

Figure 96. Deviation from log linear relation for hyperbolic sine law creep

We observe that h-t curves converge toward each other at longer indentation times or larger indentation depths, which is a result of reduction of hyperbolic sine law equation to power law equation for small arguments. In addition to hyperbolic sine law behavior, finite elasticity is also expected to contribute to the transient behavior. The effect of this elastic transient will be discussed in detail in later sections. Indentation h-t curves for various input parameters are shown in Figure 97. These curves represent indentation results for a hyperbolic sine law creeping solid with various hyperbolic sine law creep coefficients A_1, hyperbolic sine law creep multipliers A_2 and loading rates for an exponent of m=1. As seen from Figure 97, different values of elastic properties and uniaxial hyperbolic sine law creep parameters produce different indentation h-t curves when normalized using the dimensional analysis. Analogous to the study of indentation of an elastic – power law creeping solid, the next step is to investigate the feasibility of a normalization method that produces a unique h-t curve solely dependent on the creep exponent of the material. This is conducted in a manner similar to the elastic normalization process for an elastic – power law creeping solid.

Elastic normalization

Analogous to indentation of a power law creeping solid, elastic normalization simplifies the boundary value problem. In indentation of an elastic – hyperbolic sine law creeping solid, the significant indentation variables are h, t, A_1, A_2, and m. Among these variables, h, t, and A_2 may be normalized using elastic properties and geometric features of the indenter. The elastic depth (equation (28) or equation (49)) is used in normalizing the indentation depth. According to the way in which we write the hyperbolic sine law constitutive law in this study, A_2 is expressed in units of inverse of stress.

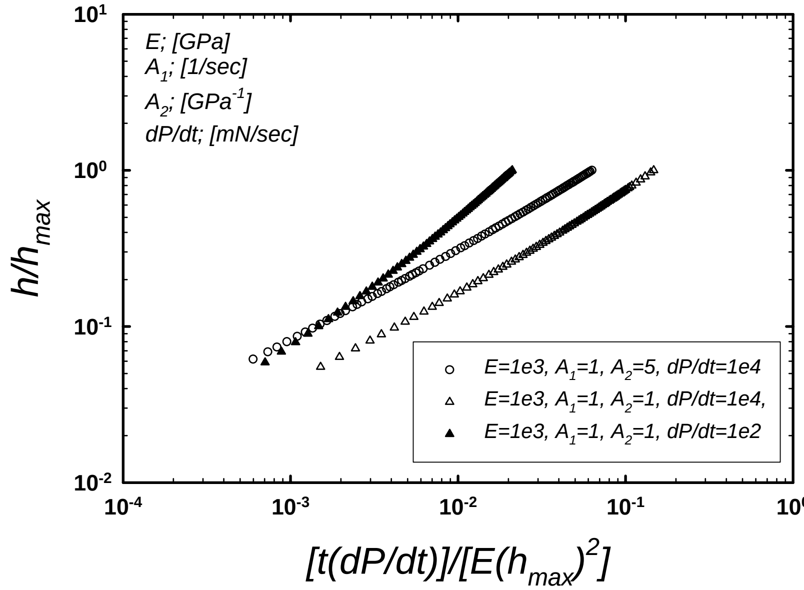

(a) conical indentation (70° cone, CRL)

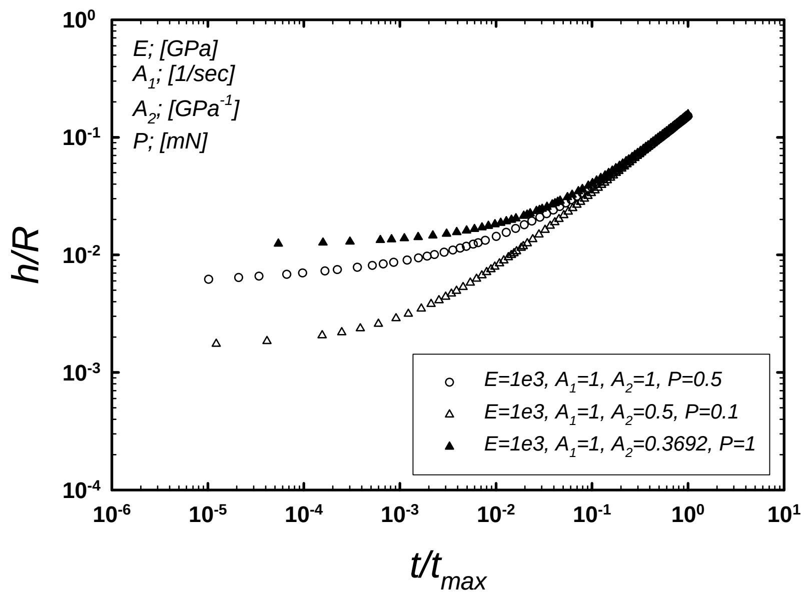

(b) spherical indentation (CLH)

Figure 97. *h*-*t* curves for hyperbolic sine law creep (*m*=1)

Therefore, we select the elastic mean pressure (equation (30) or equation (51)) as the normalizing parameter, or:

$$\left(A_2\right)_{\text{ElasticNormalized}} = A_2\left[\left(p_{\text{mean}}\right)_{\text{elastic}}\right] \tag{92}$$

To normalize indentation time, a characteristic time is required. The characteristic time is derived in a manner similar to that for indentation of a power law creeping solid. For conical indentation, substituting h_{creep} with the elastic depth (equation (49)) in equation (90) and solving for time t, we obtain the characteristic time. This is termed the characteristic time for hyperbolic sine law creep for conical indentation under constant rate of loading, $t_{\text{sinhconeCRL}}$. The mathematical expression for $t_{\text{sinhconeCLR}}$ is

$$t_{\text{sinhconeCRL}} = \left\{\left(\frac{m+1}{2m}\right)\left[\frac{P\left(1-\nu^2\right)}{2B_2\dot{P}E}\right]^m\left(\frac{\pi^{2m}}{B_1}\right)\left(c^{2m-1}\right)\left(\tan\beta\right)^{m-1}\right\}^{\frac{1}{m+1}} \tag{93}$$

For spherical indentation, substituting h_{creep} with the elastic depth (equation (28)) in equation (91) and solving for time t, we obtain the characteristic time for hyperbolic sine law creep for spherical indentation under a constant rate of loading, $t_{\text{sinhsphereCRL}}$. This is given by:

$$t_{\text{sinhsphereCRL}} = \frac{\left[\frac{3\left(1-\nu^2\right)}{E}\right]^{\frac{2m+1}{3}}\left(\pi^m\right)\left[P^{\frac{1}{3}(1-m)}\right]}{B_1\left(B_2\right)^m\left(m+\frac{1}{2}\right)\left(c^{1-2m}\right)\left(2^{\frac{2m+7}{6}}\right)\left[R^{\frac{2}{3}(1-m)}\right]} \tag{94}$$

Figure 98 presents the results of Figure 97 replotted to include elastic normalization. As a result, h-t curves with the same value of $A_2[(p_{\text{mean}})_{\text{elastic}}]$ form a single normalized h-t curve. Different elastic normalized h-t curves are produced for different values of $A_2[(p_{\text{mean}})_{\text{elastic}}]$.

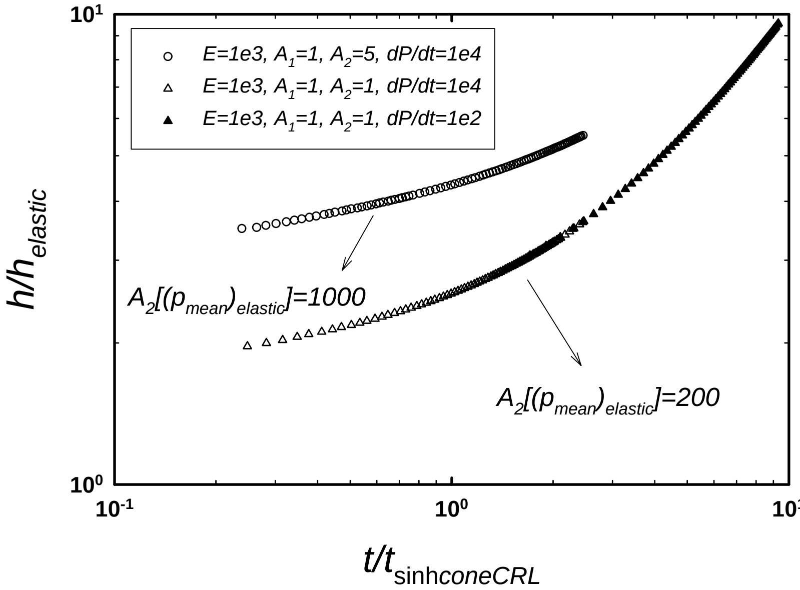

(a) conical indentation (70° cone, CRL)

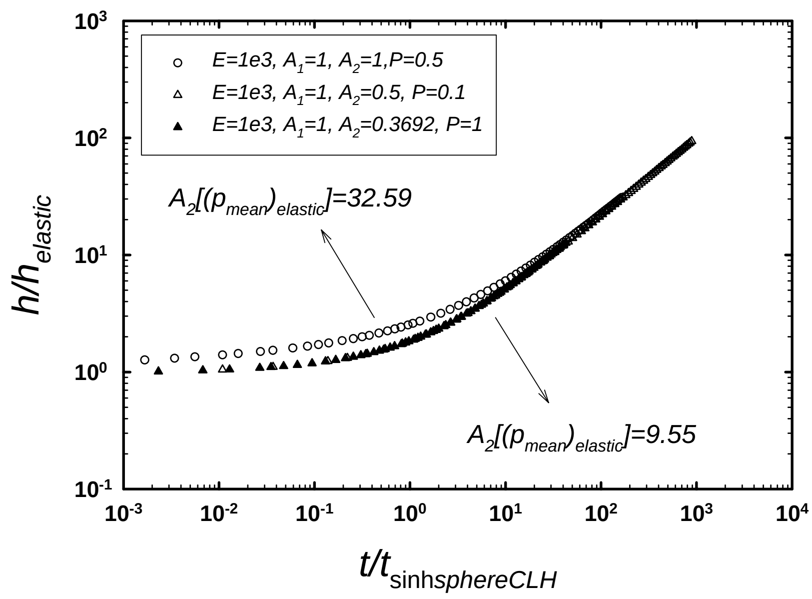

(b) spherical indentation (CLH)

Figure 98. Elastic normalized *h*-*t* curves for hyperbolic sine law creep (*m*=1)

Therefore, master *h-t* curves solely dependent on creep exponent are not possible.

Method of determining A_2 from indentation

m and $A_1(A_2)^m$ are directly determinable from indentation *h-t* curves. Since A_2 is related to the power law breakdown in hyperbolic sine law equation, we compare indentation *h-t* curves from power law creep and indentation *h-t* curves from hyperbolic sine law creep. This is shown in Figure 99 for both conical indentation under the CRL method and spherical indentation under the CLH method. In Figure 99, three different indentation *h-t* curves are shown. The two curves represented by a solid and a broken line are the results of indentation of a power law creeping solid. The solid line represents indentation results of an elastic – power law creeping solid (Model-*I*). The broken line represents indentation results of a rigid – power law creeping solid (Model-*II*). These results (Model-*I* and Model-*II*) may be compared with *h-t* curves from the hyperbolic sine law creeping solid for the determination of A_2. However, in indentation experiments, power law creep *h-t* curves with accurate description of the elastic transient may not be easily obtained. Therefore, Model-*II* may be the only practical way to evaluate A_2. As a result of elastic normalization of hyperbolic sine law *h-t* curves, a semi-master *h-t* curve can be constructed for a particular value of $A_2[(p_{\text{mean}})_{\text{elastic}}]$. Therefore, by varying the $A_2[(p_{\text{mean}})_{\text{elastic}}]$, we can obtain different *h-t* curves for hyperbolic sine law creep. This is demonstrated in Figure 100. Each of these *h-t* curves, when compared to *h-t* curves from power law creeping results, exhibits different deviations. This difference is used in correlating A_2 with measurable indentation parameters. We compute the ratio of normalized depth of hyperbolic sine law creep to the normalized depth of power law creep at a given normalized time.

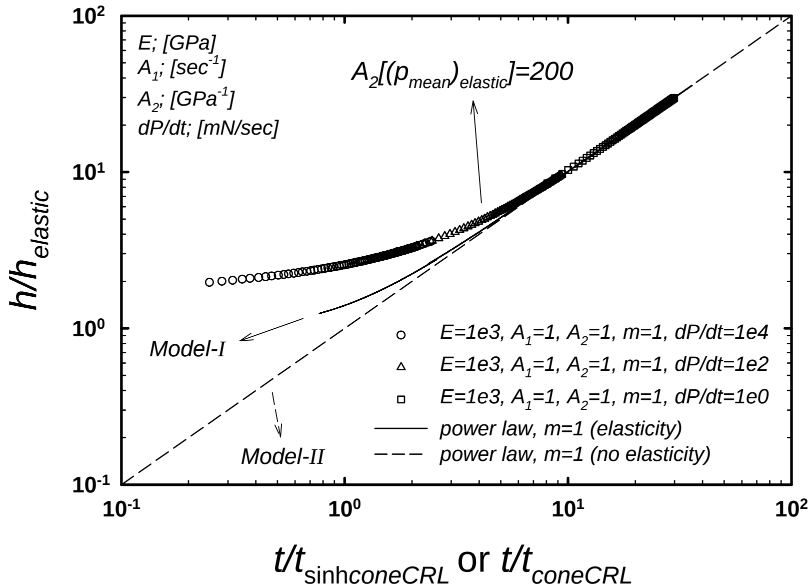

(a) conical indentation (70° cone, CRL)

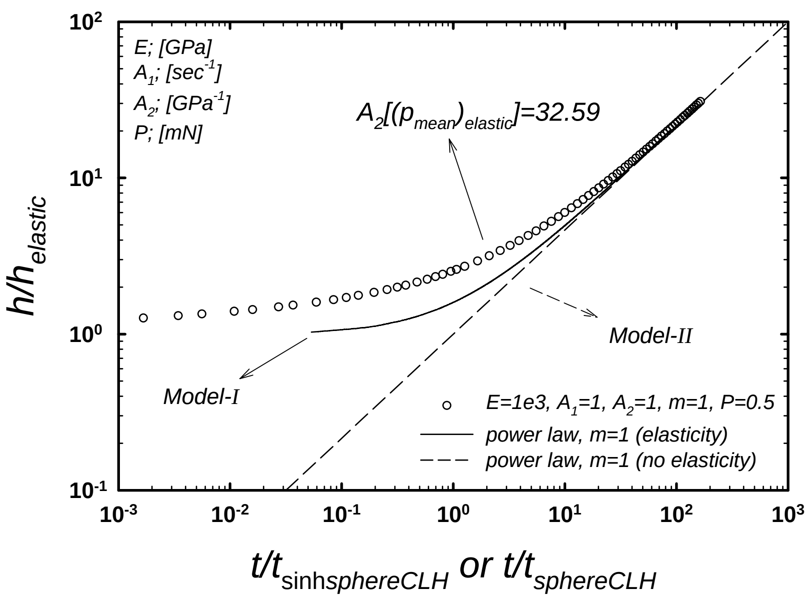

(b) spherical indentation (CLH)

Figure 99. Comparison of normalized *h-t* curves for different creep constitutive laws

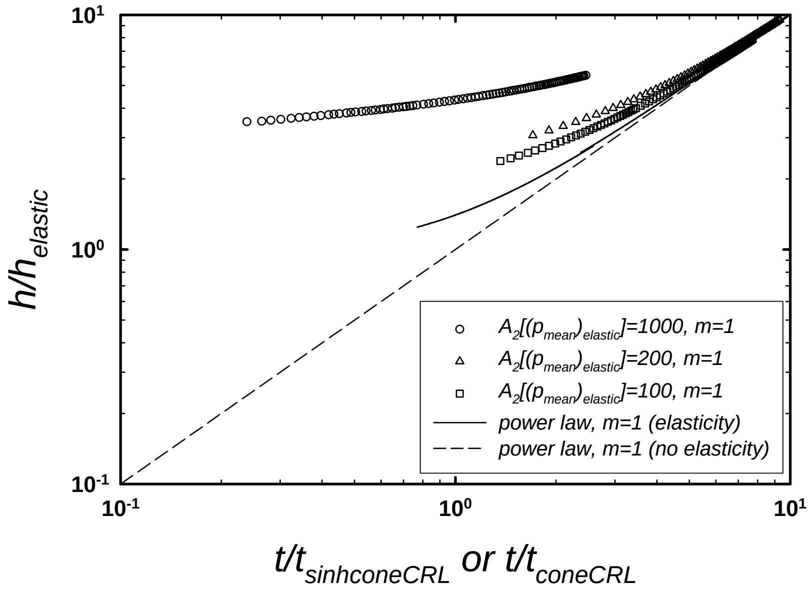

(a) conical indentation (70° cone, CRL)

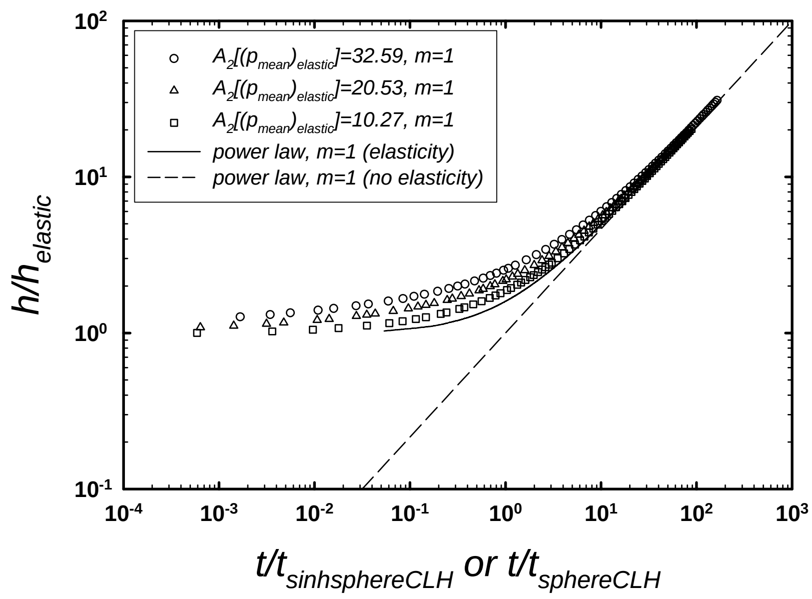

(b) spherical indentation (CLH)

Figure 100. *h-t* curves for different values of $A_2[(p_{mean})_{elastic}]$

For convenience, we choose the normalized time to be unity, mainly because the deviation between *h-t* curves from hyperbolic sine law creep and *h-t* curves from power law creep is different enough to be measured at this value. By varying the A_2 parameter in the finite element simulations, we are able to obtain the manner in which $A_2[(p_{mean})_{elastic}]$ varies as a function of the normalized depth ratios outlined above.

Results for A_2 correlation – conical indentation under the CRL method

Here, we consider the results for conical indentation under the CRL method. Under this boundary and loading condition, $A_2[(p_{mean})_{elastic}]$ is expressed by:

$$\frac{A_2 E}{2\left(1-\nu^2\right)\tan\beta} \tag{95}$$

All the variables in equation (95) are readily available except A_2. Correlation of $A_2[(p_{mean})_{elastic}]$ to the depth ratio is shown in Figures 101 and 102. Table 15 lists all the simulation parameters involved in Figures 101 and 102. Figure 101 is the result when indentation of an elastic – hyperbolic sine law creep is compared to indentation of an elastic – power law creeping material (Model-*I*). Figure 102 is the result when indentation of an elastic – hyperbolic sine law creep is compared to indentation of a rigid – power law creeping material (Model-*II*). The curves show results for creep exponents of m=1, 3, and 5. The minimum value of $A_2[(p_{mean})_{elastic}]$ considered in this study was 10. When $A_2[(p_{mean})_{elastic}]<10$, regardless of creep exponent, the hyperbolic sine law creep *h-t* curves show practically no distinction from power law creep *h-t* curves. Figure 103 shows an example of similar *h-t* curves for power law and hyperbolic sine law creep when $A_2[(p_{mean})_{elastic}]<10$ for spherical indentation under the CLH method. The result of these non-distinguishable *h-t* curves corresponds to depth ratios less than 1.03 (3% in depth ratio between hyperbolic sine law creep and power law creep).

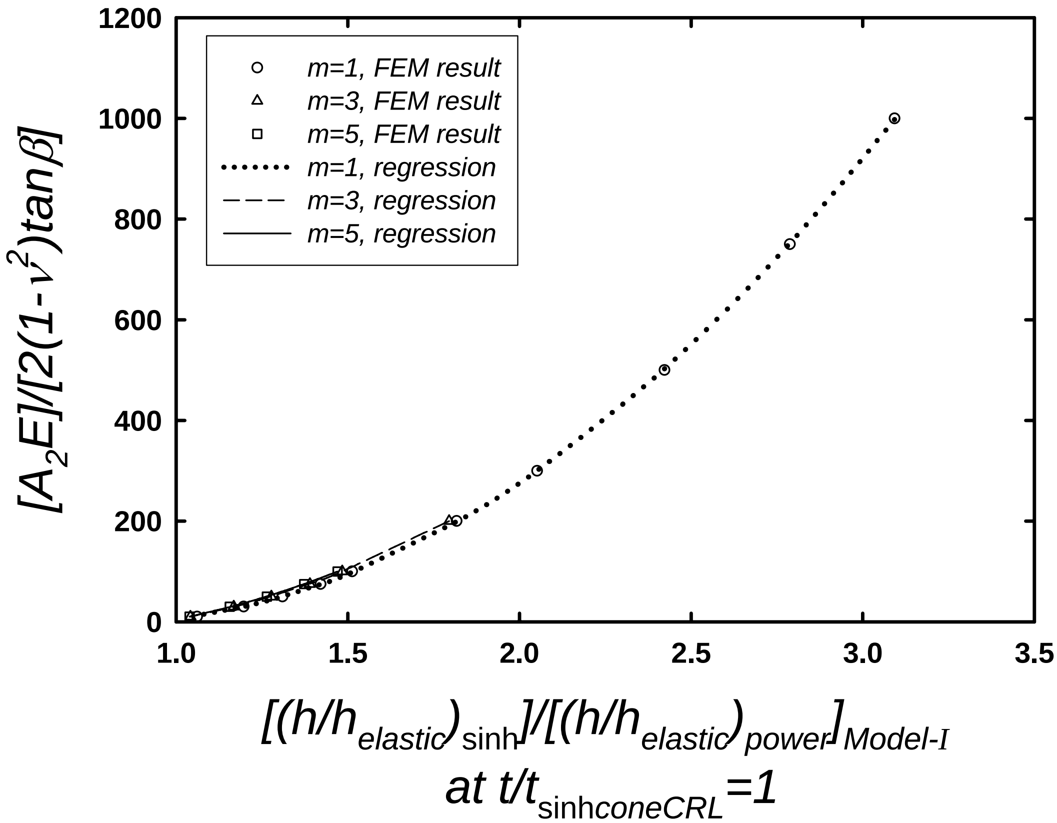

Figure 101. Correlation of $A_2[(p_{\text{mean}})_{\text{elastic}}]$ to depth ratio for Model-*I* (70° cone, CRL)

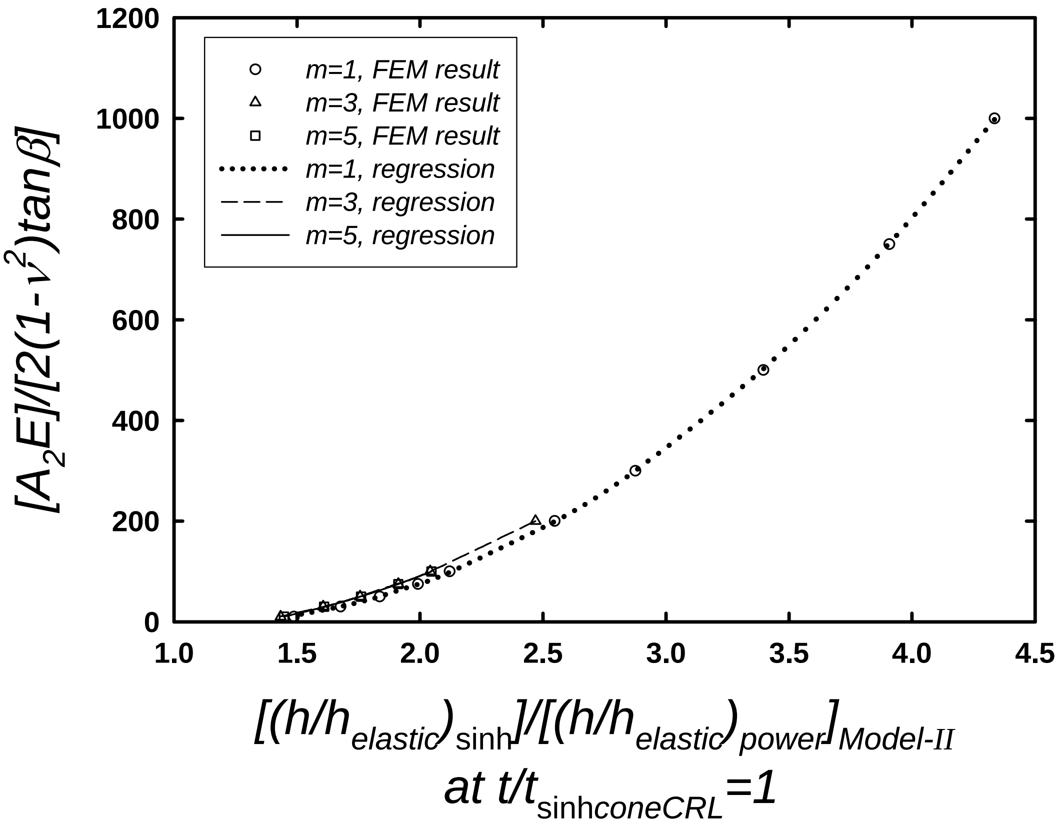

Figure 102. Correlation of $A_2[(p_{mean})_{elastic}]$ to depth ratio for Model-*II* (70° cone, CRL)

Table 15. Simulation parameters used in obtaining results for Figures 101 and 102

m	$A_2[(p_{mean})_{elastic}]$	E, [GPa]	A_1, [sec^{-1}]	A_2, [GPa^{-1}]	dP/dt, [mN/sec]
1	1000	500	1	5	1e4
	750	500	1	3.75	1e4
	500	500	1	2.5	1e4
	300	500	1	1.5	1e4
	200	500	1	1	1e4
	100	500	1	0.5	1e4
	75	500	1	0.375	1e3
	50	500	1	0.25	1e3
	30	500	1	0.15	1e3
	10	500	1	0.05	1e3
3	200	500	1	1	1e6
	100	500	1	0.5	1e6
	75	500	1	0.375	1e4
	50	500	1	0.25	1e4
	30	500	1	0.15	1e4
	10	500	1	0.05	1e3
5	100	500	1	0.5	5e6
	75	500	1	0.375	1e6
	50	500	1	0.25	3e5
	30	500	1	0.15	1e5
	10	500	1	0.05	1e3

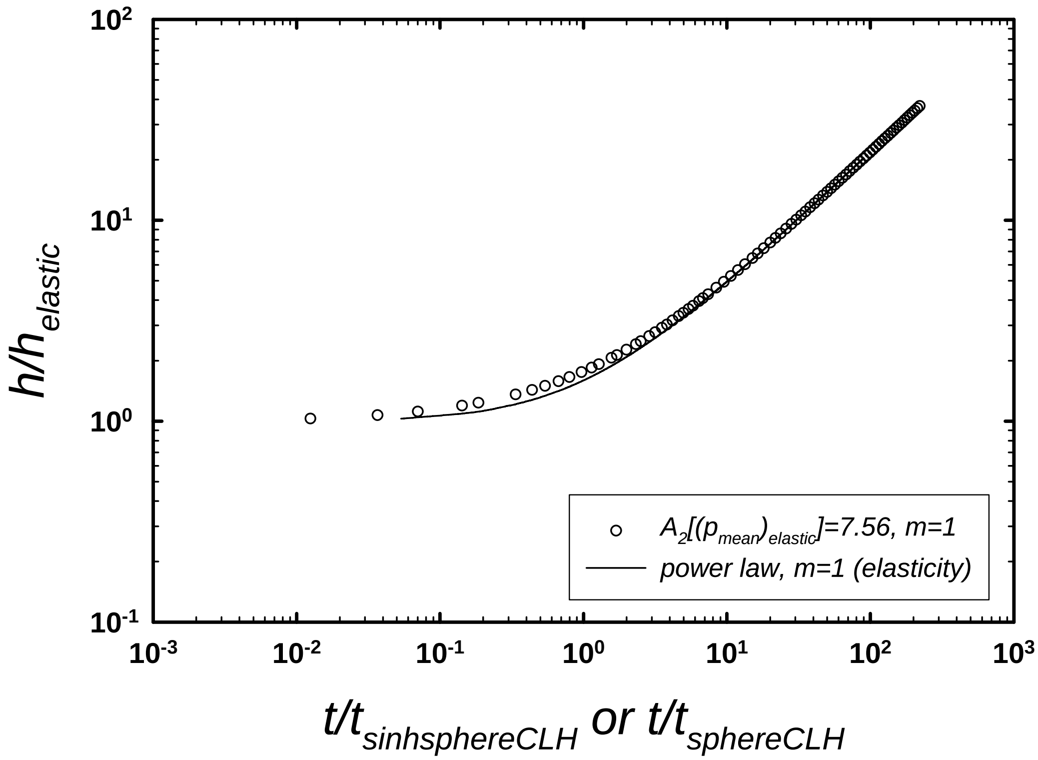

Figure 103. Hyperbolic sine law creep *h*-*t* similar to power law *h*-*t* curve for $A_2[(p_{\mathrm{mean}})_{\mathrm{elastic}}] < 10$ (sphere, CLH)

The maximum values of $A_2[(p_{mean})_{elastic}]$ in this study are influenced by simulation convergence. Fast indentation strain rates in the early stages of indentation give rise to large numbers of time increment refinement. This phenomenon gets worse as the creep exponent gets larger. Thus, larger creep exponents are limited by smaller maximum $A_2[(p_{mean})_{elastic}]$ values. The curves shown in Figures 101 and 102 both fit well to a 2rd order polynomial regression given by

$$y = x_0 + x_1 x + x_2 x^2 \tag{96}$$

The parameters of the regression are shown in Table 16.

Sensitivity of uniaxial creep properties prediction to the transient – conical indentation under the CRL method

Based on the previous section, we are able to obtain A_2 directly by comparing *h-t* curves from hyperbolic sine law creep and power law creep assuming that power law creep results are available (note: from an experimental standpoint, this is probably not the case). Potential error in predicting A_2 results from the accuracy of the A_2 prediction curves given by Figures 101 and 102. m and A_1 are obtained from *h-t* curve of the hyperbolic sine law creep in the log-linear regime. Therefore, deviation from log linearity in the *h-t* relationship has a direct impact on the accuracy of the estimated m and A_1. The resulting errors are shown in Figure 104 with the simulation parameters involved in extracting results listed in Table 17. The *h-t* data collected in computing m and A_1 are local values representing 10 data points. The depth represents an average value of these 10 data points. Creep exponent prediction is less sensitive to errors from the transient, with overestimation of creep exponent by approximately 80% at $h/h_{elastic}$=2. For A_1 estimation, transients in the *h-t* curves have a more significant effect on the error.

Table 16. Regression results for A_2 curve (70° cone, CRL)

	Model-*I*			Model-*II*		
m	x_0	x_1	x_2	x_0	x_1	x_2
1	110.45	-290.97	186.86	110.46	-207.60	95.12
3	43.62	-196.76	158.10	43.68	-143.12	83.58
5	9.59	-146.09	141.14	9.86	-105.22	72.88

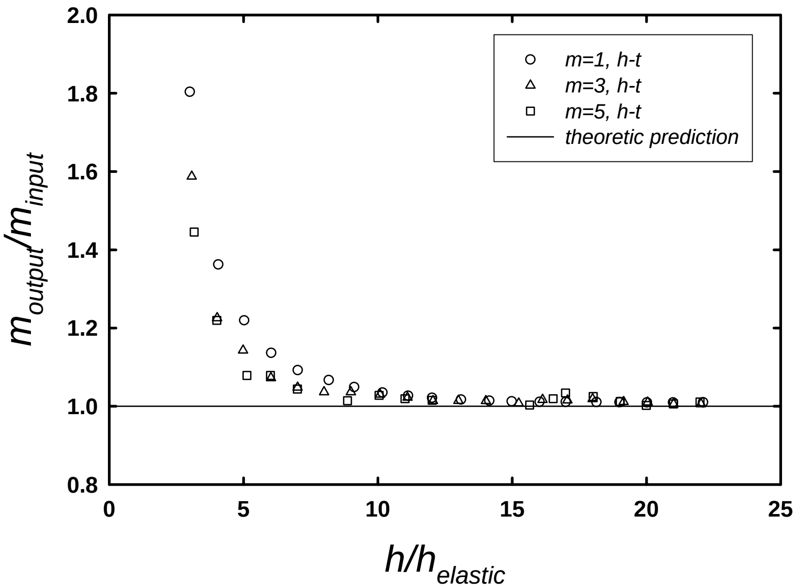

(a) Output uniaxial hyperbolic sine law creep exponent calculation

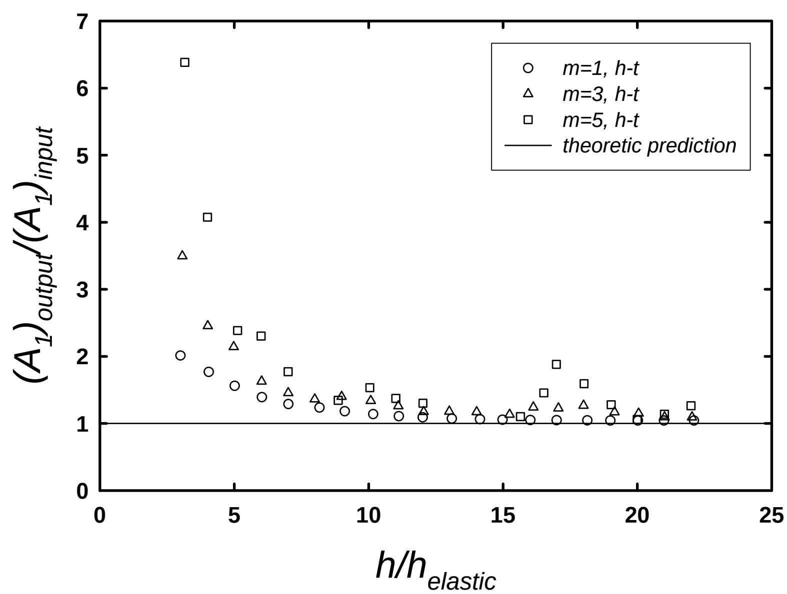

(b) Output uniaxial hyperbolic sine law creep coefficient calculation

Figure 104. Hyperbolic sine law uniaxial creep parameter estimation (70° cone, CRL)

Table 17. Simulation parameters involved in Figure 104

m	$A_2[(p_{mean})_{elastic}]$	E, [GPa]	A_1, [sec^{-1}]	A_2, [GPa^{-1}]	dP/dt, [mN/sec]
1	100	1000	1	0.5	1e2
	100	1000	1	0.5	1e0
3	100	1000	1	0.5	1e2
	100	1000	1	0.5	1e0
	100	1000	1	0.5	1e-2
	100	1000	1	0.5	1e-4
5	100	1000	1	0.5	1e2
	100	1000	1	0.5	1e-1
	100	1000	1	0.5	1e-4
	100	1000	1	0.5	1e-7

Based on Figure 104b, a minimum indentation depth of $h/h_{elastic}$=20 is needed to ensure the prediction to be within 10%.

Result for A_2 correlation – spherical indentation under the CLH method

Results are now presented for spherical indentation under the CLH method. $A_2[(p_{mean})_{elastic}]$ in this case is expressed by:

$$A_2\left[\frac{16PE^2}{9\pi^3\left(1-\nu^2\right)^2 R^2}\right]^{\frac{1}{3}} \tag{97}$$

Correlation between the parameters shown in equation (97) and the depth ratio is shown in Figures 105 and 106. Table 18 lists all the simulation parameters involved in Figures 105 and 106. When $A_2[(p_{mean})_{elastic}]<7.6$, the depth ratios are less than 1.03, which are too small for distinction. The maximum values of $A_2[(p_{mean})_{elastic}]$ were limited by simulation convergence. For the selected range of $A_2[(p_{mean})_{elastic}]$, results show a linear dependence described by

$$y = x_0 + x_1 x \tag{98}$$

The parameters of the regression are shown in Table 19.

Restrictions in modeling conical indentation under the CLH method and spherical indentation under the CRL method

For conical indentation under the CLH condition, simulation was unsuccessful. This is due to convergence issues caused by limitations in the minimum value of time (10^{-40}, in terms of seconds in this problem) set by ABAQUS™ [27]. Under the CLH method, the surface undergoes initial elastic deformation. Upon completion of elasticity, deformation makes a transition to creep.

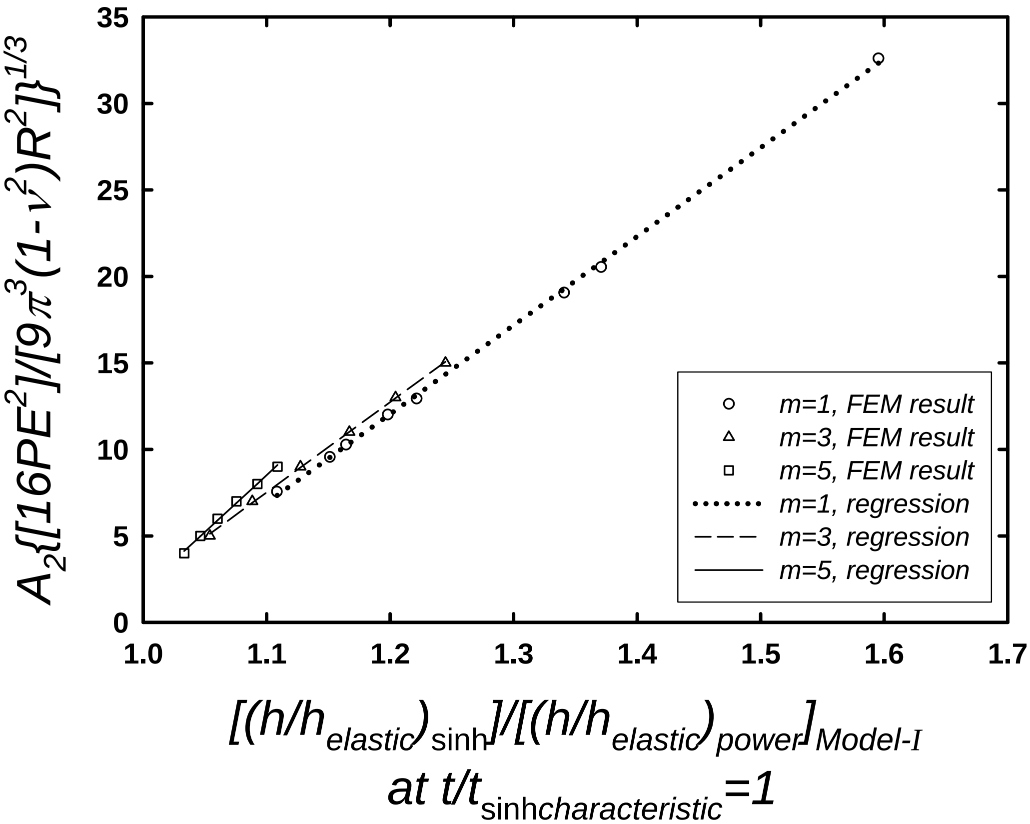

Figure 105. Correlation of $A_2[(p_{mean})_{elastic}]$ to depth ratio for Model-*I* (sphere, CLH)

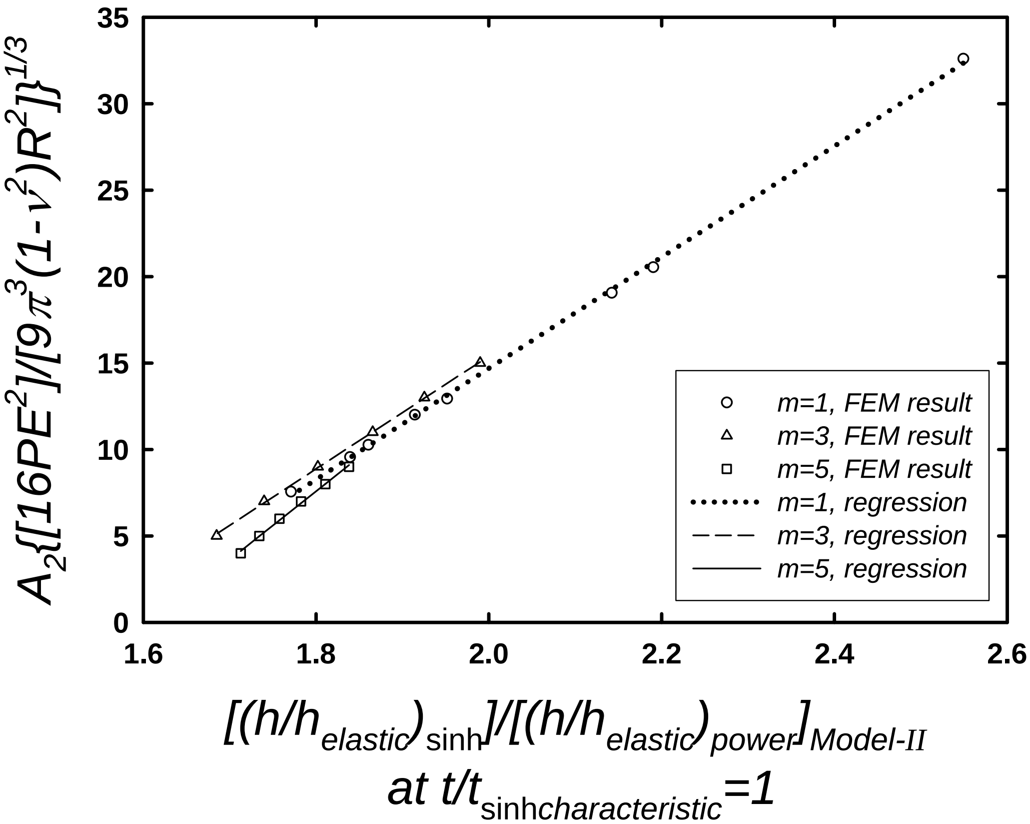

Figure 106. Correlation of $A_2[(p_{mean})_{elastic}]$ to depth ratio for Model-*II* (sphere, CLH)

Table 18. Simulation parameters used in obtaining results for Figures 105 and 106

m	$A_2[(p_{mean})_{elastic}]$	E, $[GPa]$	A_1, $[sec^{-1}]$	A_2, $[GPa^{-1}]$	P, $[mN]$
1	32.59	1000	1	1	5e-1
	20.53	1000	1	0.5	1e0
	19.06	1000	1	1	1e-1
	12.93	250	1	1	5e-1
	12.01	500	1	1	1e-1
	10.27	1000	1	0.25	1e0
	9.55	500	1	0.3692	1e0
	7.56	250	1	1	1e-1
3	15	1017	1	1	4.7124e-2
	13	881	1	1	4.0841e-2
	11	746	1	1	3.4558e-2
	9	610	1	1	2.8274e-2
	7	475	1	1	2.1991e-2
	5	339	1	1	1.5708e-2
5	9	1221	1	0.5	5.6550e-2
	8	2170	1	0.25	1.0053e-1
	7	4748	1	0.1	2.2000e-1
	6	81	1	5	3.7700e-3
	5	34	1	10	1.5700e-3
	4	271	1	1	1.2570e-2

Table 19. Regression results for A_2 curve (sphere, CLH)

	Model-*I*		Model-*II*	
m	x_0	x_1	x_0	x_1
1	-49.57	51.33	-49.57	32.13
3	-49.87	52.16	-49.86	32.63
5	-63.74	65.68	-63.76	39.63

In order to satisfy force and moment equilibrium at the first increment of the creep stage, the indentation time has to be very small. This limit is set by the finite element code. Once the limit of the minimum time increment has been reached, the finite element code determines that convergence is not achievable and aborts further calculation. For conical indentation of an elastic – hyperbolic sin law creeping solid, the 70° cone experiences this problem.

For spherical indentation under the CRL method, problems in obtaining useful data were encountered related to producing hyperbolic sine law creep *h-t* curves that are distinguishable from power law creep *h-t* curves. To observe power law breakdown, faster loading rates are required. Unlike conical indentation, distinguishable *h-t* curves (at least 3% deviation of depth ratio at $t/t_{\text{characteristic}}$=1) were not produced even at the maximum permissible loading rates set by ABAQUS™. Without being able to distinguish between hyperbolic sine law creep *h-t* curves and power law creep *h-t* curves, there is no means to provide a correlation of measurable parameters to A_2.

Indentation Results Compared with Existing Uniaxial Test Results

Luthy *et. al.* [2] have provided uniaxial creep test results for pure aluminum using a hyperbolic sine law creep constitutive law. A mathematical expression of their result can be written according to equation (3), which is:

$$\left(\frac{\dot{\varepsilon}_{\text{ss}}}{D_{\text{eff}}}\right) = K'\left[\sinh\left(\alpha\frac{\sigma}{E}\right)\right]^m \tag{3}$$

When we compare equations (2) and (3), we are able to find a relationship between A_2 and α. This relationship involves the elastic modulus and is given by:

$$A_2 = \left(\frac{\alpha}{E}\right) \tag{99}$$

For conical indentation the elastic mean pressure is expressed by equation (51). Therefore, $A_2[(p_{mean})_{elastic}]$ may be rewritten by combining equations (51) and (99) to give:

$$A_2\left[\left(p_{mean}\right)_{elastic}\right] = \left[\frac{\alpha}{2\left(1-\nu^2\right)\tan\beta}\right] \tag{100}$$

In the Luthy *et. al.* data, α=2600 and m=4.8. For materials with Poisson's ratio considered in this dissertation (ν=0.3) and an indenter with half-included cone angle of 70°, $A_2[(p_{mean})_{elastic}]$=520. Unfortunately, for the given indentation simulation conditions, the results of this dissertation provides A_2 only up to $A_2[(p_{mean})_{elastic}]$=100 for m=5. Therefore, a direct comparison of the proposed method in determining A_2 from indentation data cannot be implemented.

CHAPTER 8 – CONCLUSIONS FOR INDENTATION OF AN ELASTIC – HYPERBOLIC SINE LAW CREEPING SOLID

In this chapter, finite element simulations for indentation of an elastic – hyperbolic sine law creeping solid are presented. The feasibility of extracting uniaxial hyperbolic sine law creep parameters from indentation is examined, and the necessary correlations are provided. The conclusions may be summarized as follows:

1) Indentation of a hyperbolic sine law creeping solid may be characterized by an analogous hyperbolic sine law for the $\dot{\varepsilon}_I$ versus p_{mean} relationship. Although a mathematical proof may not be possible, FEM data in Figure 92 are provided that show the analogy seems to hold.

2) For small mean pressures, indentation of a hyperbolic sine law creeping materials reduces to power law behavior. In terms of the *h*-*t* curve, this corresponds to large indentation depths or long indentation times. In this regime, indentation solutions for power law creep are used in estimating the uniaxial hyperbolic sine law creep exponents. Additionally, a lumped coefficient comprising the uniaxial hyperbolic sine law coefficient A_1 and uniaxial hyperbolic sine law multiplier A_2 is available from the power law regime.

3) A method is developed that enables one to predict the hyperbolic sine law multiplier A_2 from normalized indentation *h*-*t* curves using measurable indentation parameters for

particular indentation geometries and loading methods. In determining A_2 by the proposed method, $A_2[(p_{mean})_{elastic}]$ defined by equations (95) and (97) becomes a significant parameter. The method developed in this study is applicable to practical indentation situations only for a limited range of $A_2[(p_{mean})_{elastic}]$.

4) The complete process of determining the three uniaxial hyperbolic sine law creep parameter is shown in Figure 107. h-t curves with indentation creep solutions developed for power law creep are used in determining the creep exponent m and the lumped coefficient $A_1(A_2)^m$. In addition, an auxiliary correlation developed in this study is used in determining the hyperbolic sine law multiplier A_2.

5) Experimental implementation may be difficult due to the difficulties in obtaining the depth ratio at the characteristic time.

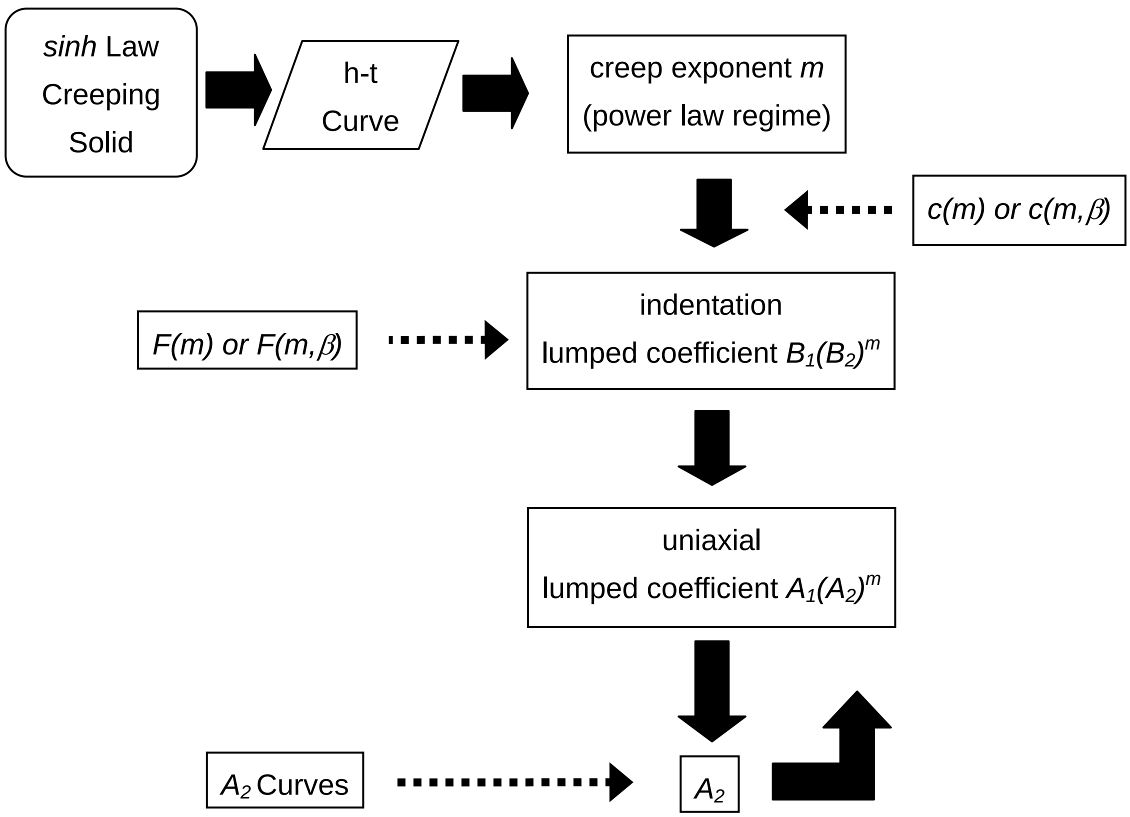

Figure 107. Flowchart of uniaxial hyperbolic sine law creep parameter extraction process from indentation

REFERENCES

[1] M.F. Ashby, D.R. Jones, "Engineering Materials 1", 1996

[2] H. Luthy, A.K. Miller, O.D. Sherby, *Acta Metallurgica*, Vol.28, pp.169-178, 1980

[3] P. M. Sargent, M.F. Ashby, *Materials Science and Technology*, Vol.8, pp.594-601, 1992

[4] T.O. Mulhearn, D. Tabor, *Journal of the Institute of Metals*, Vol.89, pp.7-12, 1960-1961

[5] A.G Atkins, A. Silverio, D. Tabor, *Journal of the Institute of Metals*, Vol.94, pp.369-378, 1966

[6] R. Hill, *Proc. R. Soc. Lond. A*, Vol.436, pp.617-630, 1992

[7] Y.T. Cheng, C.M. Cheng, *Philosophical Magazine Letters*, Vol.81, No.1, pp.9-16, 2001

[8] A.C. Fischer-Cripps, *Materials Science and Engineering A*, Vol.385, pp.74-82, 2004

[9] D.S.Wilkins, M.F. Ashby, *Acta Metallurgica*, Vol.23, pp.1277-1285, 1975

[10] S.N.G. Chu, J.C.M. Li, *Journal of Materials Science*, Vol.12, pp.2200-2208, 1977

[11] G.E. Lucas, C. Pendleton, *Journal of Nuclear Materials*, Vol.103&104, pp.1539-1544, 1981

[12] M.J. Mayo, W.D. Nix, *Acta Metallurgica*, Vol.36, pp.2183-2192, 1988

[13] V. Raman, R. Berriche, *Journal of Materials Research*, Vol.7, No.3, pp.627-638, 1992

[14] W.H. Poisl, W.C. Oliver, B.D. Fabes, *Journal of Materials Research*, Vol.10, No.8, pp.2024-2032, 1995

[15] S.A. Syed Asif, J.B. Pethica, *Philosophical Magazine A*, Vol.76, No.6, pp.1105-

1118, 1997

[16] P. Grau, G. Berg, H, Meinhard, S. Mosch, *Journal of American Ceramics Society*, Vol.81, No.6, pp.1557-1564, 1998

[17] B.N. Lucas, W.C. Oliver, *Metallurgica and Materials Transactions A*, Vol.30A, pp.601-610, 1999

[18] J.L. Bucaille, E. Felder, G. Hochstetter, *Journal of Materials Science*, Vol.37, pp.3999-4011, 2002

[19] A.F. Bower, N.A. Fleck, A. Needleman, N. Ogbonna, *Proc. R. Soc. Lond. A*, Vol.441, pp.97-124, 1993

[20] B. Storakers, P.L. Larsson, *Journal of Mechanics and Physics of Solids*, Vol.42, No.2, pp.307-332, 1994

[21] N. Ogbonna, N.A. Fleck, A.C.F. Cocks, *International Journal of Mechanics and Science*, Vol. 37, No.11, pp.1179-1202, 1995

[22] F. Yang, J.C.M. Li, C.W. Shih, *Materials Science and Engineering A*, Vol.201, pp.50-57, 1995

[23] I.N. Sneddon, "Fourier Transforms", 1951

[24] V.I. Fabrikant, *Advanced Applied Mechanics*, Vol.27, p.153, 1990

[25] L.Prandtl, *Göttinger nachr. Math. Phys. Kl.*, Vol.74, P.37, 1920

[26] R. Hill, *Q. J. Mech. Appl. Math.*, Vol.2, p.40, 1949

[27] ABAQUS USER'S MANUAL, Version 5.8, Hibbitt, Karlsson & Sorenson, Inc.

[28] M.C. Potter, C. Wiggert, " Mechanics of Fluids", pp.210-222, 1991

[29] K.L. Johnson, "Contact Mechanics", 1985

[30] D. Tabor, "The Hardness of Metals", 1951

[31] I.N. Sneddon, *International Journal of Engineering Science*, Vol.3, pp.47-57, 1965

[32] R.M. Davies, *Proc. R. Soc. Lond. A*, Vol.197, pp.416-432, 1949

[33] G.M. Pharr, *Scripta METALLURGICA*, Vol.19, pp.134-1349, 1985

VITA

Sangjoon Sohn was born on May 31, 1971 in Seoul, Republic of Korea. He was raised in Seoul, Republic of Korea and also in New Jersey, USA. He attended elementary school in New Jersey, USA and continued his junior high school and high school education in Seoul, Republic of Korea. He graduated from high school in Seoul, Republic of Korea in 1990. Upon graduating from high school, Sangjoon enrolled at Chung-Ang University in Seoul, Republic of Korea where he earned his Bachelor's and Master's Degree of Engineering majoring in Mechanical Engineering in February of 1997 and February of 1999.